THE UNIVERSITY *of* EDINBURGH

Robust Capsules for Biomedical Applications

William Rufus Grantham

A Thesis Submitted for the Degree of Doctor of Philosophy

School of Chemistry

Faculty of Science and Engineering

The University of Edinburgh

September 2019

Abstract

Metallosupramolecular capsules represent a facile route to three-dimensional structures that possess a central cavity. The synthetic accessibility is provided by self-assembly, which allows carefully designed components to form complex three-dimensional structures under thermodynamic control. The cavities allow the non-covalent binding of guests, changing their properties in a quick and reversible manner, thereby making capsules promising for catalytic, storage, extraction and biomedical applications.

However, the requirement for thermodynamic control makes capsules susceptible to degradation by changes in conditions such as heat, dilution, pH, or the presence of nucleophiles, making them insufficiently robust for biomedical applications. This project constitutes the continuation of a project which sought to synthesise more robust capsules. This was achieved by exploiting the cobalt II/III redox couple, assembling the tetrahedra with labile cobalt (II) and then oxidatively "locking" them as inert cobalt (III). This led to the development of the tetrahedron **C19**, which proved stable over a range of temperatures, dilutions and pH values. **C19** was shown to bind the common SPECT imaging agent precursor $[^{99m}Tc]TcO_4^-$, suggesting radioimaging as a potential application of the cage.

During this project, **C19** was found to be degraded in biological environments by reducing agents such as glutathione. Therefore, a ligand with electron donating amine groups, **L20**, was developed to increase the strength of interaction with metal centres, and overall stability. A two-step assembly using **C19** as a template and substituting **L20** into this prearranged tetrahedron was required to prevent kinetically trapped byproducts. The resulting cage, **C20**, was found to have increased resistance to biological conditions relative to **C19**, and was able to significantly alter the uptake of $[^{99m}Tc]TcO_4^-$ *in vivo*, proving the potential of the system to act as a delivery agent.

Further functionalisation of **C20** was explored to allow bioconjugation and targeting. To this end, the ligand was functionalised with a terminal alkyne to allow versatile Huisgen "click" functionalisation. A methyl ether was trialled as an alternative to the amines of **L20**, and the resulting ligand, **L38**, was found to confer similar properties onto its assemblies. Incorporation of alkyne Raman labels into a cage allowed stimulated Raman scattering imaging of its interaction with cells.

Overall, a robust cage system capable of retaining and altering the uptake of a significant diagnostic agent *in vivo* was developed. Progress was also made towards improving the properties, targeting and monitoring of the system.

Lay Summary

This thesis aims to explore the medical applications of small stable molecular capsules. These capsules are easily made by combining carefully designed components which can be induced to self-assemble into the desired capsule under appropriate conditions. These capsules are then chemically locked in order to make them robust enough to remain intact inside a living organism.

They can be used to encapsulate molecules reversibly in order to alter their properties without physically altering them. This means that these capsules can be used as delivery agents for pharmaceuticals. It was found that the sequential substitution of the components of an already locked container made a capsule that was able to bind a radioactive cargo inside living mice to provide images of their internal organs.

Attempts were then made to develop means to label the outside of this capsule in order to allow targeting of specific tissues. Alternative capsules were labelled with groups which absorb infrared radiation in a manner that cells do not, allowing the capsule to be detected within cells without interference from the cell itself.

Table of Contents

Acknowledgements

Firstly, thank you to my supervisor to Dr Paul Lusby for the opportunity to work on this project, and the advice, guidance and support over the past four years.

Thank you to Professor Scott Cockcroft for the funding, collaboration, supervision and excellent choice in morning rolls.

Thank you to Professor Alison Hulme, Professor Stephen Archibald, Professor Scott Cockcroft, Dr Annamaria Lilienkampf and Professor Colin Campbell for the use of your laboratories and equipment, and the guidance of your students and staff.

Thank you to the Lusby group old and new. Thanks to Michael Burke and David August for welcoming me to Edinburgh and the lab. Thanks to Patrick, Aaron, Garima, Vicente, Julia, Sam and Cora for all the company and friendship over the years. Thanks to Bec for all your help along the way. I know I wouldn't have got this far without you; your friendship, help and company have been amazing. Thank you to Helen for all the guidance, support and introduction to excellent pubs. Thank you to my project students Sofia, Cora and Katherine for all your hard work, patience and teaching me so much about science, people and myself. Good luck in all your future endeavours.

Thanks to James Cooper, Stefan Borsley, Sara Schmidt, Alisia Sim, Krystal Sepp, Samuel Oldknow, Mathew Owens, Benjamin Burke and Sally Vanden for your collaboration. Thank you to Lorna Murray, Juraj Bella, Faye Cruicshank and Logan Mackay for assistance with the NMR and Mass Spec facilities. Thanks to the Hulme group for the use of their freeze drier despite the lack of cake payment.

Special thanks for the University of Edinburgh Conservation volunteers for welcoming me, giving me an excuse to get outside and muddy, making me feel part of a community and letting me meet so many interesting people.

Thank you to my friends and family for your company, love and support. Thank you to Emma for putting up with me and making the last three years amazing.

Declaration

I hereby declare that except where specific reference is made to other sources, the work contained in this thesis is the original work of the author. It has been composed by the candidate and has not been submitted, in whole or in part, for any other degree, diploma, or other qualification.

William Rufus Grantham

Format of the Thesis

Chapter 1: Biomedical Applications of Supramolecular Coordination Complexes

- An overview of the biomedical applications of supramolecular coordination complexes

Chapter 2: Kinetically Robust $Co^{III}_4L_6$ Tetrahedra for *In Vivo* Anion Binding and SPECT Imaging

- Chapter 2 is made up of a contribution to the following published peer-reviewed paper: B. P. Burke, W. Grantham, M. J. Burke, G. S. Nichol, D. Roberts, I. Renard, R. Hargreaves, C. Cawthorne, S. J. Archibald and P. J. Lusby, *J. Am. Chem. Soc.*, 2018, **140**, 16877–16881; DOI: 10.1021/jacs.8b09582. It has been reformatted to fulfil the requirements of the University of Edinburgh regarding the preparation and submission of a thesis for the degree of PhD.

Chapter 3: Functionalisation and Conjugation of Robust $Co^{III}_4L_6$ Tetrahedra

- Chapter 3 builds on the work from Chapter 2, and explores how other functionalisations of the ligand, both pre- and post-assembly, might be used to create tuneable robust capsules.

Chapter 4: *In Vitro* Raman Spectroscopy of Alkyne Labelled $Co^{III}_4L_6$ Tetrahedra

- Chapter 4 makes use of Raman-active alkyne ligands for the synthesis of supramolecular coordination cages. Once synthesised, stimulated Raman scattering microscopy imaging was performed to examine the cellular uptake of the cages.

External Contributions

Imaging: David Roberts, Isaline Renard, Rebecca Hargreaves, Christopher Cawthorne and Benjamin P. Burke at the University of Hull

Chapter 1: Introduction: Biomedical Applications of Supramolecular Coordination Complexes

1.1 Supramolecular Coordination Complexes

Compounds within the thesis are numbered in the following manner: Assemblies and ligands have been numbered sequentially with a qualifying letter to describe nature of the species. Ligands are denoted as **L#**, cages as **C#**, helicates as **H#** and metallocycles as **M#**. Non-ligand organic species are numbered sequentially as **N#** with no relation to ligand or assemblies.

Supramolecular interactions are incredibly important in the world around us, with much of the function of biological systems driven by supramolecular interactions; from the hydrogen bonding between nuclear bases defining the structure of the DNA double helix, to the hydrophobic effects maintaining the folding of proteins to form receptors, enzymes, and biological machinery.

Supramolecular coordination complexes (SCCs) are discrete two- or three-dimensional compounds containing multiple metal centres and multitopic ligands held together by coordination bonds. These complexes are synthesised through coordination driven self-assembly, in which careful design of the components leads to the selective self-assembly of the architecture under appropriate conditions. The self-assembly of complex three-dimensional architectures is aided by the "maximum site occupancy" principle, which states that a system will seek to satisfy the maximum number of possible "non-covalent" or coordination bonds. Therefore, combining metal centres of defined coordination geometry with semi-rigid multitopic ligands of appropriate dimensions in the correct stoichiometry will lead to an assembly that satisfies all the possible bonds.

The process of self-assembly requires reversible interactions between the metals and ligands in order to allow the system to reach equilibrium, and self-correcting interactions which do not lead to the thermodynamic product. Coordination assemblies offer advantages over other forms of supramolecular assemblies, such as those driven by hydrogen bonding, in that the metal centres offer well-defined geometries and have tuneable interaction strengths intermediate between covalent and hydrogen bonds to provide both accessibility and reasonable kinetic stability.

Metallosupramolecular cages possess an intrinsic central cavity in which guests may be bound (Fig. 1.1). This provides the opportunity for applications such as catalysis,[1] storage,[2] as well as biomedical opportunities such as anion transport and drug delivery. Binding is affected by a number of different factors including the nature of the cavity, guest, solvent

and the counterions in the system. There are both enthalpic and entropic factors that govern the strength of the binding. Enthalpic contributions can be made by electrostatic interactions, π-π stacking, and hydrogen bonding between the guest and cavity of the cage. However, these can often be complicated by competition with solvent molecules or the counterions.[3]

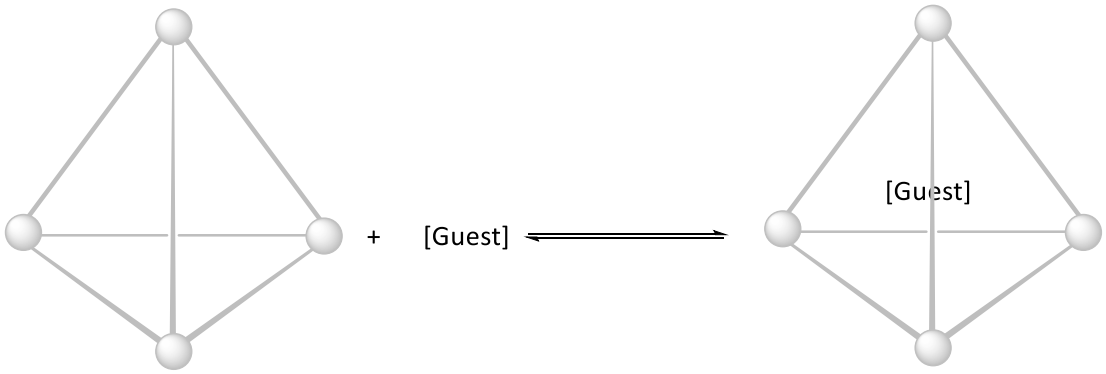

$$K_a = \frac{[\text{Host} - \text{Guest complex}]}{[Host][Guest]}$$

Figure 1.1: Depiction of guest binding within a tetrahedral cage, and the formula of the binding constant.

Many systems utilised in water rely on the hydrophobic effect to drive the binding of nonpolar guests in the hydrophobic cavities of capsules. This relies on the liberation of high energy water molecules, which possess unsatisfied hydrogen bonds within the constrained environment of the cavity. The displacement of these species enthalpically drives the binding of neutral molecules.[4] Charged species can also be bound within supramolecular capsules, and indeed, a large number of assemblies are templated by their counterions, implying that the binding of the guest is the driving force in the assembly. Oppositely charged species will have increased electrostatic interactions due to ion pairing with the charged capsules but at the potential cost of increased affinity of the guest for polar bulk solvent.[5]

1.2 Challenges in Using Supramolecular Coordination Complexes in Biological Systems

The nature of coordination complexes can lead to some issues when attempting to use them in biological applications. Many species are not intrinsically water soluble and require functionalisation with solubilising groups in order to be suitable for aqueous applications,

such as hydroxyl groups[6] or polyethylene glycol groups.[7] However, it has been demonstrated that selection of appropriate metal ions and anions can render these highly charged species water-soluble and stable (Fig. 1.2.1).[8]

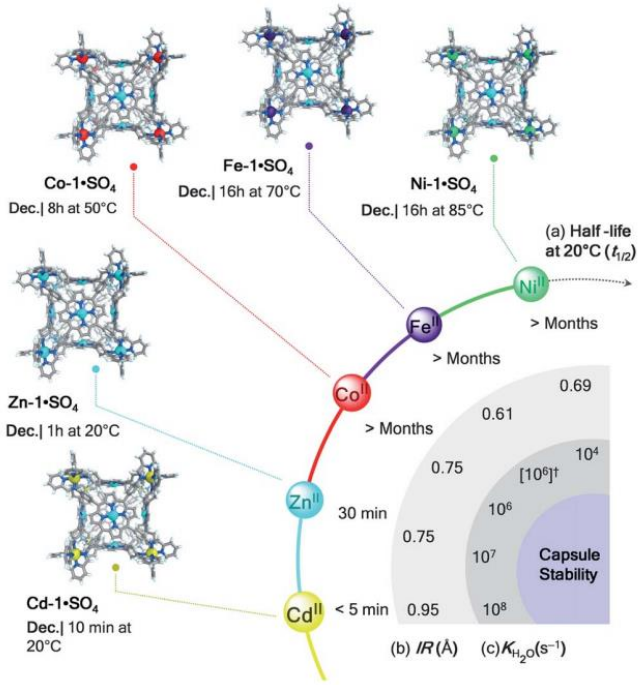

*Figure 1.2.1: Representation of how the different choice of metal ion can drastically affect the relative stability of M_8L_6 cubes (**C1**$_{a,b,c,d,e}$) in water. (a) Half-lives ($t_{1/2}$) at 20 °C, (b) ionic radii (IR, Å), and (c) ligand-exchange rates for water (K_{H_2O}, s^{-1}) for the different metal ions. Figure adapted from reference 8.*

However, when moving into aqueous systems, the dynamic nature of supramolecular systems is a fundamental issue that at present limits their effective use in biological applications. Self-assembly inherently requires the system to possess some dynamic properties that allows the desired "equilibrium" product to be accessed. While it is hoped that cooperative chelate effects will make the assembly a significant energy minima, offering some kinetic stability, the system is still effectively in equilibrium. Therefore, the desired assembly may no longer be the favoured product when removed from the assembly conditions, leading to rearrangement or disassembly.

This can mean that dilution, increase in temperature, exposure to coordinating solvents or competing ligands, or extremes in pH can lead to degradation of the cages. As water is a highly coordinating solvent, it poses a particular challenge to supramolecular systems,

especially as it is present in vast excess, meaning many systems require specific design features to be stable in water.

Stability issues become even more prominent under biological conditions, which can be considered relatively harsh compared to those under which coordination assemblies are commonly formed. Biological conditions are chemically complex, containing a plethora of reactive biological compounds and competing ligands that can compete for the structural metals of any coordination assembly,[9] an example of which is seen in Crowley and co-workers' amine-based Pd_2L_4 cages **C2** (Fig. 1.2.2).[10] This competitive environment, coupled with the low cage concentration required for biological use, makes rapid cage degradation both highly probable and irreversible. This loss of structure would remove the capacity to retain an encapsulated guest. It is therefore highly likely that almost all current SCCs are not robust enough for *in vivo* applications, certainly for any that require structural integrity.

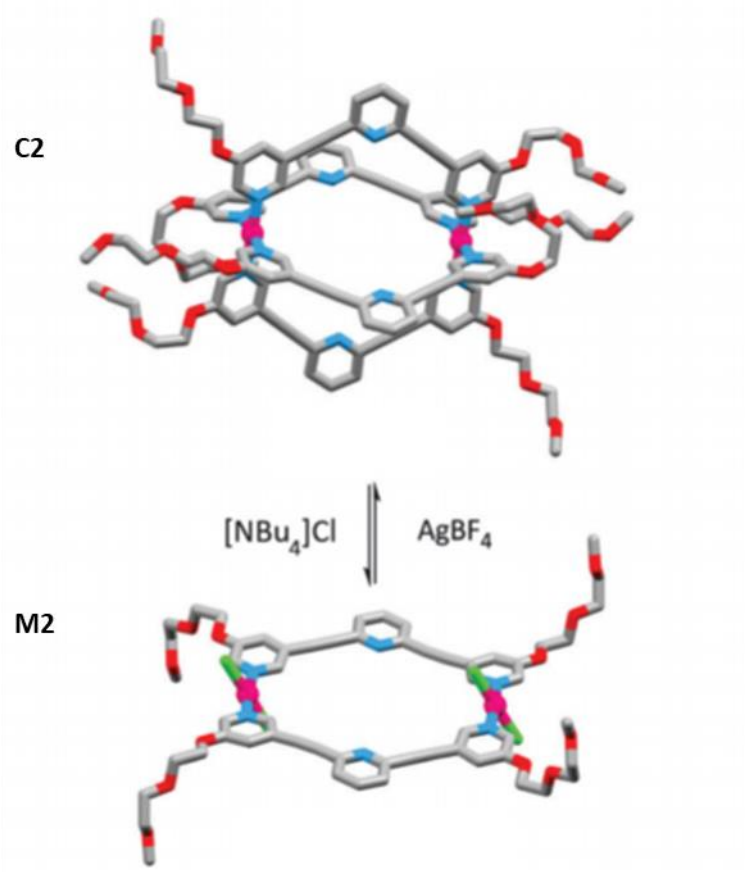

*Figure 1.2.2: Depiction of Pd_2L_4 (**C2**) cage undergoing reversible nucleophilic attack by chloride anions to form a $Pd_2L_2Cl_2$ metallocycle (**M2**). Modified from reference 10.*

1.3 Direct Biomedical Application of SCCs

Many SCCs have been reported to be biologically active in their own right, often as cytotoxic anti-cancer agents. Their methods of activity vary, including interactions with cellular components or acting as prodrugs with cytotoxic metabolites.

A large number of cytotoxic platinum, palladium and ruthenium metallocycles have been reported with range a of activities against various cell lines. The platinum metallocycle (**M3**, Fig. 1.3.1) was shown to be more cytotoxic and selective than the ubiquitous anticancer agent cisplatin. It was also shown that the cytotoxicity is greater than the sum of its individual components.[11]

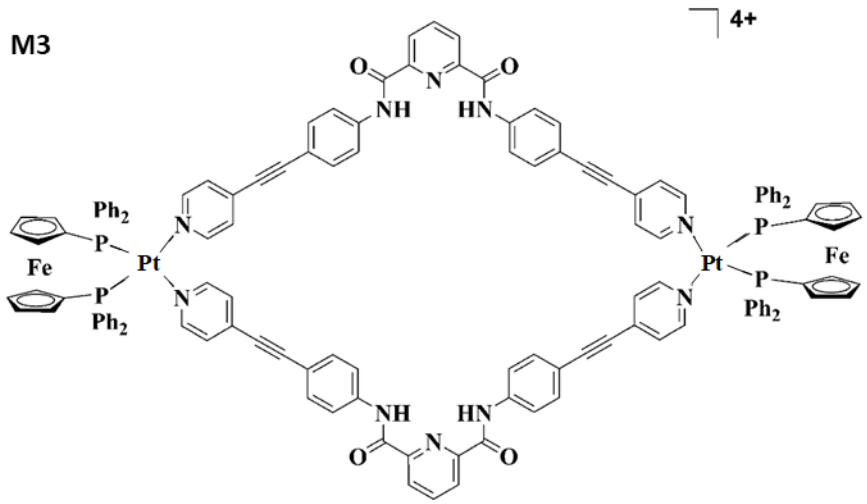

*Figure 1.3.1: Chemical structure of the cytotoxic hetero-bimetallic metallocycle (**M3**). Figure adapted from reference 11.*

Yoshizawa and co-workers developed two anthracene containing spherical M_2L_4 capsules **C4$_{a,b}$**, which were shown to be cytotoxic against a range of cancer lines (Fig. 1.3.2). Interestingly, the cytotoxicity of the cages appeared to be related to the degradation of the cages within the cells, with the palladium **C4$_a$** variant being the more active, while being demonstrated to be more easily degraded by chemical assay and fluorescence microscopy.[12]

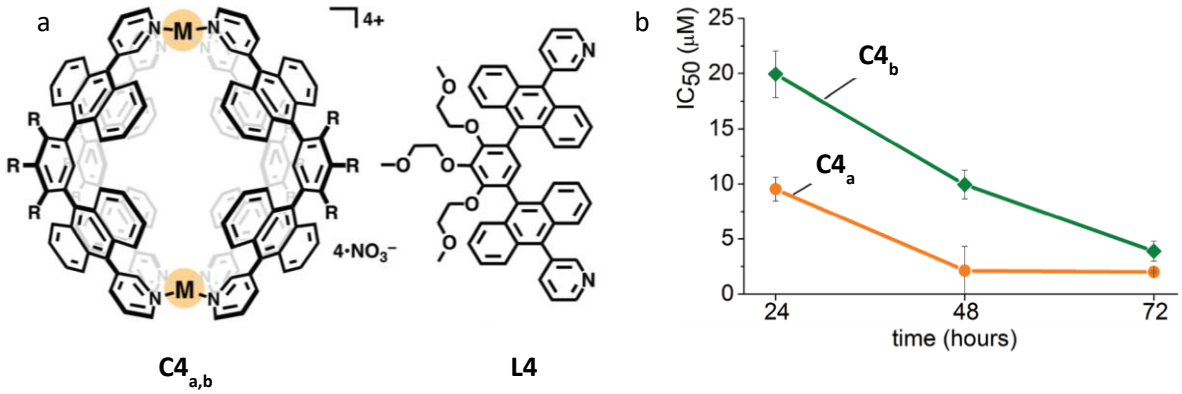

Figure 1.3.2: (a) Chemical structure of a M_2L_4 capsules (M = Pd, ***C4$_a$*** *or Pt,* ***C4$_b$****, R = -$OCH_2CH_2OCH_3$). (b) Time dependent cytotoxicity of* ***C4$_b$*** *and* ***C4$_a$*** *against HL-60, estimated as IC_{50} (in μM) at different time intervals. Figure adapted from reference 12.*

Conversely, Crowley and co-workers found that the cytotoxicity of several Pd_2L_4 constructs against cancer lines was found to increase with stability (Fig. 1.3.3). Their results indicated that the activity stemmed from the assembly's three-dimensional architecture disrupting cell membranes rather than the release of palladium complexes. Interestingly, the stability of the most active helicate was believed to be caused by shielding of the metal centres by appended alkyl chains.[13]

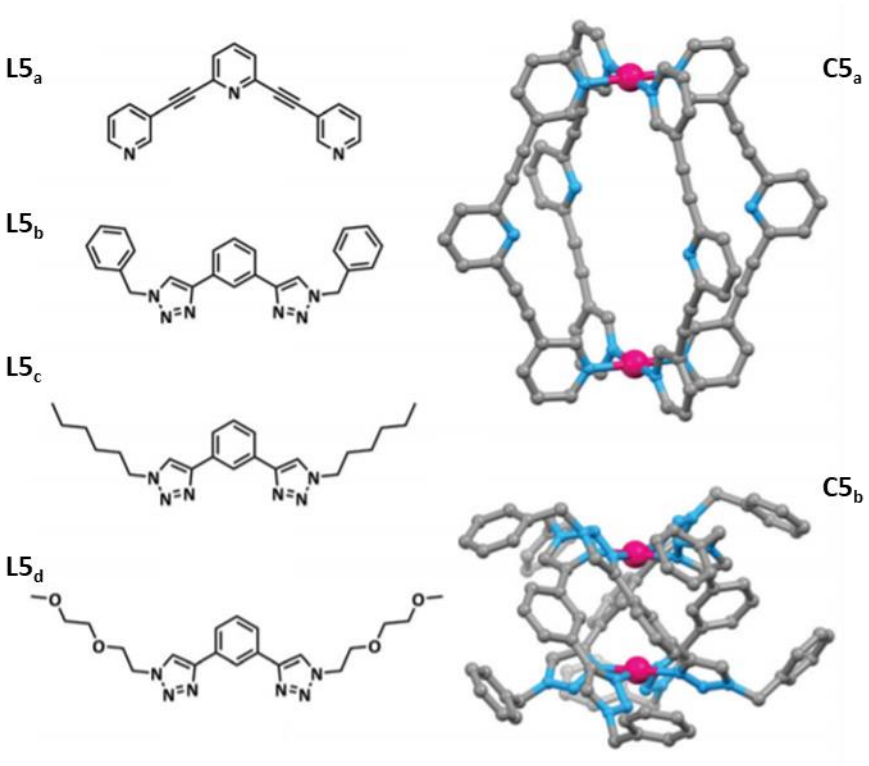

*Figure 1.3.3: (left) Chemical structures of the ligands used to form Pd_2L_4 capsules (**$L5_{a,b,c,d}$**) . (right) Molecular structures of **$C5_a$** (top) and **$C5_b$** (bottom). The order stability to nucleophilic attack is **$C5_a$**<**$C5_b$**<**$C5_c$**≈**$C5_d$**. The cytotoxicity follows the same order **$C5_a$**<**$C5_b$**<**$C5_c$** apart from **$C5_d$** which showed negligible toxicity. Figure adapted from reference 13.*

Other helicates have been shown to interact with other cell components, including a number of Fe_2L_3 helicates which are able to bind to a various DNA and RNA structures including the major groove of DNA,[14] RNA 3-way junctions,[15] and G-quadruplex DNA (**H6,** Fig. 1.3.4).[16] The specificity of these interactions imply the potential for targeting of specific cellular processes or cell cycle control.

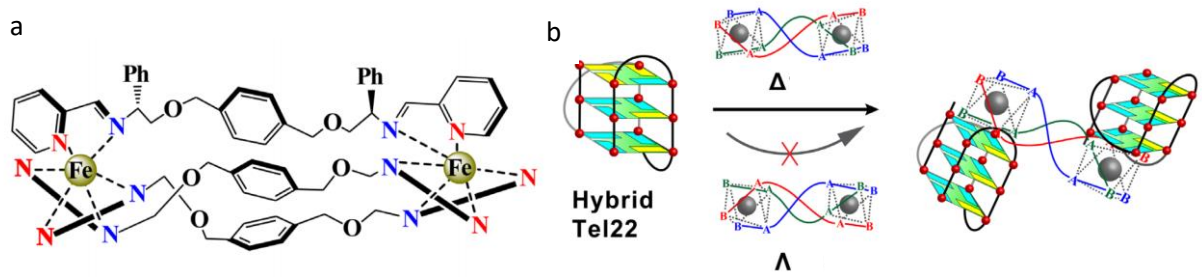

*Figure 1.3.4: (a) Depiction of the (Δ)-Fe_2L_3 cationic helicate (**H6**). (b) Schematic representation of how **H6** selectively interacts with the human telomeric hybrid G-quadruplex DNA. Figure adapted from reference 16.*

Overall, it has been demonstrated that many assemblies are "biologically active", some appearing to act as prodrugs which become active upon degradation and some being active while intact due to their overall structure. Many of these complexes are non-selectively cytotoxic but promise of specific targeting has been indicated.

1.4 Utilisation of SCCs for Drug Delivery

The access that self-assembled coordination capsules give to architectures with internal cavities make them an obvious candidate for drug delivery. The aim is to bind a pharmaceutical or diagnostic agent in order to alter its pharmacokinetics and increase activity and selectivity.

The enhanced permeability and retention effect (EPR) is one of the reasons for the interest in using macromolecules for drug delivery. The EPR effect is a consequence of poor circulation and clearance in tumours, which can lead to increased uptake and retention of macromolecules in solid tumours, providing passive selectivity.[17] While many SCCs are not large enough to be generally considered viable for the EPR effect, they do present a platform for small molecule hosts which can be conjugated in order to take advantage of the EPR effect. However, the efficacy of the EPR effect has come under question, with limited success in human trials,[18] raising further doubt about its significance in the use of metallocapsules, though their potential for use as targeted capsules remains.

There has been some exploration of the binding of medically significant compounds within metallosupramolecular capsules, with varying levels of success. A number of groups have reported the binding of other anticancer agents including Zhou and co-workers, who reported PEG functionalised copper species capable of binding 5-fluorouracil. However,

release of the drug was shown to be challenging and they do not report any biological assays.[19]

A Pd_2L_4 paddle wheel complex from Crowley and co-workers (**C5$_a$**) has been shown to bind two molecules of cisplatin (Fig. 1.4.1).[20] Functionalisation was required to render the cage sufficiently water soluble but unfortunately, and perhaps unsurprisingly, the binding was found to not occur in water.[21]

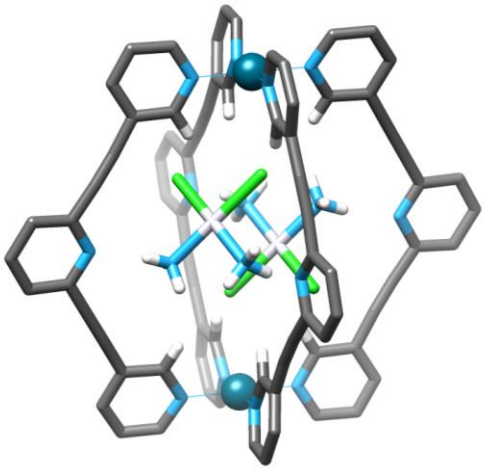

*Figure 1.4.1: Crystal structure of a **C5$_a$** with two molecules of cisplatin bound.*

Despite the reported challenges associated with binding cisplatin in water, Kuhn, Cassini and co-workers reported 20-fold increased cytotoxicity when a Pd_2L_4 was administered simultaneously with the cisplatin to cancer cells, implying some unidentified form of synergy between the two species.[22]

Therrien and co-workers have had more success in developing drug delivery systems. While their highly water soluble ruthenium capsules possess intrinsic toxicity[23] which limits their potential applications, this could be considered advantageous in the case of anti-cancer treatments. The capsule bound palladium and platinum acetylacetonates, which are more effectively bound than cisplatin due to their hydrophobic nature. This also rendered them inactive without encapsulation due to poor bioavailability. The host-guest complex exhibited far greater cytotoxicity compared to individual components, implying synergistic effects between the species.[24]

The same group probed this further when they developed an alternative cage system (**C7**, Fig. 1.4.2),[25] which was able to bind a fluorescent compound. When encapsulated, the guest's fluorescence was quenched, meaning that the liberation of the guest by cage degradation

could be visualised. Through fluorescence imaging of the cells dosed with **C7** and stained with lysosome and endocytosis markers, found that the guest appeared to be delivered into cells by endocytosis of the host-guest complex followed by degradative liberation.

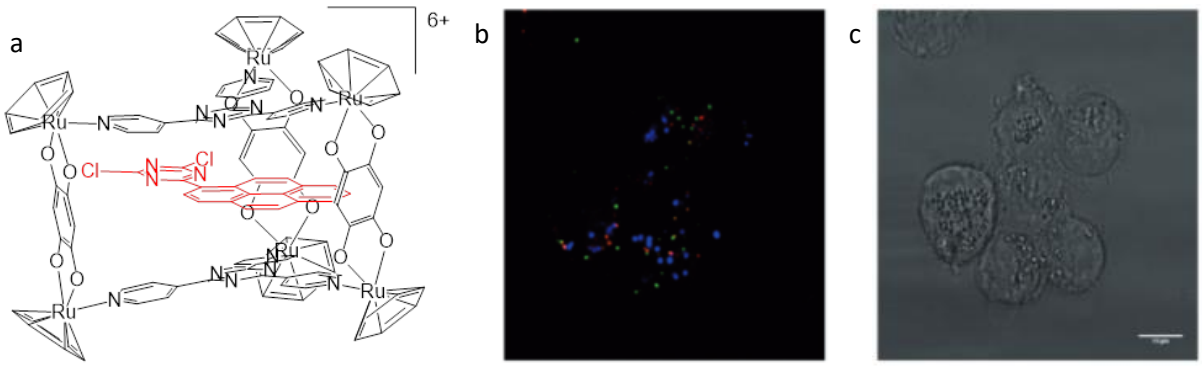

*Figure 1.4.2: (a) Chemical structure of the ruthenium trigonal prism (**C7**) with bound pyrene guest. (b and c) Confocal microscopy of A2780 cells incubated with Host-Guest complex 2mM for 24 h. Pyrene-R fluorescence (blue), FITC-dextran (fluid-phase endocytosis marker, green) and Lysotracker Red (red) were imaged. (b) Fluorescence image. (c) Transmitted-light picture (scale bar = 10mm). Figure adapted from reference 25.*

Similarly, Zheng and co-workers were able to bind a fluorescein molecule with a tethered platinum prodrug in a previously developed Fujita cage (**C8**, Fig. 1.4.3).[26] **C8** was formulated into nanoparticles through the use of an anionic block copolymer, methoxy polyethylene glycol-block-polyglutamic acid. These nanoparticles were able to release the drug through pH stimuli but were found to not exhibit greater toxicity than cisplatin.

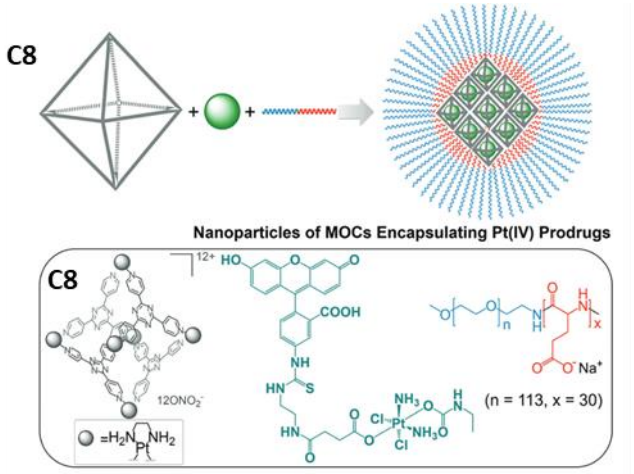

*Figure 1.4.3: Prodrug-containing Pt_6L_4 capsules (**C8**) are formulated into block copolymer-based nanoparticles. Figure adapted from reference 26.*

Isaacs and co-workers have explored two methods for cages to aid in the delivery of the anti-cancer drug doxorubicin. One capsule (**C9a**) had the drug tethered to the exterior of the cage through supramolecular interactions with cucurbit[*n*]urils and was found to increase the cytotoxicity of the drug 10-fold (Fig. 1.4.4a).[27] They then went on to develop a cage covalently functionalised with a cucurbit[*n*]uril (**C10**), through which they tethered alkyl chains which occupy the cavity of the cage to form a hydrophobic pocket within which doxorubicin could be bound (Fig. 1.4.4b). Though an interesting approach, the system behaved similarly to **$C9_b$**, though with greater selectivity toward cancer cells.[28]

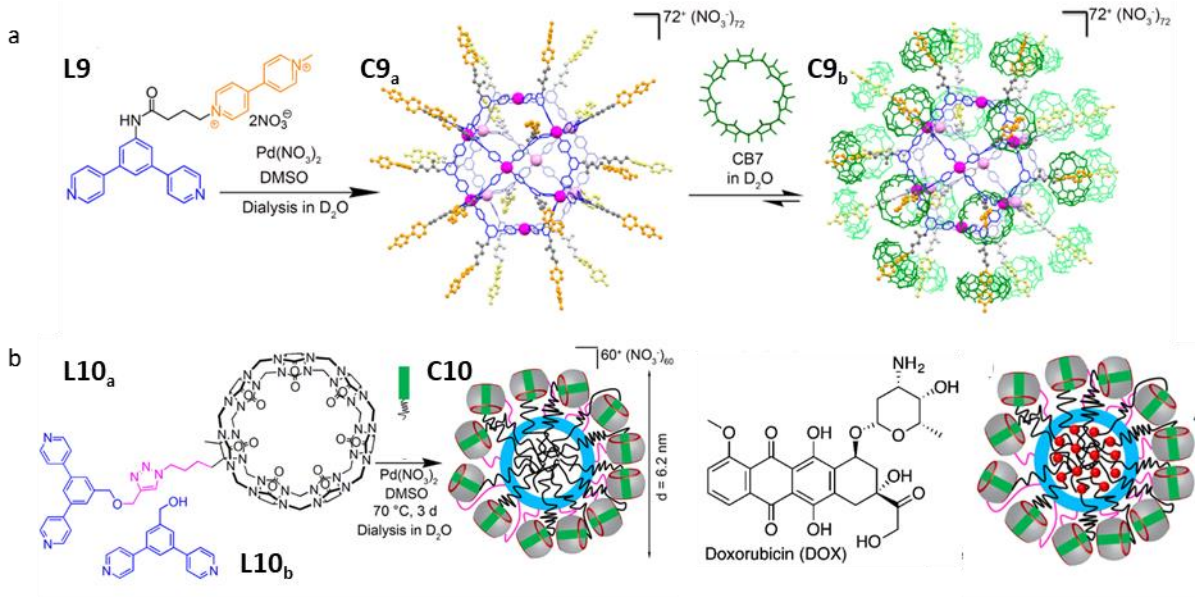

*Figure 1.4.4: (a) $Pd_{12}L_{24}$ system (**$C9_a$**) self-assembled with viologen moieties on the periphery, which are able to bind cucurbit[7]uril molecules. (b) A modified mixed ligand (**$L10_{a,b}$**) $Pd_{12}L_{24}$ system can self-assemble to **C10**, allowing the encapsulation of doxorubicin in the hydrophobic core. Figure (a) and (b) adapted from references 27 and 28, respectively.*

As previously discussed, biological systems present serious challenges for the use of SCCs and this is particularly true for *in vivo* environments. A number of metallocycles have been shown to be effective anti-tumour agents in mouse models, including ruthenium and platinum

examples.[29,30] An example of a metallocage utilised *in vivo* is a platinum square prism developed by Chen, Stang and co-workers (**C11$_a$**, Fig. 1.4.5).[31] The cage is comprised of porphyrins, platinum salts and terephthalate building blocks with the aim of combining their activity in a single system. The platinum salts and terephthalate are known anticancer agents, and the porphyrins act as both fluorophores and a photosensitiser to generate $^1O_2$ for tumour suppression. The supramolecular architecture was used to prevent π-stacking of the porphyrins and enhance their activity. In order to render them more suitable for *in vivo* application, the cage was embedded with nanoparticles comprised of two amphiphilic diblock polymers. These nanoparticles were found to have long blood circulation time and good accumulation within tumours, and to be more effective than separate treatment with cisplatin and light therapy in both exonographs and mouse models, with excellent anti-metastatic effect.[31]

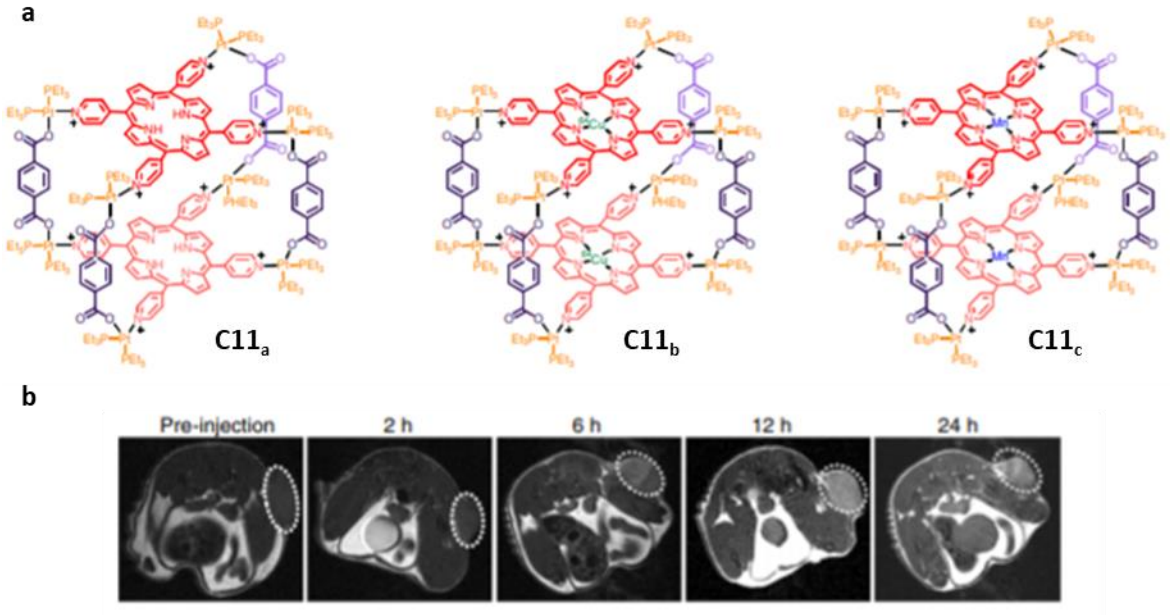

*Figure 1.4.5: (a) Depiction of cages incorporated into nanoparticles for use as anticancer (**C11$_a$**), PET (**C11$_b$**) and MRI (**C11$_c$**) agents. (b) In vivo T1-weighted axial MRI images (7T) of the mice pre-injection and post-injection of **C11$_c$**-loaded nanoparticles. (White circle denotes the tumour site). Figure adapted from reference 31.*

The porphyrins can also be utilised as binding sites for the functional metals, ^{64}Cu (**C11$_b$**) or manganese (**C11$_c$**). **C11$_b$** allows monitoring of the cage *in vivo* through PET imaging of the positron emitting ^{64}Cu or MRI detection of the paramagnetic manganese. These techniques, combined with near infrared fluorescence imaging, allowed the distribution of the cage to be detected and monitored *in vivo,* providing direct evidence for high concentrations of the nanoparticles being maintained in mouse tumours for more than 24 hours after administration.[31]

With the vast array of approaches available for synthesising metallosupramolecular cages, a cage which possesses intrinsic solubility should theoretically be accessible without the need to embed within a stabilising matrix.

1.5 Stabilisation of Supramolecular Assemblies

As aqueous and biological systems are particularly challenging for supramolecular coordination complexes, those intended for biomedical applications will often require specific design to render them suitably robust to resist degradation or rearrangement. Generally, this requires stronger interactions between the components of the assembly, which conflicts with the requirement for reversible interactions to allow for error-correction. Therefore, many approaches to "locking" the architectures after assembly have been explored.

A common approach to the problem has been to use assemblies with stronger interactions, producing species which are kinetically trapped. As the literature shows, one approach for this is to use third row transitions metals, which are considerably more coordinatively inert than the first and second row.[32,33] These inert metals require labilisation in order to undergo self-assembly. This is commonly done by heating,[34] the addition of strongly coordinating solvents,[35] or by weakening the metal ligand bonds with light (Fig. 1.5.1).[36]

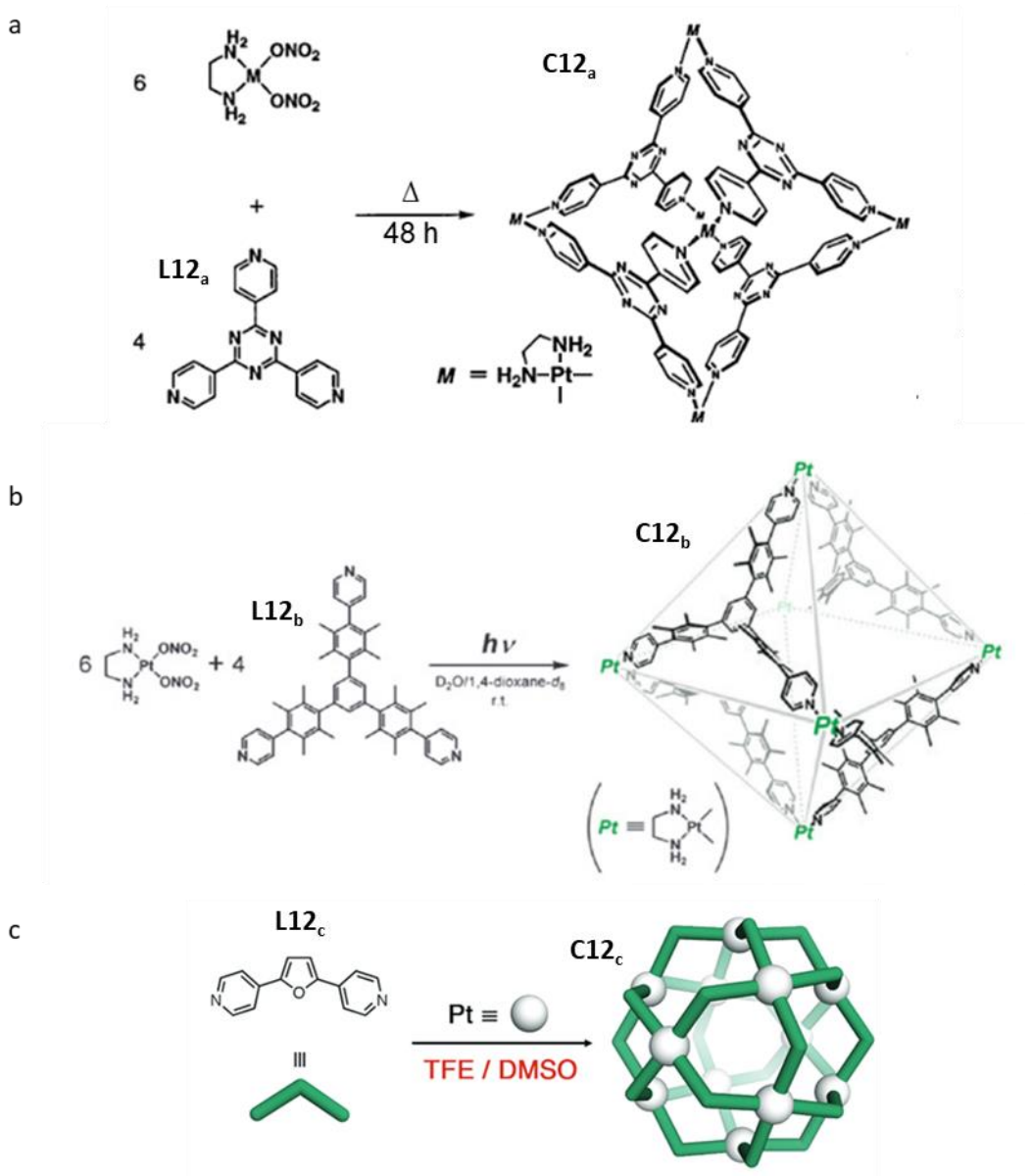

*Figure 1.5.1: Fujita and co-workers have employed different assembly conditions to promote the formation of kinetically trapped metallosupramolecular systems: (a) To form the kinetically inert M_6L_4 system containing Pt cations (**C12$_a$**), the system required extensive heating. (b) An alternative approach used light to labilise the Pd-N bonds to form **C12$_b$**. (c) Trifluoroethanol (TFE) and DMSO were used as strongly coordinating solvents to displace the **L12$_c$** ligand to help error-correct the system to form **C12$_c$**. Figures (a), (b), and (c) were adapted from references 34, 35, and 36, respectively.*

These approaches are held back by limited applicability. For instance, the use of high temperatures is not always suitable, as this will influence the equilibrium when speciation is associated with a change in entropy. For instance, two molecules of M_2L_3 helicates are

entropically more favoured than a single M_4L_6 tetrahedron, meaning the helicate is favoured at elevated temperatures (Fig. 1.5.2).[37]

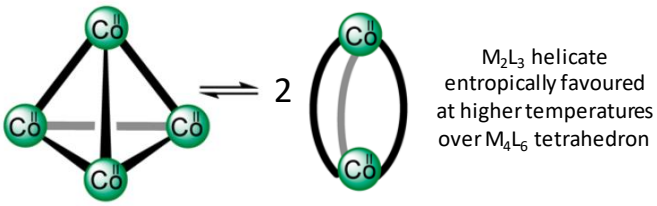

Figure 1.5.2: Using heat in the self-assembly of these species can lead to the formation of disfavoured products, for example, M_2L_3 helicates will be entropically favoured at higher temperatures over M_4L_6 tetrahedra. Figure adapted from reference 37.

This problem was encountered by Lindoy and co-workers when they attempted to produce ruthenium analogues of a previously developed iron cage. After extensive heating at 225 °C, only a 36% yield of the helicate could be isolated after silica gel chromatography of the product mixture, with no tetrahedron detected.[38]

Restriction of the coordination sphere of the metal through auxiliary capping ligands can reduce the possible arrangements of a system and increase the viability of thermal activation. Thomas and co-workers were able to use [9]aneS3 to occupy three *fac* coordination sites in a ruthenium complex, allowing only three *fac* sites for monodentate pyridine ligands to coordinate to form a M_8L_{12} cube (**C13**, Fig. 1.5.3).[39] Similarly, half sandwich complexes of inert metal have been used extensively by Therrien and co-workers to allow the sequential coordination by bridging dihydroxyquinone and then pyridine ligands to form a series of stable prisms.[40]

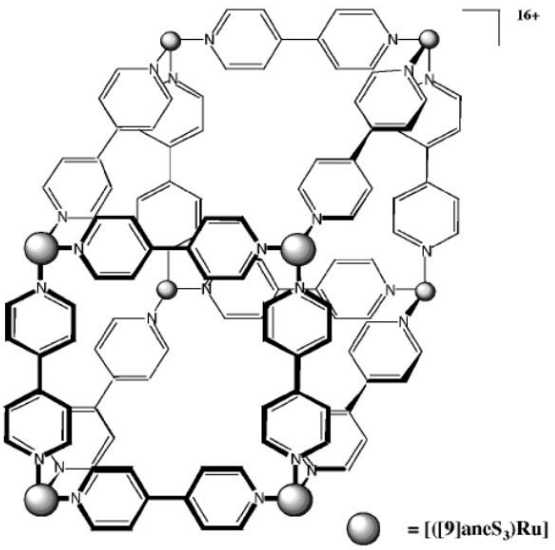

*Figure 1.5.3: Chemical structure of a Ru_8L_{12} cube **C13**. Figure adapted from reference 39.*

With more labile metal-based assemblies, post assembly modification can be utilised to "lock" the architectures once assembled. An example of this was shown by Lindoy and co-workers when they used reductive amination to covalently bridge the ligands at the vertices of an iron tetrahedron and helicate to prevent their interconversion.[38]

Rather than covalent alterations, redox changes at the metal centres of an assembly can also be exploited to alter the lability of the metal centre. An early example of this was the oxidation of cobalt (II) helicates by the addition of bromine. This oxidised the labile cobalt (II) metal centres to the inert cobalt (III), for which the higher charge, lack of Jahn-Teller distortion and low spin d^6 electron configuration rendered the helicates stable enough to purify by chromatography.[41,42]

The Lusby group have continued this route to chemical robustness with an "assembly-followed-by-fixing" procedure (Fig. 1.5.4).[43] This method also exploits the redox couple of cobalt (II/III) to allow the facile formation of cages with labile cobalt (II), before chemical locking (fixing) yields robust cobalt (III) assemblies.

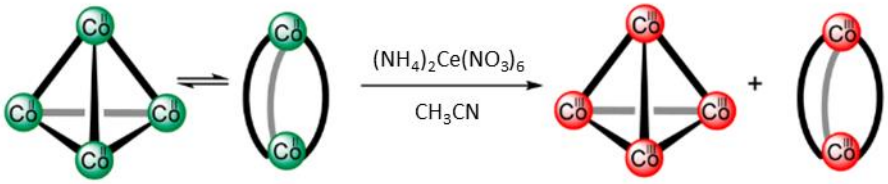

Figure 1.5.4: General procedure for "assembly-follow-by-fixing" method. The cobalt (II) species are in equilibrium between tetrahedron and helicate. Upon addition of an oxidising agent, this equilibrium is locked by the kinetically inert cobalt (III). Figure adapted from reference 43.

Initially, this approach was developed with a pyridine-triazole system (**L14**). This was utilised due to ease of ligand synthesis and functionalisation; in this case, a short PEG chain for solubility (Fig. 1.5.5). This tetrahedron (**C14**) was found to be highly water soluble but not entirely water stable.

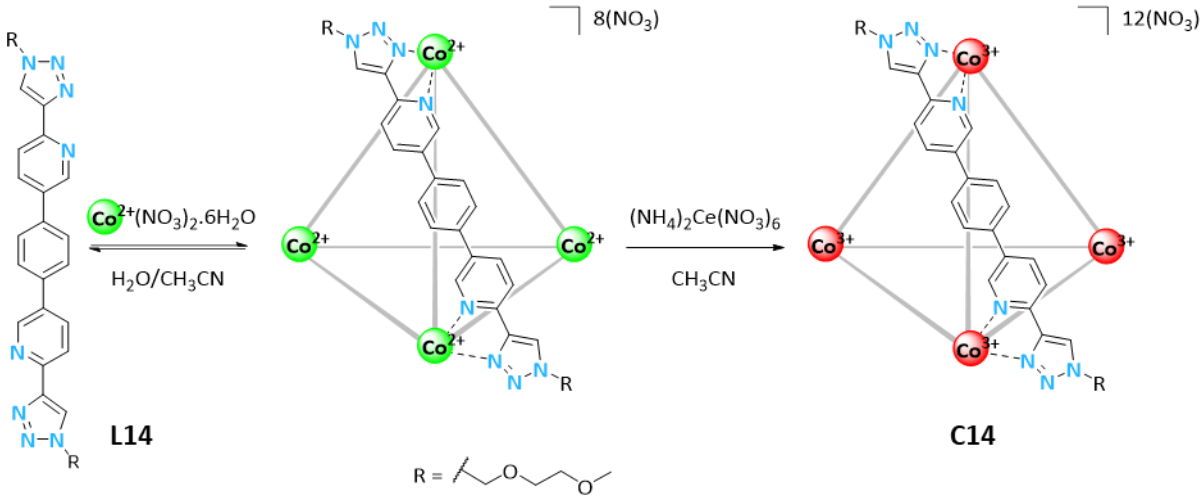

*Figure 1.5.5: Scheme showing the formation followed by fixing synthesis of water-soluble nitrate tetrahedra **C14**.*

Solutions of **C14** were found to have native pH values of 2.98 in a 2.5 mM solution. Ward and co-workers made a similar observation with a cobalt (II), Co_8L_{12} 16+ cube.[44] As acidic conditions are not biologically compatible, **C14** was tested at various pH; adjustment of the pH through use of phosphate buffer showed that the cage had limited stability above pH 5. Additionally, as shown in Figure 1.5.6, simple dilution of **C14** solutions led to an accelerated loss of NMR signals and precipitation of the ligand and attempted dissolution in cell media also led to rapid precipitation.

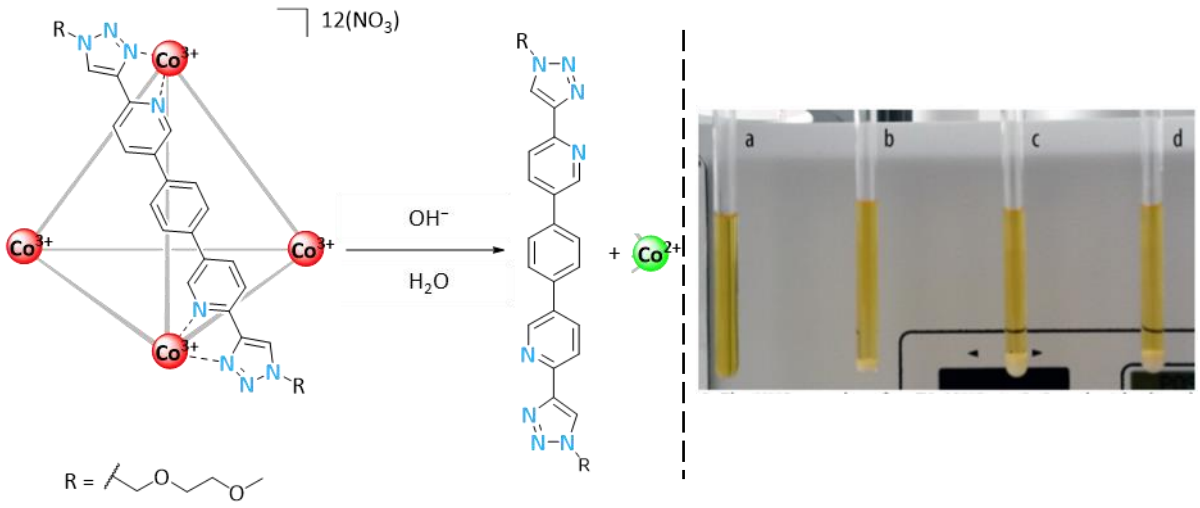

*Figure 1.5.6: (Left): The pyridine-triazole system (**C14**) is unstable to non-acidic conditions leading to rapid disassembly and precipitation of ligand from solution. (Right): (a) **C14** in D_2O. **C14** in phosphate buffer at (b) pH 6, (c) pH 7, (d) pH 8. Figure adapted from reference 43.*

This degradation was hypothesised to be due to nucleophilic attack of hydroxide ions on the cobalt metal centres.[45] It was suggested that this process is exacerbated by the cages experiencing a higher local pH than the bulk solution. This is ascribed to the macro-cationic cage binding hydroxide ions and decreasing the relative concentration in comparison to protons in the bulk solution, thereby leading to the decrease in pH.[44] The binding of hydroxide ions bound to the cationic cage would be expected to increase the local concentration of nucleophiles around the cage, accelerating degradation.

In order to overcome this instability, ligands with different coordination motifs, **L15** and **L16** (Fig. 1.5.7), where developed and investigated. The tetrahedra derived from these ligands were found to be far more stable at higher pH values, retaining their structure for multiple days in pH 7 phosphate buffer solutions.[37]

L15 **L16**

*Figure 1.5.7: Ligand **L15** and **L16** which formed more stable Co (III) assemblies than **L14**.*

1.6 Summary

Overall, supramolecular coordination complexes have been investigated for a variety of biomedical applications. The majority of systems have applications as anti-cancer agents,

potentially due to the toxicity of the third-row transition metals. However, it is worth noting that some examples do exist of the supramolecular architecture of the assemblies being the cause of activity within cells.

Additionally, many of the systems have required some form of functionalisation or further formulation in order to render them suitable for aqueous biological environments. This often involved the requirement for the use of inert third row transition metals or post-assembly modification to increase stability. In the case of many of the assemblies employed *in vivo*, the assemblies were incorporated into nanoparticles. This allows the exploitation of the supramolecular properties of the assemblies while avoiding issues of solubility, stability and pharmacokinetics.

In contrast, the Lusby group have developed a family of cages that are kinetically locked post-assembly to give stable cobalt (III) tetrahedra. These cages have the advantages of high solubility and stability without the requirement for expensive and toxic third row transition metals. This may give them significantly different biological activity to the majority of capsules that have been explored *in vivo*. They hold potential as delivery agents for therapeutic or diagnostic compounds, and offer a platform for further functionalisation and conjugation. This could further increase their stability, allow bioconjugation for targeting, or incorporate spectroscopic labels for improved monitoring.

1.7 References

1 A.-L. Lee, *Nat. Chem.*, 2016, **8**, 8–9.

2 P. Mal, B. Breiner, K. Rissanen and J. R. Nitschke, *Science*, 2009, **324**, 1697–1699.

3 D. P. August, G. S. Nichol and P. J. Lusby, *Angew. Chem. Int. Ed.*, 2016, **55**, 15022–15026.

4 F. Biedermann, W. M. Nau and H.-J. Schneider, *Angew. Chem. Int. Ed.*, 2014, **53**, 11158–11171.

5 D. Zhang, T. K. Ronson, J. Mosquera, A. Martinez, L. Guy and J. R. Nitschke, *J. Am. Chem. Soc.*, 2017, **139**, 6574–6577.

6 A. J. Metherell, W. Cullen, N. H. Williams and M. D. Ward, *Chem. Eur. J.*, 2018, **24**, 1554–1560.

7 D. Preston, A. Fox-Charles, W. K. C. Lo and J. D. Crowley, *Chem. Commun.*, 2015, **51**, 9042–9045.

8 E. G. Percástegui, J. Mosquera, T. K. Ronson, A. J. Plajer, M. Kieffer and J. R. Nitschke, *Chem. Sci.*, 2019, **10**, 2006–2018.

9 L. E. H. Paul, B. Therrien and J. Furrer, *Inorg. Chem.*, 2012, **51**, 1057–1067.

10 D. Preston, S. M. McNeill, J. E. M. Lewis, G. I. Giles and J. D. Crowley, *Dalton Trans.*, 2016, **45**, 8050–8060.

11 A. Mishra, S. Chang Lee, N. Kaushik, T. R. Cook, E. H. Choi, N. Kumar Kaushik, P. J. Stang and K.-W. Chi, *Chem. Eur. J.*, 2014, **20**, 14410–14420.

12 A. Ahmedova, R. Mihaylova, D. Momekova, P. Shestakova, S. Stoykova, J. Zaharieva, M. Yamashina, G. Momekov, M. Akita and M. Yoshizawa, *Dalton Trans.*, 2016, **45**, 13214–13221.

13 S. M. McNeill, D. Preston, J. E. M. Lewis, A. Robert, K. Knerr-Rupp, D. O. Graham, J. R. Wright, G. I. Giles and J. D. Crowley, *Dalton Trans.*, 2015, **44**, 11129–11136.

14 E. Moldrheim, M. J. Hannon, I. Meistermann, A. Rodger and E. Sletten, *JBIC J. Biol. Inorg. Chem.*, 2002, **7**, 770–780.

15 S. Phongtongpasuk, S. Paulus, J. Schnabl, R. K. O. Sigel, B. Spingler, M. J. Hannon and E. Freisinger, *Angew. Chem. Int. Ed.*, 2013, **52**, 11513–11516.

16 A. Zhao, S. E. Howson, C. Zhao, J. Ren, P. Scott, C. Wang and X. Qu, *Nucleic Acids Res.*, 2017, **45**, 5026–5035.

17 H. Maeda, J. Wu, T. Sawa, Y. Matsumura and K. Hori, *J. Control. Release*, 2000, **65**, 271–284.

18 F. Danhier, *J. Control. Release*, 2016, **244**, 108–121.

19 D. Zhao, S. Tan, D. Yuan, W. Lu, Y. H. Rezenom, H. Jiang, L.-Q. Wang and H.-C. Zhou, *Adv. Mater.*, 2011, **23**, 90–93.

20 J. E. M. Lewis, E. L. Gavey, S. A. Cameron and J. D. Crowley, *Chem. Sci.*, 2012, **3**, 778–784.

21 J. E. M. Lewis, A. B. S. Elliott, C. J. McAdam, K. C. Gordon and J. D. Crowley, *Chem. Sci.*, 2014, **5**, 1833–1843.

22 A. Schmidt, V. Molano, M. Hollering, A. Pöthig, A. Casini and F. E. Kühn, *Chem. Eur. J.*, 2016, **22**, 2253–2256.

23 B. Therrien, *CrystEngComm*, 2015, **17**, 484–491.

24 M. A. Furrer, F. Schmitt, M. Wiederkehr, L. Juillerat-Jeanneret and B. Therrien, *Dalton Trans.*, 2012, **41**, 7201.

25 N. P. E. Barry, O. Zava, P. J. Dyson and B. Therrien, *Chem. Eur. J.*, 2011, **17**, 9669–9677.

26 Z. Yue, H. Wang, D. J. Bowers, M. Gao, M. Stilgenbauer, F. Nielsen, J. T. Shelley and Y.-R. Zheng, *Dalton Trans.*, 2018, **47**, 670–674.

27 S. K. Samanta, D. Moncelet, V. Briken and L. Isaacs, *J. Am. Chem. Soc.*, 2016, **138**, 14488–14496.

28 S. K. Samanta, J. Quigley, B. Vinciguerra, V. Briken and L. Isaacs, *J. Am. Chem. Soc.*, 2017, **139**, 9066–9074.

29 A. Dubey, Y. J. Jeong, J. H. Jo, S. Woo, D. H. Kim, H. Kim, S. C. Kang, P. J. Stang and K.-W. Chi, *Organometallics*, 2015, **34**, 4507–4514.

30 I. V. Grishagin, J. B. Pollock, S. Kushal, T. R. Cook, P. J. Stang and B. Z. Olenyuk, *Proc. Natl. Acad. Sci.*, 2014, **111**, 18448–18453.

31 G. Yu, S. Yu, M. L. Saha, J. Zhou, T. R. Cook, B. C. Yung, J. Chen, Z. Mao, F. Zhang, Z. Zhou, Y. Liu, L. Shao, S. Wang, C. Gao, F. Huang, P. J. Stang and X. Chen, *Nat. Commun.*, 2018, **9**, 4335.

32 A. V. Davis and K. N. Raymond, *J. Am. Chem. Soc.*, 2005, **127**, 7912–7919.

33 G. I. Pascu, A. C. G. Hotze, C. Sanchez-Cano, B. M. Kariuki and M. J. Hannon, *Angew. Chem. Int. Ed.*, 2007, **46**, 4374–4378.

34 F. Ibukuro, T. Kusukawa and M. Fujita, *J. Am. Chem. Soc.*, 1998, **120**, 8561–8562.

35 D. Fujita, A. Takahashi, S. Sato and M. Fujita, *J. Am. Chem. Soc.*, 2011, **133**, 13317–13319.

36 K. Yamashita, K. Sato, M. Kawano and M. Fujita, *New J. Chem.*, 2009, **33**, 264–270.

37 M. J. Burke, G. S. Nichol and P. J. Lusby, *J. Am. Chem. Soc.*, 2016, **138**, 9308–9315.

38 C. R. K. Glasson, G. V. Meehan, M. Davies, C. A. Motti, J. K. Clegg and L. F. Lindoy, *Inorg. Chem.*, 2015, **54**, 6986–6992.

39 S. Roche, C. Haslam, S. L. Heath and J. A. Thomas, *Chem. Commun.*, 1998, 1681–1682.

40 A. Garci, J.-P. Mbakidi, V. Chaleix, V. Sol, E. Orhan and B. Therrien, *Organometallics*, 2015, **34**, 4138–4146.

41 A. F. Williams, C. Piguet and G. Bernardinelli, *Angew. Chem. Int. Ed. English*, 1991, **30**, 1490–1492.

42 C. Piguet, G. Bernardinelli, B. Bocquet, O. Schaad and A. F. Williams, *Inorg. Chem.*,

1994, **33**, 4112–4121.

43 M. J. Burke, The University of Edinburgh, 2016.

44 W. Cullen, A. J. Metherell, A. B. Wragg, C. G. P. Taylor, N. H. Williams and M. D. Ward, *J. Am. Chem. Soc.*, 2018, **140**, 2821–2828.

45 D. Nicholls, in *The Chemistry of Iron, Cobalt and Nickel*, ed. D. Nicholls, Elsevier, 1973, pp. 1053–1107.

Chapter 2: Kinetically Robust $Co^{III}_4L_6$ Tetrahedra for *In Vivo* Anion Binding and SPECT Imaging

2.1 Introduction

Metallosupramolecular capsules are of great interest for a large number of applications including catalysis,[1] storage,[2] and biomedical use (see Chapter 1). This is because self-assembly is a powerful tool to synthesise well-defined complex three-dimensional structures; however, many implementations of self-assembled species are limited by their instability. Therefore, a means to use the power of self-assembly to produce capsules possessing high kinetic stability would be very desirable.

Metallosupramolecular capsules are designed using rigid ligands and metals with well-defined coordination spheres with the aim of making the desired architecture the thermodynamic product. This is designed to be species with all coordination sites occupied, minimised strain and maximised favourable interactions. Selective synthesis of a desired architecture utilises reversible bonds that allow effective exploration of the energy landscape to find the desired thermodynamic product. However, sometimes the system design, and thereby the global energy difference, can be insufficient to drive the quantitative synthesis of a single species. Entropy will favour the smallest assembly, meaning that small amounts of flexibility in the ligand can lead to smaller assemblies being favoured over large species. Byproducts can also become kinetically trapped if the energy barriers to rearrange are too high, locking some of the material into local energy minima.

Such an example of mixed speciation challenges was encountered when the Lusby group first developed the "assembly-followed-by fixing" method (Scheme 2.1.1). While the assemblies could be accessed in excellent yield, this did require careful control of reaction conditions. In particular, the assembly of the M_4L_6 tetrahedron encountered the common problem of competing M_2L_3 helicate formation. A number of factors were found to play important roles in the speciation of the products. Lower temperatures and high concentration favoured the tetrahedron over the entropically favoured helicate.

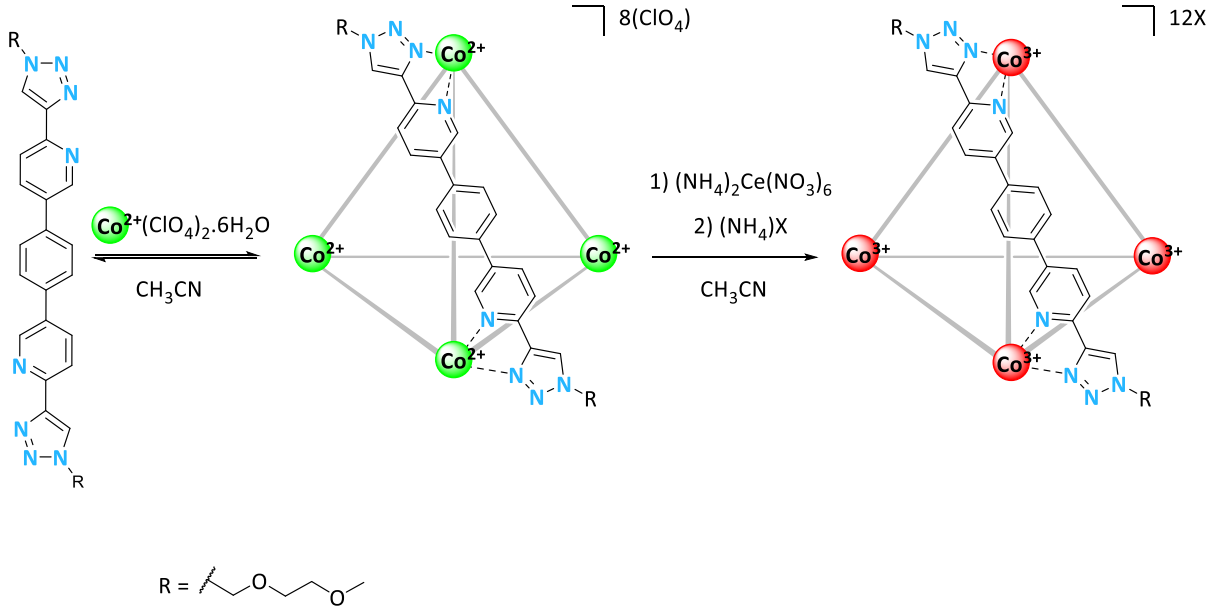

*Scheme 2.1.1: Protocol for "assembly-followed-by-fixing" cage assembly with **L14**.*

While these effects were useful for biasing the system towards the tetrahedron, further studies found that the equilibrium of the cobalt (II) species could not be induced to selectively give the tetrahedra, with small quantities of helicate remaining. The oxidation itself was found to be crucial for quantitative tetrahedron formation. Specifically, it was found that slow addition of oxidant led exclusively to the tetrahedron, while in contrast rapid addition led to a mixture of species. This is believed to be a result of the higher preference of cobalt (III) for ideal octahedral geometry. During slow addition of oxidant, the reaction mixture will contain cobalt centres in both the (II) and (III) oxidation states. This will lead to assemblies which contain metal centres of both oxidation states. It was theorised that in these species, the cobalt (III) centres will cause more strain in the distorted helicates than in the tetrahedron. This strain would induce the more labile cobalt (II) centres present to rearrange to tetrahedra before being oxidised, resulting in pure tetrahedra.[3]

These studies were initially carried out with organic soluble salts of **C14**, utilising classic hydrophobic, non-coordinating anions (ClO_4, PF_6 and BF_4) in acetonitrile. For biological applications cages must be both water soluble and stable. Cages usually use high charge and hydrophilic anions to infer water solubility,[4,5] although functionalisation of the ligand with water solubilising groups is sometimes employed.[6] Previous studies in the Lusby group using hydrophilic cobalt (II) salts, most commonly $Co(NO_3)_2.6H_2O$, found that mixtures of water and acetonitrile were required to effectively solvate both the ligand and the metal salt and allow coordination. The ratio of solvents was found to have a significant effect on speciation; mixtures of greater than 50% water were found to preferentially form tetraheda, while mixtures less than 50% showed preference for the helicate. As discussed in Chapter 1, water can be a challenging environment for metallosupramolecular assemblies, and

Co_4(**L14**)$_6$(NO_3)$_{12}$ was found to have limited stability in neutral pH aqueous solutions (see Chapter 1). Therefore, **L15** and **L16** were developed and found to give more stable cobalt (III) tetrahedra and helicates (Fig. 2.1.2).

The assemblies based on ligands **L15** and **L16** were found to be less labile in the cobalt (II) state than the previous triazole system (Fig. 2.1.1). Rearrangement between the helicate and tetrahedron upon change in concentration or temperature was found to be far slower. By extension, the slow addition of oxidant was also found to have a far less pronounced effect on the speciation of the final locked products. Nonetheless, pure tetrahedra and helicates could be obtained by careful optimisation of procedures.

*Figure 2.1.2: Ligands **L15** and **L16**.*

Electrochemical investigation of the hexafluorophosphate salts of the triazole, benzimidazole and bipyridine cages were undertaken. Interestingly, reduction potentials did not fall in line with experimental stability tests as **C14** and **C16** had more negative reduction potentials than **C15**. This implies that the reduction potential does not directly correlate to cobalt (II) kinetic stability and is affected by factors such as octahedral distortion, bite angle, and π-back bonding character.

2.1.1 Aims and Previously Developed Cages

With the Lusby group having identified a method for generating cages with what was anticipated to be the prerequisite robustness for biological investigations, studies towards identifying suitable applications were undertaken. Furthermore, the project did not just pursue cages with inherent biological properties but also aimed to utilise their host-guest chemistry. In many ways, this presents an even greater challenge than constructing robust cages. Indeed, it is a common misconception, or is not acknowledged, that almost all guests are not trapped within a host's cavity. In fact, many exhibit fast exchange on the NMR timescale, which suggests a very low energy barrier to ingress-egress. Nonetheless, the group started investigations with possible guests, which would at least show a thermodynamic binding preference that would allow preliminary biological investigations to be pursued.

Previously, the three "robust" tetrahedra previously prepared in the group using **L15**, **L16** and **L14** were found to bind a variety of organic guests. However, this binding was judged to be too weak (K_a < 10^3 M^{-1}) to carry forward for further study. The poor binding of organic molecules was postulated to

be a consequence of the high charge; while this is good for ensuring "unfunctionalised" cages are water soluble, it is very likely that their cavities do not possess the necessary hydrophobic properties to bind apolar species in water. Instead, the group's focus shifted to binding anions, anticipating that the high charge on the cage could be exploited to coulombically attract an oppositely charged species.

Anion binding is of interest for a number of biological applications and has been well explored by the supramolecular community.[7] Due to their charge, cationic metallosupramolecular cages are well suited to binding anions in non-aqueous media, or mixed aqueous/organic solvent systems. In addition to size-shape complementarity,[8] additional electrostatic interactions and ion pairing can lead to far stronger binding of charged species which are poorly solvated in less polar solvents.[9]

More challenging, and far more applicable for biological applications, is the binding of anions in water. Water is a polar, highly competitive solvent, able to both accept and donate hydrogen bonds and effectively solvate charged species. This prevents the exploitation of the hydrophobic effect, or at least minimal apolar contributions, which is often a major component of neutral guest binding within metallosupramolecular cages in water.[10]

Despite these challenges, some examples of aqueous anion binding in coordination cages are known. This includes the binding of numerous anions within an azaphosphatrane based Fe_4L_4 tetrahedra (**C17**, Fig. 2.1.2a).[11] The binding in this cage was ascribed to hydrogen bonding interactions, electrostatic interactions and high structural flexibility. In this instance, the less hydrophilic anions such as bistriflamide and perrhenate bind more strongly than hydrophilic anions such as nitrate. Indeed, the preferential binding of "hydrophobic" anions has been a common theme to emerge. Ward and co-workers have found that their Co_8L_{12} cube (**C18**) binds hydroxide, halogens and phenolates in the portals of their cages rather than the cavity (Fig. 2.1.2b), and again, the strength of binding was found to be proportional to hydrophobicity.[4]

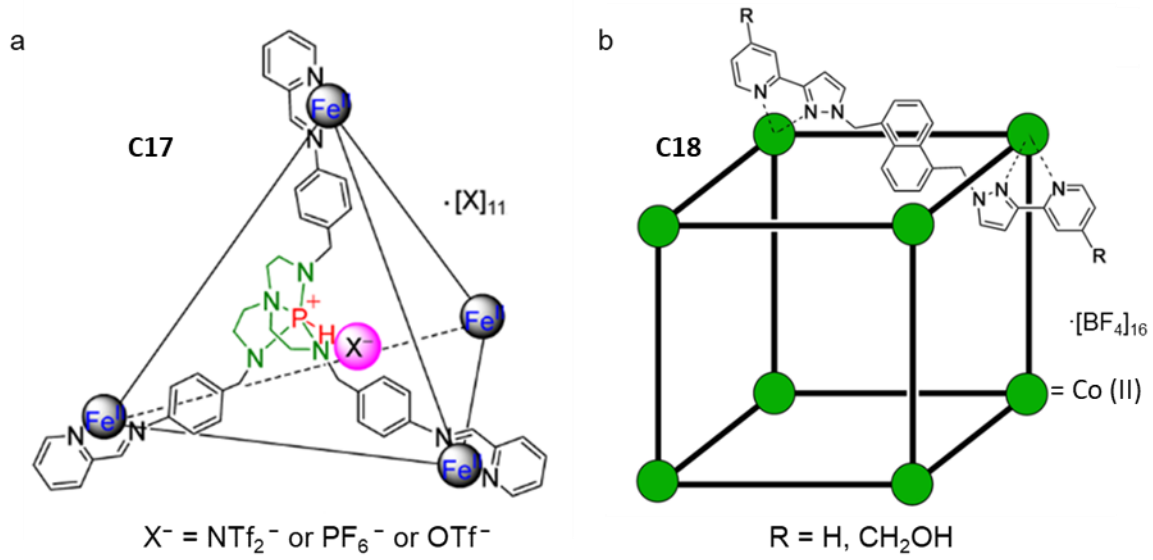

*Figure 2.1.3: (a) The azaphosphatrane-based Fe_4L_4 tetrahedra (**C17**) using hydrogen bonding and electrostatic interactions coupled with high structure flexibility to bind a variety of anions. (b) The Co_8L_{12} cube (**C18**) binds anions in the portals of the cage rather than in the cavity. Figures (a) and (b) have been adapted from references 11 and 4, respectively.*

Within the Lusby group, it was found that the smaller tetrahedron Co_4(**L19**)$_6(NO_3)_{12}$ was a suitable size for binding common anions (Fig. 2.1.3).[8] Specifically, **C19** was shown to bind a number of anions in water with association constants in the range of 10-10^5 M^{-1} (Table 2.1.1). The strength of binding is dependent upon a number of factors such as charge, hydrophobicity and shape-volume complementarity with the cavity of the cage. The cavity volume of **C19** was estimated from the crystal structures to be 134 $Å^3$ and the larger anions appeared to have larger binding constants, though SiF_6^- and SbF_6^- were found to not bind, implying that the optimal size lies between these and PF_6^-.[12]

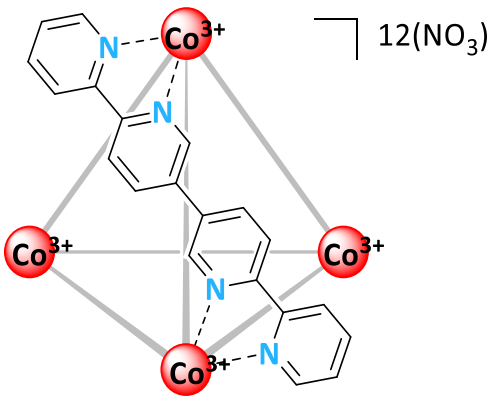

*Figure 2.1.4 Representation of "small" nitrate tetrahedra of **C19**.*

*Table 2.1.1: Volumes and binding constants of anions in **C19**. Binding constant experiment errors estimated to be ±50%. Data collected by Michael Burke.*

Anion	K_a / M^{-1}	Volume $Å^3$
SO_4^{2-}	100	60
BF_4^-	500	56
ClO_4^-	7100	61
ReO_4^-	61000	64
PF_6^-	91000	78
HPO_4^{2-}	-	75

The less hydrophilic anions bind more strongly, with the very hydrophilic sulfate anion binding less strongly than the similarly sized perchlorate. This is likely due to solvation effects, where there is a significant thermodynamic penalty for the binding of the 2− anion. The lack of strong interaction with phosphate, presumably due to similar reasons, was also considered promising from a biological application perspective due to its prevalence *in vivo*. The suggestion that this common biological anion will not interfere with the binding of other guests is a large advantage for biomedical applications. The binding of perrhenate and the fluoroanions is significant for nuclear medicine applications. Hypothetically, the fluoroanions could be substituted with ^{18}F,[13,14] which is commonly used in PET imaging. ^{188}Re is used a therapeutic agent and rhenium is commonly used as a cold analogue of ^{99m}Tc,[15] the most widely used diagnostic agent in nuclear medicine.[16]

2.1.2 Radiochemistry and Molecular Imaging

Nuclear medicine is concerned with the diagnostic and therapeutic use of radioactive elements. Imaging techniques such as positron-emission tomography (PET) and single-photon emission computerised tomography (SPECT) are often combined with radiotherapeutic treatments. The use of an internalised radio-source is very powerful in both applications but comes with associated risks in exposing the patient to radiation.

To this end, radionuclides with short half-lives are selected, so that the patient's exposure is as limited as possible. The imaging agent is also required to be selective in order to reduce the overall dose required to get a necessary quality image. Therefore, radionuclides are usually reacted with a "radioligand" which is able to coordinate the nuclide and imbue the required properties and tissue selectivity. As the half-lives of the radionuclides are so short, they often have to be generated at the point of use, meaning that procedures to formulate the imaging agent must be as straight forward as possible so that they may be carried out by non-expert operators.

^{99m}Tc is a γ-emitter with an half-life of six hours and is eluted from a ^{99}Mo generator as a saline solution of [^{99m}Tc]TcO_4^-. This oxoanion had been assumed not be suitable for ligation without further reaction. It is commonly reduced using harsh reducing agents, such as $SnCl_2$, to allow coordination by conventional chelating ligands. However, this reduction procedure represents a portion of the nuclide's half-life and must be performed by an operator, increasing their exposure to radiation. The fact that **C19** had been shown to bind the isostructural ReO_4^- and ClO^{4-} anions suggested that it could potentially act as a ligand for [^{99m}Tc]TcO_4^-. The binding of the pertechnetate anion has been identified as desirable goal,[17] and cages make attractive radioligands due to their well-defined three-dimensional structure, solubility, and the speed and ease of host-guest interactions.

In the case of pertechnetate, common radiopharmaceuticals do not target specific sites and have not even been fully structurally characterised. Instead they rely on physiochemical properties such as hydrophilicity, charge and size to alter tissue uptake through means that are not fully understood.[18,19] This means that any perturbation of pertechnetate's uptake, for instance by encapsulation within a large 12+ cation such as **C19**, would be of significant interest.

When using a cage as a supramolecular radioligand, the interaction between host and guest would ideally be as stable as possible to simplify the monitoring of uptake, distribution and elimination. This would require not only the capsule to be particularly stable *in vivo*, but also its corresponding host-guest complex. This is the significant challenge on which this project is initially focused.

2.2 Results and Discussion

2.2.1 $Co_4(L19)_6(NO_3)_{12}$ as a Radioligand for $[^{99m}Tc]TcO_4$

With a potential host for $[^{99m}Tc]TcO_4^-$, a collaboration with the Archibald group in the University of Hull was begun to explore the cage's potential as a radioimaging ligand. Due to the limitations of working with radioactive material, the cage was assessed for binding $[^{99m}Tc]TcO_4^-$ through chromatographic methods as depicted by Figure 2.2.1. When $[^{99m}Tc]TcO_4^-$ is deposited onto a silica plate, and then eluted with H_2O, it moves with the solvent front. **C19** is not eluted by water when deposited onto a silica plate and is effectively immobilised, therefore $[^{99m}Tc]TcO_4^-$ bound within the cage will remain on the baseline within the immobilised cage. $[^{99m}Tc]TcO_4^-$ can be detected by its γ-emittance and comparison of radiation at the baseline and the solvent front can be used to calculate the radiochemical yield of the $[^{99m}Tc]TcO_4^-$ as a measure of the cage's affinity for the anion.

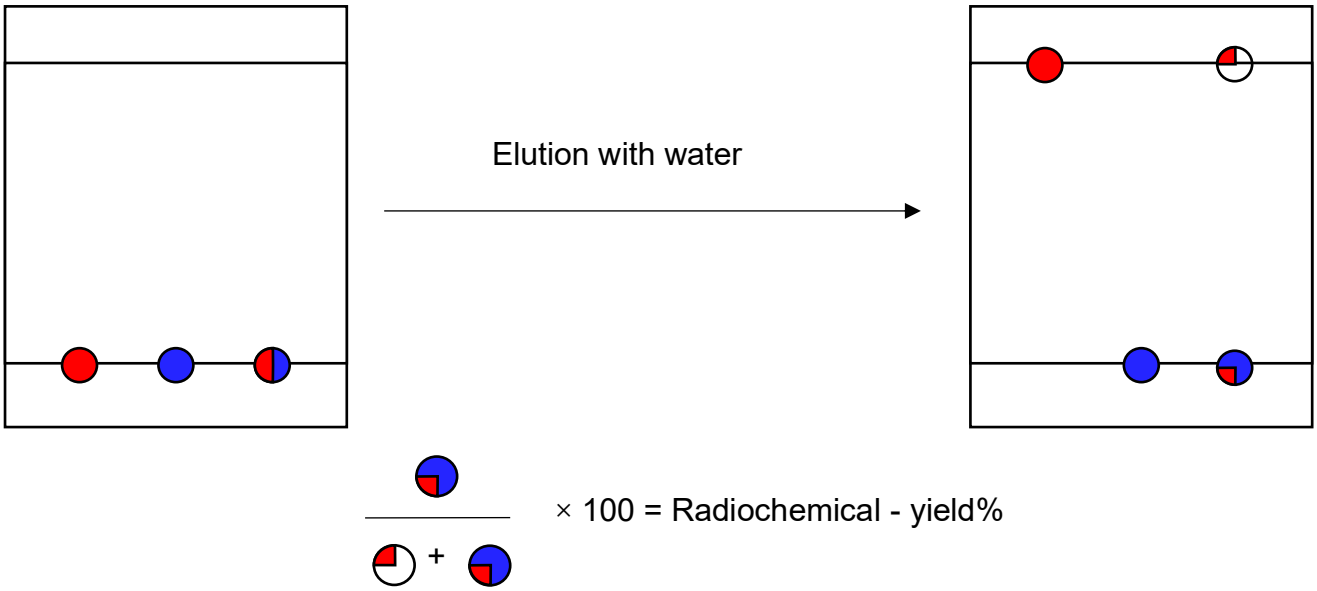

*Figure 2.2.1: Cartoon depiction of $[^{99m}Tc]TcO_4^-$ binding assay. $[^{99m}Tc]TcO_4^-$ (red), **C19** (blue), mixtures of two depicted by fractions of circles. Equation for calculation of radiochemical yield.*

Initial results of these tests showed that the cage was able to bind the $[^{99m}Tc]TcO_4^-$ anion. The concentration of cage required to bind half the activity in 1 MBq of $[^{99m}Tc]TcO_4^-$ was found to be 13.8 µM, while 126 µM was required for 95% retention (Fig. 2.2.2).

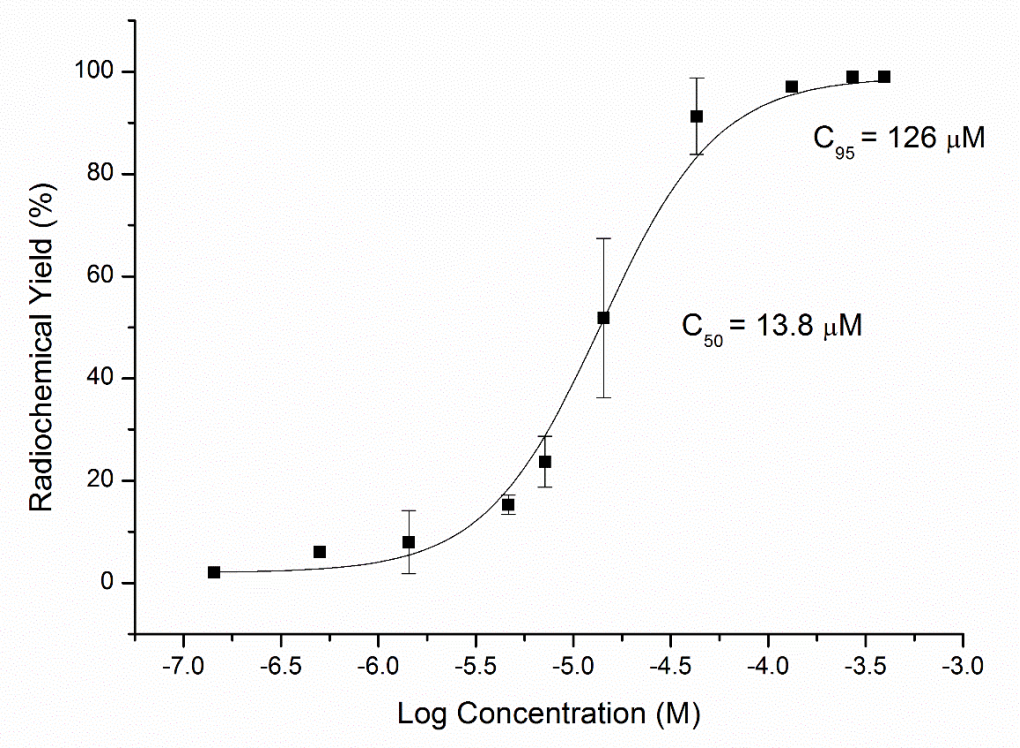

*Figure 2.2.2: Radiochemical yield for [^{99m}Tc]TcO_4^- encapsulation **C19** as a function of concentration. [^{99m}Tc]TcO_4^- (1 µL, 1 MBq) was added to cage solution (100 µL), incubated at five minutes at room temperature, before assessment by chromatography. Experiment performed in triplicate by Benjamin Burke.*

Incubating the solutions of **C19** and [^{99m}Tc]TcO_4^- for different periods of time (one minute to thirty minutes) prior to deposition on silica was found to have no effect on retention of the anion. This confirmed that the encapsulation equilibrium is reached in less than a minute and that host-guest chemistry could allow the formulation of an effective radiopharmaceutical by simply mixing solutions of the cage and radionuclide, without the need for any covalent chemistry. To verify that [^{99m}Tc]TcO_4^- binds within the cavity in the same manner as ReO_4^-, binding studies were carried out in the presence of high concentrations of ReO_4^-. The binding of [^{99m}Tc]TcO_4^- decreased in the presence of an ReO_4^- (Fig. 2.2.3), showing that the two anions bind in a competitive manner within the cavity of the cage rather than through ion pairing with the exterior of the cage.

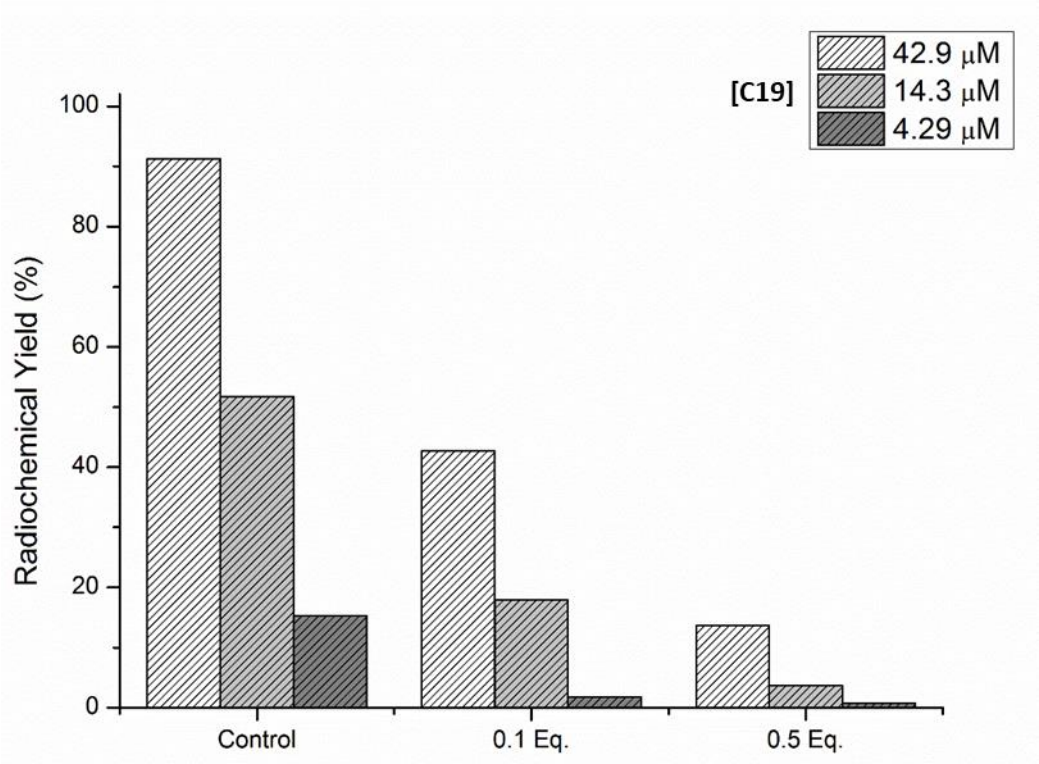

*Figure 2.2.3: Radiochemical yield of [^{99m}Tc]TcO_4^- by encapsulation within **C19** in the presence of different equivalents (Eq.) of ReO_4^- with respect to **C19**. [^{99m}Tc]TcO_4^- (1 µL, 1 MBq) was added to $KReO_4$ solution (50 µL, concentration 0/0.1/0.5 of **C19**) before addition to cage solution (100 µL, 42.9/14.3/4.29 µM), incubated at five minutes at room temperature, before assessment by chromatography. Experiment performed by Benjamin Burke.*

To further prove that the binding of [^{99m}Tc]TcO_4^- is a host-guest interaction with the cavity of the cage rather than non-specific ion pairing, binding studies were carried out with assemblies of different sizes. For a larger cavity, **C15** (Table 2.2.1), was used, while for a smaller cavity it was proposed that a helicate was used. The helicate of **L19** could not be isolated due to the increased steric strain in the smaller ligand. Instead, the helicate of **L15** was identified as a reasonable substitute, as it also has negligible cavity and shares the same metal coordination motif as **C19** (Table 2.2.1)**.** The structure obviously differs in the overall size (Table 2.2.1) and possesses a phenylene "linker" that would not be present in the smaller helicate. However, it was theorised that this was a useful control representing a highly charged assembly of similar size that lacks a cavity for binding.

Table 2.2.1: Representations of the assemblies trialled for [^{99m}Tc]TcO_4^- binding and estimates of their metal-metal distances and cavity volumes. Estimated measurements acquired using Spartan 10' models of assemblies.

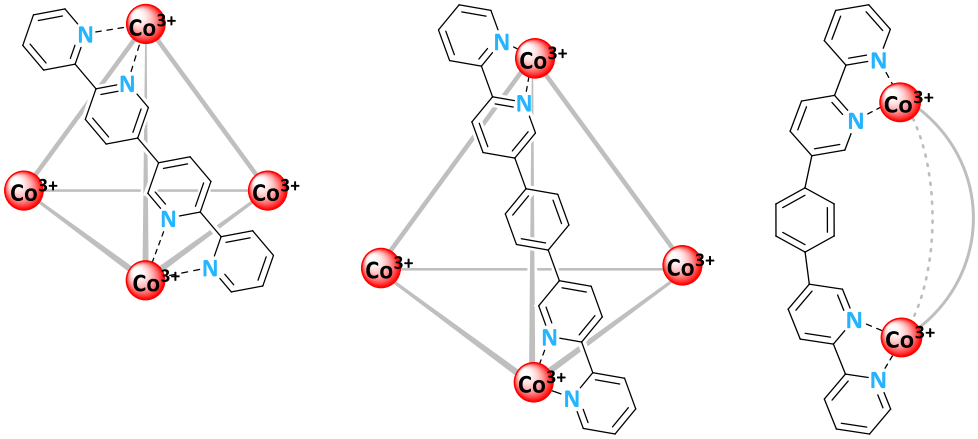

Structure	**C19**	**C15**	**H15**
Co-Co distance / Å	9.3	13.2	11.4
Cavity volume / Å^3	134	302	N/A

When these assemblies were utilised in the same binding experiments as **C19**, neither showed any retention of [^{99m}Tc]TcO_4^-, even at concentrations exceeding the C_{95} of **C19**. The fact that these differently sized assemblies show no binding of [^{99m}Tc]TcO_4^- provides strong evidence that the binding in **C19** is due to the strong size and shape complementarity with the cavity. This suggests that the interaction is likely to be more selective than ion pairing and that the bound guest will be effectively "partitioned" within the cavity of the cage.

To investigate the resilience of the binding of [^{99m}Tc]TcO_4^- within **C19** to a range of different chemical environments, the encapsulation studies were repeated in a number of different solutions. This included salts of strongly binding anions, weakly binding anions and biologically relevant solutions to gain insight into the viability of binding *in vivo* (Fig. 2.2.4).

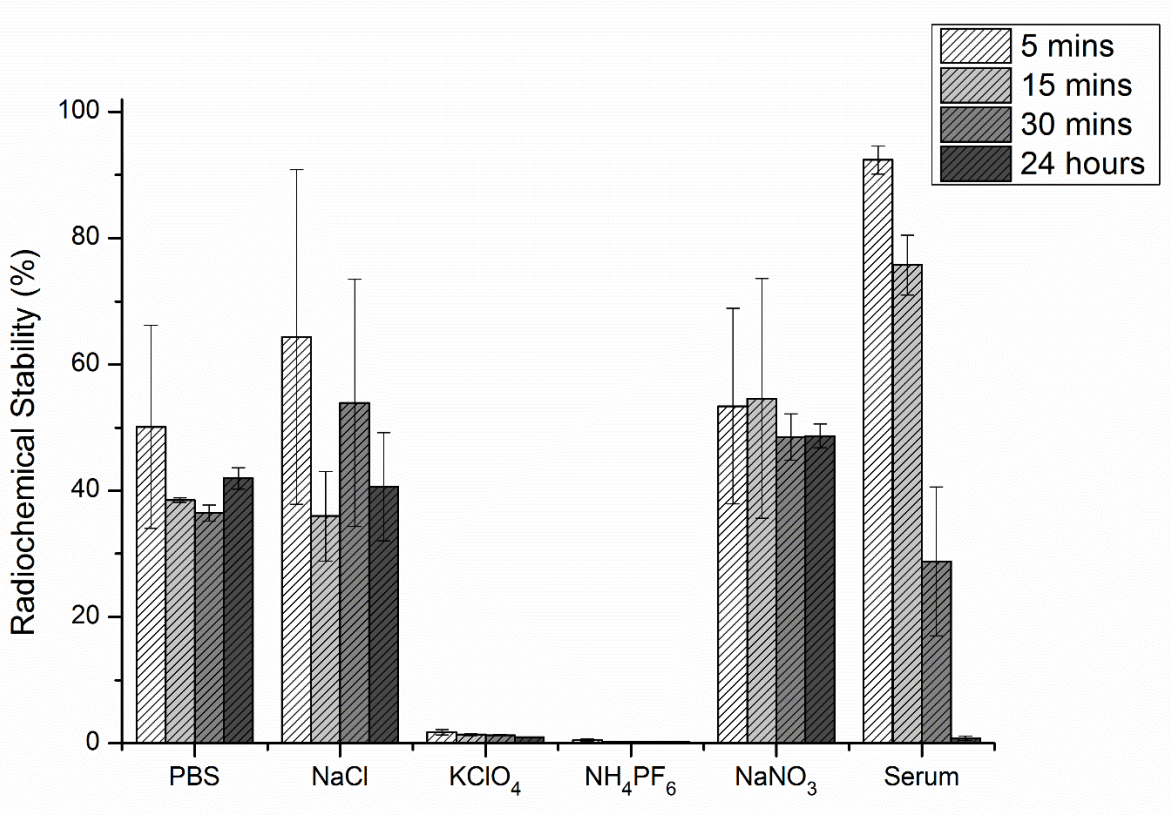

*Figure 2.2.4: Radiochemical yield of [^{99m}Tc]TcO_4^- (1 MBq) in **C19** (132 µM) in various solutions (100 µM) over time. [^{99m}Tc]TcO_4^- (1 µL, 1 MBq) and salt solution (50 µL, 0.1mM) were added to cage solution (100 µL), incubated for stated time at room temperature, before assessment by chromatography. Experiment performed in triplicate by Benjamin Burke.*

As predicted, an excess of the strong guests, perchlorate and hexafluorophosphate, was able to almost completely prevent the binding of [^{99m}Tc]TcO_4^-. Less predictably, the hydrophilic anions, chloride, nitrate and phosphate also lowered [^{99m}Tc]TcO_4^- binding. These anions would be expected to be poor guests due to their affinity for aqueous solution and poor spatial fit for the cavity of **C19** but it appears that some (weak) interaction is occurring.

C19 retained a significant amount of radiochemical yield in phosphate buffered saline; however, in pure serum the yield was observed to decline over a period of 24 hours. All other yields remained relatively constant over the same time frame, as would be expected from guest binding equilibria. This decrease in binding over time was therefore attributed to degradation of the cage, decreasing the effective quantity of cage able to bind the [^{99m}Tc]TcO_4^- over longer time frames (Scheme 2.2.1).

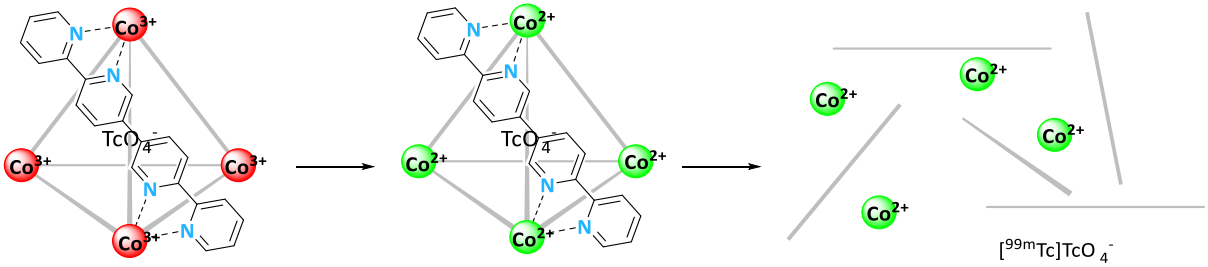

*Scheme 2.2.1: Depiction of reductive degradation of **C19** to release bound guest.*

Both phosphate buffered saline and serum are commonly used biological models, representing analogues of biological environments. Serum is a close biological model and is present in most cell media. Hence, the degradation of **C19** by serum implied that the cage would not be stable *in vivo* and was therefore not suitable as a radioligand. Therefore, the aim of the project going forward was to develop a suitable robust capsule for use a as radioligand for $[^{99m}Tc]TcO_4^-$. It was proposed that this would be best performed by gaining greater insight into the process of this degradation. This insight would then hopefully allow a countermeasure for the degradation to be proposed and implemented.

2.2.2 Biological Reductant Degradation of C19

To continue the project, the nature of this instability was explored. Serum is a direct *in vivo* analogue as it is an extract of calf blood with only the clotting agents removed. It is therefore a complex mixture of the lipids, sugars, amino acids, hormones, biological growth factors and proteins (largely albumin) found in the blood of living organisms. These species possess a variety of chemistries which could be expected to degrade cages in a number of different ways.

Serum contains a number of molecules which could act as competing ligands for the metal centres, such as chloride, histidine and cysteine which have been shown to disassemble a number of cage structures.[20] Serum also contains a number of biological redox agents, such as glutathione and ascorbic acid (Scheme 2.2.2). Often referred to as antioxidants, these compounds are present in living tissue in high concentrations, estimated to be 0.5-10 mM in mammalian cells.[21]

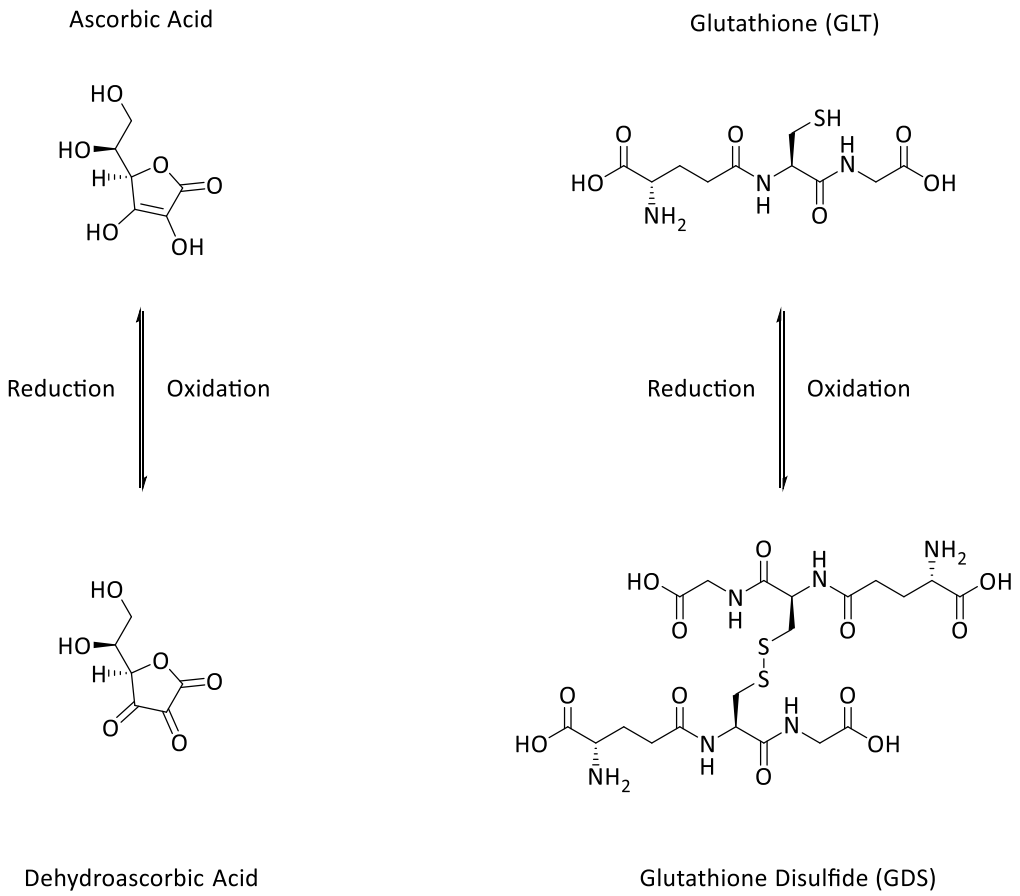

Scheme 2.2.2: Common biological redox agents.

These biomolecules could be expected to reduce the cobalt centres of the **C19** to labile cobalt (II), effectively "unlocking" the kinetically "locked" system, making it susceptible to degradation by nucleophiles and competing ligands present in solution (Scheme 2.2.3). Glutathione has been shown to trigger the disassembly of palladium capsules,[22] and both compounds have been oxidised by a ruthenium-based cage.[23]

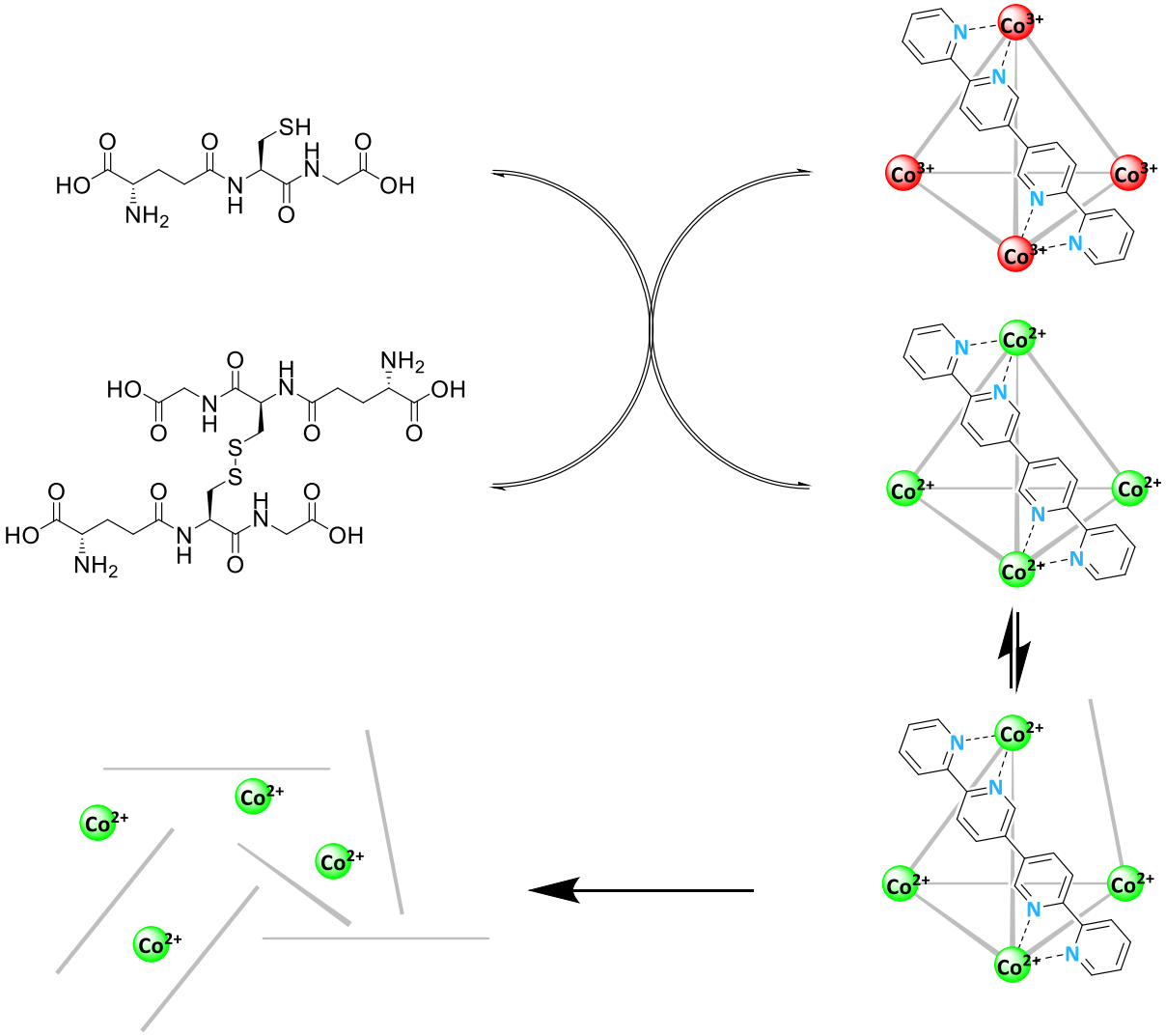

*Scheme 2.2.3: Proposed route of degradation of **C19** by reduction by biomolecules and subsequent disassembly of the cobalt (II) cage.*

To test this proposed degradation mechanism of **C19**, the cage was exposed to phosphate buffered saline and an excess of glutathione. Solutions of **C19** in phosphate buffered saline without glutathione showed no loss of cage concentration over time when monitored by ^{1}H NMR, concurring with the [^{99m}Tc][TcO_4]$^-$ binding studies. However, when ten equivalents of glutathione were added, **C19** was found to degrade within twenty minutes (Fig. 2.2.5).

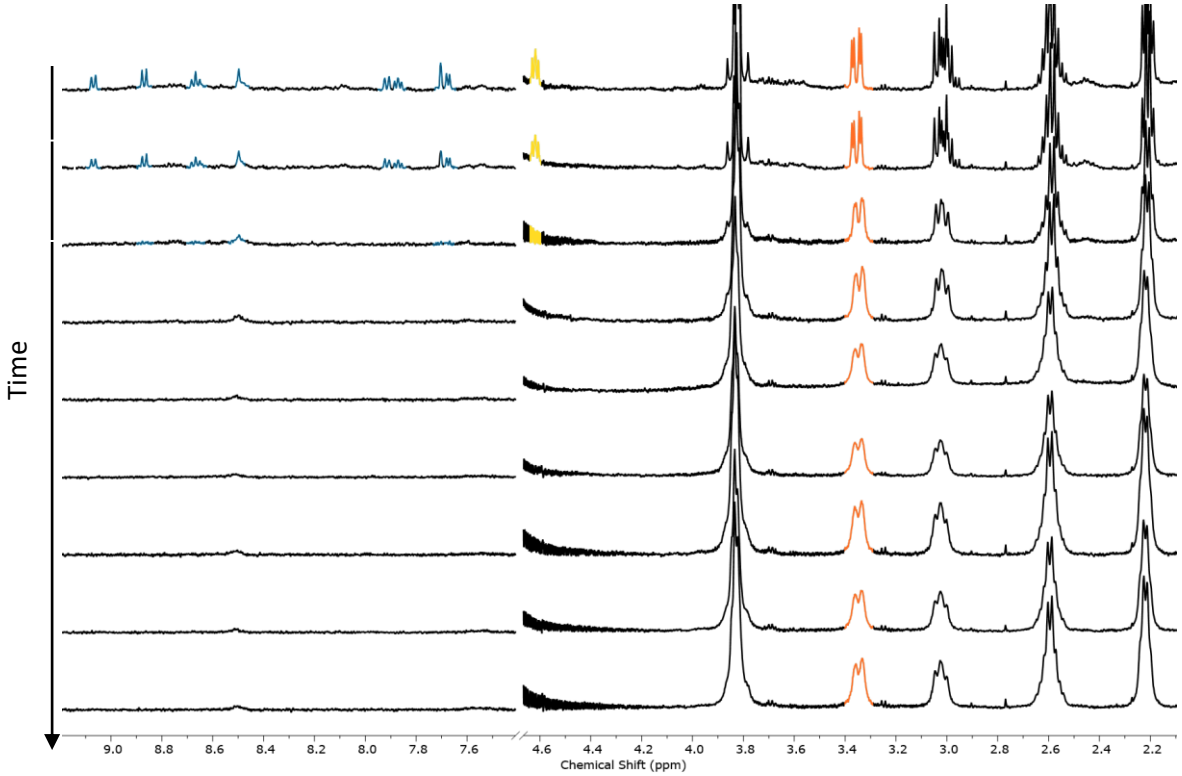

*Figure 2.2.5: Partial ^{1}H NMR (600 MHz, D_2O, 1 M PBS) of **C19** (0.1 mM) in deuterated PBS in presence of 10 equivalents glutathione over time (descending: 0 h, 0.5 h, 5 h, 10 h, 22 h, 26 h, 30 h, 52 h, 70 h). **C19** (dark blue), glutathione (yellow), glutathione disulphide (orange).*

The ^{1}H NMR signals of the cage were rapidly lost from the spectra within the first hour, implying a significant decrease in concentration of the cobalt (III) species. The cage signals were almost entirely gone after twenty-four hours (Fig. 2.2.6). A precipitate was also observed in the NMR sample, implying the disassembly of the cage and precipitation of the ligand. A number of paramagnetic signals also developed in the 10–20 ppm range, the nature of this species could not be identified but they appeared to be of low symmetry and concentration, implying multiple partially disassembled species.

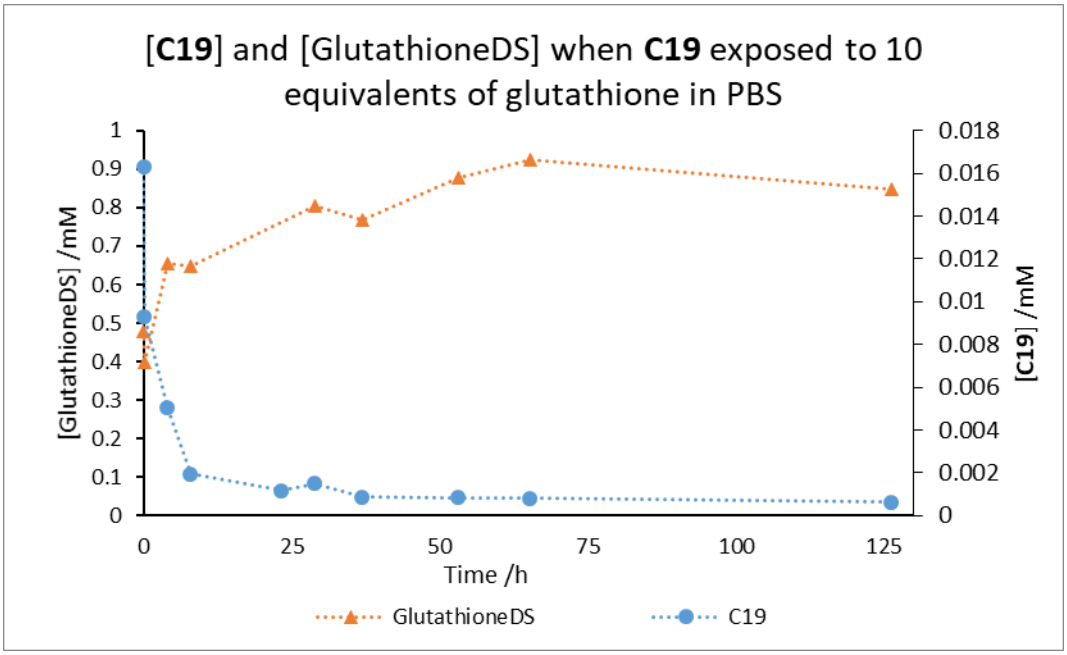

*Figure 2.2.6: Concentrations of glutathione disulphide (glutahthioneDS) and **C19** (1 mM), when **C19** exposed to 10 equivalents of glutathione in pH 7.4 phosphate buffered saline.*

Interestingly, as shown in Figure 2.2.6, the oxidation of glutathione continues after the complete consumption of cage, which may indicate that the cobalt species remaining in solution are able to continue the oxidation. Oxidation of glutathione by cobalt (III) complexes and other transitions metals has been reported and is likely the case here.[24–26]

This rapid depletion of **C19**'s ^{1}H NMR signals and the precipitation of the ligand indicate that glutathione is able to reduce the cage complex, leading to its disassembly. This confirms our hypothesis that reduction by "antioxidants" is one of the likely routes to degradation of **C19** by biological conditions.

2.2.3 Development of a Functionalised Ligand for Stabilised Cages

With the knowledge that the "locked" cage was unstable to representative biological conditions, further stabilisation of the tetrahedra was proposed. Substitution of an amine group *para* to the coordinating nitrogen of the outer pyridine groups was proposed to increase the σ-donor strength of the ligand (Fig. 2.2.7). The increased donor strength was expected to stabilise the cobalt (III) oxidation state and decrease the cage's susceptibility to reduction, providing resistance to biological degradation. It was also proposed that the stronger interactions would slow the rate of ligand substitution in both (II) and (III) oxidation states.

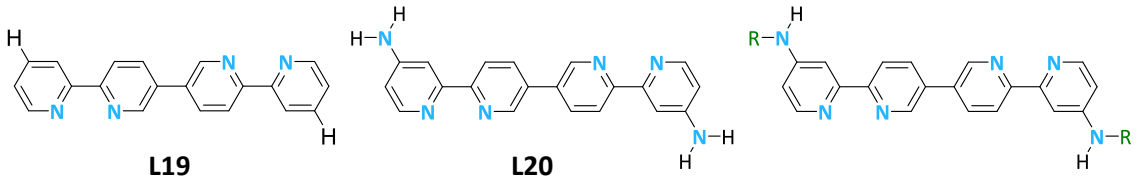

Figure 2.2.7: Left to right. ***L19****, proposed amine functionalised ligand* ***L20*** *and potential functionalised amine ligand.*

The amine also provides a potential functionalisation handle for appending groups to the cage in order to alter properties such as solubility and biological targeting.[27] A similar approach was reported by Crowley and co-workers, who added amine groups to the coordinating pyridine in Pd_2L_4 paddlewheel cages (**C21$_{b,c}$**, Fig. 2.2.8). **C21$_b$** and **C21$_c$** showed much greater kinetic stability and longer lifetimes in the presence of nucleophiles such as cysteine and chloride than **C21$_a$**.[28]

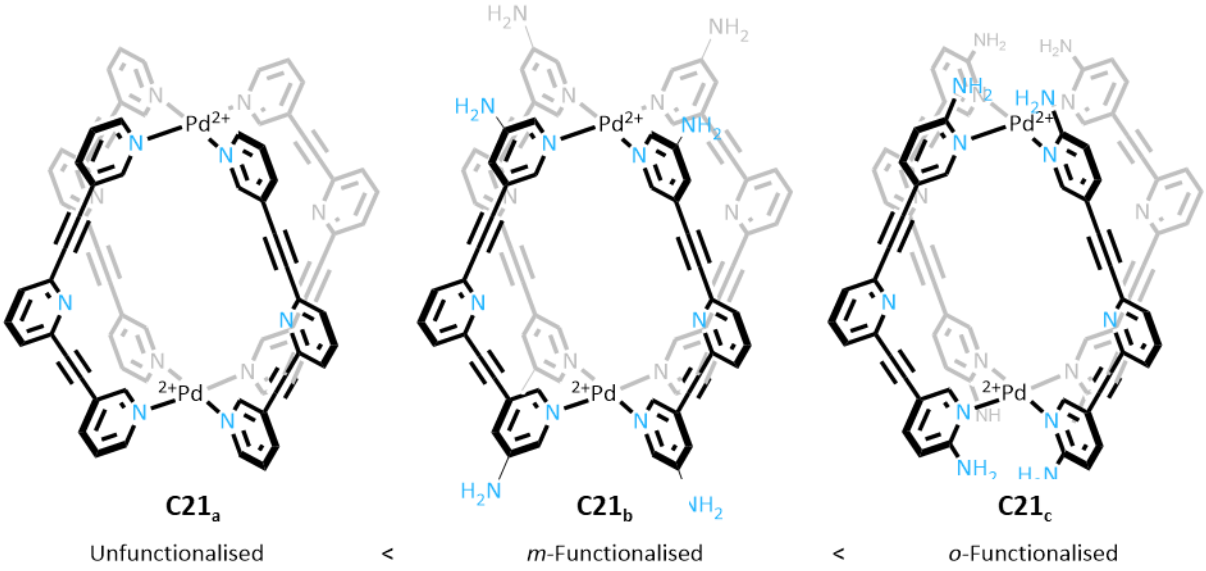

*Figure 2.2.8: Parent (****C21$_a$****) and functionalised cages (****C21$_{b,c}$****) in order of stability to nucleophiles.*

For the synthesis of this new ligand, Stille couplings were proposed as the most dependable coupling reaction to form the substituted 2,2'-bipyridine building blocks. Direct reaction of **N4** with **N1** would have been ideal (Scheme 2.2.4).[29] However, this was unsuccessful, potentially due the electron rich nature of the amine-containing substrate.

Instead, nitro groups were identified as an amine precursor that might be more compatible with the Stille coupling conditions (Scheme 2.2.4). Indeed, **N3** was successfully reacted with **N2** to give the compound **N5**. The *N-oxide* protected **N3** was selected as it was readily available. Initial yields of the reaction were poor, with a number of significant side products and extensive decomposition. Changing

the solvent from dimethyl formamide to toluene significantly increased yields, though side products persisted.

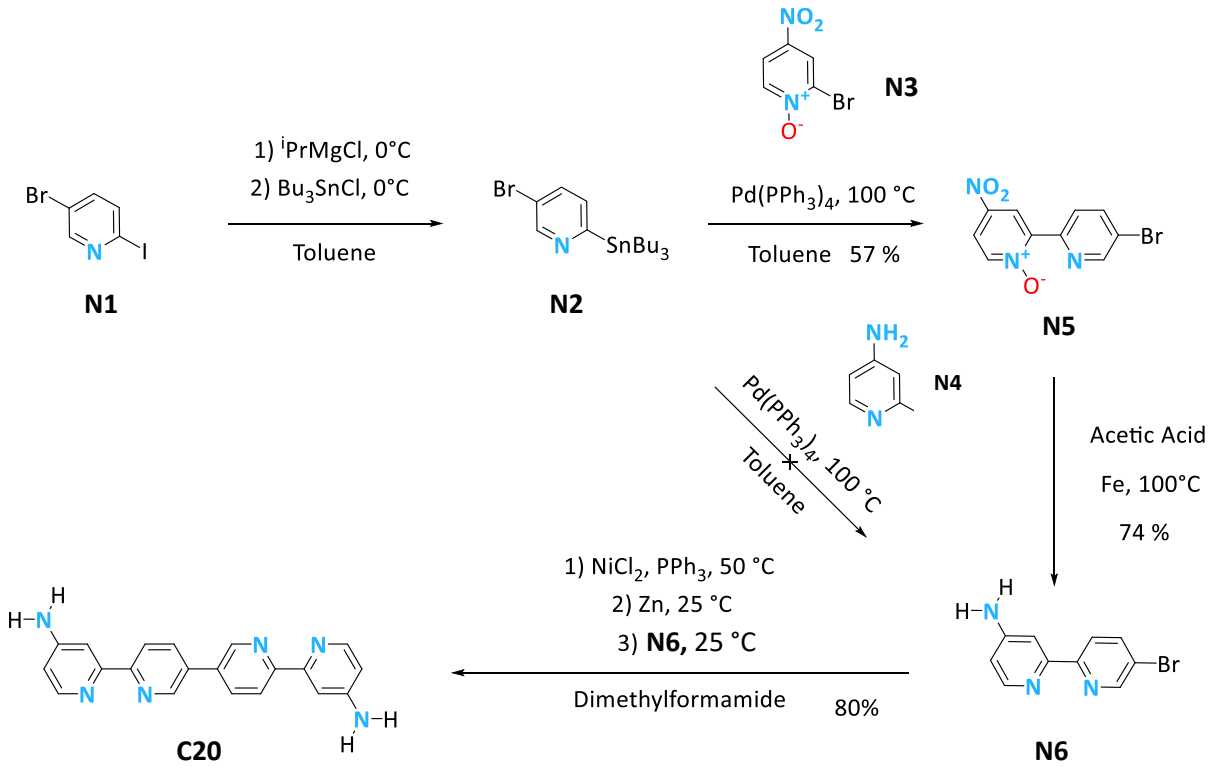

*Scheme 2.2.4: Synthesis of **L20** ligand.*

One of the side products was identified to be the reduced form of **N5**, **N7** (Scheme 2.2.5). The reduction was hypothesised to have been caused by the triphenylphosphine present in the catalyst. As **N5** is still a viable intermediate of the desired ligand, the Stille coupling was then repeated with the unprotected **2.7** (Scheme 2.2.6). This reaction successfully gave **N7** but without a significantly increased yield.

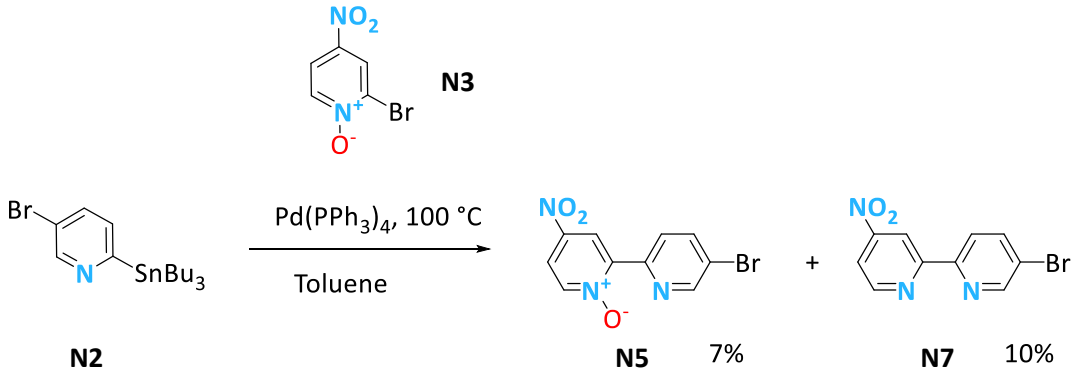

*Scheme 2.2.5: Products of the Stille coupling of **N2** and **N3**.*

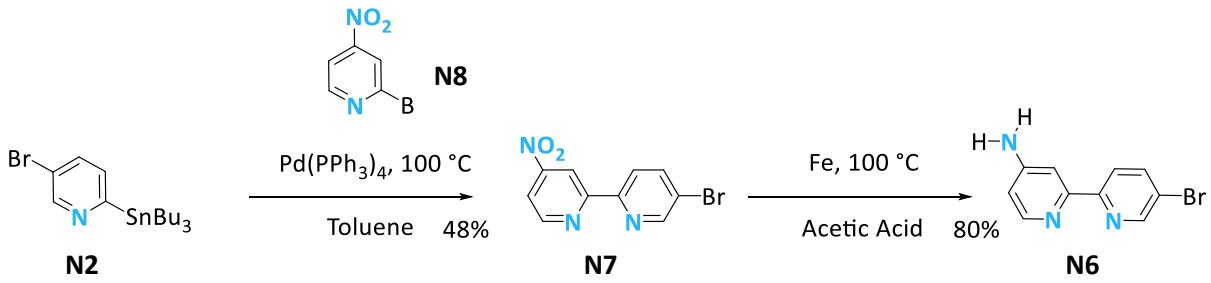

*Scheme 2.2.6: Alternative synthesis of **N6** from different starting material **N8**.*

The previously utilised Ullman-type homocoupling was found to be ineffective with **N7**, likely due to reaction of the stoichiometric metals with the redox active nitro groups. The nitro compound(s) were therefore reduced to give the amine **N6** (Scheme 2.2.6). This was found to be suitable for the homo-coupling and the product was successfully synthesised in a good yield of 80%.

L20 displayed significantly lower solubility than **L19** and the ^{1}H NMR showed a similar spectrum that was far more shielded, especially the electron rich functionalised pyridine ring (Fig. 2.2.9).

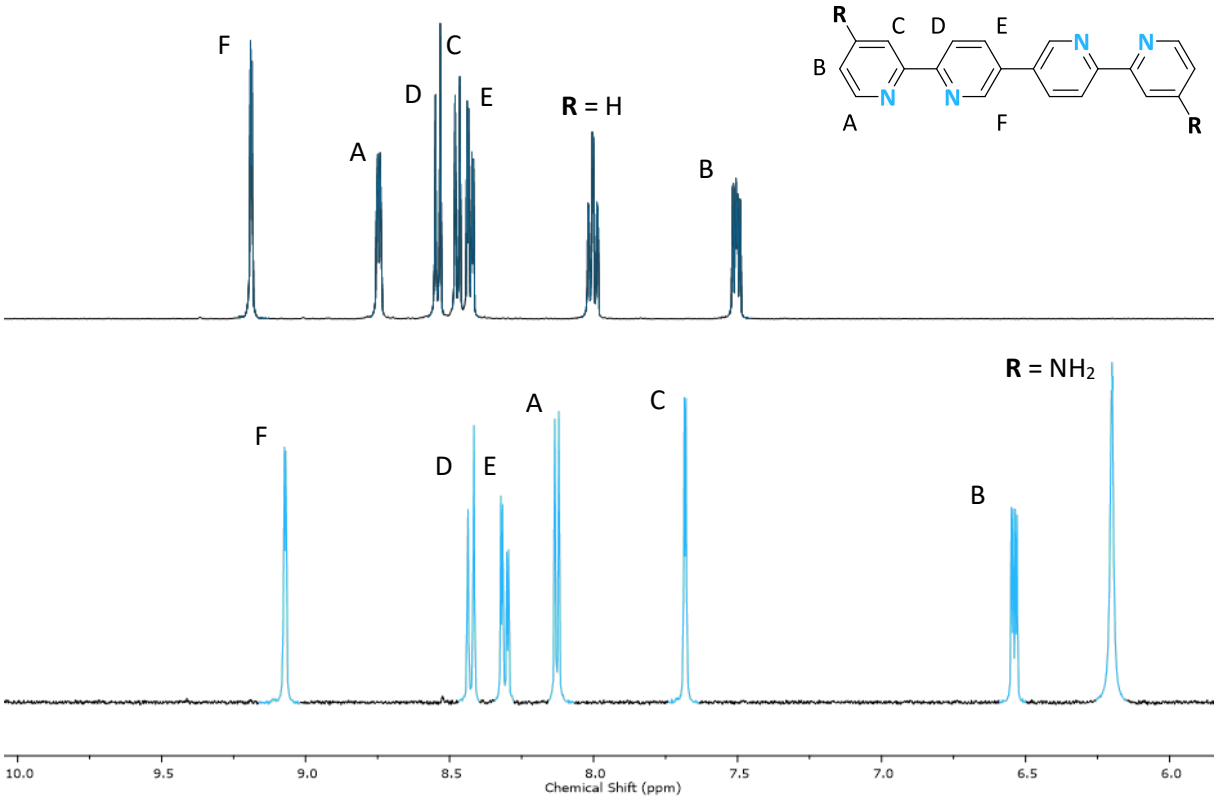

*Figure 2.2.9: Partial ^{1}H NMR (600 MHz, d_6-DMSO) of **L19** (top) and **L20** (bottom).*

2.2.4 Attempted Direct Formation of $Co_4(L20)_6(NO_3)_{12}$ Tetrahedron

Initial attempts at cage formation with **L20** using the conditions developed for the previous **L19** ligand systems (Scheme 2.2.7) were found to not produce pure **C20**. ^{1}H NMR of the crude product showed peaks consistent with the desired tetrahedron but also other peaks and a broad, raised baseline (Fig. 2.2.10). An almost exact repetition of the reaction with slight variation in conditions gave similar complex spectra but with a slightly different range of peaks.

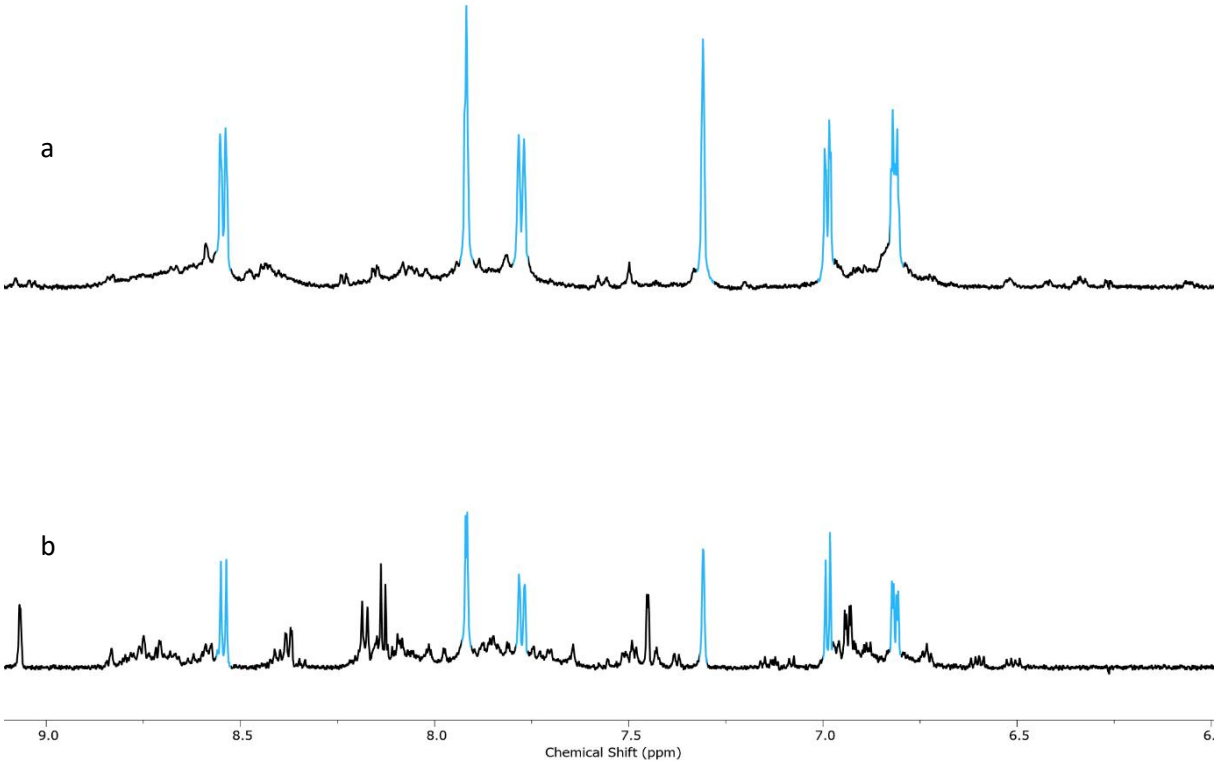

*Figure 2.2.10: Partial ^{1}H NMR (500 MHz, D_2O) of the products of cage formation with **L20** using standard cage formation conditions. **C20** peaks highlighted in light blue.*

The well-defined impurity peaks are likely to be alternate assemblies and the broad baseline to be oligomeric material. This mixture of products could be caused by the stronger coordinating properties of **L20** reducing reversibility in the cobalt (II) state. The $Co_4(\mathbf{L19})_6(NO_3)_{12}$ system has previously been shown to be more sluggish to rearrange in the cobalt (II) oxidation state than $Co_4(\mathbf{L^{TZPEG}})_6(NO_3)_{12}$, indicating higher kinetic stability. Further stabilisation of these assemblies could increase these energy barriers until the intermediate species become kinetically "trapped" (Scheme. 2.2.8).

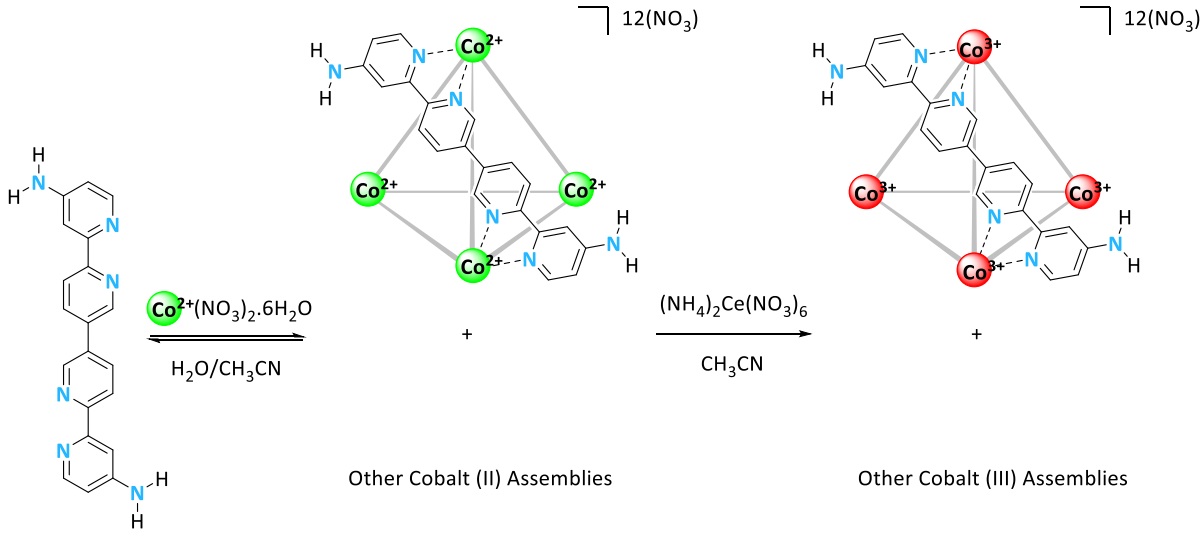

*Scheme 2.2.7: Attempted synthesis of **C20**.*

Similar issues have been reported when attempting to form species with inert third row transition metals, which required extended heating in order to access a low yield of desired product.[30] It was therefore hoped that higher temperatures would overcome the energy barriers of dissociation, allowing these intermediates to rearrange to the tetrahedron. Higher temperatures might be expected to increase the preference for the entropically favoured helicate but it was hoped that it would prevent the formation of oligomeric material. Therefore, the reaction was repeated at a variety of temperatures including 60, 70, 80 and 90 °C, but all give similar mixtures of products. Additionally, at 90 °C the material was found to be very difficult to re-dissolve, potentially due to presence of oligomeric material which degraded upon removal of solvent.

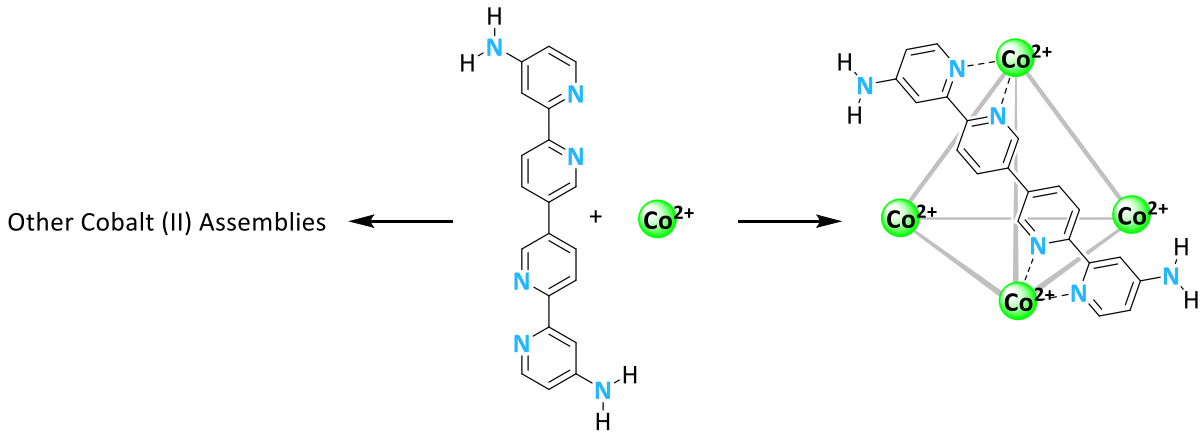

*Scheme 2.2.8: Depiction of lack of dissociation of **L20** and cobalt (II) ions, leading to impure tetrahedron.*

Investigation of the cobalt (II) speciation by paramagnetic NMR was precluded by the apparent lower solubility of system. Upon heating, the ligand would enter solution but a precipitate would form over

time. The cause for this could not be identified but it prevented the accurate study of the species in solution.

The M_2L_3 helicate **H20** (Figure 1.5.2) is the most likely discrete byproduct of the reaction; it is the smallest assembly which fully satisfies all coordination sites and would represent an energy minimum. Indeed, a recurring impurity in the product mixture, which exhibited the same symmetry as the cage, and was found to have a smaller hydrodynamic radius (Fig. 2.2.11, 7.99 Å), was theorised to be the helicate.

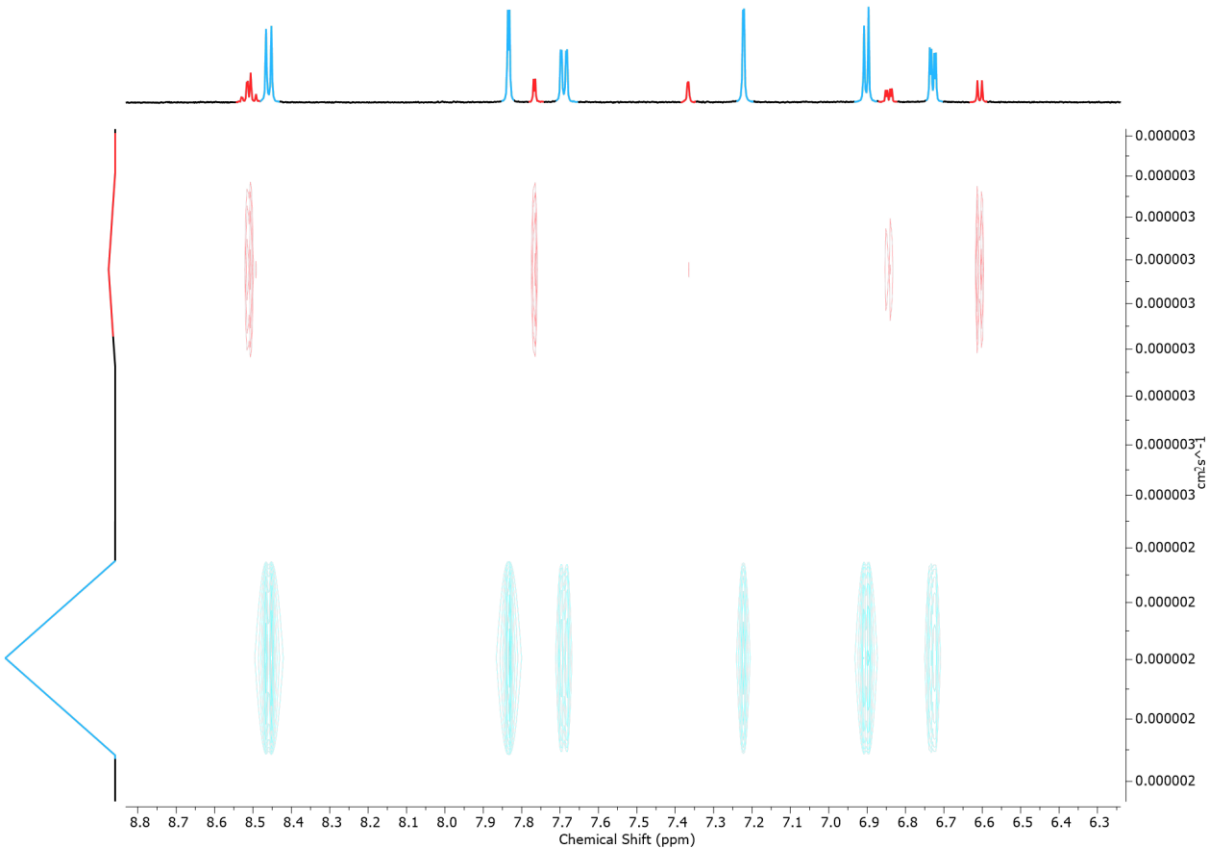

*Figure 2.2.11: Partial DOSY NMR (500 MHz, D_2O) of **C20** (blue) and **H20** (red).*

After finding it challenging to directly synthesise pure **C20**, separation of the product from the impure mixtures was attempted. Crystallisation and selective precipitations were attempted with a variety of solvents and solvent mixtures. The assemblies were found to have high solubility in water/acetonitrile mixtures but could be precipitated with addition of acetone or methanol. The slow diffusion of acetone into water/acetonitrile mixtures caused mixtures of orange block, needle and hexagonal crystals to form, in addition to precipitated powder. Unfortunately, these proved too small to effectively collect by filtration and re-dissolution did not provide any significant increase in purity.

Alternatively, Lindoy and co-workers were able to separate iron tetrahedron from helicate using chromatography on silica gel.[31] However, attempts at chromatography on both standard and reverse

phase silica proved ineffective - the nitrate assemblies could not be eluted with water, sodium nitrate solutions, acetonitrile, DMF or mixtures of the previous.

Size exclusion chromatography was also trialled as a means of purification of the cage. It was predicted that **C20**, **H20** and oligomeric species would be considerably different sizes, allowing separation by this method. While the technique initially did yield a small quantity of pure material, it remained problematic. In particular, the separation of the tetrahedron from other discrete species proved unreliable, with the helicate frequently co-eluting with the tetrahedron (Fig. 2.2.12). This separation was found to vary from batch to batch of cage, giving poor and unreliable yields.

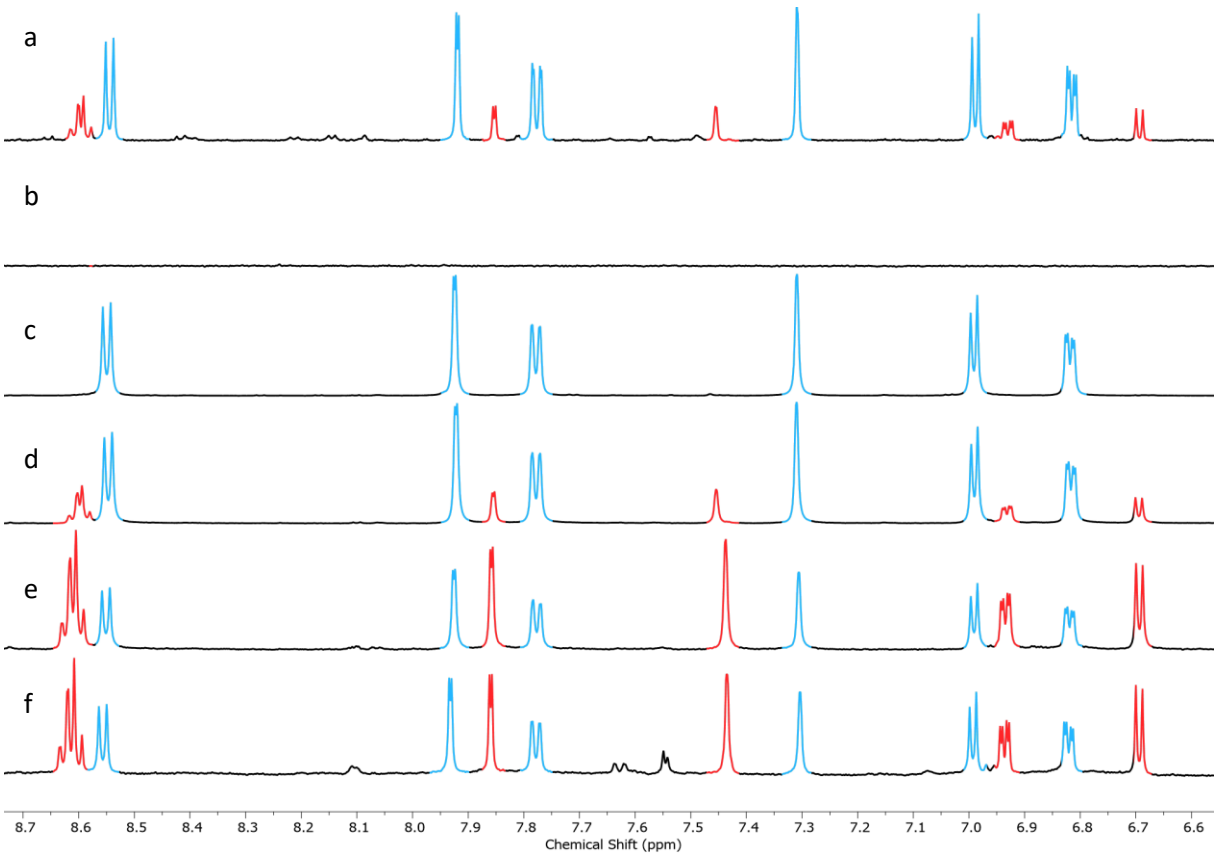

Figure 2.1.12: Partial ^{1}H NMR (500 MHz, D_2O) of size exclusion fractions of cage formation reaction. From top: (a) Crude product, (b) Fraction 1-3, (b) Fraction 4-5, (d) Fraction 6-7, (e) Fraction 8, (f) Fraction 9-12. ***C20*** *highlighted in blue,* ***H20*** *highlighted in red.*

2.2.5 Investigation of Alternative Conditions for $Co_4(L20)_6(NO_3)_{12}$ Formation

With previously utilised cage formation conditions only partly successful in the selective formation of the **C20**, it was proposed that a wider range of conditions be trialled. It was suggested that changes in the solvation of the components and/or intermediates may affect the equilibrium.

Unfortunately, as Figure 2.2.13 shows, none of the solvent systems offered clear improvement, with significant impurities present in all reactions. The reaction using acetone as a co-solvent displayed

particularly good solubility and thus was revisited as mixed co-solvent with acetonitrile. While this offered an improvement on the pure acetone reaction, the product still left much to be desired.

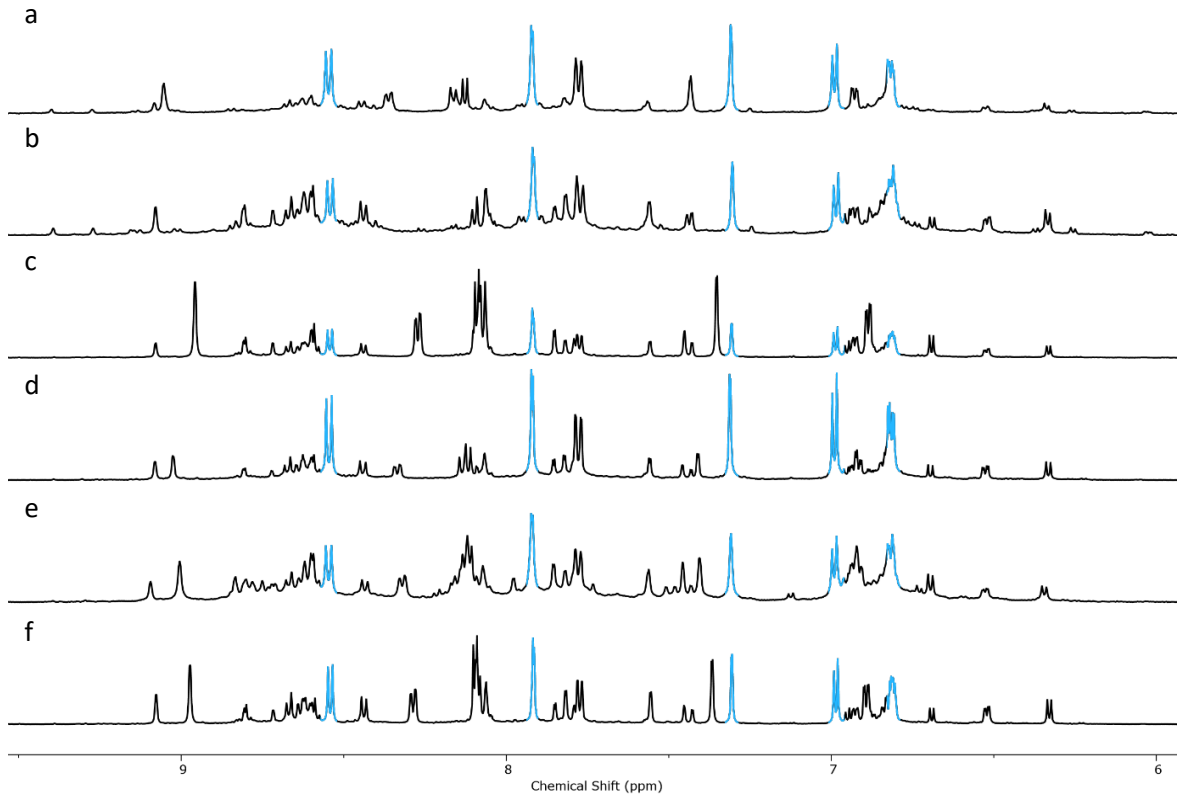

*Figure 2.2.13: Partial ^{1}H NMR (500 MHz, D_2O) of attempted **C20** formations in various co-solvent. (a) acetone/acetonitrile, (b) acetone, (c) tetrahydrofuran, (d) ethanol, (e) trifluoroethanol, (f) methanol. **C20** signals highlighted in blue.*

Since common solvents proved ineffective at improving the selectivity of the reaction, strongly coordinating solvents were suggested. It was hoped that strongly coordinating solvents such as dimethylformamide, dimethylsulfoxide and pyridine would coordinate the metal centres and better solvate the ligands to thereby stabilise the uncoordinated metals and ligands. The strongly coordinating solvents, may also act as nucleophiles to displace the **L20** ligands coordinated to metal centres to "unlock" kinetically "locked" structures. The use of DMSO as co-solvent was not completely effective, though it did show a far better purity when the reaction was carried out at 80 °C (Fig. 2.2.14a).

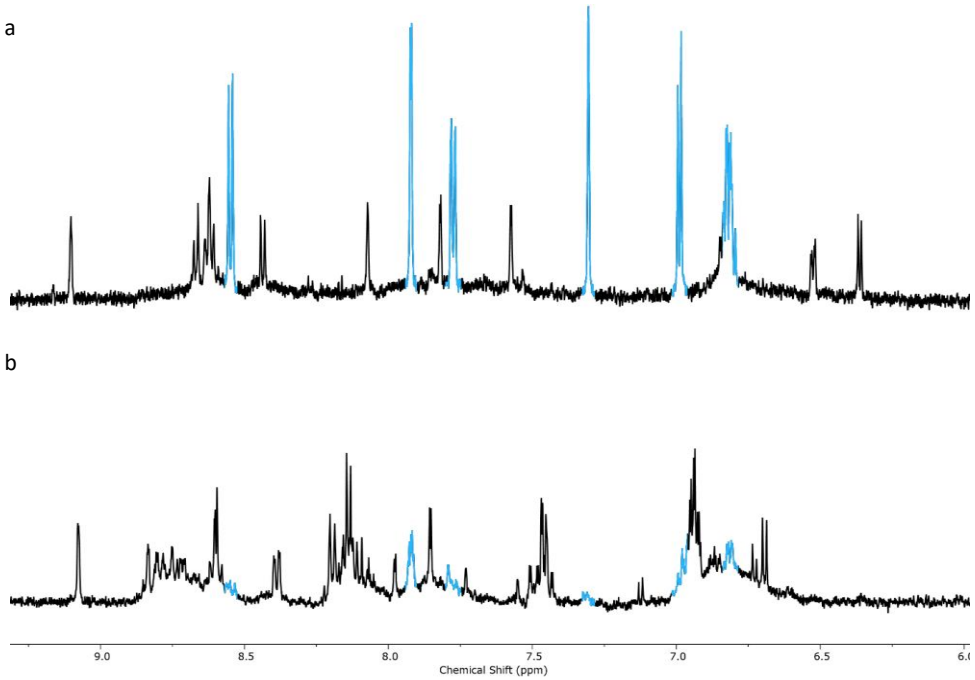

*Figure 2.2.14: Partial ^{1}H NMR (500 MHz, D_2O) of product of **C20** formation reaction with DMSO as a co-solvent. (a) 80 °C, (b) 60 °C. **C20** peaks picked out in blue.*

DMF showed a similar trend, though the product of the reaction at 80 °C precipitated in two batches (Fig. 2.2.15a and b), one appearing to largely contain a single impurity (Fig. 2.2.15b). This impurity was observed in many product mixtures and could not be identified as it did not have high enough solubility to be analysed by DOSY but appeared to have lower symmetry than homochiral tetrahedra, and was theorised to be a lower symmetry tetrahedron.

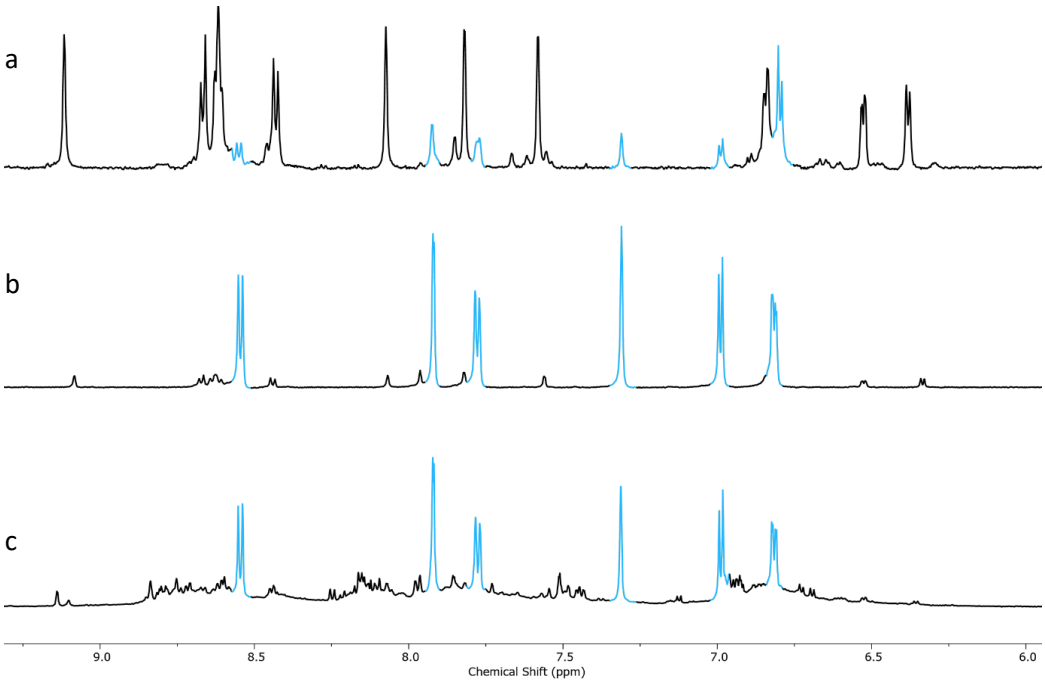

*Figure 2.2.15: Partial ^{1}H NMR (500 MHz, D_2O) of products of **C20** formations with DMF co-solvent. (a) 80 °C first product, (b) 80 °C second product, (c) 60°C. **C20** signals highlighted in blue.*

Reactions in which pyridine was used as co-solvent led to poorly soluble products which could not be redissolved once the solvent was removed, preventing further investigation. Another approach to attempt to increase the reversibility of the metal-ligand bonds was to decrease the pH of the reaction mixture. It was suggested that decreasing the pH would increase the protonation of **L20**, which should disfavour the coordination of the ligand to the metals (Scheme 2.2.9).

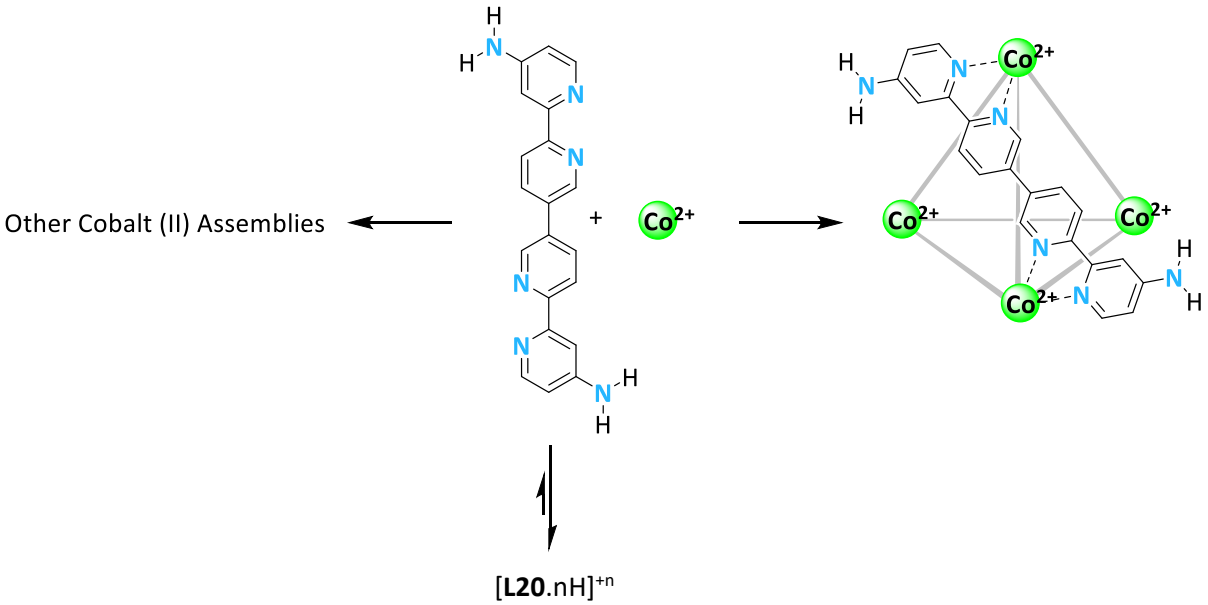

*Scheme 2.2.9: Proposed acid mediation of **L20** speciation.*

Therefore, cage assembly reactions were attempted utilising 5 M, 1 M, 10 mM, 1 mM, 0.1 mM concentrations of nitric acid in the place of water (Fig. 2.2.7). The two most acidic reactions showed no change after heating at 50 °C for 12 hours and then 80 °C for a further 2 hours, with no colour change or dissolution of the ligand observed. The three other reactions did exhibit coordination and were investigated further. None of the reactions gave pure products and none of the observed species had the shifts prescribed to **C20**. The dominant species in the reactions appeared to possess similar symmetry to **C20** (green, Fig. 2.2.16) but could not be identified. An entirely different set of assemblies seemed unlikely and it was theorised the peaks may be shifted by excess nitrate salts or acetate from the acidic hydrolysis of the acetonitrile in the reaction.

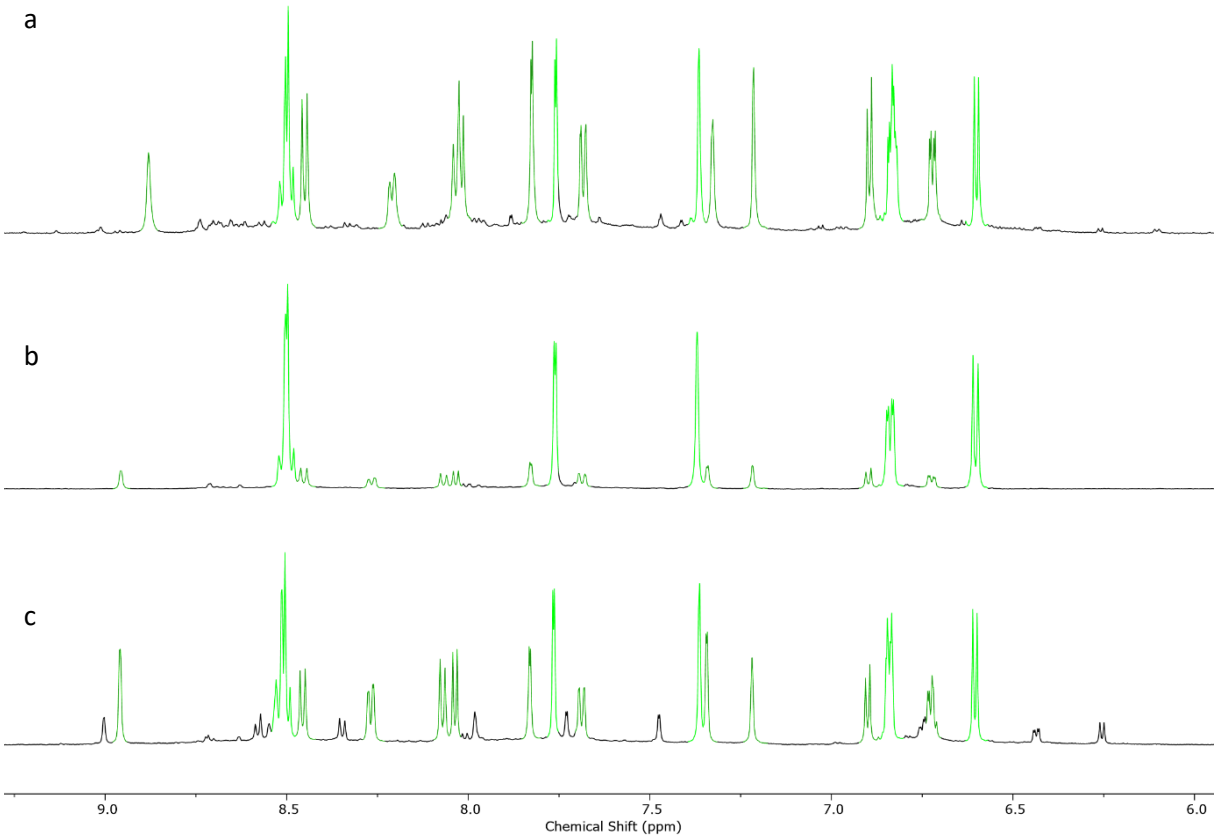

*Figure 2.2.16: Partial ^{1}H NMR (600 MHz, D_2O) of products of **C20** formations using nitric acid in place of water. (a) 10 mM, (b) 1 mM, (c) 0.1 mM acid solutions. Major species highlighted in green.*

2.2.6 Electron-Withdrawing Protecting Groups

After being unable to identify conditions that would formation of pure **C20**, it was proposed that modification of the ligand might be required. It was proposed that substituting a *tert*-butyloxycarbonyl (BOC) protecting group onto the amine would reduce its electron donation to the pyridine ring, decreasing the σ-donor strength of the ligand and reduce the kinetic stability of byproducts. This protecting group could then be removed post-assembly – not least as the cobalt (III) cages had shown tolerance to acidic conditions (Fig. 2.2.17).

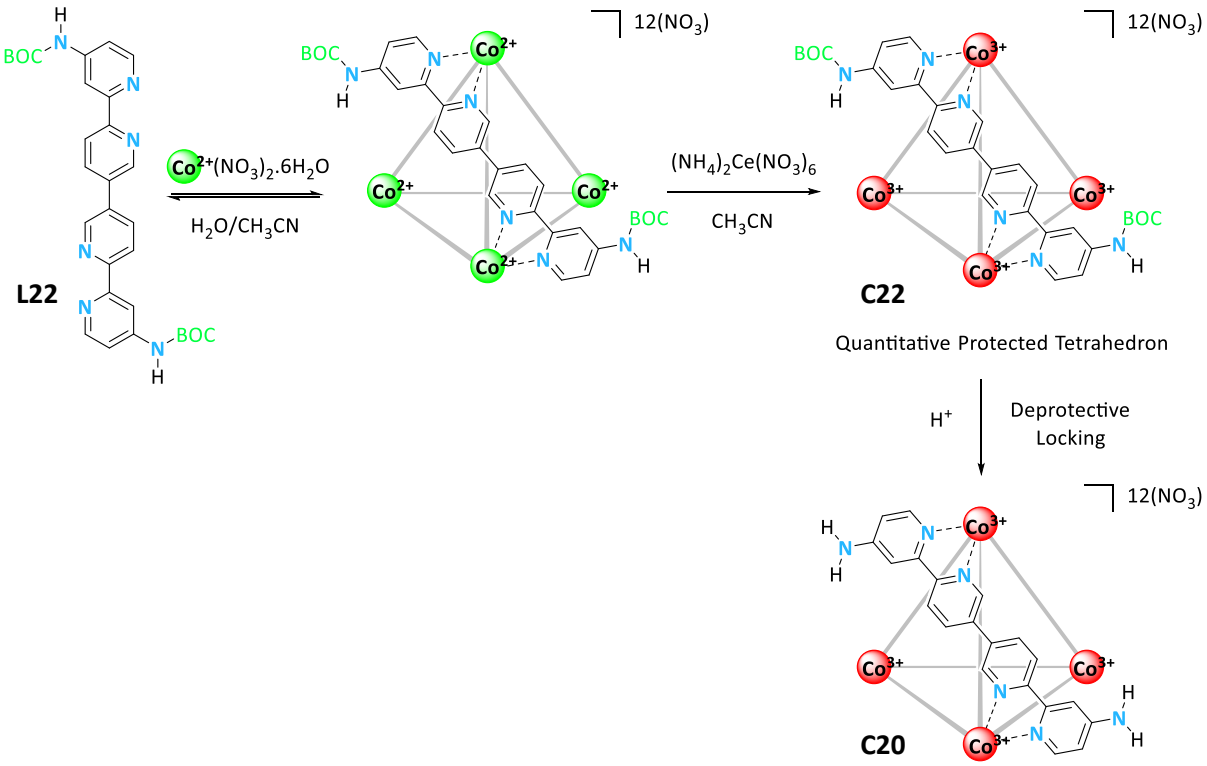

*Figure 2.2.17: Proposed route to **C20** via protection of the ligand, tetrahedral formation followed by deprotection.*

It was also suggested that a *tert*-Butyloxycarbonyl protected amine could serve as an alternative to the nitro group as an amine precursor and give a better route to the ligand (Scheme 2.2.10). The *tert*-Butyloxycarbonyl pyridine monomer **N9** was synthesised according to a literature procedure but was found to not undergo Stille coupling using the previously developed conditions. Therefore **N6** was reacted directly with *tert*-Butyloxycarbonyl to give the protected bipyridine **N10**, which was then homo-coupled to give **L22** (Scheme 2.2.10), though both reactions had poor yields, possibly due to the poor reactivity of the electron poor amine and decomposition of the carbamate groups to unidentified impurities.

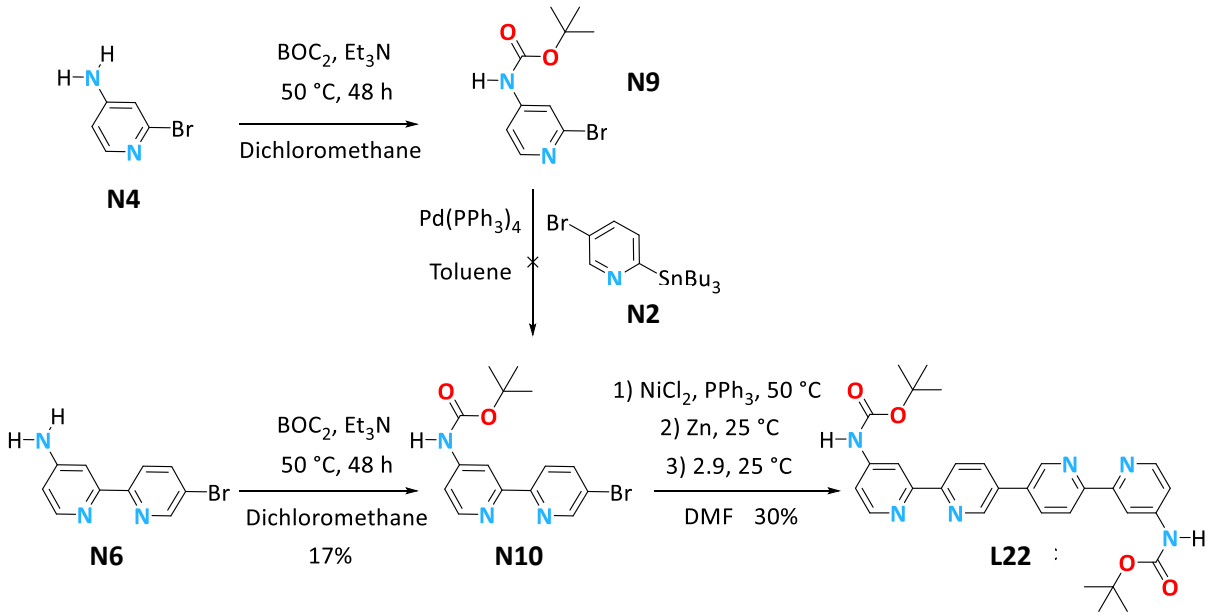

*Scheme 2.2.10: Synthesis of **L22**.*

When **L22** was utilised in a cage formation reaction, it dissolved less readily than **L20** but otherwise behaved in a similar manner. However, when the product was analysed by NMR, it appeared to be an impure sample of **C20** rather than the expected cage (Fig. 2.2.18).

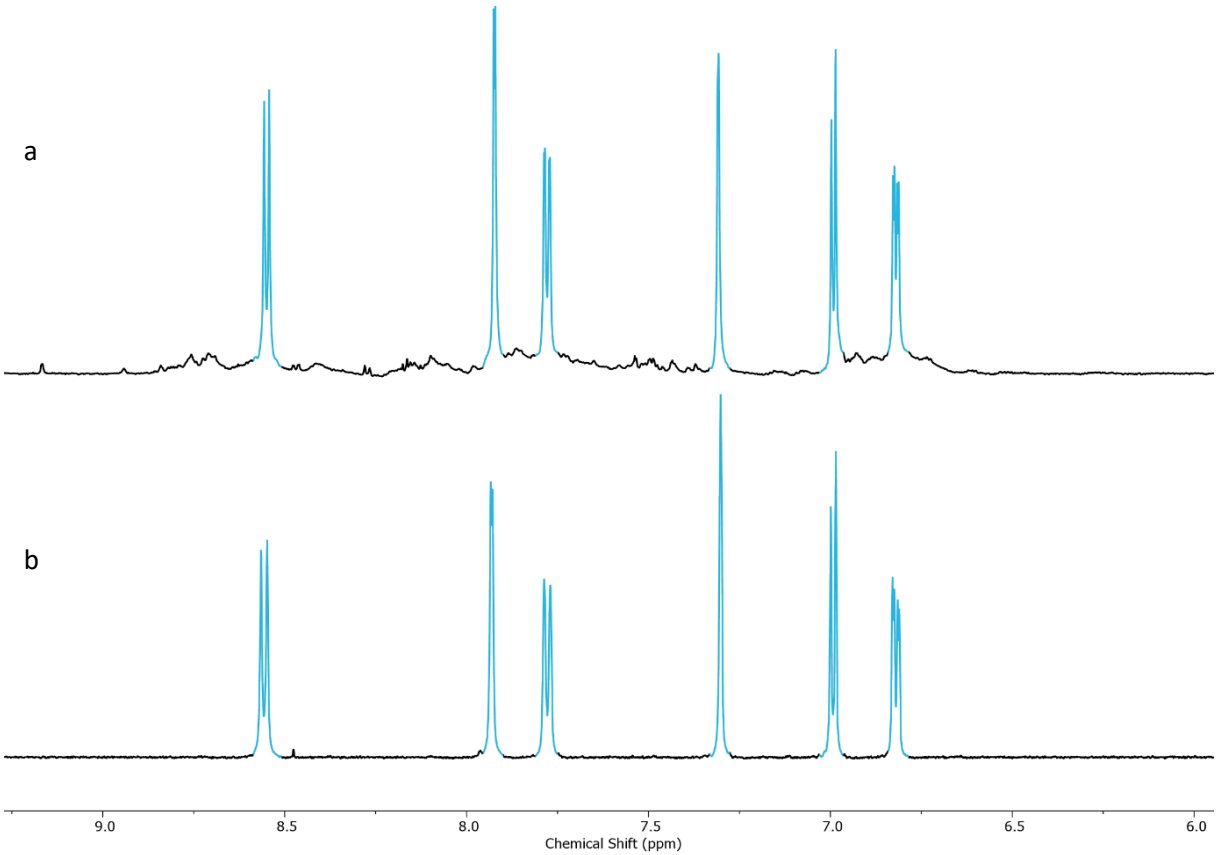

*Figure 2.2.18: Partial ^{1}H NMR (600 MHz, D_2O) comparison of (a) product of cage formation using **L22**, (b) pure **C20** below for comparison. **C20** highlighted in light blue.*

The main species in the spectra was consistent with **C20** and there was no evidence of the *tert*-butyl group. It appeared that the protecting group had been cleaved in the reaction, leading to a similar product mixture as reactions with **L20**.

It appeared that the cage formation conditions were harsh enough to be able to cleave the acid labile protecting group, possibly because the cage formation conditions have a similar acidity to cage solutions. Whether the groups were cleaved before or after coordination cannot be said without further investigation.

As the protected ligand offered limited improvement in the selectivity of the cage formation and posed a greater synthetic workload, this approach was abandoned. It is possible that a more robust protecting group, such as acyl, may withstand the formation conditions and allow for facile cage formation.

Another possible approach would be the use of a template to favour the formation of the tetrahedron. Templating is a powerful tool in the synthesis of three-dimensional assemblies, though removal of the template post-assembly can be challenging.[32] This means that although common anions such as tetrafluoroborate, hexafluorophosphate and triflate may template the formation of the tetrahedron, they would likely then occupy the cavity and reduce its ability to bind other guests such as $[^{99m}Tc]TcO_4$.[33] However, there are examples of careful anion selection allowing anion templated cages to bind guests, and it is possible that the weak binding of the sulfate anion might make it suitable to drive selective formation of the tetrahedron while only minimally interfering with guest binding.[11]

2.2.7 C20 Synthesis by Ligand Exchange

Due to continued difficulty in synthesising **C20**, a less common synthesis approach was suggested. In this strategy, the idea was to use a template tetrahedra with less strongly bound ligands that would undergo sequential displacement by **L20** (Fig. 2.2.19). It was hypothesised that the negligible concentration of free cobalt ions would prevent the formation of intermediates species.

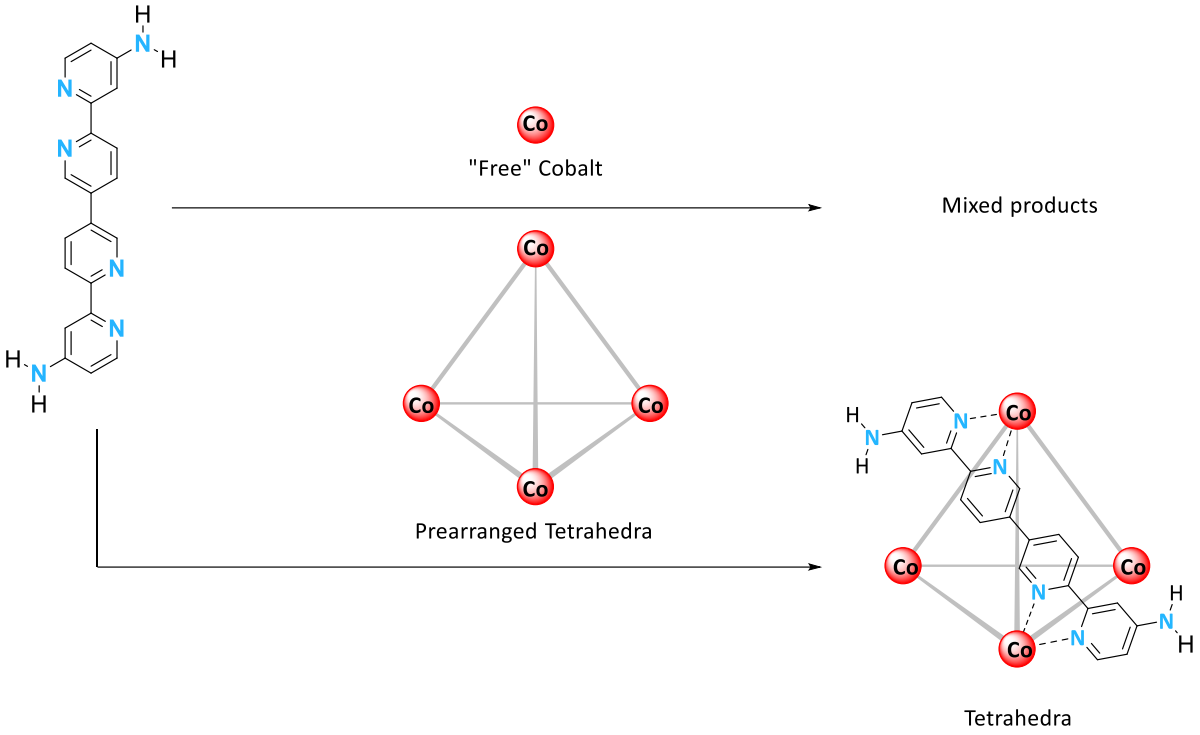

*Figure 2.2.19: Proposed route to synthesis of pure **C20** tetrahedron by ligand exchange.*

Ligand exchange and the substitution of ligands into existing assemblies has been reported a few times. An example was reported by Hardie in which two analogous ligands appeared to form cages of significantly different stabilities.[34] This leads to the preferred formation of one cage over the other and the sequestering of the metal ions by the uncoordinated stronger ligand. Michl and co-workers used prearrangement to access a challenging kinetically locked structure. In their method, they use reversible pyridine-Pt interactions (facilitated by strong *trans*-directing phosphine capping groups) to generate square (**M23$_a$**) in high yield. They then substituted these neutral "weak" ligands for strongly coordinating acetylides **L23b** to yield **M23$_b$** (Fig. 2.2.20).[35]

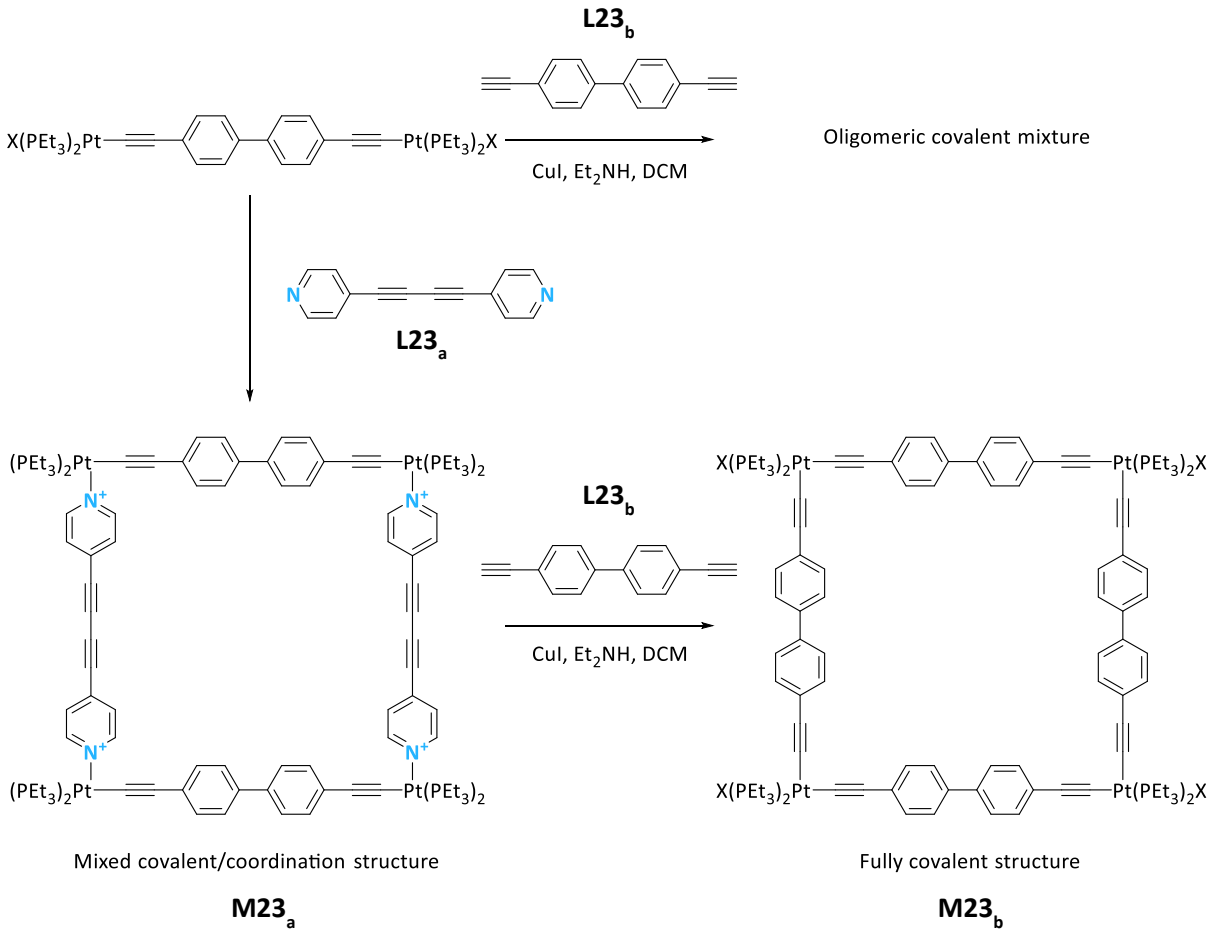

Figure 2.2.20: Synthesis of fully covalent square assembly ***M23$_b$*** *through initial formation of* ***M23$_a$*** *with* ***L23$_a$*** *followed by substitution with* ***L23$_b$****.*

These examples lead us to propose the possibility of exchanging the ligands in an assembled **L19** tetrahedron with **L20**. The cooperativity of the cage could be expected to maintain the integrity of cage, thus allowing stepwise substitution of the ligands, effectively using the existing tetrahedra as a template. **L19** was considered an effective sacrificial ligand as it will have a weaker interaction with the metal, making ligand exchange is thermodynamically favoured. This equilibrium could be further biased with an excess of **L20**, and it was also possible that the kinetic stability of the coordinated **L20** would lead to formation of **L20** through an irreversible pathway.

Initially it was suggested that the cobalt (II) tetrahedron of **L19** would be suitable for this substitution, as the lability of the system would allow the fast and facile incorporation of the ligand into the assembly. However, as discussed previously, it has been shown that it was very difficult to quantitatively form the cobalt (II) tetrahedron in solution. While paramagnetic ^{1}H NMR had been a powerful tool when working with cage systems in acetonitrile, attempts at investigation of cobalt (II) nitrate assemblies of **L19** in aqueous solution were less effective (Fig. 2.2.21). Solubility was an issue

and NMRs of the solutions obtained did not show high symmetry species. An attempt was made to isolate the Co_4(**L19**)$_6$(NO_3)$_8$ by crystallisation, which also proved ineffective due the high solubility of the cobalt (II) assemblies.

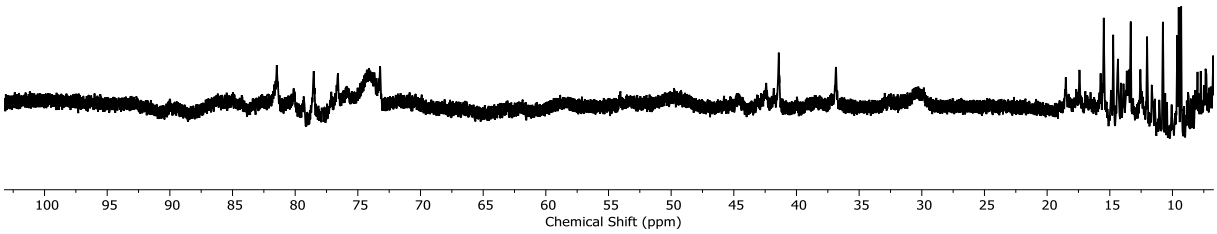

Figure 2.2.21: ^{1}H NMR (500 MHz, D_2O/CD_3CN 9:1) of mixed cobalt (II) assemblies of ***L^{BB}****.*

Substitution of the cobalt (III) tetrahedron was proposed as an alternative approach, as shown in Figure 2.2.22. Though these cobalt (III) species have been targeted as kinetically "locked" assemblies, the previous triazole based **C14** and **C24** was shown to undergo ligand scrambling when two cages composed of different ligands were mixed. **H14** was shown to rearrange to the **C14** upon heating and the two tetrahedra were shown to scramble ligands after extended heating. Though the **L19** system has been demonstrated to be considerably less labile than the **L14**, it was still anticipated that it could exhibit some lability. In particular, it was suggested that scrambling by adding an uncoordinated ligand would substantially speed up this process. Indeed, it has previously been shown that ligand scrambling with intact cages gives an artificially high assessment of their stabilities due to the very low steady state concentration of free components.

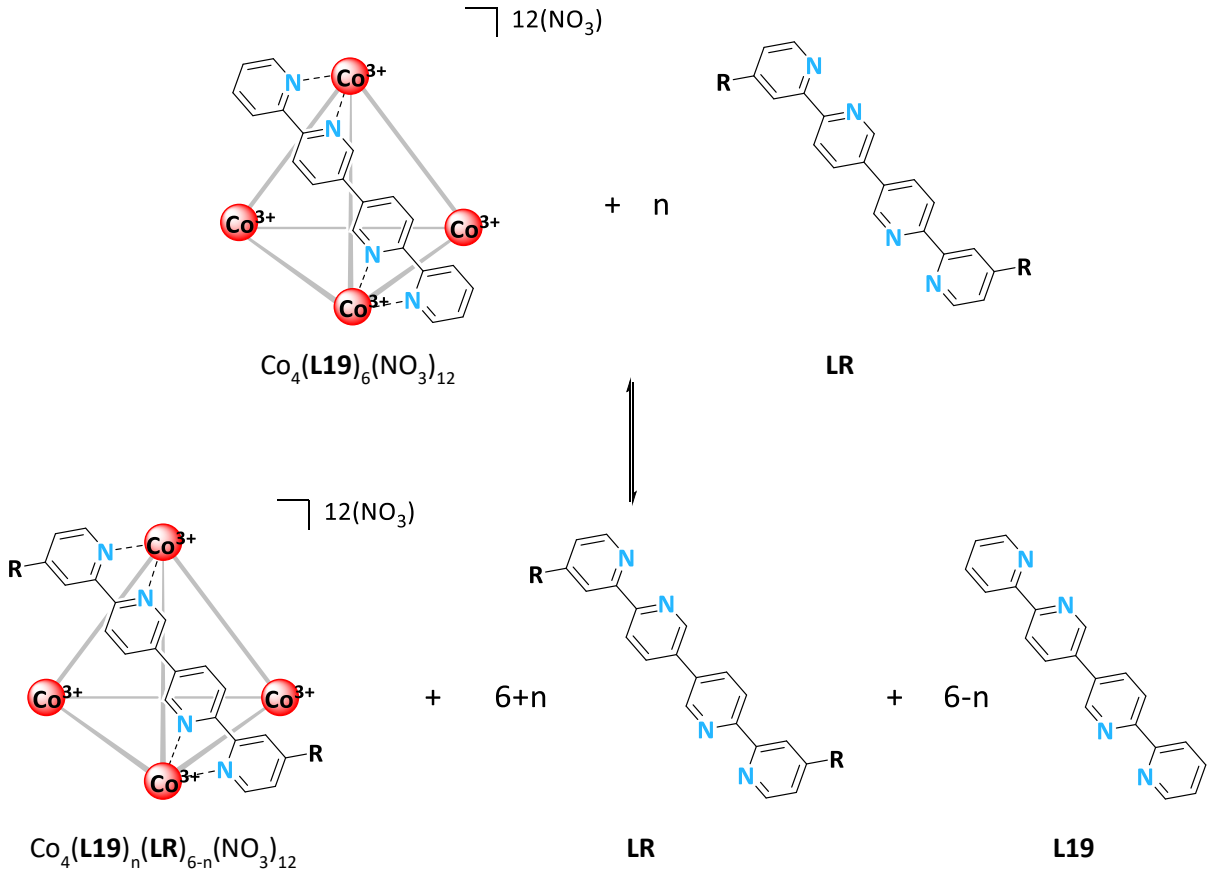

*Figure 2.2.22: Proposed substitution of functionalised ligands into **C19**.*

Therefore, a sample of the **C19** was dissolved in a 9:1 mixture of D_2O/CD_3CN and nine equivalents of **L20** were added as a solid. The mixture was sealed, heated to 75 °C and monitored by NMR (Fig. 2.2.23). The yellow colour of the **C19** solution quickly changed to the orange colour of **C20** and the NMR showed the rapid loss of **C19** peaks in favour of ones consistent with **C20**. Continued heating after three days caused little further change in speciation, implying that an equilibrium had been reached.

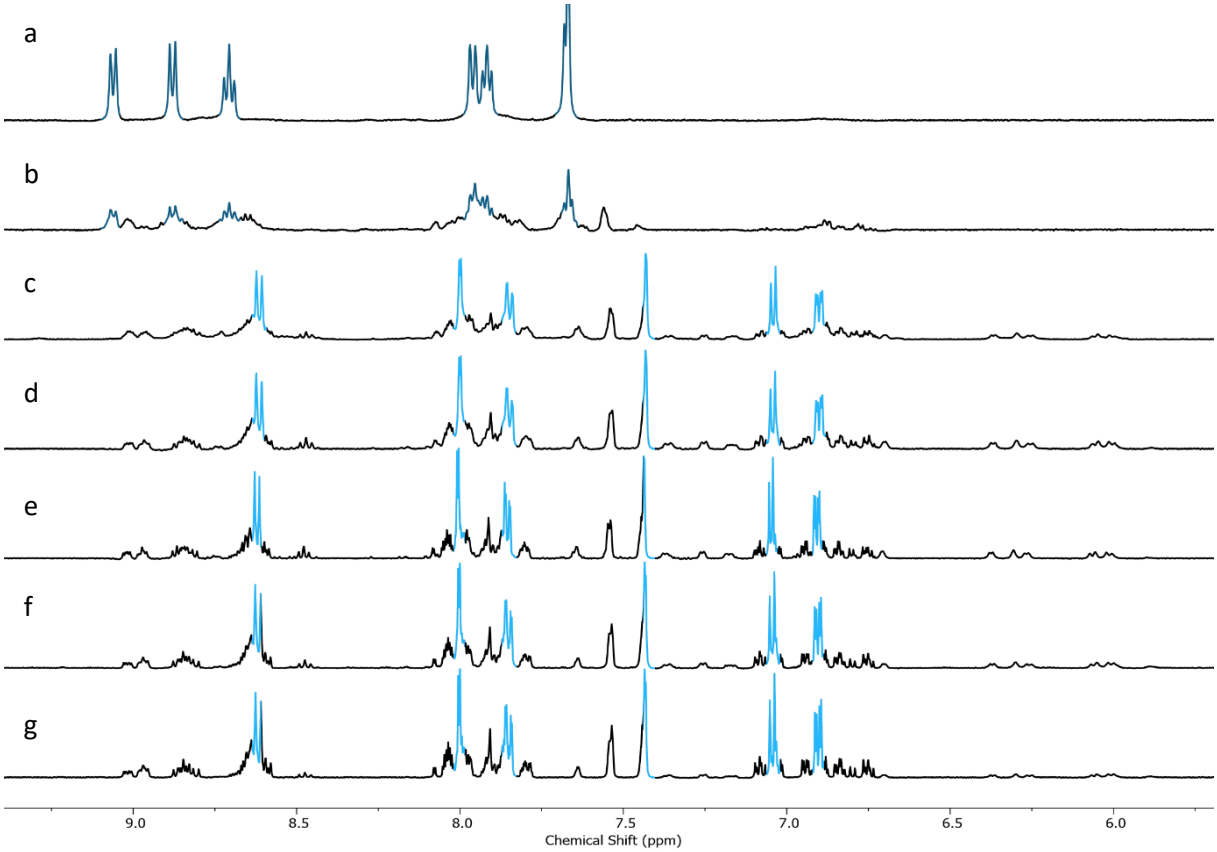

*Figure 2.2.23: Partial ^{1}H NMR (600 MHz, 9:1 D_2O/CD_3CN) of **C19** with 9 equivalents of **L20**. (a) Before addition of **L20**, then after heat at 75 °C for (b) 0 h, (c) 1 h, (d) 12 h, (e) 36 h, (f) 50 h, (g) 71 h. **C19** highlighted in dark blue and **C20** in light blue.*

The other species present are likely to be heteroleptic species with mixed ligands (Figure 2.2.24). These heteroleptic cages would be expected to represent a complex mixture of species with different symmetries, depicted in Figure 2.2.24.

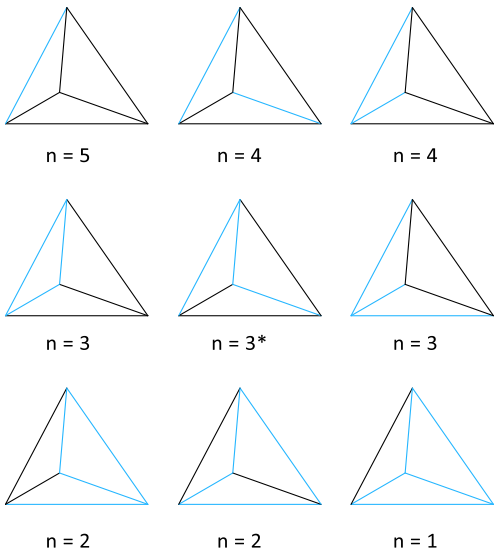

*Figure 2.2.24: Depictions of nine potential substitution patterns of heteroleptic tetrahedra formed in the reaction. Ligands depicted in black and blue. (*Possess additional chirality)*

While these heteroleptic cages might be of interest due to their lowered symmetry and intermediate properties, they threatened to make isolation of pure cage difficult. The persistence of these intermediates implied that the excess of **L20** was too small to effectively out-compete **L19** in the exchange equilibrium. Therefore, the reaction was repeated with twelve equivalents of **L20**, making the total **L20**/**L19** ratio two to one. This reaction appeared to show a smaller number of other species in the NMR spectra even after 13 days. Unfortunately, the solid ligand present in solution caused bad shimming and line broadening (Figure 2.2.25).

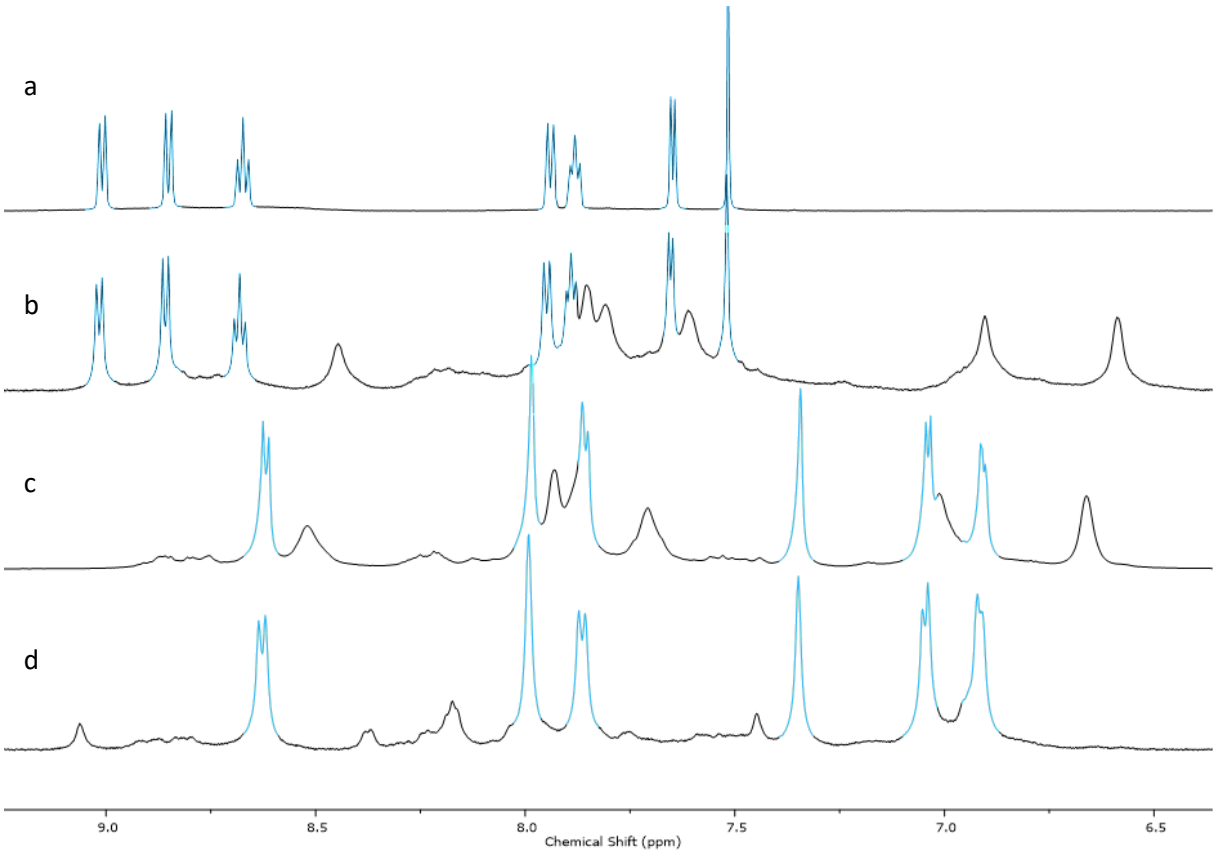

*Figure 2.2.25: Partial ^{1}H NMR (600 MHz, 9:1 D_2O/CD_3CN) of **C19** with 12 equivalents of **L20**. (a) Before addition of **L20**, then after heating at 75 °C for: (b) 0 h, (c) 48 h, (d) 13 days. **C19** highlighted in dark blue and **C20** in light blue.*

It was hypothesised that these persistent impurities may be caused by metastable intermediates. Higher temperatures may overcome this problem but could also lead to a rearrangement to the helicate over extended periods of time. Therefore, it was proposed that energy barrier to ligand exchange be lowered by exploiting the redox activity of cobalt.

It was hypothesised that the inclusion of a catalytic amount of cobalt (II) into the system would facilitate exchange. Under an inert atmosphere, these cobalt (II) centres could propagate through the system by electron transfer between complexes. These reduced sites would be expected to be far more labile, increasing the overall rate of substitution without destabilising the cage. This is a similar concept to the slow oxidation of the system, which exploits rearrangement of the mixed oxidation state species. While **L20** cobalt (II) assemblies appeared to be slow to rearrange, it was hypothesised exchange may be more effective with uncoordinated ligand.

Addition of cobalt (II) nitrate was proposed as the most practical means of introducing cobalt (II) into the system. Another NMR study was undertaken, shown in Figure 2.2.26, this time introducing 0.25

mol% $Co(NO_3)_2.6H_2O$ (with respect to cage) before degassing and sealing of the reaction vessel prior to heating.

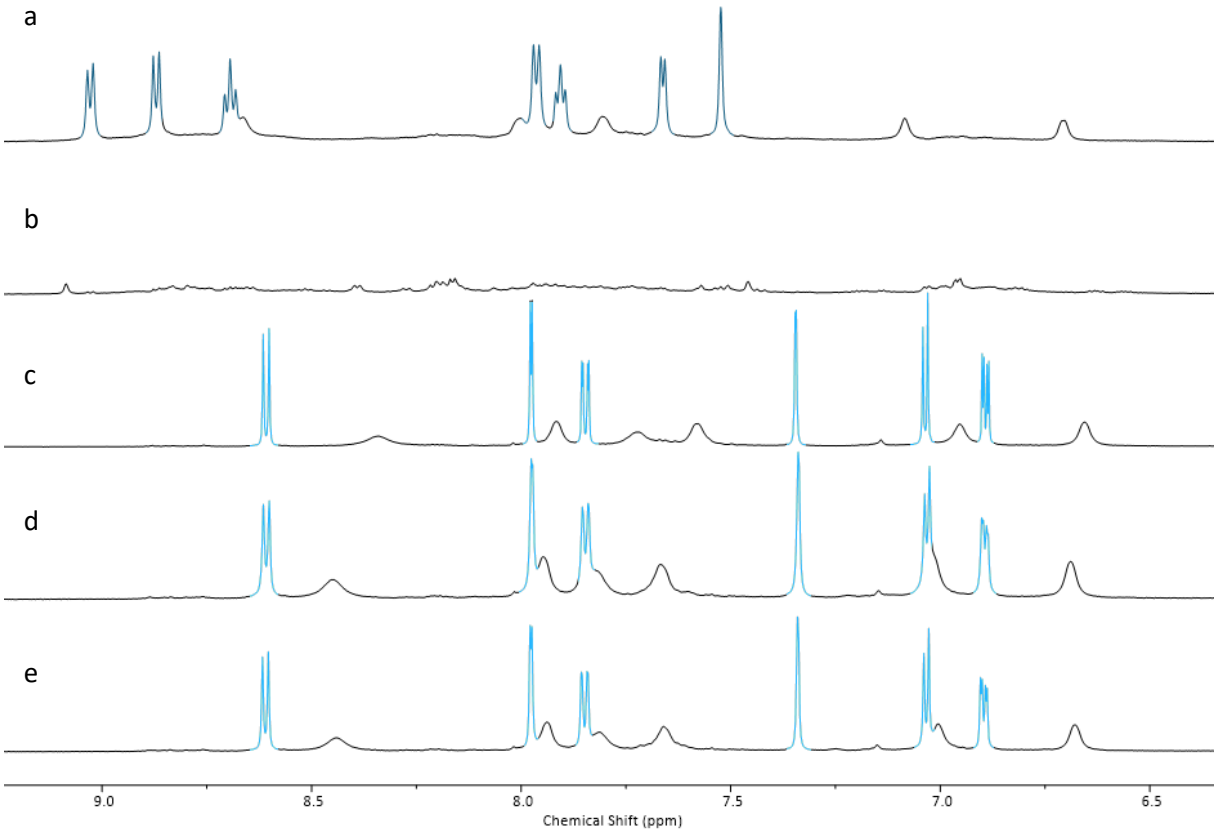

*Figure 2.2.26: Partial ^1H NMR (600 MHz, 9:1 D_2O/CD_3CN) of **C19** with 12 equivalents of **L20** and 0.23 mol% $(CoNO_3)_2.6H_2O$. After heating at 75 °C for: (a 0 h, (b) 24 h, (c) 4 days, (d) 5 days, (e) 6 days. **C19** highlighted in dark blue and **C20** in light blue.*

The results of this cobalt (II) "catalysed" reaction (Fig. 2.2.26) appeared to show a large reduction in the impurities, with only a single broad set of other signals. DOSY investigation of these peaks appeared to show that they had a smaller hydrodynamic radius than the tetrahedron, though the broadness of the peaks might imply a dynamic or cobalt (II) species. Encouraged by this improvement, the reaction was filtered and the product dried and isolated. Size exclusion chromatography was trialled on the product mixture and found to be effective at isolating the pure cage from these impurities. Whether this separation was caused by the DOSY-implied size difference, or some chemical differentiation by the saccharide-silicone gel could not be determined, but the cage was isolated in a respectable 70% yield.

The reaction was repeated on a preparative scale and found to be reproducible, consistently giving pure **C20** with greater than 50% yields (Scheme 2.2.11). While this synthesis may be considered resource- and time-intensive, it was the most reliable and reproducible method to synthesise **C20**.

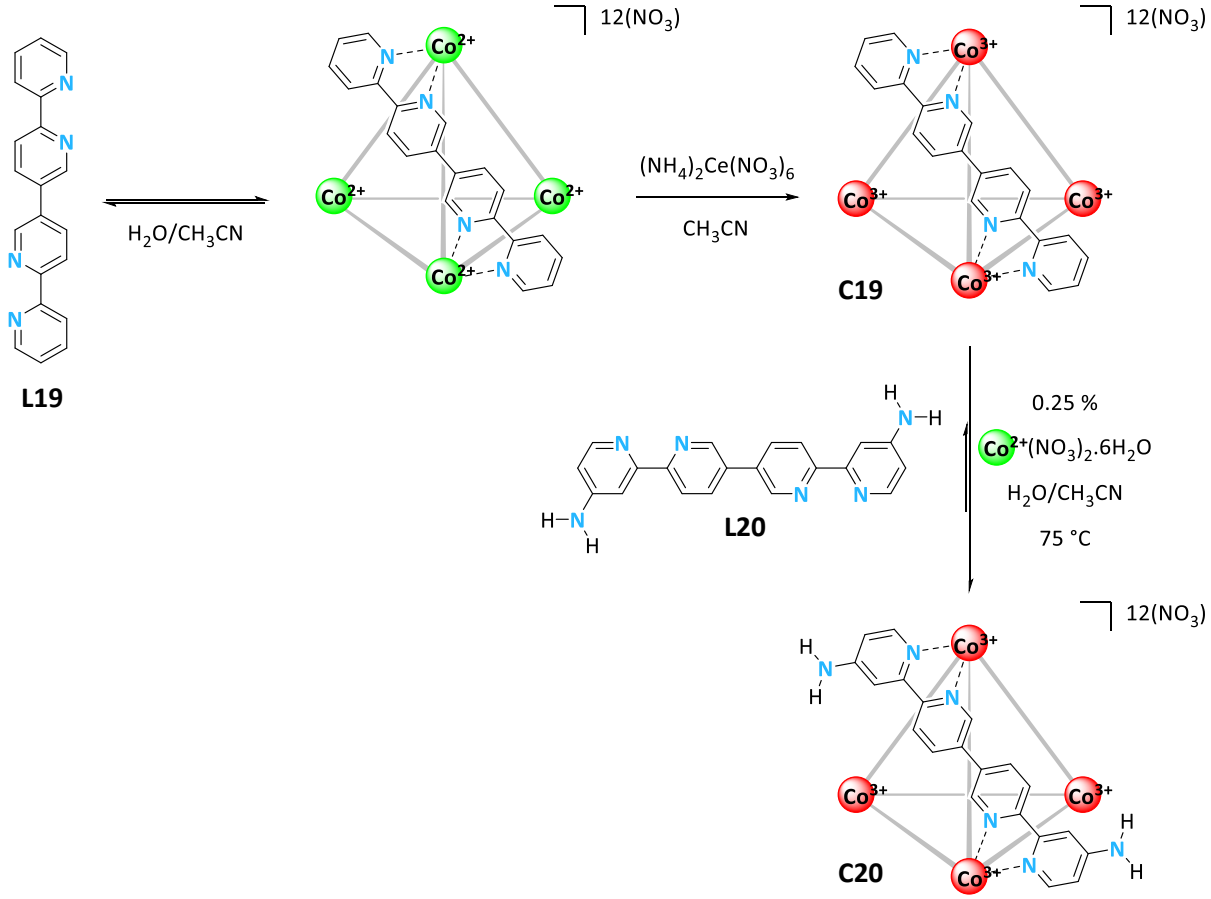

*Scheme 2.2.11: Successful route to **C20** via the formation of **C19** and substitution with **L20** ligands.*

The reaction is less resource intensive than it may first appear, as the excess ligand and the byproducts are recoverable. The excess ligands are collected by filtration during the work up and are easily separated according to their different solubilities. The impure byproducts can also be disassembled through demetallation with EDTA to recover the ligands in a similar manner.

While the reaction was found to be effective, greater understanding may allow its improvement. Identification of the intermediates, byproducts and impurities of the reaction might give insight into the kinetic and thermodynamic factors in the exchange and allow optimisation.

The rapid progress of the reaction implies that the temperature of the reaction could be lowered to allow closer monitoring of the intermediate stages of the reaction. It may also prevent any possible rearrangement to helicate occurring during the reaction. Temperature variation may also provide more information about the role of the cobalt (II) additive in the reaction. The inverse reaction, attempting to exchange of an excess of **L19** into **C20**, would also be a poignant experiment, illuminating whether the greater ligating strength of **L20** is significant.

2.2.8 Properties of C20

Once isolated, **C20** was characterised; The proton NMR of the cage showed that the shielding observed in the ligand was also apparent in the cage indicating a more electron rich system, shown in Figure 2.2.27.

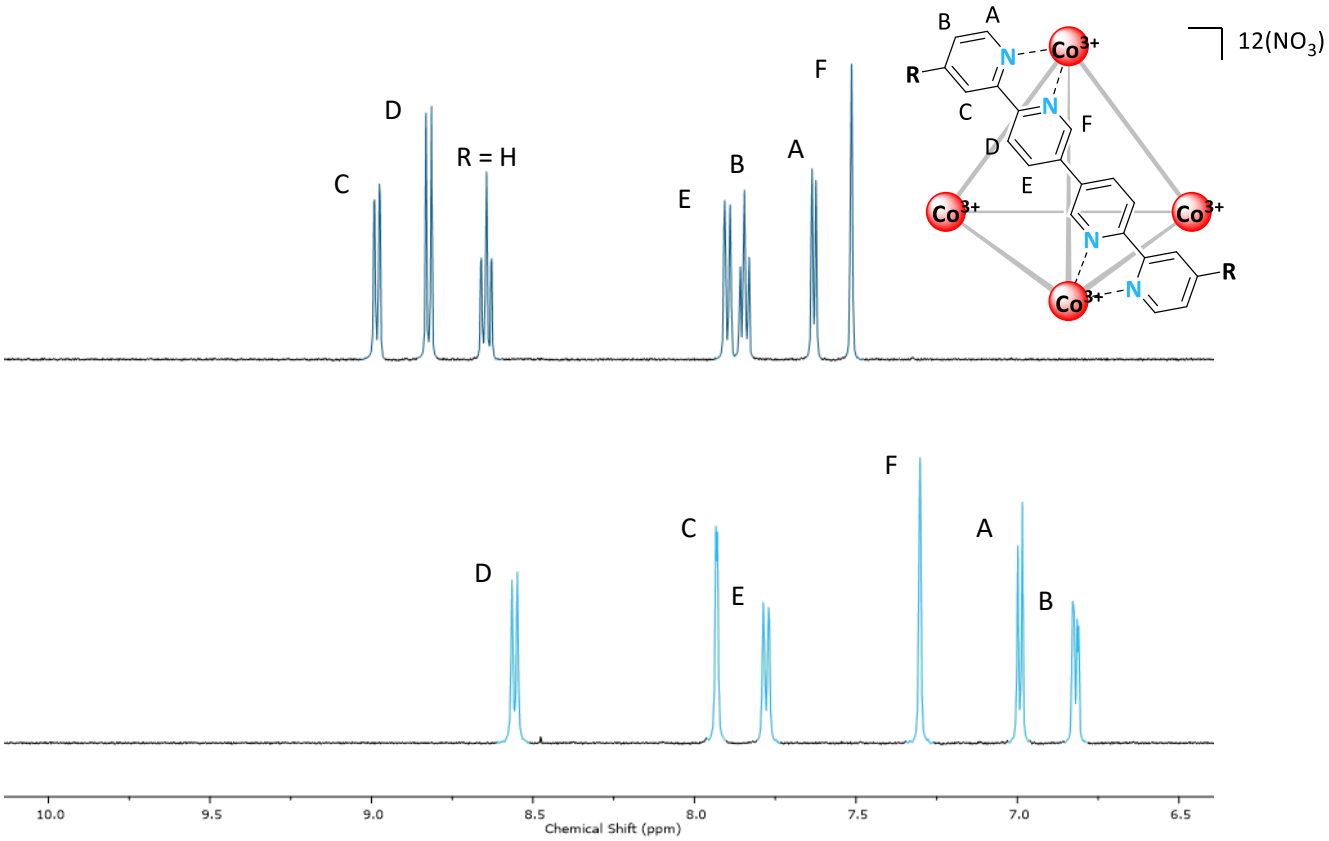

*Figure 2.2.27: Partial ^{1}H NMR (500 MHz, D_2O) of **C19** (top, R = H, dark blue) and **C20** (bottom, R = NH_2, light blue), NH_2 signals not observed due to deuterium exchange.*

As **C20** does not differ in size or charge in comparison with **C19**, it was predicted that it would have very similar guest binding properties. A number of guest binding studies with **C20** were performed; perchlorate and perrhenate were both found to bind within **C20** to a similar extent as **C19** (Table 2.2.2). Perrhenate with a binding constant of 46000 M^{-1} and perchlorate with a binding constant of 21000 M^{-1}.

*Table 2.2.2: Binding constants of perchlorate and perrhenate in **C19** and **C20**. Experimental error estimated to be ±50%. Binding constants for **C19** collected by Michael Burke.*

	K_a M^{-1}	
Anion	**C19**	**C20**
ClO_4^-	7100	21000
ReO_4^-	61000	46000

Additionally, a crystal structure of [ReO_4⊂**C20**] was obtained by the slow diffusion of acetone into a solution of the cage saturated with [NMe_4][ReO_4], shown in Figure 2.2.28. Though the angle of diffraction was insufficient for in-depth measurements and analysis, it provides further proof of both the connectivity of the capsule and the binding of the guest within its cavity. Interestingly the anion was only bound within the cavity of the cage with a 50% occupancy in this crystal structure, though the reason for this remains unclear.

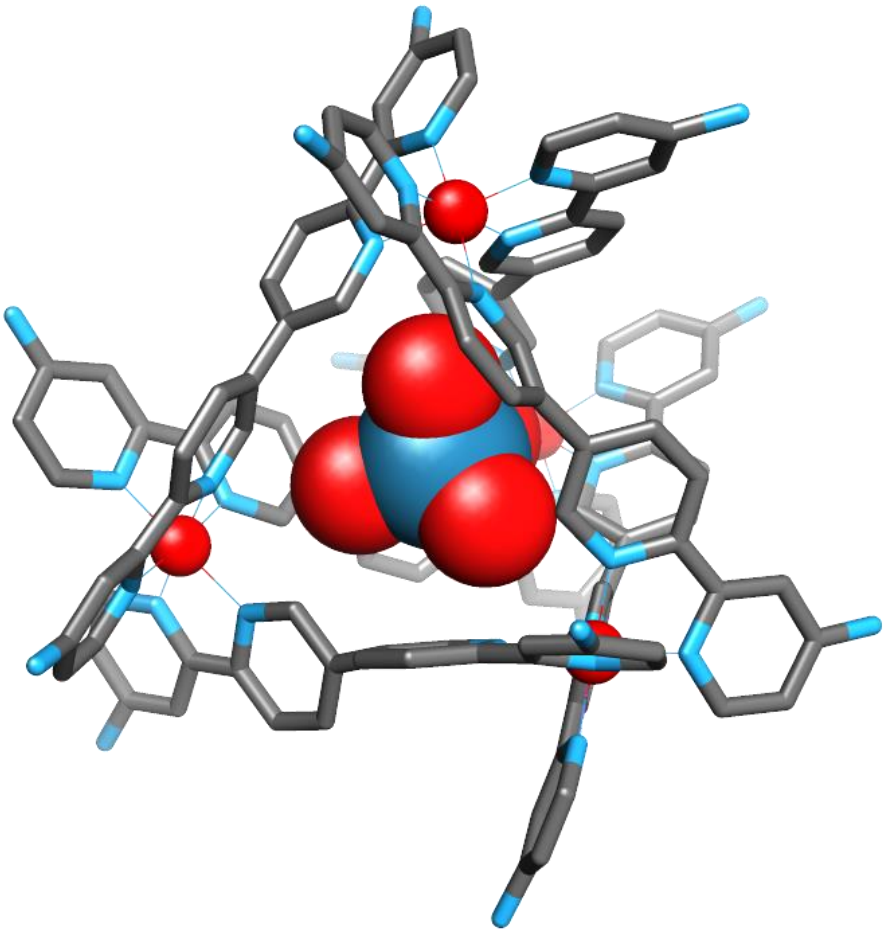

*Figure 2.2.28: Partial crystal structure of [ReO_4⊂**C20**]. Protons, solvent molecules, and anions have been omitted for clarity.*

C20 was characterised and found to retain the desirable qualities of **C19** regarding solubility, structure and guest binding of "cold" anions. In order to assess the stability of the new cage, the glutathione assay previously utilised with **C19** was repeated. As expected, **C20** was found to be stable in pH 7.4 phosphate buffered saline with negligible loss of ^{1}H NMR signals over several weeks (Figure 2.2.29).

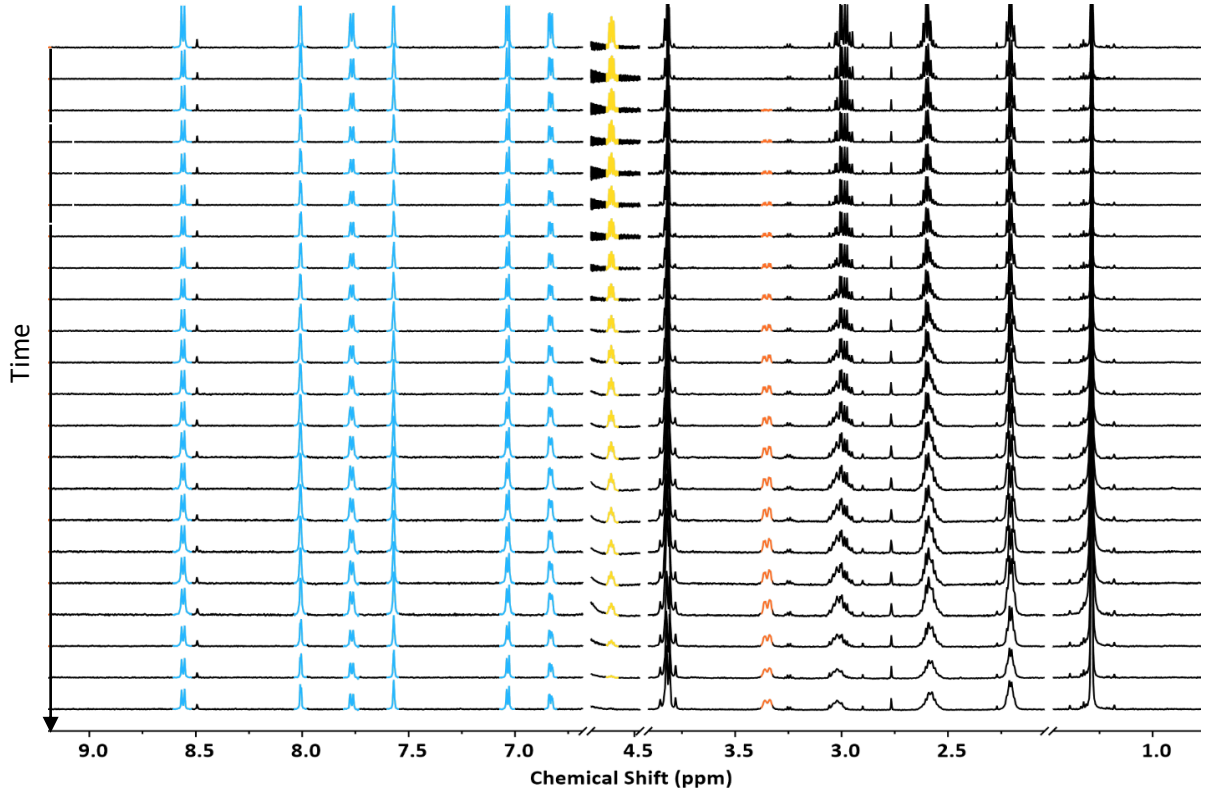

*Figure 2.2.29: Partial ^{1}H NMR (600 MHz, D_2O, 1 M PBS) of **C20** (0.1mM) in presence of 10 equivalents of glutathione over time (descending: 0 h, 0.5 h, 1 h, 2 h, 2.5 h, 3 h, 3.5 h, 4 h, 4.5 h, 5 h, 5.5 h, 6 h, 6.5 h, 7 h, 7.5 h, 8 h, 8.5 h, 9 h, 9.5 h, 10 h, 10.5 h, 11 h, 24 h, 36h, 42 h). **C20** (blue), glutathione (yellow), glutathione disulphide (orange).*

Following the addition of 10 equivalents of glutathione to a PBS solution of **C20**, it appeared to exhibit better stability than **C19**. The ^{1}H NMR signals of the cage are present for far longer; in fact, the signals of the cage appear to still be present after 40 hours, whereas **C19** had been almost completely consumed within one hour (Fig. 2.2.30).

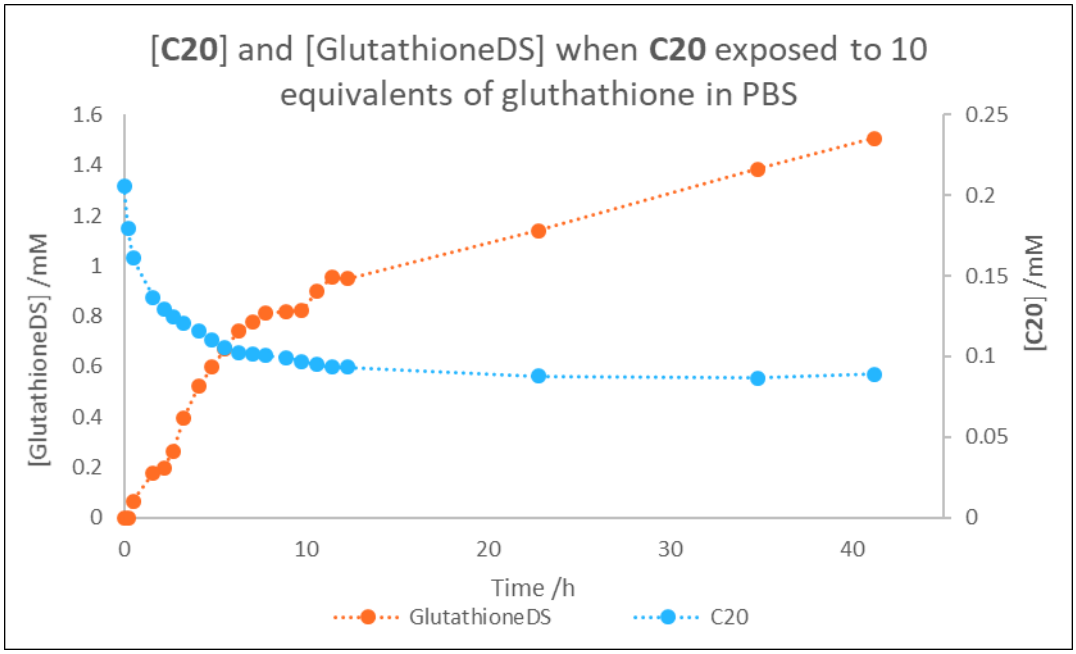

*Figure 2.2.30: Concentration of **C20** and glutathione disulfide (GlutathioneDS), when **C20** (1 mM) exposed to 10 equivalents glutathione in pH 7.4 phosphate buffered saline.*

Analysis of the concentration of the cage and glutathione disulfide showed that the concentration of the cage did not fall below half of the initial concentration during the experiment. The concentration of glutathione could not be accurately monitored due to overlap with the water peak; however, it was apparent that all ten equivalents of glutathione were consumed, even after the concentration of the **C20** had stabilised. One explanation for the consumption of glutathione in the absence of consumption of **C20** could be other reactions. The previous experiments have shown that degraded **C19** appeared to catalyse the oxidation of glutathione. It is possible that this also occurring in this instance before the complete consumption of **C20**. However, continued consumption of **C20** might be expected in this were the case.

Another possibility is that the cage concentration is being regenerated. It is possible that the cobalt (II) form of **C20** may be sufficiently stable to remain in solution and react with atmospheric oxygen to regenerate the cobalt (III) species. This would allow **C20** to effectively catalyse the oxidation of glutathione by atmospheric oxygen. Though, as the **C20** concentration remains stable rather than increasing or decreasing, it implies that the system had reached some form of equilibrium. That this was observed with **C20** and not **C19** could be explained by the greater stability of the cobalt (II) or mixed valent assemblies of **C20**. **L20**-cobalt (II) assemblies were shown to be stable by the apparent perseverance of kinetically trapped byproducts. This observed stability could imply that the cobalt (II) assemblies of **L20** are kinetically stable enough to survive in phosphate buffered saline long enough to be re-oxidised.

The mechanism of the reaction cannot be known without further study and is likely to be complex. Many reported glutathione oxidations include the coordination of the glutathione to the metal centres and the supramolecular nature of our system provides many interactions that may be significant to the reaction. Cage solutions in buffer represent a complex mixture of chemical species and environments. The cage's counterions, cavity, portals, exterior surface and coordination sphere all represent different chemical micro-environments. Additionally, the buffer also contains a large number of ions, including various phosphate, chloride and nitrate. Therefore, the complexity of the system may make identification of the reaction mechanism difficult.

At pH 7.4, glutathione would be expected to possess two anionic carboxylic acid groups, one protonated amine and the thiol group, all of which will be expected to interact with the cage and solution ions. By ^{1}H NMR the peaks of glutathione and **C20** in PBS only shift marginally when combined, suggesting there is little non-covalent interaction (Figure 2.2.31).

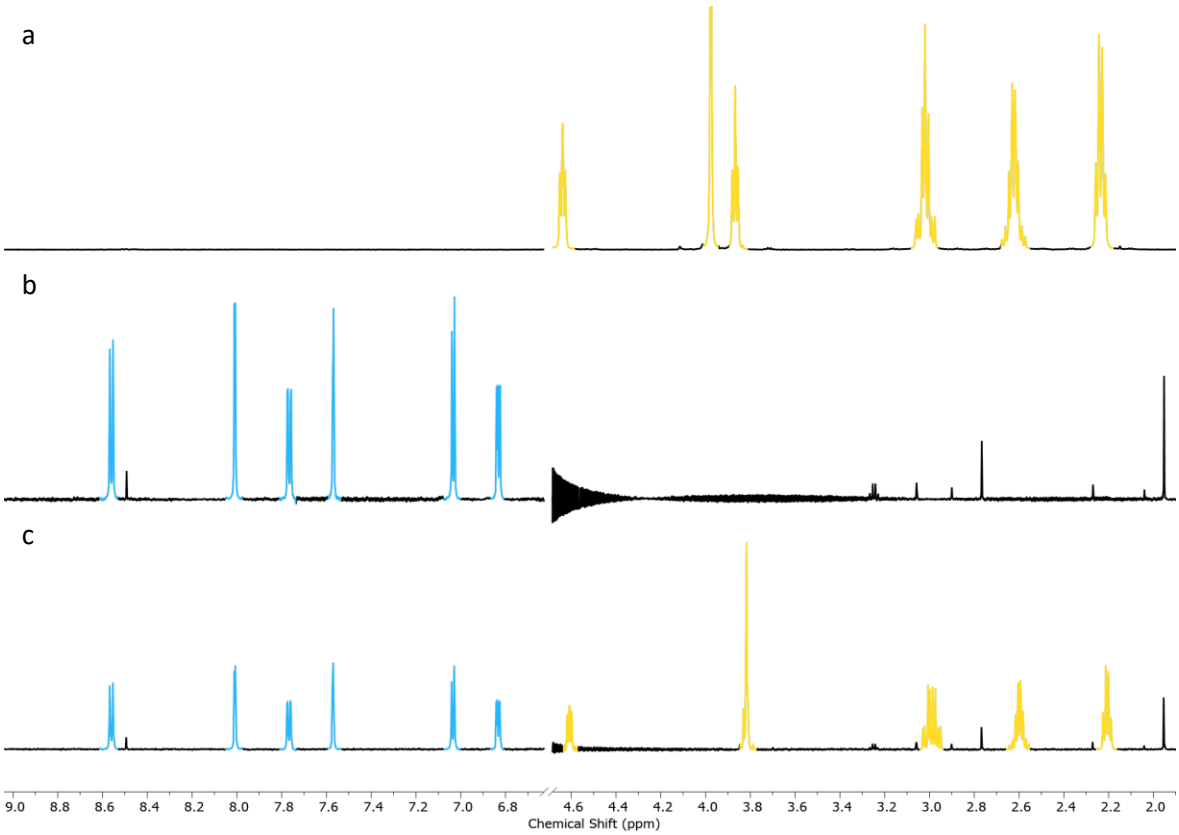

*Figure 2.2.31: Partial ^{1}H NMR (600 MHz, D_2O, 0.1 M PBS) of solutions of (a) glutathione, (b) **C20**, (c) glutathione and **C20**.*

The peaks of the cage do not shift, though its concentration has dropped considerably upon the addition of glutathione, implying that the glutathione is interacting with some form of degraded or reduced cage that is not visible to ^{1}H NMR.

In an attempt to gain more insight into this interaction between glutathione and **C20** the reaction was repeated in D_2O rather than phosphate buffered saline. This was expected to simplify the system by reducing the number of ions in solution, allowing the cage to decrease the pH. Treating the cage with glutathione in D_2O was found to degrade the cage at a slower rate. Unexpectedly, a second set of peaks appeared (Figure 2.2.32, purple peaks) and these peaks increase in intensity as the peaks of **C20** decrease (Figure 2.2.32, blue peaks). These peaks possess the same symmetry as the cage and appear to be diamagnetic but also migrate over time.

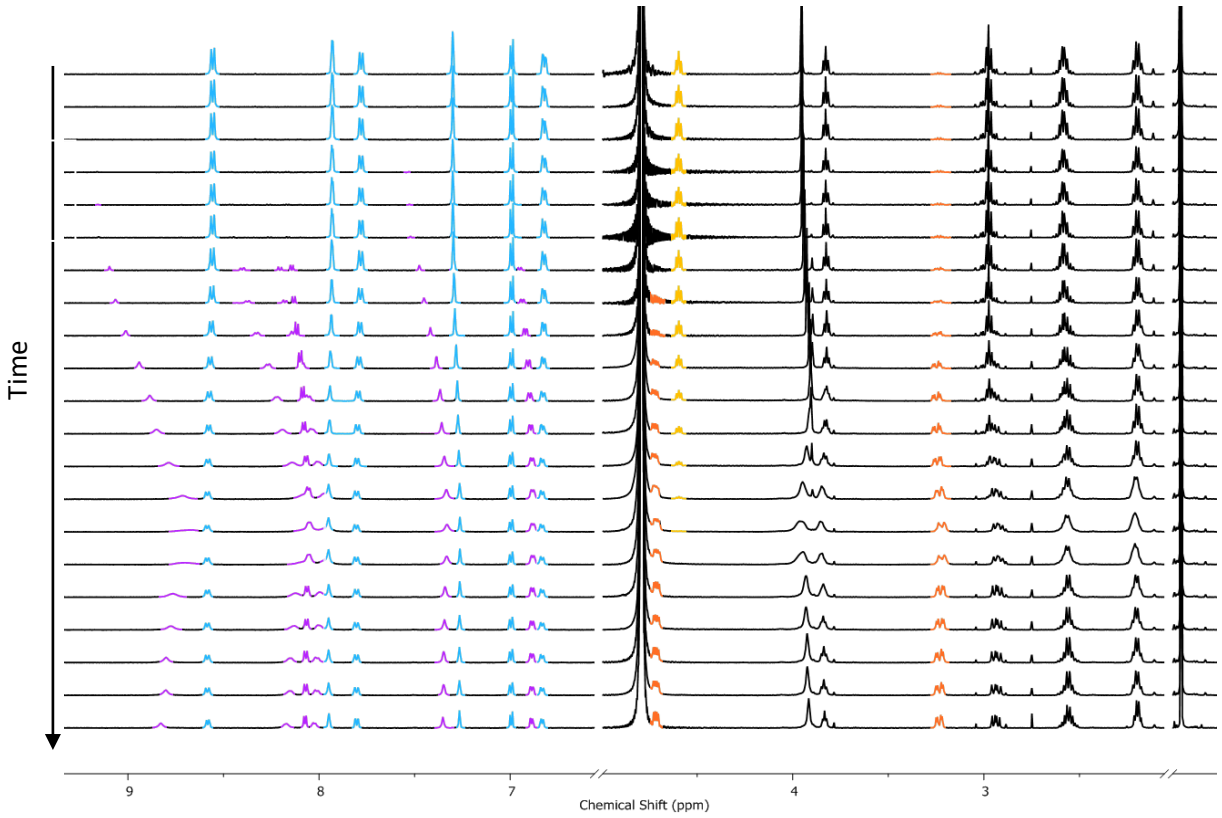

*Figure 2.2.32: Partial ^1H NMR (600 MHz, 600 MHz, D_2O, 1 M PBS) of **C20** and Glutathione over time (descending). **C20** (blue), **C20*** (purple), glutathione (yellow, select peaks), GlutathioneDS (orange, select peaks).*

The properties of this species imply that is either an entirely different cobalt (III) **L20** assembly of the same symmetry or the original cage shifted by an exchange process that is slow on the NMR timescale. The movement of the second cage species over time implies either a fast exchange process or a response to a change in solution, potentially pH changes. The slower rate of overall degradation could be explained by the lower pH either reducing interactions between the cage and glutathione or the more likely the lower concentration of glutathione thiolate compared to thiol.

2.2.9 [^{99m}Tc]TcO_4^- binding in C20

With this new, more stable cage, the pertechnetate binding studies were revisited. When the binding studies were carried out with **C20**, it was found to also bind the radiotracer better than **C19** (Fig. 2.2.33).

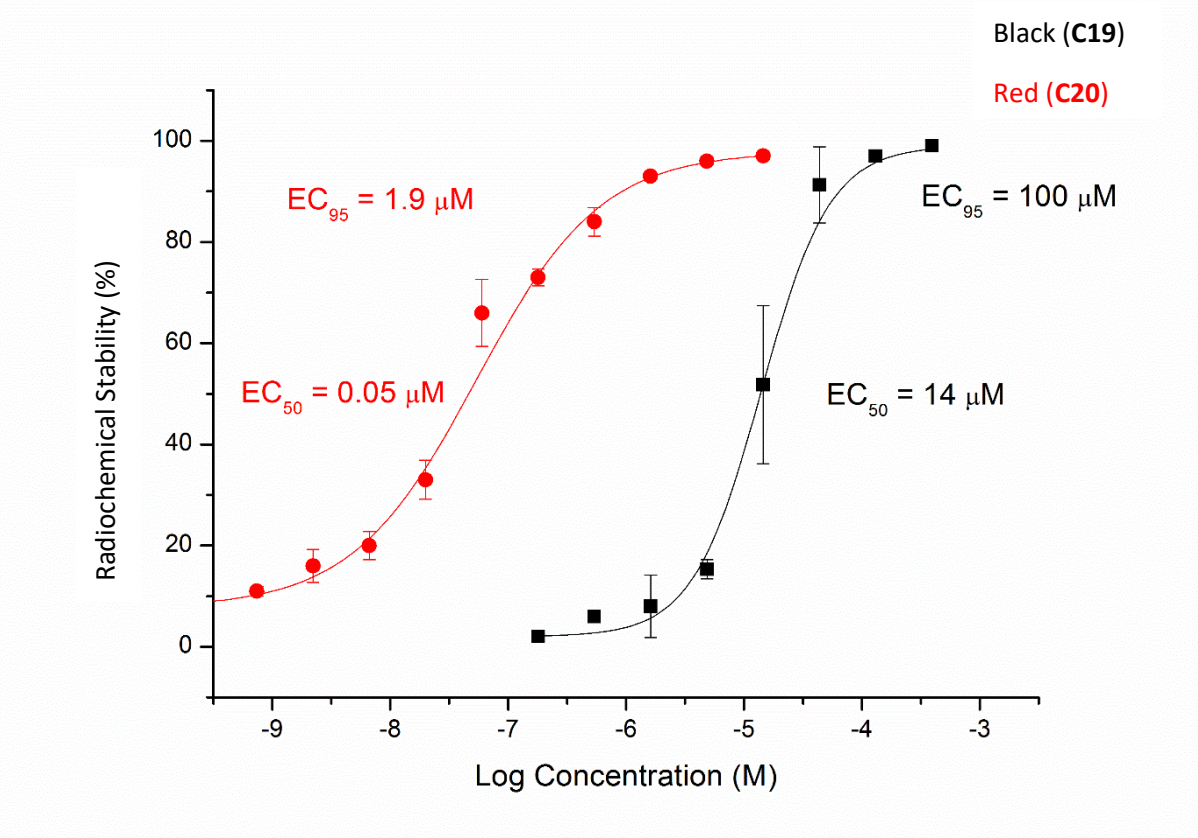

*Figure 2.2.33: Radiochemical yield for [^{99m}Tc]TcO_4^- encapsulation against concentration of **C19** (black) and **C20** (red). [^{99m}Tc]TcO_4^- (1 µL, 1 MBq) were added to cage solutions (100 µL), incubated for stated time at room temperature, before assessment by chromatography. Experiment performed in triplicate by Benjamin Burke.*

C20 appears to be 50 times more effective than **C19** at binding [^{99m}Tc]TcO_4. This result is surprising as it is not reflected in the results of the NMR studies with "cold" anions, which showed very similar binding of perrhenate in the two cages. **C20** being a better host than **C19** for [^{99m}Tc]TcO_4^- is difficult to rationalise as the cages are believed to be largely isostructural. The discrepancy between the results of the two techniques could either be caused by difference in the anion or the techniques.

Perrhenate is commonly used as a cold model for pertechnetate but some differences are apparent in their properties and interactions with hosts.[16] It is possible that these differences allow **C20** to differentiate between the two anions when **C19** cannot. The other explanation is the differences

between the techniques. The chromatographic analysis differs from the NMR studies as it does not monitor the interaction in solution but rather deposited on silica.

Deposition onto silica is regarded as a harsh procedure, known to degrade sensitive chemical groups. It is possible that **C19** is degraded by this deposition while the more stable **C20** is not, thereby artificially lowering the effective concentration of **C19**. However, the cages have been shown to be stable to both silanols and acid conditions which are the main chemical features of silica.[3]

Encapsulation of $[^{99m}Tc]TcO_4^-$ by **C20** was investigated in a number of different solutions (Fig. 2.2.34). These experiments showed similar results to those for **C19**, though the improved affinity of **C20** for $[^{99m}Tc]TcO_4^-$ was reflected by increased radiochemical yields. This implies that **C20** is actually more selective towards TcO_4^- but could still be explained by a higher concentration of undegraded cage. Again, this did not reflect the NMR analysis, which showed **C20** being slightly better than **C19** at binding perchlorate.

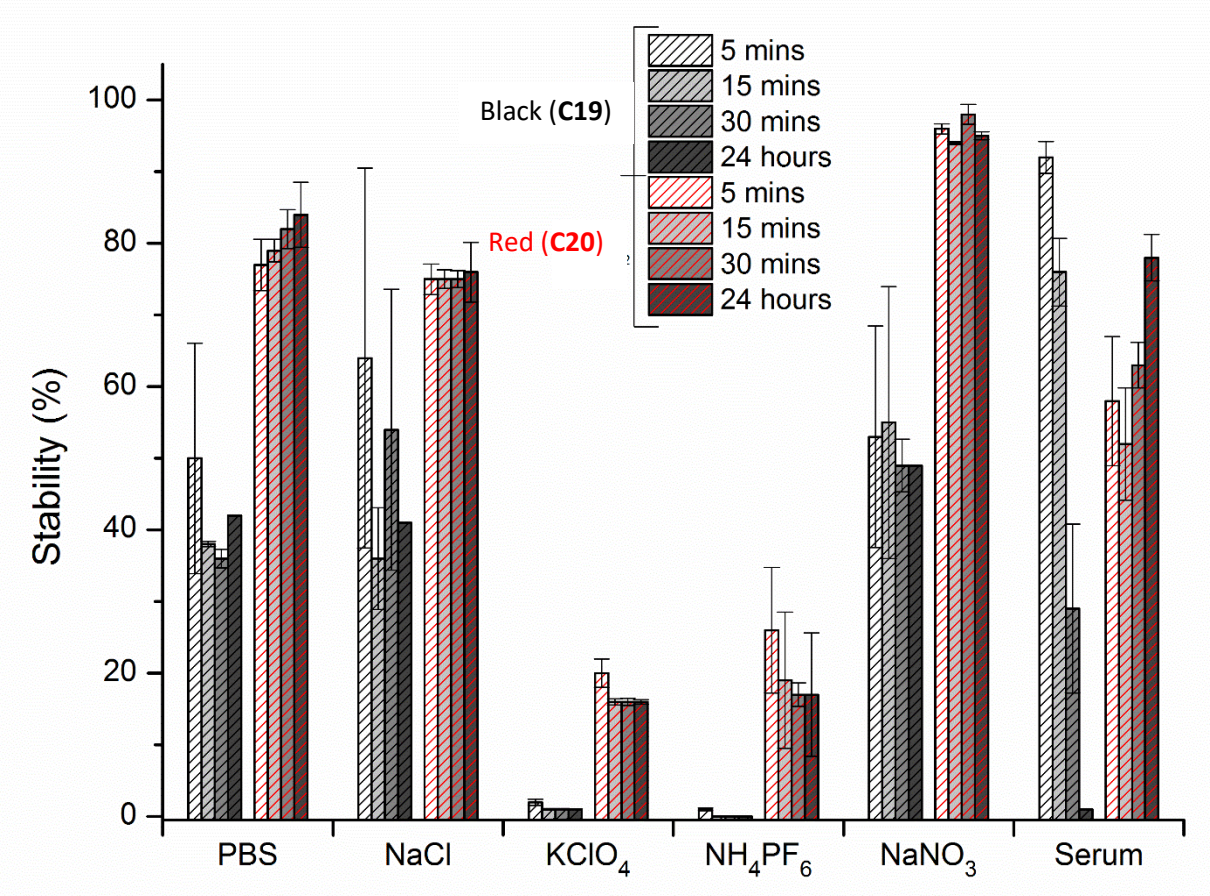

*Figure 2.2.34: Radiochemical yield of $[^{99m}Tc]TcO_4^-$ (1 MBq) in **C20** (132 µM) in various solutions over time. $[^{99m}Tc]TcO_4^-$ (1 µL, 1 MBq) and salt solution (50 µL, 0.1mM) were added to cage solutions (100 µL), incubated for stated time at room temperature, before assessment by chromatography. Experiment performed in triplicate by Benjamin Burke.*

Most importantly, the presence of serum did not cause **C20** to show a reduction of $[^{99m}Tc]TcO_4^-$ retention over time. No significant drop of radiochemical yield was observed over a 24 hour period indicating that the cage remains intact and able to bind the $[^{99m}Tc]TcO_4^-$ under these conditions.

These results, in combination with the glutathione studies, indicate that the functionalisation of the cage was effective at stabilising the cage against biological breakdown while retaining its ability to bind $[^{99m}Tc]TcO_4^-$. These properties suggested that **C20** may be suitable to act as radioligand for $[^{99m}Tc]TcO_4^-$ and so investigations turned to SPECT imaging.

2.2.10 *In vivo* SPECT imaging with $[^{99m}Tc]TcO_4^-[TcO_4\subset$**C20**$]$

With evidence that **C20** is able to bind $[^{99m}Tc]TcO_4^-$ under biological conditions, the cages were also assessed for cytotoxicity to get an idea of whether they could be safely administered to animals. This work, alongside imaging studies, was carried out by David Roberts, Isaline Renard, Rebecca Hargreaves, Christopher Cawthorne and Benjamin P. Burke at the University of Hull.

MTT assays found that the two cages possessed low cytotoxicity towards HeLa cells, with EC_{50} values of 31.4 μM for **C19** and 10.6 μM for **C20**. The toxicity values of the cages are low, especially in the context of the concentrations at which radioimaging agents are administered. However, a greater understanding of their biological activity and fate would be desirable.

With **C20** exhibiting good biological stability and low cytotoxicity, *in vivo* studies were initiated. Naïve anaesthetised mice were dosed with either $[^{99m}Tc]TcO_4^-$ or $[^{99m}Tc]TcO_4^-[TcO_4\subset$**C20**$]$ prior to a combined CT/SPECT acquisition. The biological uptake of pertechnetate is well understood, it is known to be taken up by sodium-iodide symporter (NIS). This receptor is mostly present in the thyroid but also the stomach and salivary and lacrimal glands, making these tissues the main location of pertechnetate uptake.[17]

The mice treated with unbound $[^{99m}Tc]TcO_4^-$ showed the expected uptake in the thyroid and stomach (Fig. 2.2.35, left). However, the mouse administered a solution of $[^{99m}Tc][TcO_4\subset$**C20**$]$ showed a marked difference in uptake with considerable activity present in the liver in addition to the stomach and thyroid (Fig. 2.2.35, right).

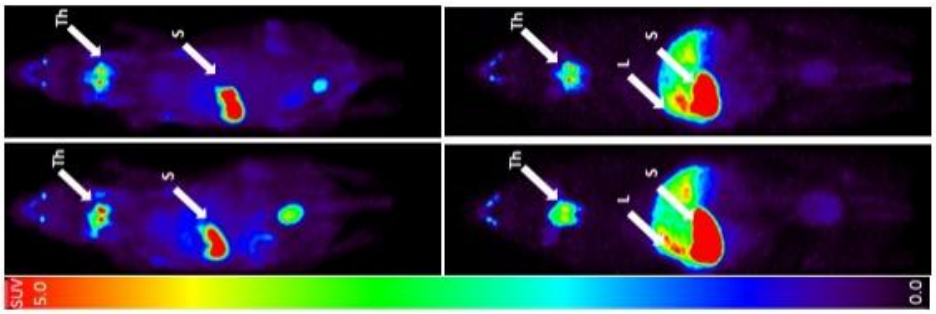

*Figure 2.2.35: (Left) Naïve mice dosed with free [^{99m}Tc]TcO_4^- solution (25-35 MBq), uptake apparent in thyroid and stomach. (Right) Naïve mice dosed with [^{99m}Tc]TcO_4^-[TcO_4⊂**C20**] (7-20 MBq), uptake apparent in liver as well stomach and thyroid . Animals dosed 20 minutes before 100-minute SPECT acquisition. Th = Thyroid, S = Stomach, L = Liver. Experiment performed by Benjamin Burke and Christopher Cawthorne.*

To further explore this difference of uptake, another three animals were dosed, killed and their organs collected and assessed for radioactivity (Fig. 2.2.36). These results confirm the host-guest complex showed considerable uptake in the liver.

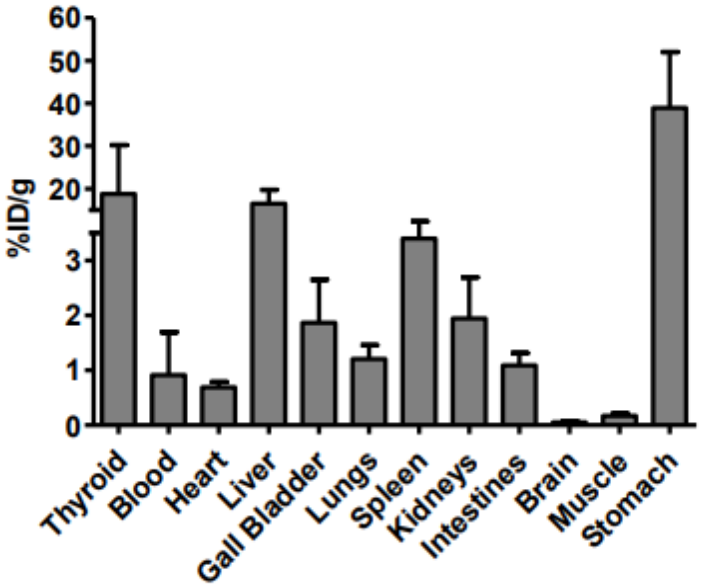

*Figure 2.2.36: Biodistribution of [^{99m}Tc][TcO_4⊂**C20**]$^{11+}$ in selected tissues from CD1-IGS mice 120 minutes after injection with [^{99m}Tc][TcO_4⊂**C20**]$^{11+}$ (6-8 MBq). All radioactivity values converted into %ID/g. Data are mean ± SD of 3 animals. Experiment performed by Benjamin Burke and Christopher Cawthorne.*

To assess the fate of pertechnetate in the liver, an aqueous extract of the dosed mouse's livers was taken, purified by centrifugation and investigated by TLC. When eluted with water, this extract exhibited 30% retention on the baseline, while elution with acetonitrile led to no retention. These

results are consistent with the extract containing $[^{99m}Tc][TcO_4 \subset \mathbf{C20}]^{11+}$, indicating that this is the species which was taken up by the liver.

The continued uptake in the thyroid and stomach likely represents dissociation of the anion from the cage. This is not unexpected and is likely due to the high dilution and prevalence of competing biological anions *in vivo*. This would lead to "bleeding" of free anion into the biological environment which will follow the standard uptake mechanism.

These results show that:

- The functionalised cage remains stable enough *in vivo* to retain a cavity fit to bind the guest
- The guest remains largely bound within the cavity of the cage *in vivo* during the experiment
- The host-cage complex exhibits significantly different uptake to the free anion

These results prove the potential for these cage systems as a radioligand capable of directly "ligating" the pertechnetate anion without the requirement for conventional chemistry. Bioconjugation of the cage prior to encapsulation would allow the synthesis of directed radioimaging agents by the simple addition of $[^{99m}Tc]TcO_4^-$ solution from the generator to these pre-formulated cages.

The results also provide evidence for the potential of this cage system for other biological applications. Examples of discrete cages that are stable *in vivo* are very rare and could have a huge number of biomedical applications in changing the biological behaviour of therapeutic or diagnostic molecules.

2.3 Summary

The previously developed Co_4(**L19**)$_6$$(NO_3)_{12}$ system was found to be promising as a radioligand for [^{99m}Tc]TcO_4^-, the precursor to all ^{99m}Tc based radioimaging agents. This suggested that the cage could be used as a supramolecular ligand for the radionuclide to provide a new and promising means of synthesising radiopharmaceuticals. However, further investigation found that Co_4(**L19**)$_6$$(NO_3)_{12}$ was susceptible to reduction by glutathione, making it insufficiently stable for *in vivo* use.

In order to counteract this instability a functionalised ligand (**L20**) was developed, which was substituted with an amine group to increase the strength of interaction with the metal centres and to improve the overall stability of the cage. Attempts at the direct formation of the tetrahedron through previously established methods were hindered by kinetic trapping of the byproducts due to the lack of reversibility in the strengthened coordination bonds.

A range of attempts made to facilitate the direct formation of the cage included elevated temperatures, strongly coordinating solvents, lowered pH, and protection of the amine group with an electron withdrawing group. Unfortunately, none of these measures were successful and purification of product mixtures was found to give very poor yields.

An effective means of synthesising the cage was found by substituting **L20** directly into Co_4(**L19**)$_6$$(NO_3)_{12}$. This allowed the exploitation of the prearrangement of the existing tetrahedra to prevent the formation of alternate assemblies. Co_4(**L20**)$_6$$(NO_3)_{12}$ was found to retain many of the properties of the previous cage and was found to be an even better host for [^{99m}Tc]TcO_4^-. The cage was also shown to be considerably more stable to biological conditions, resisting degradation by glutathione and retaining its binding of [^{99m}Tc]TcO_4^- in serum.

After determining that the cage had low cytotoxicity, *in vivo* radioimaging experiments were able to demonstrate [^{99m}Tc][TcO_4⊂**C20**]$^{11+}$ had different biological uptake to free [^{99m}Tc]TcO_4^- and that the host-guest complex could be recovered from the liver of dosed animals. This proves that **C20** is able to bind a medicinally significant guest *in vivo*, and that similar metallosupramolecular cages may be used as radioligands or drug delivery agents.

2.4 Experimental

General Information

Unless otherwise stated, all reagents and solvents were purchased from Alfa Aesar, Fluorochem, VWR or Sigma Aldrich and used without further purification. Anhydrous solvents: anhydrous DMF was obtained from Sigma Aldrich, other solvents were dried using a solvent purification system manufactured by Inert. Column Chromatography. Column chromatography was carried out using Geduran Si60 (40-63 µm), as the stationary phase. TLC was performed using pre-coated ALUGRAM plates, (0.2 mm, UV254) and observed under UV irradiation. Alumina chromatography was performed using Aluminium oxide, neutral, 50-200 microns, as the stationary phase. Size exclusion chromatography was performed using Sephadex LH-20 pre-swollen in the stated solvent. All reactions were carried out under N_2 atmosphere unless otherwise stated. Degassing of solvents was carried out by sparging with N_2 for a minimum of ten minutes.

Abbreviations used in this text:

DMSO	Dimethylsulfoxide
DMF	*N,N*-dimethylformamide
THF	Tetrahydrofuran
DCM	Dichloromethane
NMR	Nuclear Magnetic Resonance
COSY	Correlation Spectroscopy
DOSY	Diffusion ordered spectroscopy
NOESY	Nuclear Overhauser Effect Spectroscopy
HSQC	Heteronuclear Single Quantum Coherence
RT	Room Temperature
EDTA	Ethylenediaminetetraacetic acid
Na_4EDTA	Ethylenediaminetetraacetic acid tetrasodium salt
MS	Mass Spectrometry
pi	Penetration Index
MBq	Megabecquerel
MTT	3-(4,5-dimethylthiazol-2-yl)-2,5-diphenyltetrazolium bromide

All ^{1}H NMR spectra were recorded on either a 500 MHz Bruker AV III equipped with a DCH cryo-probe (Ava500) a 600 MHz Bruker AV IIIHD equipped with a TCL cryoprobe (Ava600) or a 400 MHz Bruker AV III equipped with a BBFO+ probe (Ava400). All ^{13}C NMR spectra were recorded on the Ava500. All

spectra recorded at a constant temperature of 300 K. All DOSY experiments were performed on either the Ava500 or Ava600 using bipolar gradient pulses for diffusion with two spoil gradients (ledbpg2s.compensated) pulse sequence. The sequence was carried out under automated conditions where the duration was 100 ms. Typically, in each PFG NMR experiment a series of 16 spectra on 32 K data points were collected and eddy current delay was set to 5 min in all experiments. The pulse gradients were incremented from 2 to 95% of the maximum gradient strength in a linear ramp. The temperature was set and controlled at 300 K with an air flow of 400 Lh^{-1} in order to avoid any temperature fluctuations due to sample heating during the magnetic field pulse gradients. The Stokes-Einstein equation was used to convert diffusion coefficient to hydrodynamic radius. The NMR data was processed using Topspin 2.1 and MestreLab Research MestReNova 11.0.0. Chemical shifts are reported in parts per million from low to high field and were referenced against values for the residual solvent peaks. Coupling constants (J) are reported as observed in Hz. Standard abbreviations indicating multiplicity were used as follows: m = multiplet, t = triplet, d = doublet, s = singlet, br(s/d) = broad (singlet/doublet etc.), appt = apparent triplet etc. Mass spectrometry of organic compounds was carried out on a high resolution Bruker ToF instrument, mass spectrometry (ESI-MS) of complexes was carried out using a Waters SYNAPT G2 instrument.

Synthesis of ligands

Safety Notice: Alkyltin compounds are all highly toxic and should be handled with great caution. Tributyltin chloride is highly toxic, readily absorbed through the skin, and relatively volatile; it and other tributyltin derivatives should be only be handled within a fume cupboard, and extreme vigilance is recommended in handling the viscous oil in the reaction to make **N2**. Tributyltin chloride is regenerated in Stille cross coupling reactions, meaning that the Stille couplings to make **N5** and **N7** should be carried out and worked up with the same caution. All glassware that has been in contact with tin compounds should be thoroughly washed into a clearly marked and sealable “tin waste” for proper disposal. Glassware should preferably be washed with bleach before being returned to general use.

Fragments 5-bromo-2,2’-bipyridine (**N22**) ,[36] 5-bromo-2-(tributylstannyl)pyridine (**N2**),[29] and *tert*-butyl-*N*-(2-bromopyridin-4-yl)carbamate (**N9**),[37] were synthesised according to literature procedure.

L19

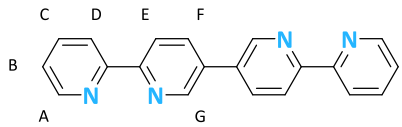

A solution of NiCl (0.174 g, 1.34 mmol) and PPh_3 (1.34 g, 5.10 mmol) in DMF (12.0 mL) was heated at 50 °C for 0.5 h under N_2. The resulting blue suspension was treated with Zn (powder, 90.3 mg, 1.38 mmol) to produce a red brown suspension after 0.5 h, to which **N22** (0.299 g, 1.27 mmol) in DMF (6.0 mL) was added and the mixture stirred at RT for 3 days. To this, Na_4EDTA (0.25 M, 60 mL, 15.0 mmol) was added and the aqueous layer washed with dichloromethane (5 × 100 mL) and brine added (20 mL). The combined organic layers were dried over $MgSO_4$, the solvent removed *in vacuo* and purified by silica flash column (dichloromethane, 1% trimethylamine, 1% methanol). This was crystallised in hot acetonitrile to give white plate crystals. Yield = 0.126 g (64%).

M.p. 233-235 °C, ^{1}H NMR (600 MHz, $CDCl_3$): δ 9.03 (dd, *J* = 2.4, 0.8 Hz, 2H, H_G), 8.75 (d, *J* = 4.8 Hz, 2H, H_A), 8.58 (dd, *J* = 8.3, 0.8 Hz, 2H, H_E), 8.50 (d, *J* = 8.0 Hz, 2H, H_D), 8.13 (dd, *J* = 8.3, 2.4 Hz, 2H, H_F), 7.89 (t, *J* = 7.6 Hz, 2H, H_C), 7.38 (dd, *J* = 7.6, 4.8 Hz, 2H, H_B). ^{13}C NMR (151 MHz, CDCl3): δ 155.8, 155.6, 149.3, 147.5, 137.0, 135.2, 133.1, 124.0, 121.2, 121.2. HR-ESI: m/z 311.12890 (predicted [M+H]+ = 311.12912), 333.11180 (predicted [M+Na]+ = 333.11107).

N5

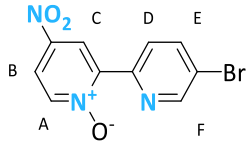

N3 (4.039 g, 18.4 mmol), $Pd(PPh_3)_4$(1.04 g, 0.901 mmol) and **N2** (8.29g, 18.5 mmol) were combined in toluene (80 mL) and heated at 100 °C for 24 h under N_2. The mixture was allowed to cool to room temperature, diluted with dichloromethane (30 mL) and filtered. The solvent was removed from filtrate *in vacuo*. The crude product was crystallised from hot ethanol and then purified by silica flash column (gradient: dichloromethane to dichloromethane, 4% diethyl ether) to give a colourless powder. Yield = 3.07 g (57%).

^{1}H NMR (500 MHz, Chloroform-*d*) δ 9.19 (d, J = 3.3 Hz, 1H, H_F), 8.90 (dd, J = 8.6, 0.7 Hz, 1H, H_A), 8.84 (dd, J = 2.4, 0.7 Hz, 1H, H_C), 8.35 (d, J = 7.2 Hz, 1H, H_D), 8.08 (dd, J = 7.2, 3.3 Hz, 1H, H_E), 8.01 (dd, J = 8.6, 2.4 4 Hz, 1H, H_B). ^{13}C NMR (126 MHz, Chloroform-*d*) δ 151.1, 147.56, 146.0, 142.7, 142.3, 139.5, 126.2, 122.9, 122.5, 119.2. HR-ESI: m/z 295.96780 (predicted [M+H]+ = 295.96653), 317.9480 (predicted [M+Na]+ = 317.94847).

N7

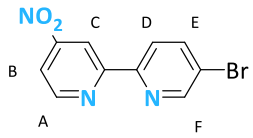

N8 (1.0008g, 4.9300 mmol), $Pd(PPh_3)_4$ (282 mg, 0.1811 mmol) and **N1** (2.268g, 5.073 mmol) were combined in toluene (25 mL) and heated at 110 °C for 48 h under N_2. The mixture was allowed to cool to room temperature, diluted with toluene (30 mL) and filtered. The solvent was removed from filtrate *in vacuo*. The crude product was purified by silica flash column (gradient: dichloromethane to dichloromethane, 2% diethyl ether) and then recrystallized from acetonitrile to give colourless needles. Yield = 660 mg, (48%).

^{1}H NMR (500 MHz, Chloroform-*d*) δ 9.12 (dd, *J* = 2.2, 0.7 Hz, 1H, H_C), 8.94 (dd, *J* = 5.3, 0.7 Hz, 1H, H_A), 8.78 (dd, *J* = 2.3, 0.8 Hz, 1H, H_F), 8.38 (dd, *J* = 8.5, 0.7 Hz, 1H, H_D), 8.03 (dd, *J* = 5.3, 2.2 Hz, 1H, H_B), 8.00 (dd, *J* = 8.5, 2.3 Hz, 1H, H_E). ^{13}C NMR (126 MHz, Chloroform-*d*) δ 158.7, 155.2, 152.6, 151.5, 150.8, 140.0, 122.8, 122.7, 116.2, 113.9. HR-ESI: m/z 279.9752 (predicted [M+H]+ = 279.9716).

N6

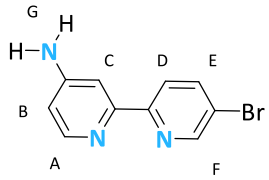

N5 (1.66g, 5.60 mmol) and Fe (fillings, 1.67g, 29.9 mmol) were combined in acetic acid (50 mL) and heated at 100 °C for 3 h under N_2. The mixture was allowed to cool to room temperature and a solution of NaOH (10.54 g, 0.27 mol), EDTA (17.564g, 60.1 mmol) in water (50 mL) and ammonium hydroxide (30 %, 100 mL) was added slowly. The mixture was then extracted with chloroform (3 x 150 mL) and the combined organic phases were dried over $MgSO_4$. The solvent was removed *in vacuo* and the crude product was crystallised from hot toluene to give pale yellow needle crystals. Yield = 1.03 g (74%).

^{1}H NMR (600 MHz, Chloroform-*d*) δ 8.68 (d, *J* = 2.4 Hz, 1H, H_F), 8.32 – 8.25 (m, 2H, $H_{A,D}$), 7.91 (dd, *J* = 8.5, 2.4 Hz, 1H, H_E), 7.64 (d, *J* = 2.5, 0.5 Hz, 1H, H_C), 6.57 (dd, *J* = 5.5, 2.4 Hz, 1H, H_B), 4.24 (s, 2H, H_G). ^{13}C NMR (126 MHz, Chloroform-*d*) δ 156.0, 155.0, 153.7, 150.1, 139.6, 122.6, 121.1, 110.0, 106.9. HR-ESI: *m/z* 249.99910 (predicted $[M+H]^+$ = 249.99744).

^{1}H NMR (601 MHz, DMSO-d_6) δ 8.74 (dd, *J* = 2.4, 0.7 Hz, 1H, H_F), 8.25 (dd, *J* = 8.5, 0.7 Hz, 1H, H_D), 8.12 (dd, *J* = 8.5, 2.4 Hz, 1H, H_E), 8.09 (d, *J* = 5.5 Hz, 1H, H_A), 7.57 (d, *J* = 2.3 Hz, 1H, H_C), 6.53 (dd, *J* = 5.5, 2.3 Hz, 1H, H_B), 6.23 (s, 2H, H_G).

L20

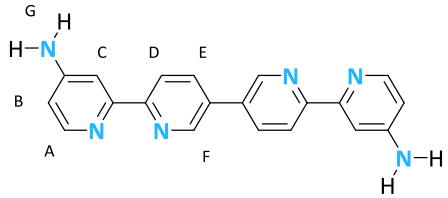

$NiCl_2$ (779.5 mg, 6.01 mmol) and PPh_3 (638.5 mg, 2.43 mmol) were combined in DMF (50 mL) and heated at 50 °C for 24 h under N_2. The mixture turned an intense blue with some yellow material visible. Zn (powder, 375.6 mg, 5.74 mmol) was added causing an immediate colour change to red and then black. The mixture was left stirring for 1 h before a solution of **N6** (1.272 g, 0.51 mmol) in DMF (5 mL) was added and then left stirring for 48 h. The solvent was removed *in vacuo* and a Na_4EDTA solution was added to the residue and then refluxed for 72 h. A beige suspension was collected by filtration and then extracted with 2 × 100 mL chloroform/methanol (1:1, 100 mL) and 2 × 100 mL THF. The solvent was removed from the extractants *in vacuo*. The residue was heated in acetonitrile (100 mL), allowed to cool and collected by filtration to give a beige solid. Yield = 695 mg (80%).

M.p. 342 °C decomposition. ^{1}H NMR (500 MHz, DMSO-d_6) δ 9.09 (dd, J =2.4, 0.8 Hz, 1H, H_F), 8.45 (dd, J = 8.3, 0.8 Hz, 1H, H_D), 8.33 (dd, J = 8.3, 2.4 HZ, 1H, H_E), 8.15 (d, J = 5.5 Hz, 1H, H_A), 7.70 (d, J = 2.3 Hz, 1H, H_C) 6.56 (dd, J = 5.5, 2.3 Hz, 1H, H_B), 6.21 (s, 2H, H_G). ^{13}C NMR (126 MHz, DMSO-d) δ 155.7, 155.2, 154.8, 149.4, 147.0, 134.8, 132.0, 120.4, 109.1, 105.6. HR-ESI: m/z 341.15240 (predicted $[M+H]^+$ = 341.15092), 363.1339 (predicted $[M+Na]^+$ = 363.1334).

^{1}H NMR (500 MHz, Methanol-d_4) δ 9.03 (dd, J = 2.3, 1.0 Hz, 1H), 8.34 – 8.28 (m, 2H), 8.16 (d, J = 5.8 Hz, 1H), 7.59 (d, J = 2.3 Hz, 1H), 6.69 (dd, J = 5.8, 2.4 Hz, 1H).

N10

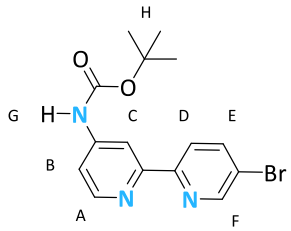

N6 (303.2 mg, 1.21 mmol) and di-*tert*-butylcarbonate (326.1 mg, 1.13 mmol) were placed in a 2-5 mL sealed vial with septum under N_2. Dichloromethane (5 mL) and trimethylamine (0.5 mL) were added and the mixture sparged with N_2 for five minutes and heated at 50 °C for 48 h. The solvent was removed *in vacuo* and the crude product purified by silica gel chromatography (19:1 dichloromethane/diethylether) to give an off-white solid. Yield= 69 mg (17%).

^{1}H NMR (601 MHz, Chloroform-d) δ 8.72 (d, J = 2.3 Hz, 1H, H_F), 8.53 (d, J = 5.5 Hz, 1H, H_A), 8.32 (d, J = 8.5 Hz, 1H, H_D), 8.22 (d, J = 2.2 Hz, 1H, H_C), 7.95 (dd, J = 8.5, 2.3 Hz, 1H, H_E), 7.58 (dd, J = 5.5, 2.2 Hz, 1H, H_B), 6.76 (s, 1H, H_G), 1.57 (s, 9H, H_H). ^{13}C NMR (126 MHZ, Chloroform-d) δ 150.5, 150.3, 139.7, 122.6, 112.7, 109.8, 28.5. Only H_C of the quaternary carbons could not be detected.

L22

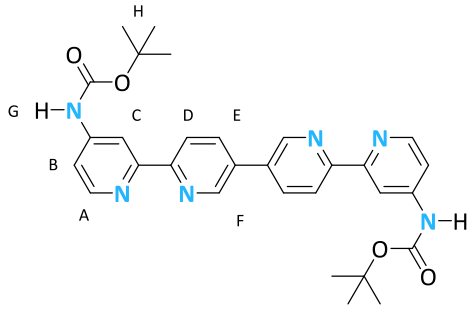

$NiCl_2$ (162.3 mg, 0.48 mmol) and PPh_3 (52.4 mg, 0.20 mmol) were combined in in DMF (2 mL) and heated at 50 °C for 1 h under N_2. The resulting blue suspension was treated with Zn (powder, 35.7 mg, 0.55 mmol) to produce a red brown suspension after 0.5 h, to which **N10** (168.6 mg, 0.48 mmol) in

DMF (2 mL) was added and the mixture stirred at RT for 3 d. A solution of EDTA (703.4 mg, 2.41 mmol) and NaOH (385.0 mg, 9.63 mmol) in ammonium hydroxide solution (30%, 20 mL) was added to the mixture and the mixture stirred for 24 h. The colourless precipitate was collected by filtration, extracted with THF (50 mL) and the solvent removed *in vacuo*. The crude product was crystallised from hot acetonitrile to give a colourless powder. Yield = 39 mg (30%).

^{1}H NMR (601 MHz, DMSO-d_6) δ 10.00 (s, 2H, H_G), 9.16 (dd, J = 2.4, 0.8 Hz, 2H, H_F), 8.67 (d, J = 2.2 Hz, 2H, H, H_C), 8.49 (d, J = 5.5 Hz, 2H, H_A), 8.49 (d, J = 8.3 Hz, 2H, H_D), 8.38 (dd, J = 8.3, 2.4 Hz, 2H, H_E), 7.48 (dd, J = 5.5, 2.2 Hz, 2H, H_B), 1.52 (s, 18H, H_H). ^{13}C NMR (126 MHz, DMSO-d_6) δ 193.2, 192.6, 190.1, 187.6, 185.2, 185.0, 172.8, 170.03, 158.2, 150.3, 146.7, 117.8, 65.6. HR-ESI: *m/z* 541.2582 (predicted $[M+H]^+$ = 541.2558), 563.2395 (predicted $[M+Na]^+$ = 563.2377).

Synthesis of capsules

C19 synthesised according to previous procedure.[38]

General procedure for attempted C20 Synthesis

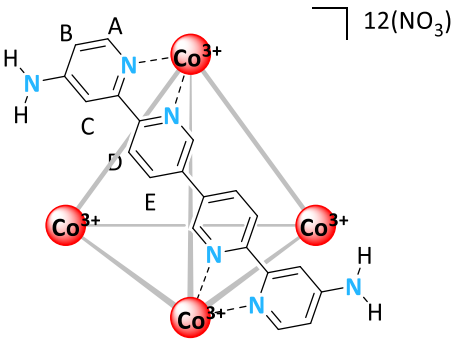

$Co(NO_3)_2.6(H_2O)$ (1 equivalent, approximately 50 µ) and **L20** (1.5 equivalents) were suspended in a mixture of degassed water and co-solvent (9:1, approx. 22.1 mM with respect to **L20**) under N_2. The reaction was heated at the stated temperature for 2-12 hours and allowed to cool. $(NH_4)_2Ce(NO_3)_6$ (1.5 equivalents) in acetonitrile (approx. 22.85 mM) and was added to the reaction mixture. Dilution with acetonitrile induced an orange precipitate which was isolated by filtration on celite and washed with acetonitrile. The retentate was eluted with water and freeze-dried to give the crude product.

Example

$Co(NO_3)_2.6(H_2O)$ (17.2 mg, 59.1 µmol) and **L20** (30.1 mg, 88.4 µmol) were suspended in a mixture of degassed water-acetonitrile (9:1, 4mL) and heated in a microwave reactor for 2 h at 80 °C. The reaction was cooled to room temperature before $(NH_4)_2Ce(NO_3)_6$ (501 mg, 91.4 µmol) in acetonitrile (4 mL) was added via syringe pump (4.2 µL min^{-1}). Dilution with acetonitrile (40 mL) induced precipitation, this was isolated by filtration onto celite and washed with acetonitrile. The retentate was eluted with

water and freeze-dried to give an orange solid. It was then purified by size exclusion chromatography on sephadex LH-20 gel in water and freeze-dried to give an orange solid. Yield = 11 mg (26%).

^{1}H NMR (600 MHz, D_2O) δ 8.55 (d, J = 8.4 Hz, 12H, H_D), 7.92 (d, J = 2.7 Hz, 12H, H_C), 7.78 (dd, J = 8.4, 1.8 Hz, 12H, H_E), 7.31 (d, J = 1.8 Hz, 12H, H_F), 6.99 (d, J = 7.0 Hz, 12H, H_A) 6.81 (dd, J = 7.0, 2.7 Hz, 12H, H_B). ^{13}C NMR (126 MHz, D_2O) δ 158.4, 156.5, 153.4, 148.5, 143.2, 137.3, 124.6, 114.7, 112.0, 110.0.. ^{1}H DOSY NMR (500 MHz, D_2O): D 22 = 2.14 x 10-6 cm^2 s^{-1} ; calculated hydrodynamic radius = 11.5 Å. ESI-MS ESI-MS (m/z): 369.5 (7+), 315.6 (8+).

Suspected helicate H20

^{1}H NMR (601 MHz, Deuterium Oxide) δ 8.56 – 8.49 (m, 24H), 7.77 (d, *J* = 2.7 Hz, 12H), 7.35 (d, *J* = 1.9 Hz, 12H), 6.85 (dd, *J* = 7.1, 2.7 Hz, 12H), 6.61 (d, *J* = 7.1 Hz, 12H). ^{1}H DOSY NMR (500 MHz, D_2O): D 22 = 2.84 x 10-6 cm^2 s^{-1} ; calculated hydrodynamic radius = 8.6 Å.

Ligand exchange reactions

NMR trial

C19 (5 mg, 1.759 µM) was dissolved in D_2O (1170 µL,) and CD_3CN (130 µL) in an NMR tube. A "zero time point" ^{1}H NMR was acquired. **L20** (9 or 12 equivalents) was added and the mixture was sonicated for five minutes. The reaction was sealed and heated at 75 °C and the mixture periodically allowed to cool before ^{1}H NMR acquired.

NMR trial with $Co(NO_3)_2.6H_2O$

C19 (5mg, 1.76 µmol) was dissolved in D_2O (854 µL) and CH_3CN (98 µL) in a NMR tube, **L20** (7.2 mg, 21.2 µmol, 12 equivalents) was added and the mixture sparged with argon. An aqueous solution of $Co(NO_3)_2.6H_2O$ (2 mM, 23 µL) was added the mixture sparged again. The reaction was sealed and heated at 75 °C and the mixture periodically allowed to cool and ^{1}H NMR acquired.

After the reaction was finished the reaction mixture was filtered onto celite and the retentate washed with water. The filtrate was freeze-dried to give the crude product. This was purified by size exclusion chromatography on sephadex LH-20 gel in water under gravity. 1 mL fractions were collected of all coloured material and the purity assessed by ^{1}H NMR. Pure **C20** fractions were combined and freeze-dried to yield the product as an orange powder. Yield = 5 mg (71%).

Preparative scale Ligand exchange

L20 (28.4 mg, 83.4 µmol) was suspended in a solution of **C19** (20.2mg, 7.04 µmol) in degassed acetonitrile (9:1, 3.9 mL), an aqueous solution of $Co(NO_3)_2.6(H_2O)$ (2 mM, 141 µL) was added, the mixture sparged with N_2 and heated at 75 °C in a sealed vial. The mixture was allowed to cool, filtered through celite and the retentate washed with water (5 mL). The filtrate was freeze-dried, dissolved in

water (2 mL), purified by size exclusion chromatography on sephadex LH-20 gel (see above) and freeze-dried to give an orange solid. Yield = 12 mg, 56%).

^{1}H NMR (600 MHz, D_2O) δ 8.55 (d, J = 8.4 Hz, 12H, H_D), 7.92 (d, J = 2.7 Hz, 12H, H_C), 7.78 (dd, J = 8.3, 1.8 Hz, 12H, H_E), 7.31 (d, J = 1.8 Hz, 12H, H_F), 6.99 (d, J = 7.0 Hz, 12H, H_A) 6.81 (dd, J = 7.0, 2.7 Hz, 12H, H_B). ^{13}C NMR (126 MHz, D_2O) δ 158.3, 156.4, 153.3, 148.4, 143.1, 137.2, 124.5, 114.6, 111.9, 109.9. ^{1}H DOSY NMR (500 MHz, D_2O): D 22 = 2.14 x 10-6 cm^2 s^{-1}; calculated hydrodynamic radius = 11.5 Å. ESI-MS ESI-MS (m/z): 369.5 (7+), 315.6 (8+).

NMR Guest Binding Studies

K_a for cage and guest combinations determined through ^{1}H NMR titration in unbuffered D_2O. A solution of compounds cage with a guest compound was titrated into a solution of cage, thereby maintaining a constant concentration of cage. With anion guests, addition of more than approximately two equivalents led to precipitation, preventing further data acquisition. Where possible, different cage peaks were plotted separately before using a global fitting technique. Some peaks omitted due to overlap with other peaks.

Fast exchange determination

All observable shifts in the ^{1}H NMR spectra had their peak position plotted against concentration of guest. A global non-linear curve fitting function was then applied to the combined plots using the 1:1 binding model given by:

$$y = y_0 + \Delta y \left(\frac{\left(1 + K_a(P + x)\right) - \sqrt{\left(1 + K_a(P + x)\right)^2 - 4K_aK_aPx}}{2K_aP} \right)$$

y_0 = $peak\ position\ wiht\ no\ guest$

Δy = $peak\ position\ with$ 100% $bound$

x = $concentration\ of\ guest$

P = $concentration\ of\ cage$

Origin Function = y=y0+DY*((1+Ka*(P+x))-sqrt(((1+Ka*(P+x))^2)-4*Ka*Ka*P*x))/(2*Ka*P)

NMe_4ClO_4 in C19

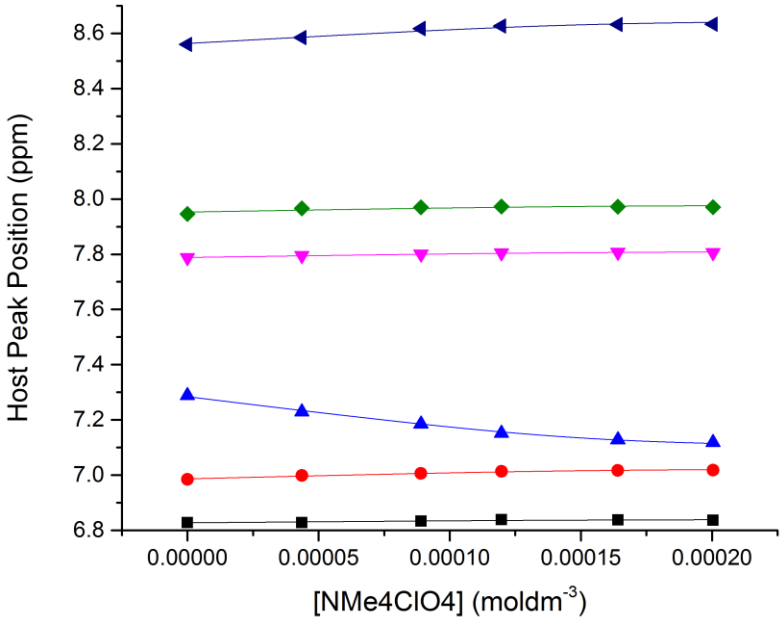

*Figure 2.4.1: Fitted curves for change in peak positions for NMe_4ClO_4 in **C19**.*

Slow exchange determination

Concentration of guest⊂cage was calculated from ^{1}H NMR integrals and plotted against guest concentration. A non-linear curve fitting function was then applied to the plot using the 1:1 binding model given by:

$$y = \frac{\left(x + P + \left(\frac{1}{K_a}\right)\right) + \sqrt{\left(x + P + \left(\frac{1}{K_a}\right)\right)^2 - (4Px)}}{2}$$

$$x = concentration\ of\ guest$$

$$y = Concentration\ of\ host\ guest\ complex$$

$$P = concentration\ of\ host$$

Origin function = ((x+h+(1/K))-((x+h+(1/K))^2-(4*h*x))^(1/2))/2

K_4ReO_4 in C19

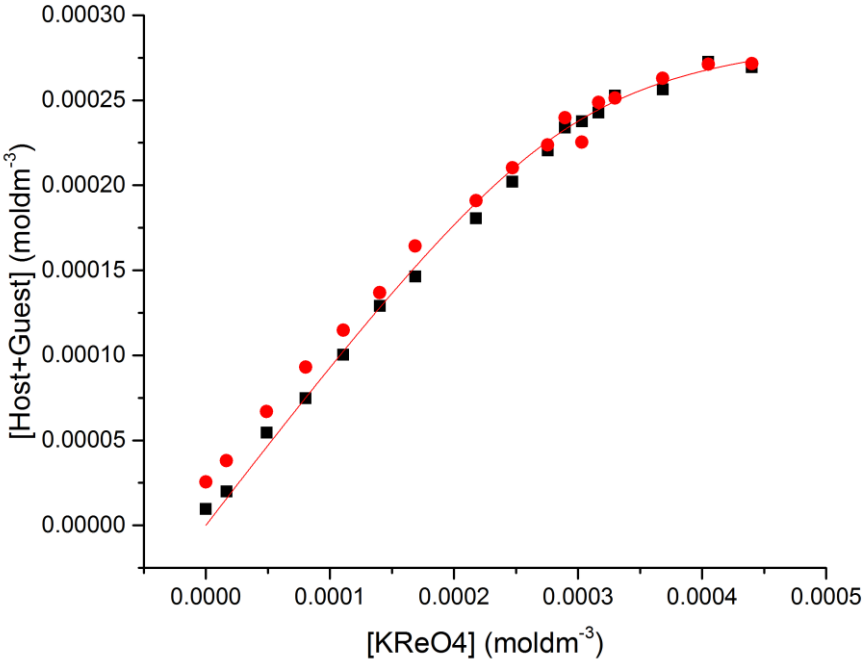

*Figure 2.4.2: Fitted curve for concentration (independent peaks plotted separately) of host+guest complex for K_4ReO_4 in **C19**.*

$KReO_4$ in C20

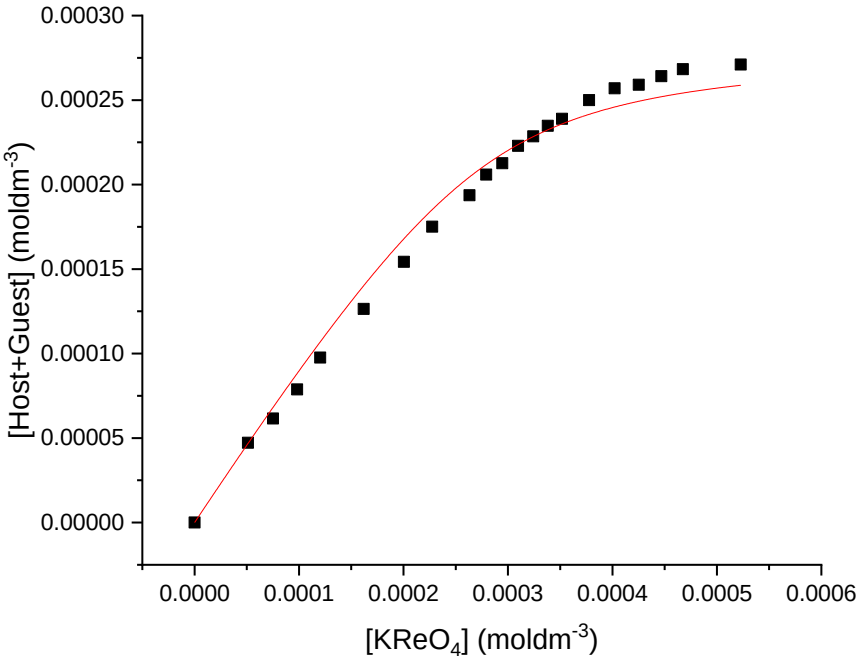

*Figure 2.4.3: Fitted curve for concentration of host+guest complex for K_4ReO_4 in **C20**.*

MTT Studies

Benjamin Burke

HeLa cells were plated onto a 96-well plate in Dulbecco's Modified Eagle Medium (DMEM) (10% in PBS) (100 µL) at approximately 8000 cells/mL. The plate was incubated for 20 h. The DMEM was removed and replaced with a solution of the stated compound in DMEM (100 µL); each concentration was added to seven wells. The plate was incubated for another 20 h before the removal of DMEM and washing of the cells with PBS. A 1.2 mM solution 3-[4,5-dimethylthiazol-2-yl]-2,5-diphenyl-2H tetrazolium bromide (5 mg) in media/PBS (7/3, 10 mL) was prepared and 100 µL added to each well. This was incubated for 3 h, at which point crystals were apparent. A solubilising solution (prepared: 5 mL Triton-X 100, 45 mL Isopropanol, 1 drop HCl (12M)) (100 µL) was added and the plate shaken on a plate shaker overnight to ensure complete dissolution of crystals. UV-visible absorbance measurements were carried out at 490 nm. For each concentration of the added compound the absorbances were averaged (discarding those more than two standard deviations from the mean). The absorbances were then normalised against those of untreated cells.

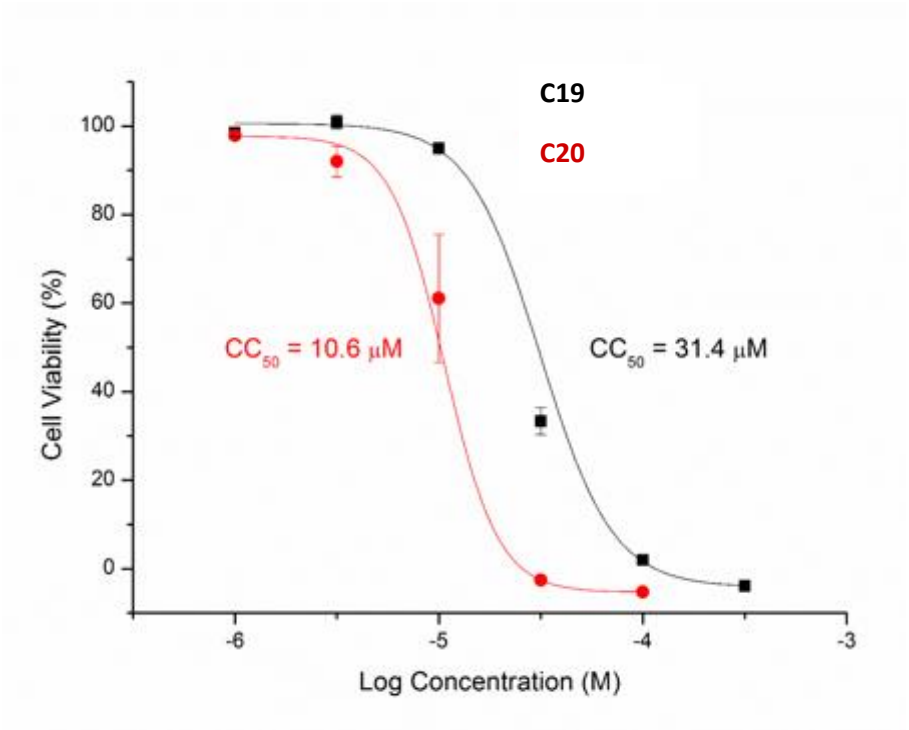

*Figure 2.4.4: Plot of cell viability versus concentration of (**C19**, black) and (**C20**, red).*

Pertechnetate Binding Studies,

Benjamin Burke

[^{99m}Tc]TcO_4 – was eluted from a 2.15 GBq Ultra-TechneKow™ DTE ^{99}Mo/^{99m}Tc generator (Mallinckrodt, UK) in 4 mL 0.9% saline solution. [^{99m}Tc]TcO4 – (1 µL, 1 MBq) was then added to **C19** or **C20** solutions (100 µl) and incubated at room temperature for 5 minutes. Pertechnetate encapsulation was assessed by silica gel thin layer chromatography, wherein eluting with DI water separates free [^{99m}Tc]TcO_4^-, which runs with the solvent front, while bound [^{99m}Tc]TcO_4^- complex remains on the baseline. The proportion of bound and free [^{99m}Tc]TcO_4^- was determined by cutting the eluted TLCs into 10 mm strips and independently analysing using a Wallac 1480 Wizard 3" automatic-gamma-counter (Perkin Elmer, USA). All reactions were carried out in DI water. [^{99m}Tc][TcO_4⊂cage]$^{11+}$ was spin filtered using a 10 kDa MWCO centrifuge filter (12,000 g, 5 minutes), during which 79% ± 1.6 of the activity passes through the filter. TLC analysis demonstrated [^{99m}Tc][TcO4⊂cage]$^{11+}$ remained >99% stable in the filtrate.

Pertechnetate Binding Controls

See table 2.2.1 for assembly structures

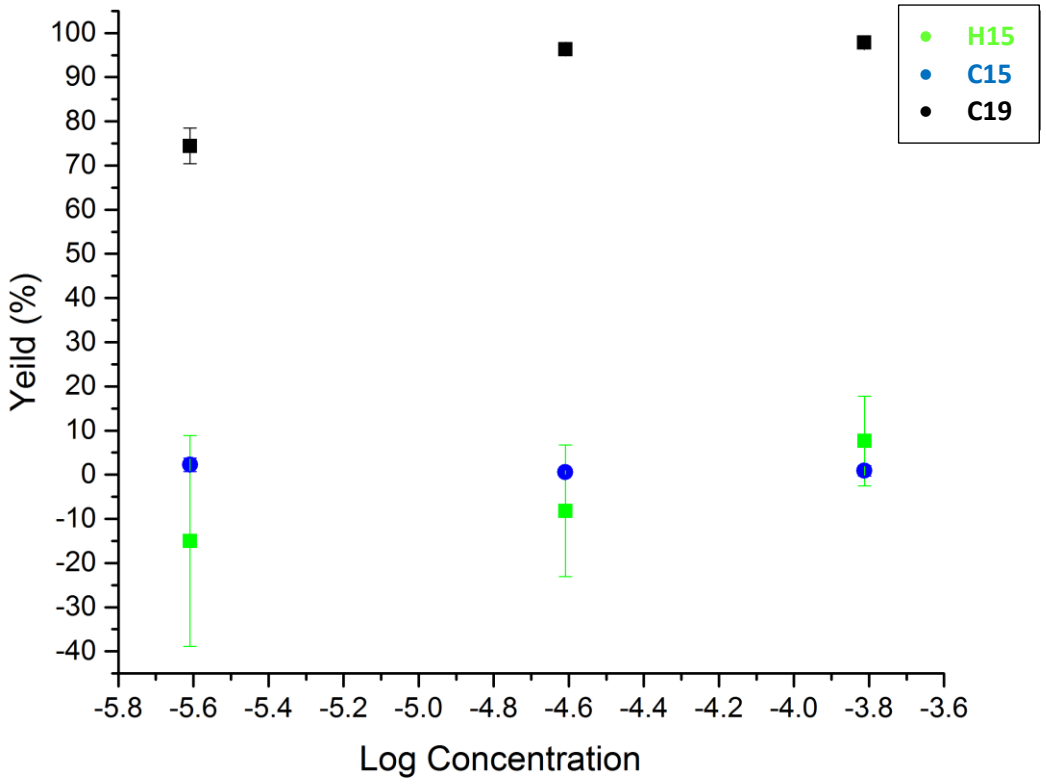

*Figure 2.4.4: Plot of yield (%) versus log concentration of **C15** (green), **C15** (blue), and **C19** (black).*

Glutathione Assays

Deuterated phosphate buffered saline (pH 7.4, 1 M) was prepared using D_2O with 1 mM ^tBuOH as an internal standard.

Stock solutions of cages were prepared to a concentration of approximately 0.3 mM in deuterated PBS or D_2O (with 1 M ^tBuOH internal standard). 0.45 mL of these solutions were placed in NMR tubes. Solutions of glutathione (25 mM, 10 equivalents) were added to samples and the samples monitored by ^1H NMR (600 MHz).

Characterisation of glutathione and glutathione disulphide

Glutathione

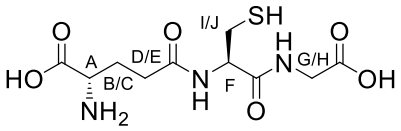

^1H NMR (601 MHz, Deuterium Oxide) δ 4.61 (dd, *J* = 6.8, 5.4 Hz, 1H, H_F), 4.01 (s, 2H, $H_{G/H}$), 3.87 – 3.83 (m, 1H, H_A), 3.02 – 2.95 (m, 2H, H, $H_{I/J}$), 2.59 (apthept, *J* = 7.8 Hz, 2H, $H_{D/E}$), 2.21 (aptq, *J* = 8.4, 7.8 Hz, 2H, $H_{B/C}$).

^1H NMR (601 MHz, Deuterium Oxide 1M PBS) δ 4.62 (d, *J* = 6.2 Hz, 1H, H_F), 3.82 (s, 2H, $H_{G/H}$), 3.82 (t, *J* = 6.3 Hz, 1H, H_A), 3.02 (dd, *J* = 13.4, 4.7 Hz, 1H, $H_{I/J}$), 2.98 (dd, *J* = 14.2, 6.9 Hz, 1H, $H_{I/J}$), 2.68 – 2.55 (m, 2H, $H_{B/C}$), 2.22 (aptq, *J* = 7.3 Hz, 2H, $H_{D/E}$).

Glutathione sulphide

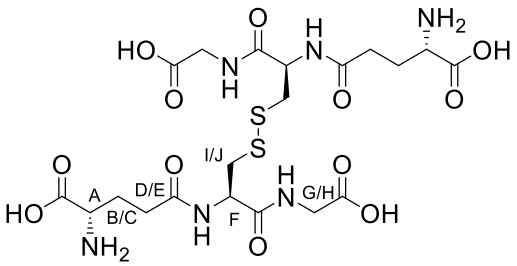

^1H NMR (500 MHz, Deuterium Oxide) δ 4.00 (s, 4H, $H_{G/H}$), 3.85 (d, *J* = 6.3 Hz, 2H, H_A), 3.32 (dd, *J* = 14.5, 4.7 Hz, 2H, H_F), 3.02 (dd, *J* = 14.3, 9.3 Hz, 2H, H_I), 2.56 (apthept, *J* = 7.6 Hz, 4H, $H_{D/E}$), 2.20 (aptq, *J* = 7.3 Hz, 4H, $H_{B/C}$). H_J covered by water peak

^1H NMR (601 MHz, Deuterium Oxide 1M PBS) δ 3.93 (s, 4H, $H_{G/H}$), 3.84 (t, *J* = 6.3 Hz, 2H, H_A), 3.34 (dd, *J* = 14.3, 4.6 Hz, 2H, H_F), 3.03 (dd, *J* = 14.3, 9.4 Hz, 2H, H_I), 2.65 – 2.52 (m, 4H, $H_{D/E}$), 2.21 (td, *J* = 7.7, 6.3 Hz, 4H, $H_{B/C}$). H_J at approximately 4.8 covered by water peak.

In vivo Studies

Benjamin Burke, Christopher Cawthorne

Mice were injected *i.v.* with 25-35 MBq of [^{99m}Tc]TcO_4^- and 7-20 MBq of caged (**C20**) [^{99mTc}]TcO_4^- under anaesthesia before being transferred to a temperature-controlled imaging bed and attached to an anaesthetic facemask (Minerve, France).

[^{99m}Tc]TcO_4^- SPECT images were acquired at ~40 minutes pi for 30 minutes under anaesthesia, [99mTc][TcO4⊂C-2]$^{11+}$ SPECT images were acquired at 20 minutes pi for 100 min. In both cases SPECT was followed by CT scan (240 projections with 1 s exposure to 55 kVp X-rays). SPECT and CT images were reconstructed with an iterative algorithm (HiSPECT, Scivis GmbH, Germany) and with exact cone beam Filtered Back Projection (VivoQuant, inviCRO LLC, USA), respectively.

Ex vivo biodistribution

Benjamin Burke, Christopher Cawthorne

Naïve female CD1-IGS mice (30-50 g) were obtained from Charles River. Animals were injected *intravenously* with 6-8 MBq of radiotracer and euthanised 2 h post-injection. Blood, liver, stomach and other selected organs were harvested and the radioactivity present measure by an Automated Gamma Counter. The biodistribution was then performed as describe above. All values were normalised and are quoted as percent injected dose per gram of tissue (%ID/g).

Liver samples were analysed to investigate the identity of technetium-^{99m}. Liver samples (ca. 200 mg) from three animals were extracted with water (200 µL) for five minutes an ultrasonic bath followed by centrifugation at 12,000 g for five minutes. TLC analysis of the supernatant showed 29.7% ± 2.4 of the radioactivity remained on the baseline in a manner consistent with [^{99m}Tc][TcO_4⊂**C20**]$^{11+}$ and the remaining radioactivity was present at the solvent front, consistent with free TcO_4^-.

Extraction of the silica plate by ultrasonication in acetonitrile (200 µL) followed by centrifugation at 12,000 g for five minutes. When analysed by TLC this extract was consistent with 100% free TcO_4^-.

2.5 References

1 V. Martí-Centelles, A. L. Lawrence and P. J. Lusby, *J. Am. Chem. Soc.*, 2018, **140**, 2862–2868.

2 C. T. Mcternan, T. K. Ronson and J. R. Nitschke, *J. Am. Chem. Soc.*, 2019, **141**, 6837–6842.

3 M. J. Burke, G. S. Nichol and P. J. Lusby, *J. Am. Chem. Soc.*, 2016, **138**, 9308–9315.

4 W. Cullen, A. J. Metherell, A. B. Wragg, C. G. P. Taylor, N. H. Williams and M. D. Ward, *J. Am. Chem. Soc.*, 2018, **140**, 2821–2828.

5 J. L. Bolliger, T. K. Ronson, M. Ogawa and J. R. Nitschke, *J. Am. Chem. Soc.*, 2014, **136**, 14545–14553.

6 M. Whitehead, S. Turega, A. Stephenson, C. A. Hunter and M. D. Ward, *Chem. Sci.*, 2013, **4**, 2744-2751.

7 N. Busschaert, C. Caltagirone, W. Van Rossom and P. A. Gale, *Chem. Rev.*, 2015, **115**, 8038–8155.

8 C. R. K. Glasson, G. V. Meehan, J. K. Clegg, L. F. Lindoy, P. Turner, M. B. Duriska and R. Willis, *Chem. Commun.*, 2008, 1190–1192.

9 C. R. K. Glasson, J. K. Clegg, J. C. McMurtrie, G. V. Meehan, L. F. Lindoy, C. A. Motti, B. Moubaraki, K. S. Murray and J. D. Cashion, *Chem. Sci.*, 2011, **2**, 540–543.

10 A. J. Metherell, W. Cullen, N. H. Williams and M. D. Ward, *Chem. Eur. J.*, 2018, **24**, 1554–1560.

11 D. Zhang, T. K. Ronson, J. Mosquera, A. Martinez, L. Guy and J. R. Nitschke, *J. Am. Chem. Soc.*, 2017, **139**, 6574–6577.

12 N. R. Voss and M. Gerstein, *Nucleic Acids Res.*, 2010, **38**, 555–562.

13 H. Jiang and T. R. DeGrado, *Theranostics*, 2018, **8**, 3918–3931.

14 H. Jiang, A. Bansal, R. Goyal, K.-W. Peng, S. J. Russell and T. R. DeGrado, *Bioorg. Med. Chem.*, 2018, **26**, 225–231.

15 A. Boschi, L. Uccelli, M. Pasquali, A. Duatti, A. Taibi, G. Pupillo and J. Esposito, *J. Chem.*, 2014, **2014**, 1–14.

16 E. A. Katayev, G. V. Kolesnikov and J. L. Sessler, *Chem. Soc. Rev.*, 2009, **38**, 1572–1586.

17 H. Stephan, R. Berger, H. Spies, B. Johannsen and F. P. Schmidtchen, *J. Radioanal. Nucl. Chem.*, 1999, **242**, 399–403.

18 S. Jürgens, W. A. Herrmann and F. E. Kühn, *J. Organomet. Chem.*, 2014, **751**, 83–89.

19 S. Vallabhajosula, R. Zimmerman, M. Picard, P. Stritzke, I. Mena, R. S Hellman, R. S Tikofsky, M. G Stabin, R. A Morgan and S. Goldsmith, *J. Nucl. Med.*, 1989, **30**, 599–604.

20 S. M. McNeill, D. Preston, J. E. M. Lewis, A. Robert, K. Knerr-Rupp, D. O. Graham, J. R. Wright, G. I. Giles and J. D. Crowley, *Dalton Trans.*, 2015, **44**, 11129–11136.

21 A. Meister and M. E. Anderson, *Annu. Rev. Biochem.*, 1983, **52**, 711–760.

22 A. Ahmedova, R. Mihaylova, D. Momekova, P. Shestakova, S. Stoykova, J. Zaharieva, M. Yamashina, G. Momekov, M. Akita and M. Yoshizawa, *Dalton Trans.*, 2016, **45**, 13214–13221.

23 L. E. H. Paul, B. Therrien and J. Furrer, *Inorg. Chem.*, 2012, **51**, 1057–1067.

24 S. Nayak, K. V. Reddy and A. C. Dash, *Transit. Met. Chem.*, 2014, **39**, 177–187.

25 A. A. Campanali, T. D. Kwiecien, L. Hryhorczuk and J. J. Kodanko, *Inorg. Chem.*, 2010, **49**, 4759–4761.

26 D. R. Frasca and M. J. Clarke, *J. Am. Chem. Soc.*, 1999, **121**, 8523–8532.

27 A. Schmidt, M. Hollering, M. Drees, A. Casini and F. E. Kühn, *Dalton Trans.*, 2016, **45**, 8556–8565.

28 D. Preston, S. M. McNeill, J. E. M. Lewis, G. I. Giles and J. D. Crowley, *Dalton Trans.*, 2016, **45**, 8050–8060.

29 Y. A. Getmanenko and R. J. Twieg, *J. Org. Chem.*, 2008, **73**, 830–839.

30 G. I. Pascu, A. C. G. Hotze, C. Sanchez-Cano, B. M. Kariuki and M. J. Hannon, *Angew. Chem. Int. Ed.*, 2007, **46**, 4374–4378.

31 C. R. K. Glasson, G. V. Meehan, C. A. Motti, J. K. Clegg, P. Turner, P. Jensen and L. F. Lindoy, *Dalton Trans.*, 2011, **40**, 10481–10490.

32 R. L. Paul, Z. R. Bell, J. C. Jeffery, J. A. McCleverty and M. D. Ward, *Proc. Natl. Acad. Sci. U. S. A.*, 2002, **99**, 4883–4888.

33 D. P. August, G. S. Nichol and P. J. Lusby, *Angew. Chem. Int. Ed.*, 2016, **55**, 15022–15026.

34 J. J. Henkelis, J. Fisher, S. L. Warriner and M. J. Hardie, *Chem. Eur. J.*, 2014, **20**, 4117–4125.

35 A. G. L. Olive, K. Parkan, C. Givelet and J. Michl, *J. Am. Chem. Soc.*, 2011, **133**, 20108–20111.

36 J. Chen, M. Kuss-Petermann and O. S. Wenger, *Chem. Eur. J.*, 2014, **20**, 4098–4104.

37 J. M. Cross, N. Gallagher, J. H. Gill, M. Jain, A. W. McNeillis, K. L. Rockley, F. H. Tscherny, N. J. Wirszycz, D. S. Yufit and J. W. Walton, *Dalton Trans.*, 2016, **45**, 12807–12813.

38 M. J. Burke, The University of Edinburgh, 2016.

Chapter 3: Functionalisation and Conjugation of Robust $Co^{III}_4L_6$ Tetrahedra

3.1 Introduction

New detection methods for different disease states remain an ongoing endeavour. Having shown that the host-guest complexes of a robust $Co_4L_6^{12+}$ cage can be utilised for *in vivo* imaging, our attention turned to biological targeting through derivatisation of the cage exterior.

The behaviour of synthetic cages *in vivo* has had limited exploration, and their pharmacokinetics are likely to be dominated by high charge.[1] Our experiments have indicated that the **C20** macro-cation is taken up by the liver, potentially due to binding by albumin and macrophages.[2,3] Control of cage pharmacokinetics, and overcoming the inherent biological fate of the "naked" cage structure would promote a far greater scope of biomedical applications.

There are several strategies for derivatisation of the cage periphery. Theoretically, the conjugation could be carried out before or after assembly, both approaches possessing advantages and challenges. Post-assembly modification requires that a functionalisation handle be incorporated into the ligand, so that the assembled cage can be readily modified. This approach requires careful consideration of chemoselectivity: the cage assembly procedure must be tolerant of the chemical handle and vice versa. Furthermore, the post-assembly modification of the cage must occur without degradation of the cage and the bio-conjugation must not be hindered by the macromolecular structure. In contrast, pre-assembly functionalisation has the advantage that the cage is not required to be stable to any conjugation reaction conditions. However, pre-functionalised ligands must assemble into the desired assembly despite additional chemical groups, which may pose chemical or steric barriers.

Both approaches can be effective, and both have been explored. The Lusby group have previously encountered issues with the pre-assembly functionalisation method, wherein it was found that a ligand containing an iridium complex could not be used to form a tetrahedron. In contrast, the Lusby group previously developed a ligand precursor (**N9**, Scheme 3.1.1) with intrinsic functionalisation handles to allow customisation using copper catalysed azide-alkyne Huisgen cycloaddition (CuAAC) reactions, which allow different constituents (**N11** and **N12**) to be externally affixed (Scheme 3.1.1). This method further utilised the triazole group as a coordinating alternative to bipyridine, facilitating the ready inclusion of a polyethylene glycol group into the ligand to improve aqueous solubility.[4] The triazole-pyridine chelating moiety, however, were found to be poorly suited to *in vivo* environments (see Chapter 2).

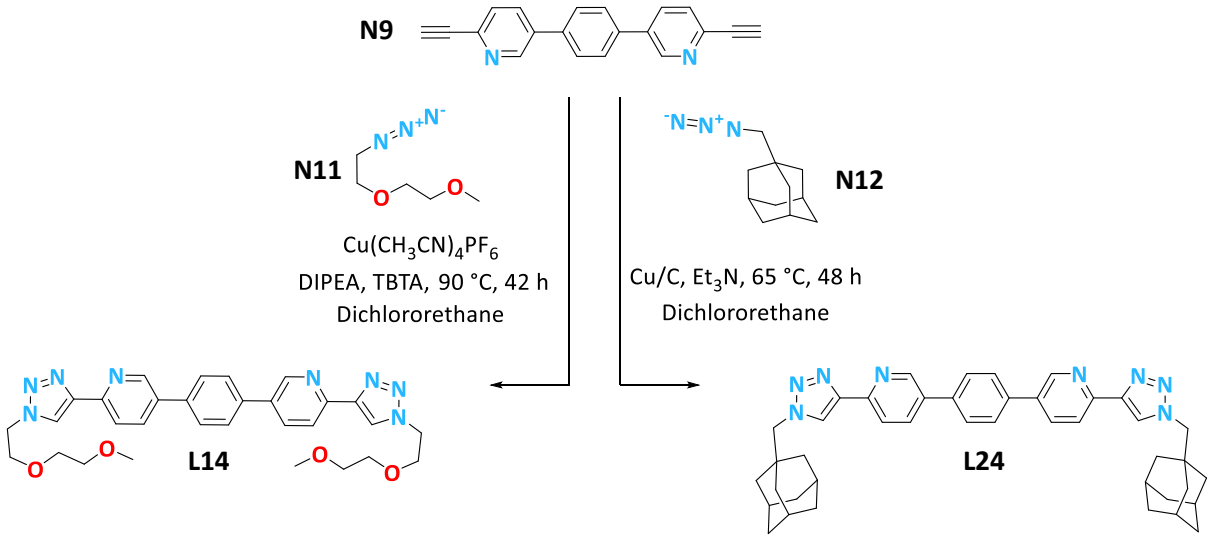

*Figure 3.1.1: Simultaneous "click" synthesis and functionalisation of triazole ligands **L14** and **L24** from ligand precursor **N9**.*

A similar approach was taken by Crowley and co-workers, who developed a ligand with a pendant azide (**L25$_a$**) to allow facile functionalisation of their ditopic ligands through CuAAC reactions with fluorescent, redox active and biologically relevant groups (**L25$_{b\text{-}j}$**, Fig. 3.1.2).[5] All of these ligands were successfully assembled into Pd_2L_4 lantern capsules, though protecting groups were required for the **L25$_c$** and **L25$_d$**. However, only **C25$_d$** was sufficiently water stable to allow biological applications to be explored.

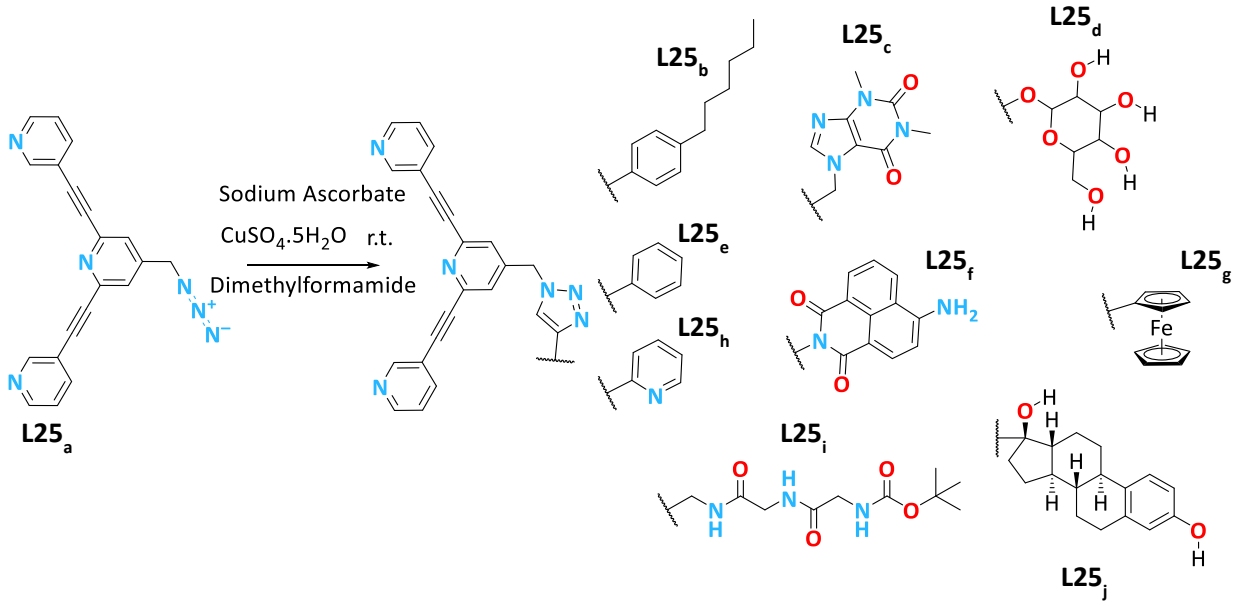

*Figure 3.1.2: CuAAC functionalisation of **L25$_a$** to generate **L25$_{b\text{-}j}$** .*

Casini and co-workers took an alternative route in conjugating proteins to similar Pd_2L_4 systems. They successfully synthesised a number of cages with four pendant proteins using an amide coupling reaction. Interestingly, attempts at post-assembly conjugation of the proteins onto the assembled cages resulted in poor yields, variable numbers of couplings, and side reactions.[6]

While these two groups found success in pre-assembly conjugation, it should be noted that Pd_2L_4 are well suited to the approach and are widely studied due to their relative synthetic accessibility. The cages form readily when the components are mixed in appropriate solvents with limited potential side-products. The assemblies are also conveniently shaped with little ligand overlap, causing conjugated groups to point away from each other to avoid steric clash. In comparison, tetrahedral systems are more complex structures with more entwined ligands. They also sometimes require multiple steps in the assembly process further complicating "chemical orthogonality".

An example of pre-assembly ligand conjugation was reported by Fujita and co-workers, who showed that a $Pd_{12}L_{24}$ macroscopic cage could be assembled around a ubiquitin protein covalently affixed to a single ligand of the assembly (**L26$_b$**, Fig. 3.1.3). This attachment was achieved by reacting a cysteine residue from the protein to **L26$_b$** using a maleimide Michael "click" reaction. Mixing the correct ratio of **L26$_a$** and **L26$_b$** with palladium salts in a water-acetonitrile mixture gave the desired cage-protein complex **C26$_c$**. While a remarkable achievement, conjugation of a cage interior is significantly different to the exterior, due to templating effects and the blocking of the cavity.[7]

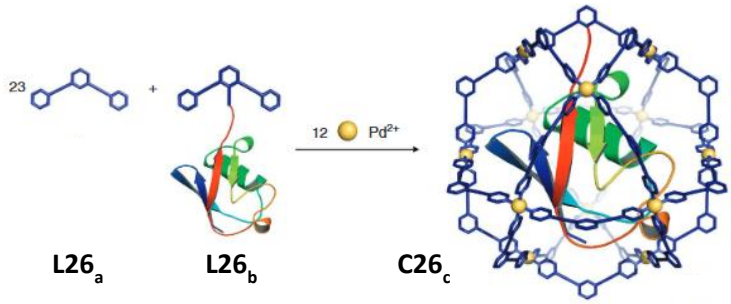

*Figure 3.1.3: Fujita and co-workers pre-functionalised the ligand **L26$_b$** with ubiquitin, such that when combined in a 1:23 ratio with the unfunctionalised ligand **L26$_a$** and a palladium salt, they assembled to give $Pd_{12}L_{24}$ **C26$_c$**. Figure adapted from reference 7.*

Post-assembly conjugation has also been reported in the literature.[8] These reactions have largely been carried out using "click" reactions exploiting highly tolerant functional groups and mild reaction conditions. The very popular "click" reaction, CuAAC, has had some success. For example, Zhao and co-workers were able to able conjugate a number of polyethylene glycol groups to their copper (II) cuboctahedra (**C27a**) to generate the far more water solubility and stability **C27$_b$** (Fig. 3.1.4). They

utilised copper (I) catalysts rather than exposing their system to the reducing agents required for the more common copper salts.[9]

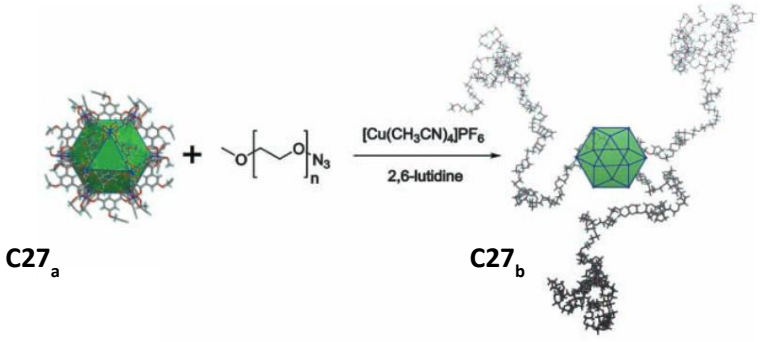

Figure 3.1.4: CuAAC was used to attach solubilising and stabilising polyethylene glycol groups to alkyne-functionalised copper (II) cuboctahedra ***C27$_a$*** *to give water soluble* ***C27$_b$****. Figure adapted from reference 9.*

Many groups have also found ways to avoid the use of redox active copper catalysts, which can prove incompatible with many coordination assemblies. One method of avoiding copper is to use electron deficient alkynes that are able to undergo cycloaddition without the need for a catalyst (Fig. 3.1.5a).[10] This allowed for the effective "click" functionalisation of a copper paddlewheel structure (**M27$_a$**), though a zinc analogue (**M28$_a$**) was still incompatible with these mild conditions (Fig. 3.1.5b).[11,12] Strain-promoted alkyne-azide cycloadditions have also been used by Stang and co-workers to attach both a fluorophore and biotin molecules to a platinum metallocycle **M29a** (Fig. 3.1.5c).[13,14]

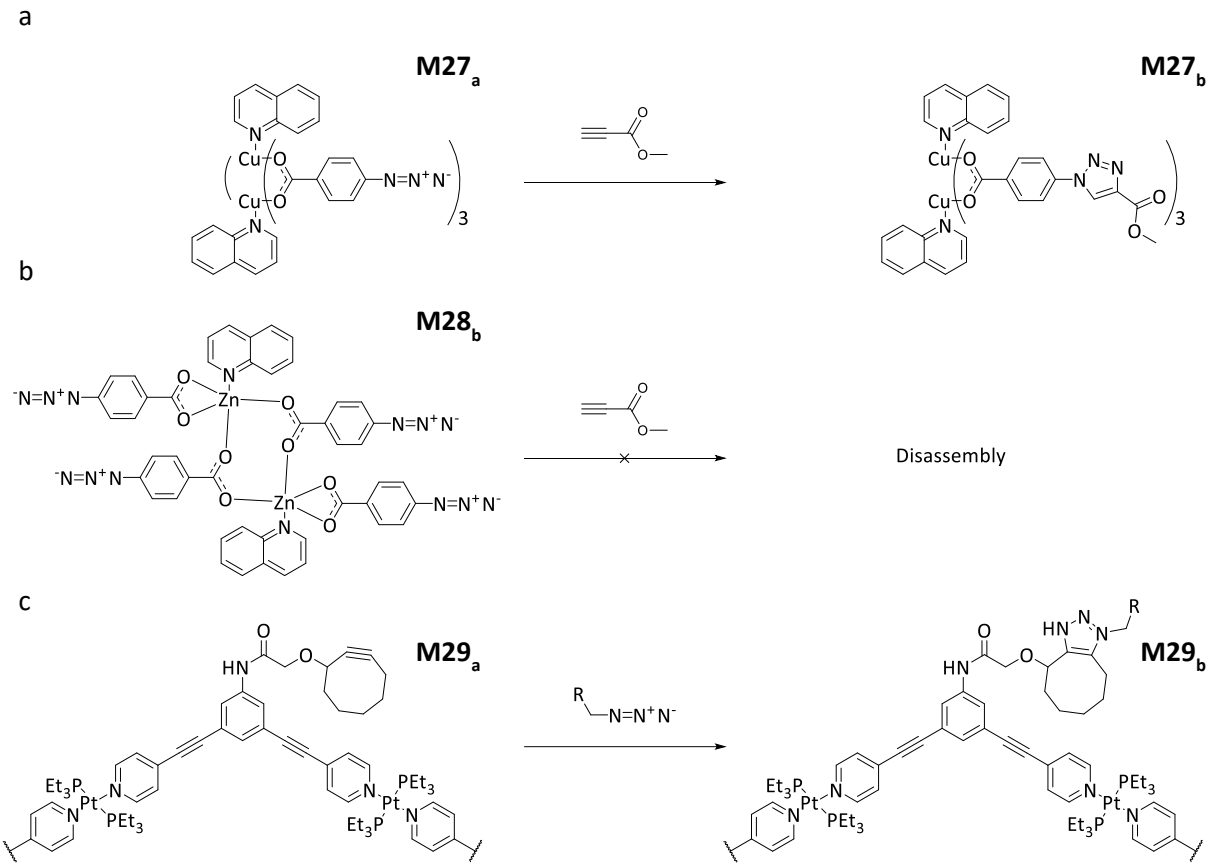

*Figure 3.1.5: Copper free post-assembly azide-alkyne cyclo additions. (a) Successful "click" reaction of copper paddlewheel (**M27$_a$**) with electron deficient alkyne (b) Unsuccessful "click" reaction of zinc metallocycle (**M28$_a$**) with electron deficient alkyne, (c) Strain promoted "click" reaction of platinum metallocycle (**M29$_a$**).*

The popularity of the alkyne-azide cycloaddition as a means of post-assembly modification is due to the low polarity of these functional groups, which prevents unwanted side reactions. However, Stang and co-workers have reported nucleophilic conjugation reactions that possess ligand based amine nucleophiles (**C30$_a$**) and maleimide electrophiles (**C30$_a$**), which could be expected to disrupt many coordination assemblies (Fig. 3.1.6).[15] The success of this bio-conjugation reaction to give **C30$_{c,d,e}$** was attributed to the stability of the platinum assembly.

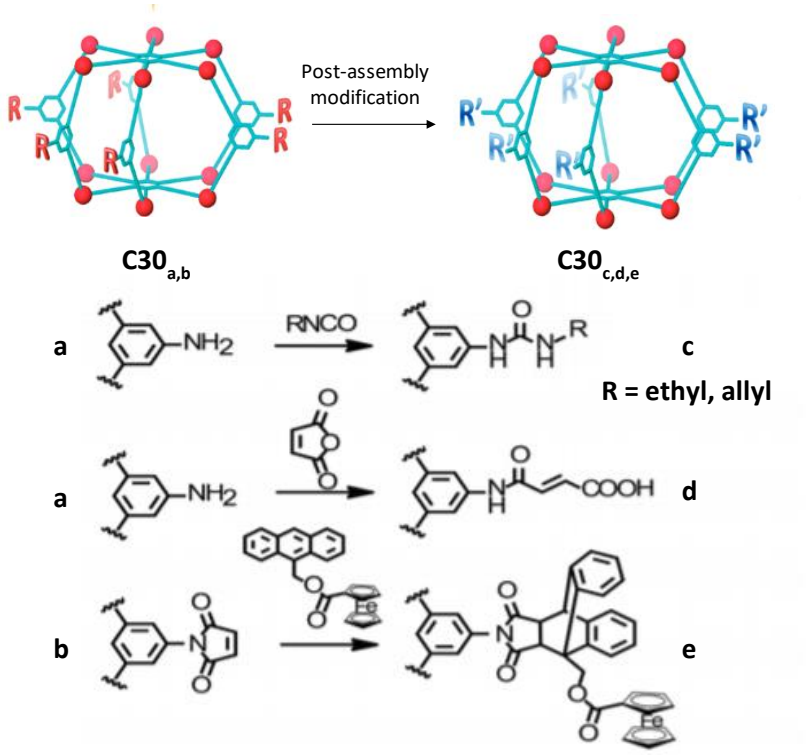

*Figure 3.1.6: Post-assembly modification of amine (**C30$_a$**) and maleimide (**C30$_b$**) appended hexagonal prisms. Figure adapted from reference 15.*

In a similar manner, Nitschke and co-workers were able to acetylate primary amines present in a meta-stable iron helicate **H31$_a$** using reactive anhydrides and carboxylic acids activated with HATU to funtionalised the helicate with range of groups (**H31$_{b,c,d,e}$**, Fig. 3.1.7).[16]

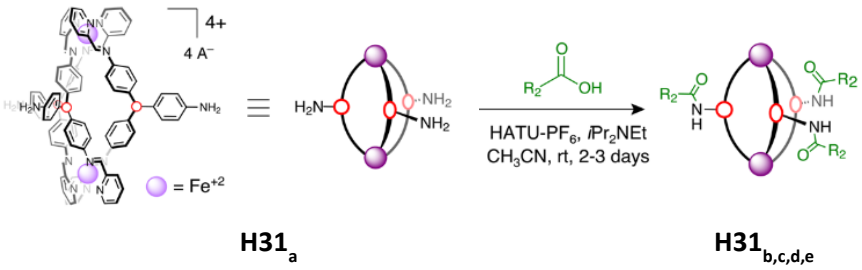

*Figure 3.1.7: Post-assembly covalent functionalisation iron helicate **H31$_a$** through acylation. (b) R_2 = 2-pyridine, (c) R_2 = 3-pyridine, (d) R_2 = 4-pyridine, (e) R_2 = 4-pyridylphenyl. Figure adapted from reference 16.*

In summary, the literature shows that that there are several possible approaches for the conjugation of metallosupramolecular capsules. The key is finding suitable key intermediates, either pre-functionalised ligands or a cage, which can allow access to a library of conjugated targets such as proteins or saccharides (Fig. 3.1.8). The robustness of our cage system, alongside the relative

complexity of our cage assembly reaction, point to post-assembly modification being desirable. However, pre-functionalisation is a valid alternative that could be explored from similar building blocks. The key is therefore to identify "click" functionalisation handles that will display the necessary chemical orthogonality to ensure compatibility with our system. This chapter will describe the synthesis of ligand and cage precursors with functionalisation handles appropriate for either pre- or post-assembly modification.

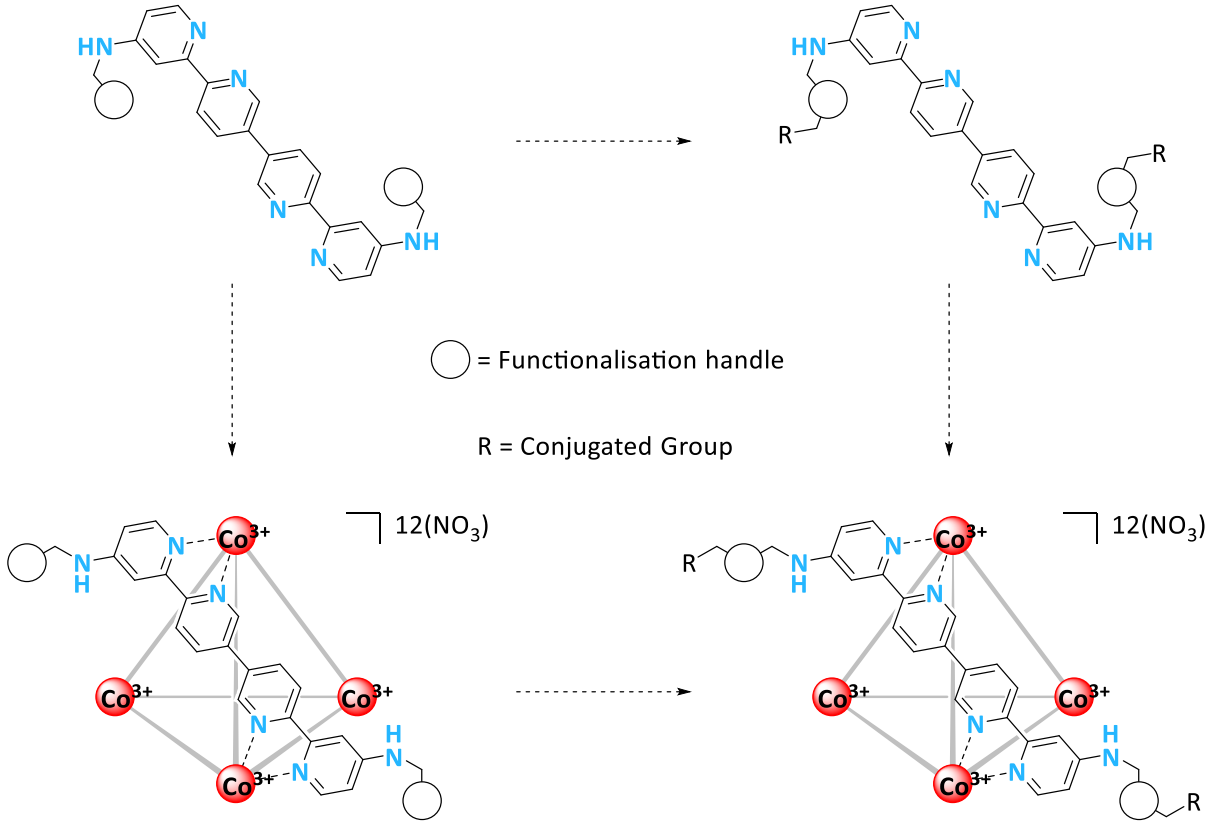

Figure 3.1.8: Proposed duel approach to cage conjugation.

3.2 Results and Discussion

3.2.1 Direct Functionalisation of L20

The external amines of **L20** might appear to be ideal groups from which to functionalise **C20**. Primary amines can undergo a plethora of high-yielding organic reactions. Unfortunately, the strong electron withdrawing properties of the pyridine ring means that the amine groups of **L20** are poor nucleophiles, especially after coordination to metal centres. While this makes post-assembly reactions of these amines highly unlikely, it was suggested that the amine groups could be functionalised pre-assembly to improve the properties of the ligands and/or to install other functional groups for post-assembly modification. In short, the incorporation of a spacer between the pyridine amine and some functionalisable group were thought to represent the most obvious chance of success.

Alkynes and esters were identified as suitable groups for this purpose, the former using CuAAC "click" chemistry and the latter using classic carbonyl chemistry. Trial reactions of **N6** (see Chapter 2) with propargyl bromide were unsuccessful in making **N13** but treatment with ethylbromoacetate afforded product (**N14**, Scheme 3.2.1). However, the direct reaction with the full **L20** ligand was found to not progress to **L32**, potentially due to the lower solubility of **L20** (Scheme 3.2.2).

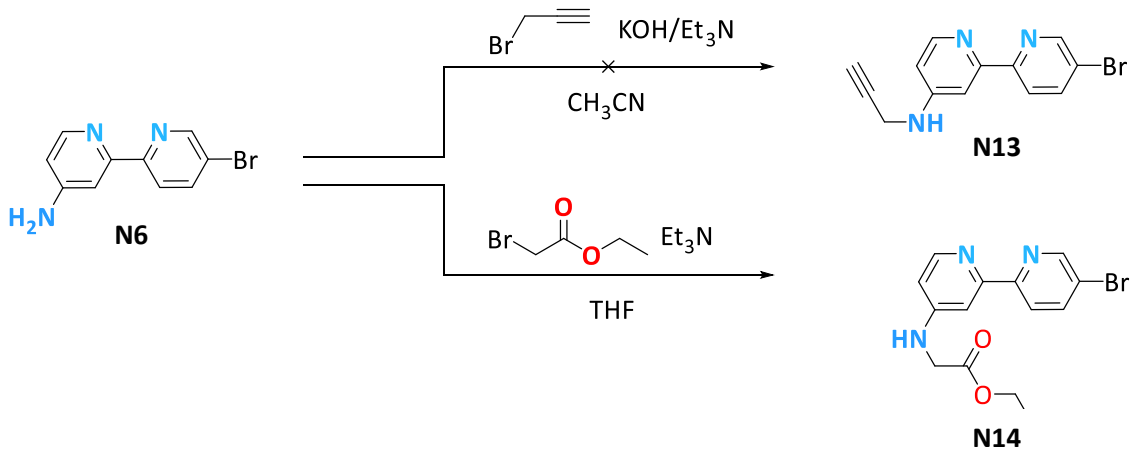

*Scheme 3.2.1: Trialled nucleophilic reactions of **N6** with alkyne and ester containing compounds.*

Dimethylacetamide was adopted as the solvent, and sodium carbonate, sodium hydroxide or Et_3N were trialled as bases. However, in all instances the reactions were found to be slow and very poor yielding (Scheme 3.2.2).

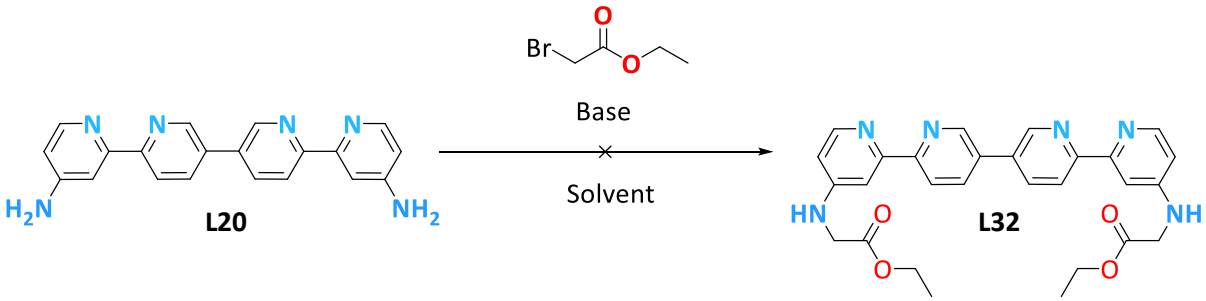

*Scheme 3.2.2: Unsuccessful reaction of **L20** with ethyl bromoacetate. Base = Et_3N, K_2CO_3 or KOH. Solvent = THF and/or dimethylacetamide.*

It was also suggested that the electron deficient amine, while a poor nucleophile, could instead be exploited as a pro-nucleophile activated by deprotonation. To explore this strategy, the electron withdrawing *o*-Nitrobenzenesulfony (Nosyl) group was identified as an activating moiety to increase pro-nucleophile acidity. This group could then be easily cleaved by reaction with soft nucleophiles via a Meisenheimer complex.[17]

Reaction of **N6** with *o*-nitrobenzenesulfonyl chloride led to the precipitation of a crystalline solid. However, the characterised solid was not consistent with the desired product **N15**, and **N6** was recovered when it was exposed to base, implying the reaction had yielded a salt (Scheme 3.2.3). Repeating the experiment using multiple solvents and bases yielded the same result and this approach was abandoned. The *tert*-Butyloxycarbonyl groups reported in the previous chapter could be a valid pro-nucleophile alternative; however, time constraints hindered further exploration.

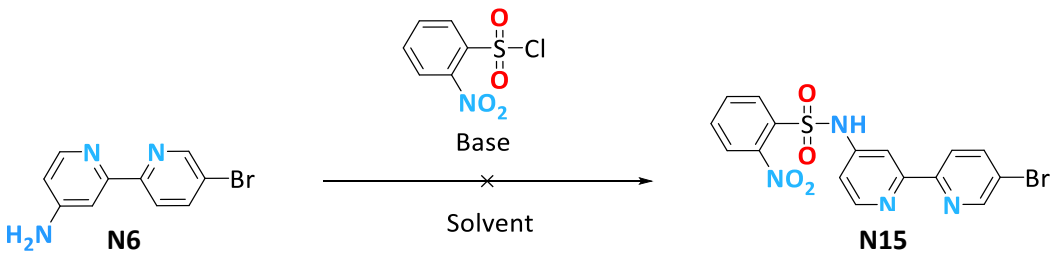

*Scheme 3.2.3: Unsuccessful reaction of **N6** with nosyl chloride. Base = K_2CO_3 and Et_3N. Solvent = THF, toluene, $CHCl_3$ and/or DMF.*

3.2.2 Development of Ligand Precursor

As the direct functionalisation of the pendent amine proved challenging, it was proposed that functionalised amines could be directly introduced, exploiting S_NAr type reactivity and a ligand precursor.

3.2.3 Nucleophilic functionalisation

Literature reports of amines substituting the nitro groups by S_NAr are common. Unfortunately, many of these reactions require high temperatures that are not always compatible with the reactants.[18] As **N5** was a key intermediate in the synthesis of **L20**, this compound was reacted with several different amines under a range of conditions (Scheme 3.2.4). In almost all instances, significant decomposition was observed. Even when products were detected, purification issues were encountered due to the presence of high boiling point amines and the products being too polar for silica gel chromatography.

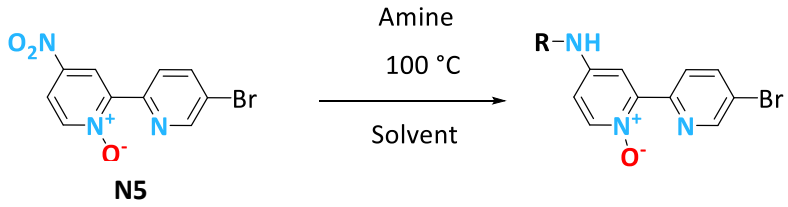

N5

*Scheme 3.2.4: Failed S_NAr substitutions of **N5**. Solvent = none, toluene, THF and/or CH_3CN. Amine = diethanolamine, ethanolamine.*

3.2.4 Sandmeyer reaction of L20

After encountering issues with the nucleophilic substitution of the nitro groups, another ligand functionalisation route was sought. A Sandmeyer reaction of **L20** would allow the substitution of the amine groups with chlorines or other halogens, opening up a range of different derivatisation reactions. Due to the poor solubility of **L20** and concerns over diazonium salts, a procedure utilising concentrated hydrochloric acid as both the solvent and source of chloride nucleophiles was selected and was found to give **L33** in good yield, as shown in Scheme 3.2.5.

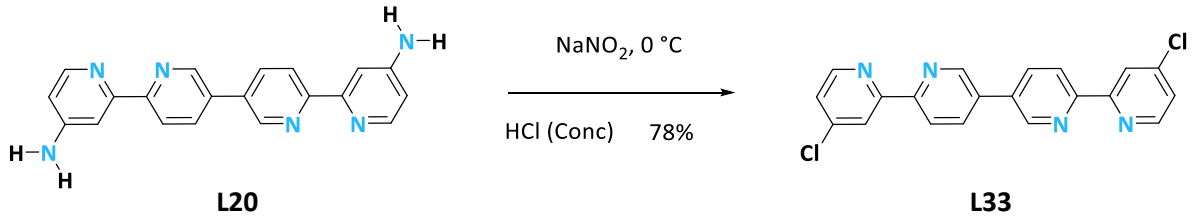

L20 **L33**

*Scheme 3.2.5: Sandmeyer reaction of **L20** to give **L33**.*

L33 could be considered a ligand in its own right, it is also a precursor that can be functionalised by a number of routes. While not synthetically trivial (requiring five synthetic steps from commercial materials), it does have the properties of a versatile ligand precursor. Furthermore, the compound was easy to handle, with good solubility in many solvents. The chloride groups could act as leaving

groups for S_NAr reactions with either alcohol or amine nucleophiles and could also be used in palladium cross-coupling transformations, such as the Buchwald-Hartwig reaction.

S_NAr reactions were initially considered as a simple means to substitute **L33**. However, these reactions gave similarly poor results to that observed with **N5**, leading to slow reaction times and decomposition of the starting material. The reaction was attempted with the corresponding lithium salt, by initially treating a protected propargylamine with ^{n}BuLi, before reaction with **L33**. This reaction yielded only starting material and the reason for this lack of reaction could not be determined.

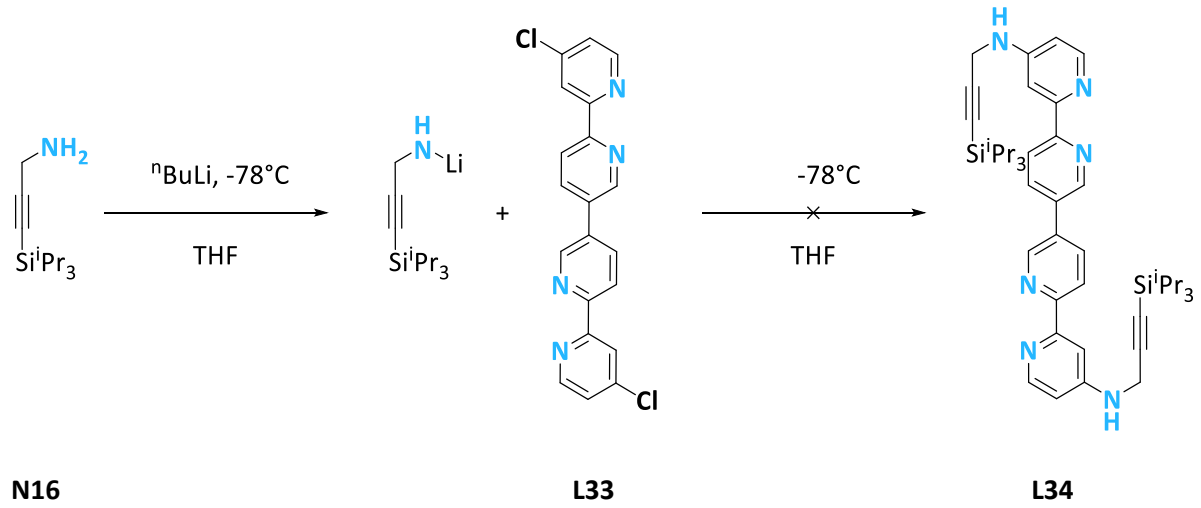

N16 **L33** **L34**

*Scheme 3.2.6: Failed reaction of **L33** with lithium amide of **3.12**.*

There are reports of Lewis acid catalysts being used to activate chloro-pyridine rings to nucleophilic attack by amines, which could be an effective means of allowing substitution of the ligand.[19] It was proposed that assembly of **L33** to give a cobalt (III) tetrahedra might activate the chlorine groups in a similar manner. Unfortunately, exposing the ligand to standard cage formation conditions was completely ineffective (Scheme 3.2.7). The ligand remained completely undissolved under the standard reaction conditions. This may be caused by both the reduced aqueous solubility of the less polar ligand and the reduced strength of the interaction with the metal.

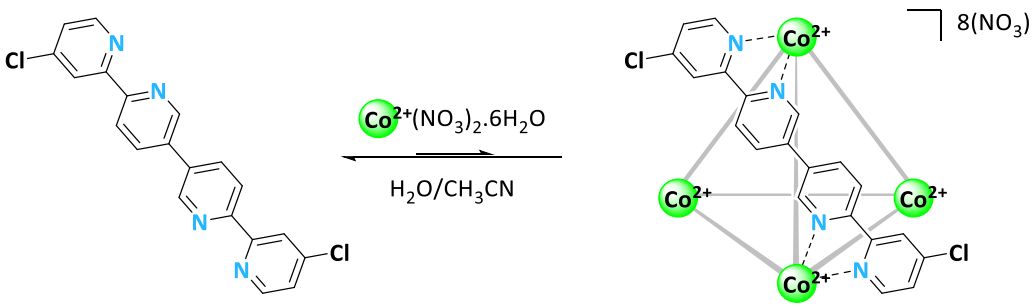

*Scheme 3.2.7: Failed cage assembly with **L33**.*

3.2.5 Buchwald-Hartwig coupling of L33

Buchwald-Hartwig reactions were trialled as an alternative to the problematic S_NAr functionalisation of the ligand. These Pd cross-coupling reactions have been shown to be an effective means of coupling amines to aryl halides.[20] Conditions adapted from a literature procedure were successful in coupling the protected propargylamine with **L33** to give **L34** in a reasonable yield of 58%.[21] Deprotection of **L34** could be achieved with tetrabutyl ammonium fluoride to give the desired terminal alkyne ligand, **L35** (Scheme 3.2.8). This ligand is suitable for CuAAc "click" conjugation, which could allow the conjugation with many azide-containing biological compound groups under very mild conditions.

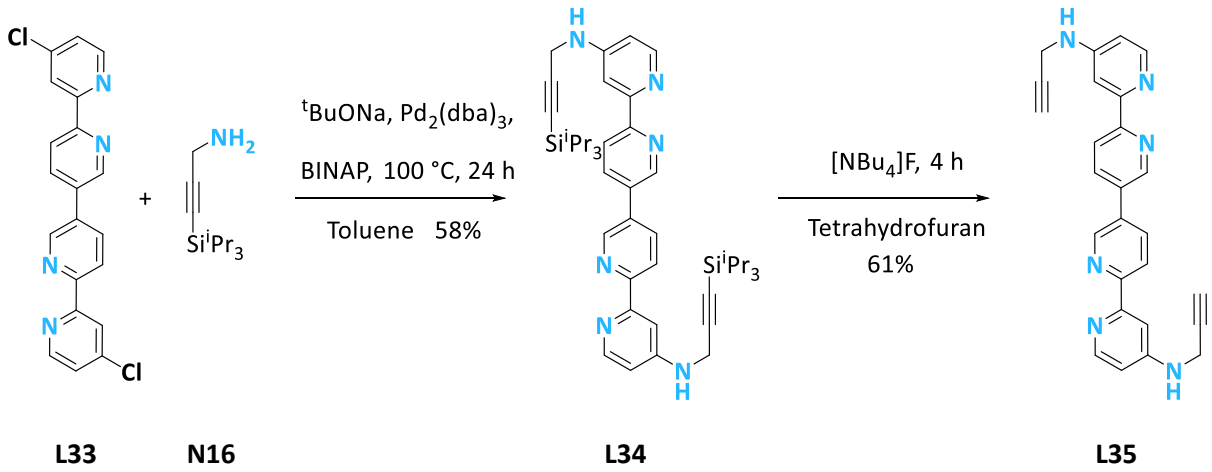

L33 **N16** **L34** **L35**

*Scheme 3.2.8: Successful synthesis of **L35**.*

3.2.6 "Click" Reactions

Polyethylene glycol (PEG) chains were identified as a group which could be conjugated to the ligand in order to modify the properties of the ligand and cage. They were also considered of interest as they could "mask" the cationic structure and thereby alter the biological behaviour of the cage.[9] Initial attempts at "click" conjugation with a PEG azide (**N11**, Fig.3.2.9), previously prepared by Dr Michael Burke, using standard copper (II) salts and ascorbic acid as a reducing agent, were met with limited success.[22] Challenges in the isolation of the product were encountered wherein the increased aqueous solubility of the product made demetallation and recovery difficult. To avoid this issue, a copper on carbon catalyst was used to prevent copper leaching.[4] While this was more successful, the product could still only be isolated in very low yield. Despite initial challenges, optimisation of the reaction and workup conditions could provide a universal method of ligand conjugation.

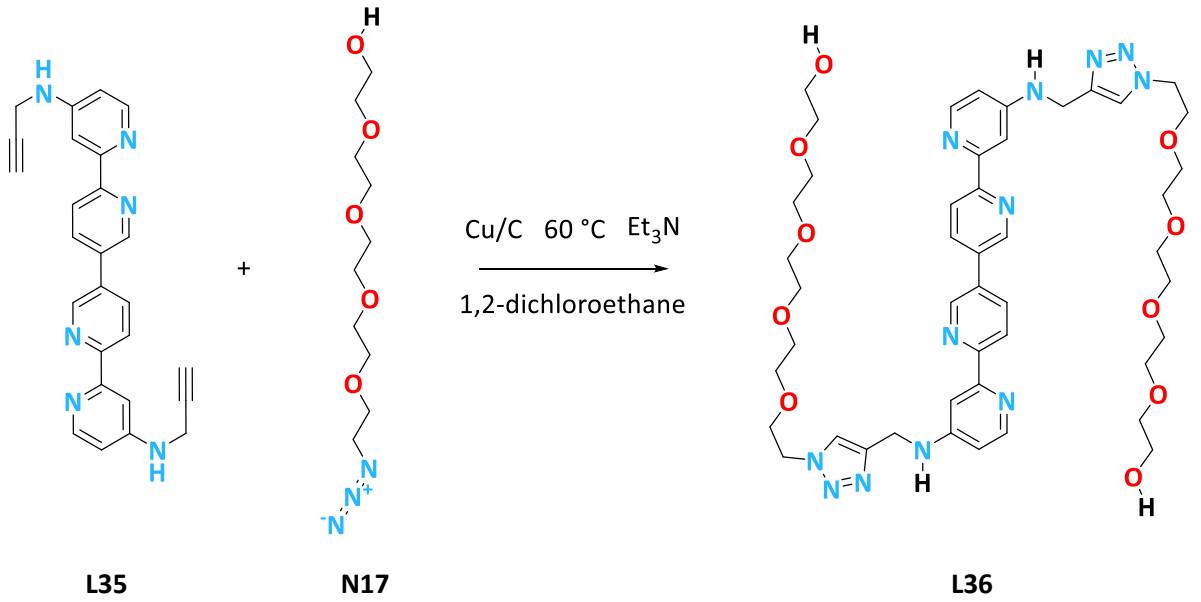

*Scheme 3.2.9: Partially successful CuAAC conjugation of **L35** with PEG azide **N17**.*

3.2.7 Maleimide Reactions

The Buchwald-Hartwig reaction itself represents a branching point for functionalisation of the ligand. Theoretically, this reaction would allow the coupling of a large range of amines directly onto the ligand, including other "click" handles. One group identified as a promising alternative were maleimides. These undergo Michael-"click" reactions with thiols under very mild aqueous conditions as demonstrated by Fujita and co-workers.[23] Therefore, the protected amine maleimide precursor **N11** was synthesised according to a literature procedure and the coupling reaction with **L33** was attempted (Scheme 3.2.10).[24] Unfortunately, the compound was found to be incompatible with the reaction conditions, which resulted in the retro-Diels-Alder reaction, thereby removing the furan protecting group and the polymerisation of the unprotected maleimide.[25]

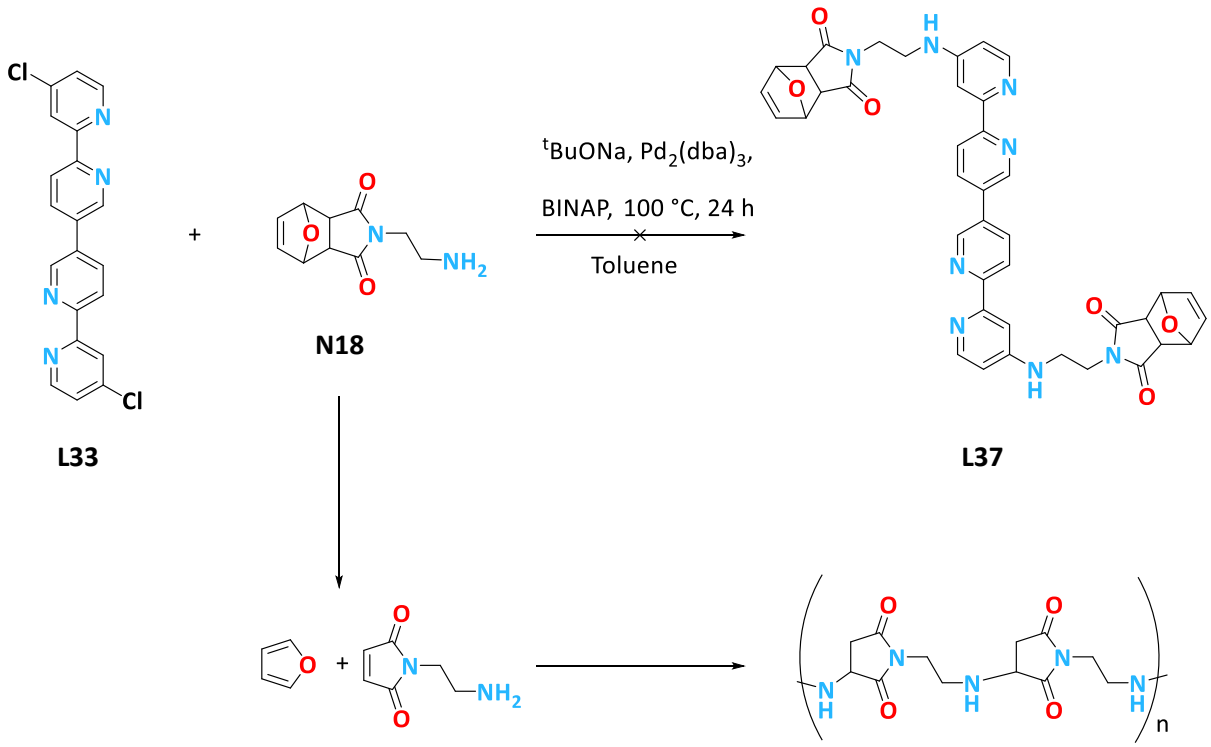

*Scheme 3.2.10: Failed Buchwald-Hartwig coupling of **L33** and **N18**.*

Alternative conditions could be used for the coupling which may not remove the protecting group.[26] Alternatively, a range of different groups could be introduced including other "click" handles such as carboxylic acids or cyclooctynes.

3.2.8 S_NAr Derived Ether Functionalised Ligands

While functionalisation of the ligand with an amine proved successful at stabilising the cages *in vivo*, it did lead to some synthetic challenges. Therefore, other electron donating groups that could imbue favourable cage-stability properties whilst providing a chemical ligation handle were considered. As such, methyl ether groups were identified as stable, strongly electron donating groups which might be suitable for cage functionalisation (Fig. 3.2.1). Methyl ether groups have a Hammett constant of -0.37, in comparison to the -0.66 amine groups and it was hoped that this intermediate electron donation would allow straightforward cage synthesis, while imparting some measure of biological stability.

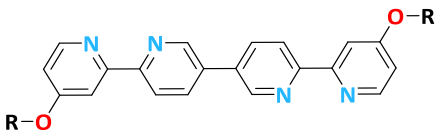

Figure 3.2.1: Proposed ligand functionalised with ether groups.

In contrast to the S_NAr reactions with amine and lithium amide nucleophiles, the nitro-containing intermediates **N5** and **N7** underwent ready substitution with methoxide, giving compounds **N19** and **N20** in excellent yield (Scheme 3.2.11).[27]

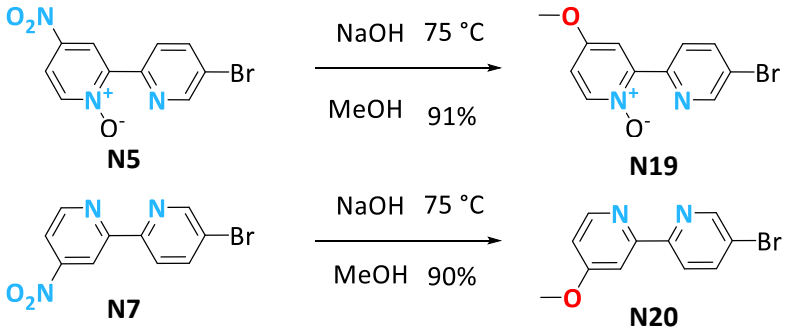

*Scheme 3.2.11: Synthesis of methyl ether ligand precursors **N19** and **N20**.*

Compound **N20** was then taken forward to homo-coupling procedures, using both nickel and Stille conditions, but neither reaction was successful (Scheme 3.2.12). Therefore, the reaction was repeated with **N19**, which successfully gave the quarter-pyridine ligand precursor **N21** in a reasonable yield of 66% (Scheme 3.2.13). With this in hand, only a reduction of the *N*-oxide was required to access **L38**.

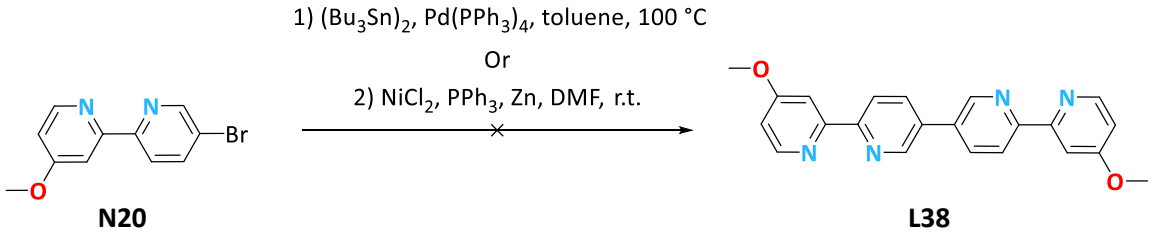

*Scheme 3.2.12: Failed homocoupling reactions of **N20** to give **L38**.*

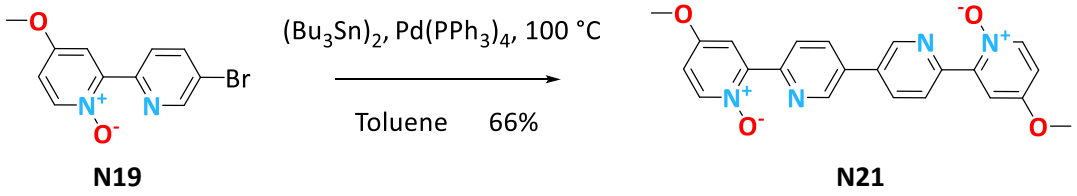

*Scheme 3.2.13: Successful Stille homocoupling of **N19**.*

3.2.9 Reduction of *N*-oxides

While *N*-oxides can aid the synthesis of pyridine species, their installation and removal represent additional synthetic steps which can prove non-trivial. A range of conditions have been reported for the reduction of the *N*-oxides, though many require specific metal catalysts or harsh conditions.[28]

Previously, **N5** had been refluxed in acetic acid with iron (0) in order to simultaneously reduce the nitro group and *N*-oxide group. While effective, these conditions require tricky workups in order to remove iron salts from the multidentate ligating product. The conditions were found to be effective for the reduction of **N19** (Scheme 3.2.14), but it was suggested that identification of milder conditions would be advantageous.

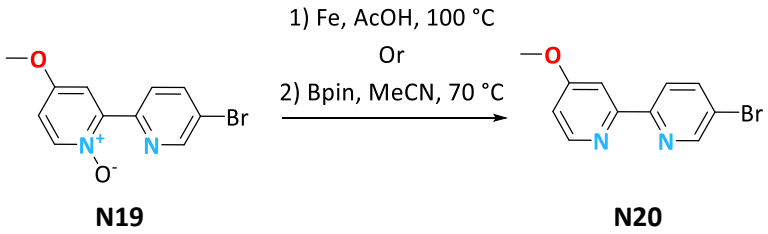

N19 **N20**

*Scheme 3.2.14: Successful methods of N-oxide reduction in **N19**.*

Triphenyl phosphine is a common, mild, reducing agent for *N*-oxides, with the strength of the formed O=P bond the driving force of the reaction. However, the triphenylphosphine oxide byproduct can be non-trivial to separate from polar products. Additionally, 4-nitro-pyridine has been noted to be a particularly challenging substrate for reduction.[29] Experimentation on an NMR scale showed that triphenyl phosphine reacts with **N5** very slowly, taking over a week to fully consume the starting material and appearing to lead to partial decomposition.

Another set of mild conditions were found that utilise bis(pinacolato)diboron (BPin), with the boron atom's affinity for oxygen driving the reaction. The reaction required only mild conditions and produced easily separable byproducts.[30] These conditions were then used to reduce **N21** to give **L38**, though with a relatively low yield of 54% (Scheme 3.2.15). This was unexpected given the mild nature of the reaction and was judged likely be due to the small scale of the reaction, with the hope that repetition of the reaction on a larger scale would give better results.

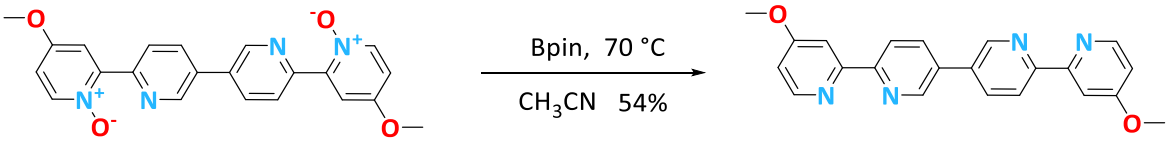

N21 **L38**

*Scheme 3.2.15: Reduction of **N21**.*

3.2.10 Synthesis of Methylether Functionalised Tetrahedron

With **L38** now synthesised, the formation of its respective tetrahedron was attempted. It was hoped that the lower σ-donor strength in comparison to **L20** would allow the formation of the Co_4(**L38**)$_6(NO_3)_{12}$ (**C38**) quantitatively without kinetic byproducts.

Unfortunately, the use of standard tetrahedron formation conditions (*i.e.* direct reaction of ligand with $Co(NO_3)_2.6H_2O$ followed by oxidation with cerium ammonium nitrate (see Chapter 2) failed to give pure tetrahedron (Scheme 3.2.16). As Figure 3.2.2 shows, a high symmetry species that likely corresponded to **C38** was present in the crude ^{1}H NMR spectrum along with a broad baseline peak indicative of polymeric material. Additionally, a large amount of insoluble material was obtained that could not be re-dissolved in water, presenting further evidence that large amounts of polymeric or oligomeric material was being produced in the reaction.

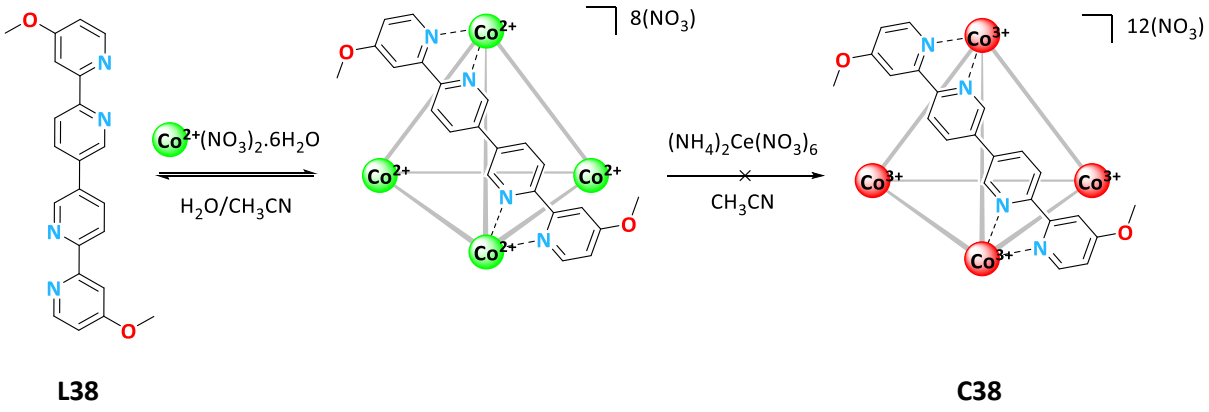

*Scheme 3.2.16: Depiction of unsuccessful formation of Co_4(**L38**)$_6(NO_3)_{12}$.*

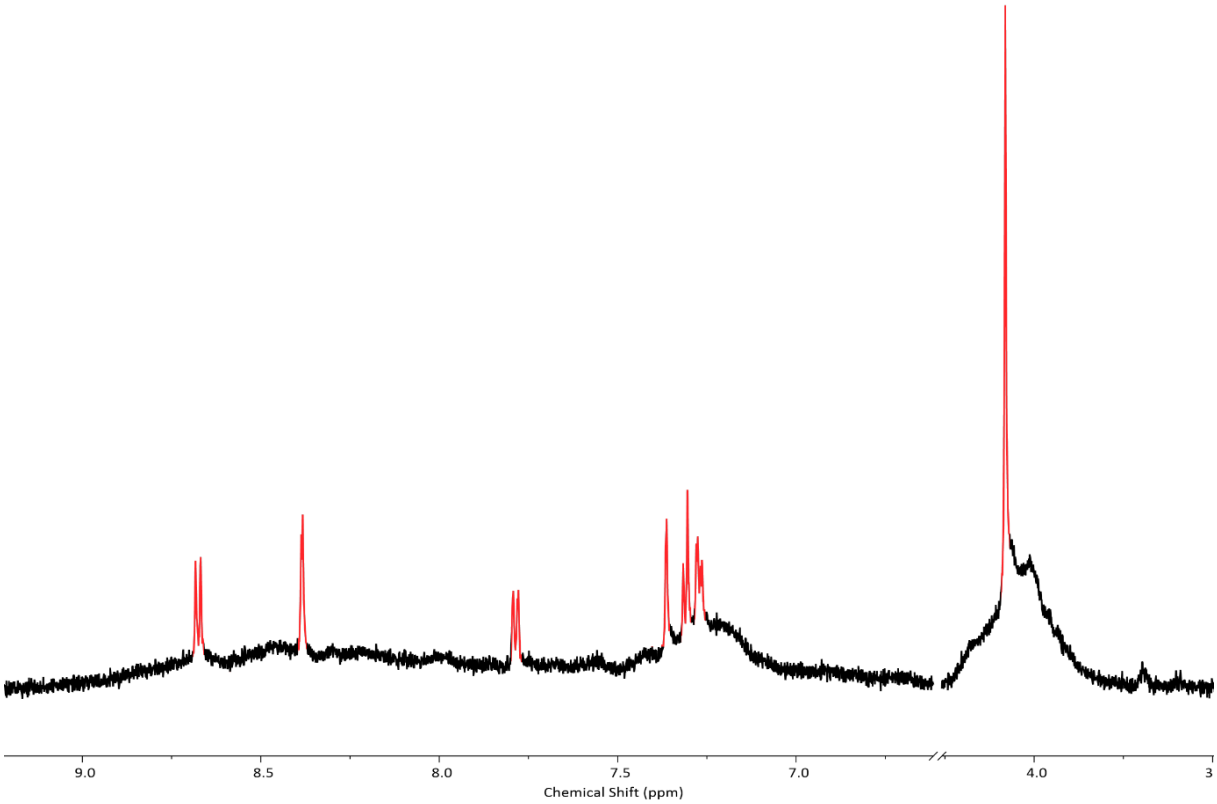

Figure 3.2.2: *Partial ^{1}H NMR (600 MHz, D_2O) of crude product of attempted direct Co_4(**L38**)$_6$(NO_3)$_{12}$ formation.*

Size exclusion chromatography allowed a very small amount of cage to be isolated (yield = 6%), proving the presence of the tetrahedron (Fig. 3.2.3). Due to limited material, the properties of this new cage could not be investigated in depth but it was possible to demonstrate that the cage was able to bind the perrhenate anion and so is likely to share the guest binding properties of **C19** and **C20**.

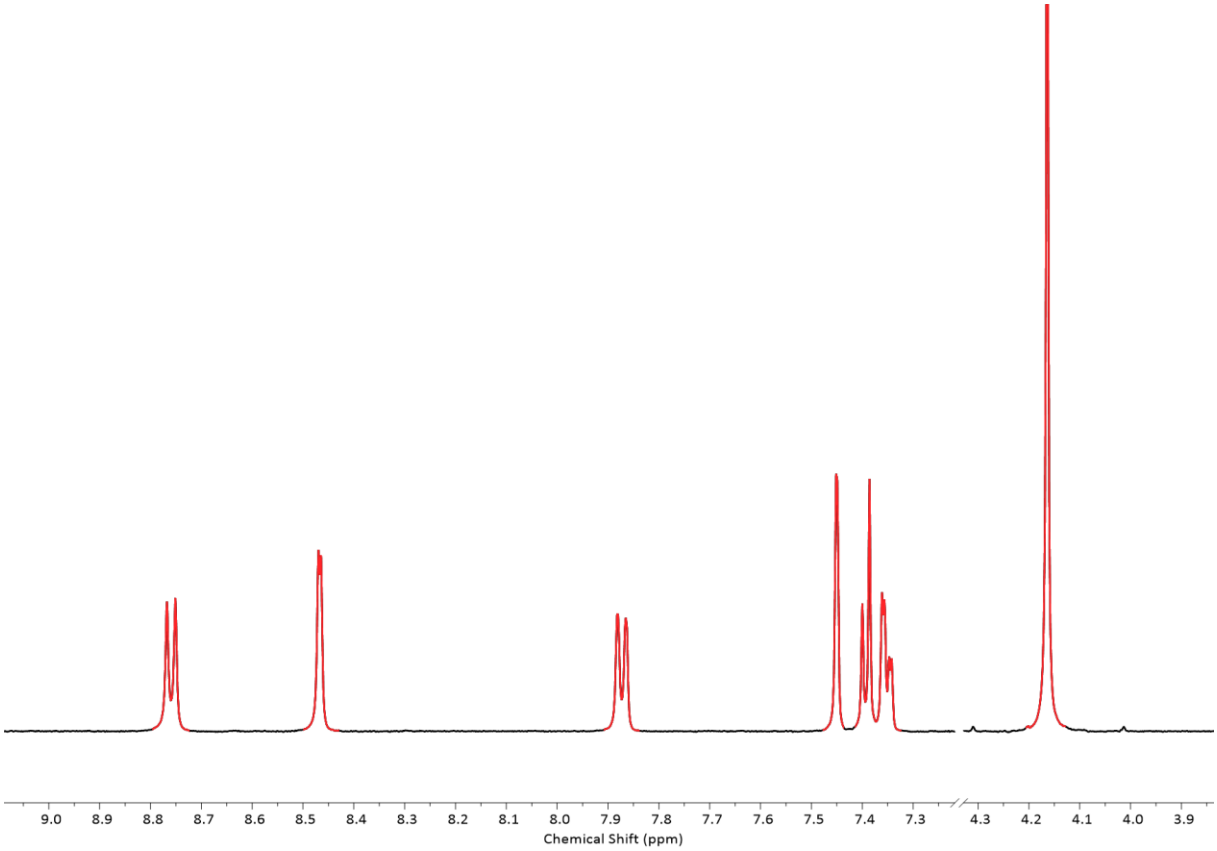

*Figure 3.2.3: Partial ^{1}H NMR (600 MHz, D_2O) of Co_4(**L38**)$_6$(NO_3)$_{12}$ synthesised by direct cage formation.*

In light of the ligand encountering similar cage formation challenges as **L20**, synthesis by ligand exchange was attempted, with an excess of the ligand added to a solution of **C19** in a water-acetonitrile mixture before heating and monitoring with ^{1}H NMR (Fig. 3.2.4).

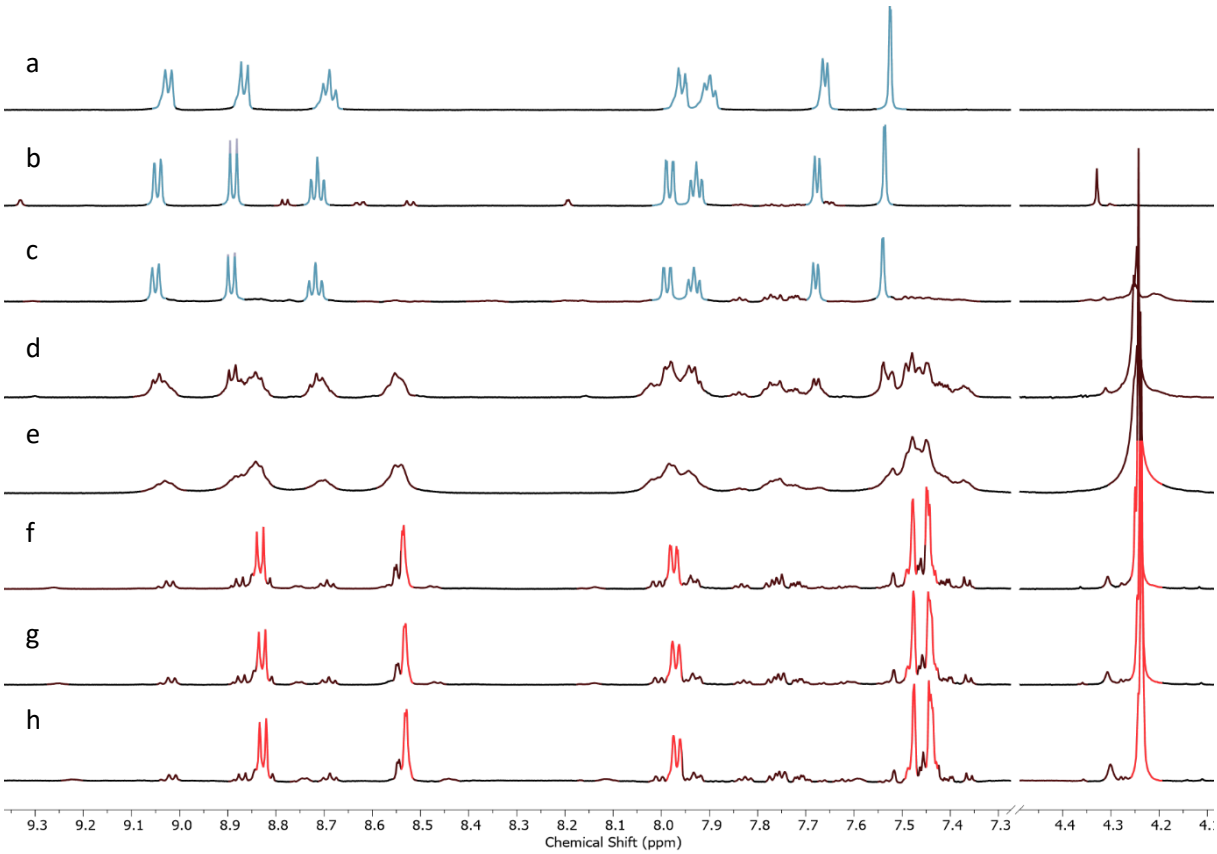

*Figure 3.2.4: Partial ^{1}H NMR (600 MHz, 9:1 D_2O/CD_3CN) of ligand exchange of **L38** into **C19**. (a) **C19**, (b) After addition of **L38,** sampled then heated at 75 °C for (c) 1 hour, (d) 1 day, (e) 4 days, (f) 12 days, (g) 13 days, (h) 15 days. **C19** peaks highlighted in blue. **C38** highlighted in red.*

This ligand exchange appeared successful, with peaks consistent with **C38** becoming dominant after 12 days at 75 °C (Fig. 3.2.5). As could be expected, the intermediate stages of the ligand exchange showed very broad signals, likely caused by the solid in solution leading to poor shimming. The greater solubility of **L38** allowed the easy workup of the reaction by extraction of the excess ligands with chloroform. The resulting solution also appears to contain several other well-defined species with apparent high symmetry, implying that they are heteroleptic species. Unfortunately, time constraints did not allow the confirmation of the nature of these species or attempts at their separation, but ligand exchange appeared a promising means of synthesising **C38**.

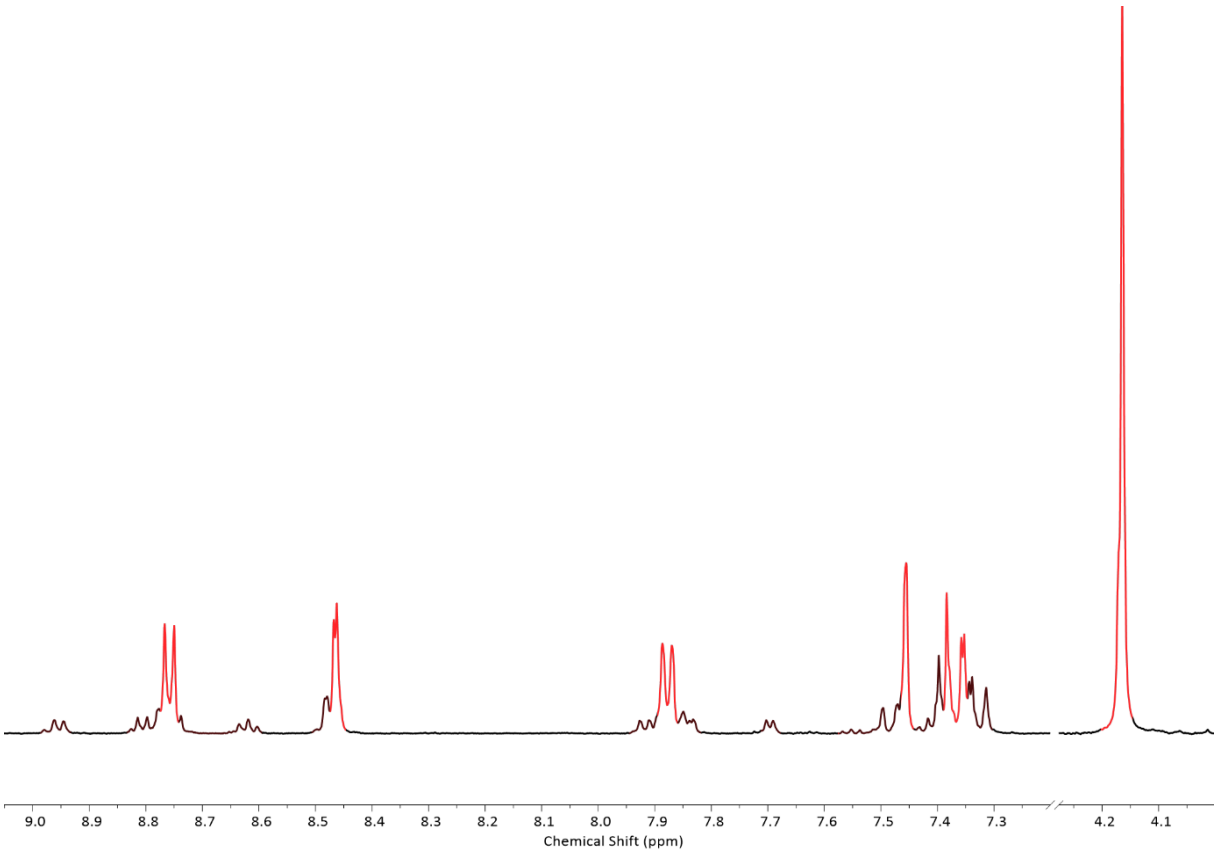

*Figure 3.2.5 Partial ^{1}H NMR (600 MHz, D_2O): Unpurified Co_4(**L38**)$_6(NO_3)_{12}$ and heteroleptic impurities.*

The properties of **C38** in comparison to both **C19** and **C20** would be of great interest. The stability offered by the ether groups should be assessed in order to ascertain whether the functionalisation imparts the necessary stability for biological applications. This could be assessed through both [^{99m}Tc]TcO_4^- binding studies and glutathione assays as with the previous systems. The development of a second isostructural ligand to **L19** presents the possibility of a greater exploration of ligand exchange reactions, as the hypothesised intermediate ligation strength of **L38** may provide information on the kinetic and thermodynamic details of the reaction.

The success of the methyl ether functionalised ligand suggests that the use of alkoxide nucleophiles could be a promising means of functionalising ligands with a variety of other groups. These groups could be reacted with **N19** in a parallel synthesis to **L38**. However, reaction with **L33** may be more lucrative, allowing the direct synthesis of functionalised ligands without the need for further homocoupling and reduction.

3.2.11 Ligand Exchange using Functionalised Ligands

The ligand exchange reaction described in Chapter 2 is a promising means of post-assembly modification, which may allow the substitution of conjugated ligands into cages without the need for

additional reagents. Theoretically, this exchange could be made either partial or complete, by using different stoichiometries.

Full exchange would be more effective for groups which seek to change the general properties of the cage, while partial exchange would be more desirable for conjugation to a single targeting group. Intermediate exchange could be useful for accessing polyvalent targeting, e.g. protein-protein interactions. Therefore, developing a synthetic procedure for either Co_4(**L35**)$_6$(NO_3)$_{12}$ or Co_4(**L20**)$_5$(**L35**)$_1$(NO_3)$_{12}$ would be a proof of concept for general cage functionalisation. The cages could theoretically be formed in different manners: the homoleptic cage is most logically synthesised by substitution of **L35** into Co_4(**L19**)$_6$(NO_3)$_{12}$ in exactly the same manner as Co_4(**L20**)$_6$(NO_3)$_{12}$. However, Co_4(**L20**)$_5$(**L35**)$_1$(NO_3)$_{12}$ would theoretically be best synthesised by starting with Co_4(**L20**)$_6$(NO_3)$_{12}$ and substituting with **L35**. Substitution into Co_4(**L20**)$_6$(NO_3)$_{12}$ should be feasible as the previous ligand exchange experiments with Co_4(**L19**)$_6$(NO_3)$_{12}$ and **L20** appeared to be under thermodynamic control. Therefore, addition of an appropriate amount of **L35** added to an exchange reaction should lead to the system being driven to a majority of Co_4(**L20**)$_5$(**L35**)$_1$(NO_3)$_{12}$.

An initial experiment appeared to show evidence of the exchange occurring by ^{1}H NMR; however, the significant loss of symmetry of caused by the substitution of single ligand makes NMR analysis a limited means of monitoring the reaction. Unfortunately, time constraints precluded the use of other techniques, such as mass spectrometry to analyse the reaction.

3.3 Summary

A means of generating functionalised variants of the **L20** was explored. Direct functionalisation of the amine groups was found to be ineffective due to their extremely electron poor nature. Substitution of nitro groups by different amines using S_NAr chemistry also proved ineffective. Instead, **L20** was utilised as a precursor itself and substituted to give the chlorine functionalised **L33.** This ligand successfully underwent Buchwald-Hartwig coupling to yield a ligand with pendant propargyl amine suitable for CuAAC reactions. Furthermore, it was shown that this ligand could be "clicked" with a PEG chain using a heterogenous Cu-C catalyst.

A ligand functionalised with methyl ether groups in the place of amines (**L38**) was also successfully synthesised using a combination of S_NAr and Stille reactions. The tetrahedron was synthesised in poor yield due to similar kinetic trapping of byproducts as observed in **C20**.

While many of the synthetic routes reported in this chapter have proved problematic, they will nonetheless allow the continuation of the project in multiple possible directions. Whether Co_4(**L38**)$_6$$(NO_3)_{12}$ shares the robustness of **C20** will be of interest to inform us as to whether it is a viable alternative for use *in vivo*.

3.4 Experimental

General Information

As described in Chapter 2.

Abbreviations used in this text:

DMSO	Dimethylsulfoxide
DMF	*N,N*-dimethylformamide
THF	Tetrahydrofuran
DCM	Dichloromethane
NMR	Nuclear Magnetic Resonance
DOSY	Diffusion ordered spectroscopy
RT	Room temperature
EDTA	Ethylenediaminetetraacetic acid
Na_4EDTA	Ethylenediaminetetraacetic acid tetrasodium salt
MS	Mass Spectrometry
DCE	Dichloroethane
BPin	Bis(pinacolato) diboron
BINAP	2,2'-Bis(diphenylphosphino)-1,1'-binaphthyl
DBA	Dibenzylideneacetone

Direct functionalisation of L20

Ethylbromoacetate

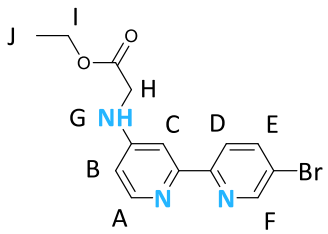

N6 (106.4 mg, 0.424 mmol), Et_3N (30 µL, 21.7 mg, 0.214 mmol), ethylbromoacetate (110 µL, 165.6 mg, 0.992 mmol) were dissolved in THF (10 mL) and stirred under N_2 for 72 h. The solvent was removed *in vacuo* and the crude product was crystallised from hot acetonitrile to give product as colourless crystalline material. Yield = 27 mg (19 %).

^{1}H NMR (500 MHz, DMSO-d_6) δ 8.85 (d, J = 2.4 Hz, 1H, H_F), 8.40 (dd, J = 8.3, 2.4 Hz, 1H, H_E), 8.26 (d, J = 7.3 Hz, 1H, H_A), 7.80 (d, J = 8.3 Hz, 1H, H_D), 7.01 (d, J = 2.7 Hz, 1H, H_C), 6.98 (dd, J = 7.3, 2.7 Hz, 1H, H_B), 5.07 (s, 2H, H_H), 4.16 (q, J = 7.1 Hz, 2H, H_I), 1.18 (t, J = 7.1 Hz, 3H, H_J).

Synthesis and reactions of L33

L33

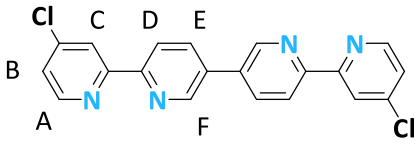

Finely ground **L20** (504.8 mg, 1.48 mmol) was added to hydrochloric acid (40% in water, 20 mL) and sonicated for 15 minutes. Additional hydrochloric acid (580 mL) was added and the mixture stirred vigorously for 30 minutes under gentle warming (beware corrosive gas evolution) and then sonicated for a further five minutes to attain complete dissolution. The mixture was cooled to 0 °C and a solution of sodium nitrite (1.0 mg, 0.02 mmol, 15 mL) was added dropwise resulting in a yellow solution. The reaction was stirred at 0 °C for 6 h then at room temperature for 24 h. Hydrochloric acid (20%, 100 mL) was added to dissolve the colourless precipitate. NaOH solution (240 g, 1 L) was added slowly, while the temperature was maintained below 20 °C. Then solid sodium carbonate was added until the pH = 8 and the mixture was extracted with $CHCl_3$ (3 × 400 mL). The combined organic phases were dried over $MgSO_4$ and the solvent removed *in vacuo* to give the product as a pale-yellow powder. Yield = 436 mg (78%).

^{1}H NMR (400 MHz, Chloroform-*d*) δ 8.99 (dd, *J* = 2.4, 0.8 Hz, 1H, H_F), 8.61 (dd, *J* = 5.3, 0.7 Hz, 1H, H_A), 8.55 (dd, *J* = 8.3, 0.8 Hz, 1H, H_D), 8.53 (dd, *J* = 2.1, 0.6 Hz, 1H, H_C), 8.11 (dd, *J* = 8.3, 2.4 Hz, 1H, H_E), 7.36 (dd, *J* = 5.3, 2.1 Hz, 1H, H_B).^{13}C NMR (126 MHz, Chloroform-*d*) δ 157.2, 154.8, 150.3, 147.7, 145.5, 135.5, 133.7, 124.3, 121.8, 121.7. HR-ESI-MS: *m/z* 379.0473 (predicted [M+H]+ = 379.0512)

*Protected propargyl amine **N16** synthesis*

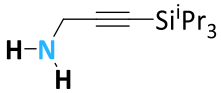

Protected propargyl amine synthesised according to literature procedure.[31]

*Buchwald-Hartwig coupling of **L33***

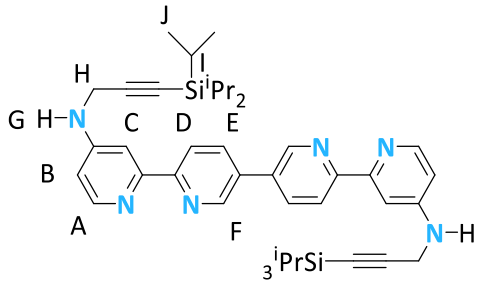

L33 (146.9 mg, 0.39 mmol), ^{t}BuONa (112.8 mg, 1.17 mmol), BINAP (435.0 mg, 0.70 mmol) and $Pd_2(DBA)_3$ (31.9 mg, 0.035) were suspended in toluene (20 mL) in a sealed vial under N_2. **N16** (0.4 mL, 0.86 g mL^{-1}, 0.47 mmol) was added via syringe and the mixture was heated at 100 °C for 48 h. The mixture was diluted with water (100 mL) and extracted with chloroform (3 × 200 mL). The organic phases were combined and dried over $MgSO_4$. The solvent was removed *in vacuo* and the crude product was crystallised from hot acetonitrile. Yield = 163 mg (58%).

^{1}H NMR (601 MHz, Chloroform-*d*) δ 8.94 (d, *J* = 2.4 Hz, 2H, H_F), 8.51 (d, *J* = 8.2 Hz, 2H, H_D), 8.37 (d, *J* = 5.6 Hz, 2H, H_A), 8.06 (dd, *J* = 8.2, 2.4 Hz, 2H, H_E), 7.77 (d, *J* = 2.5 Hz, 2H, H_C), 6.61 (dd, *J* = 5.6, 2.5 Hz, 2H, H_B), 4.49 (t, *J* = 5.7 Hz, 2H, H_G), 4.12 (d, *J* = 5.7 Hz, 4H, H_H), 1.03 – 1.02 (m, 24H, $H_{I,J}$). HR-ESI-MS: *m/z* 365.2265 (predicted [M+2H]+ = 365.2282), 729.4466 (predicted [M+H]+ = 729.4491).

L35 Synthesis: TIPS Deprotection

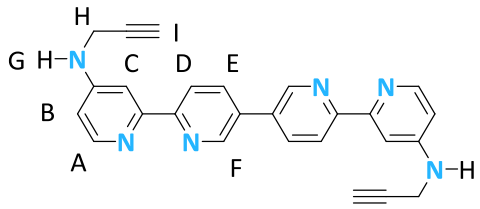

L34 (75.4 mg, 0.10 mmol) was dissolved in THF (6 mL) in a sealed microwave vial under N_2. Tetrabutyl ammonium fluoride (1 M in THF, 0.25 mL) was added dropwise. The reaction was stirred for 2 h. The reaction was diluted with water (10 mL) and the precipitate was collected by filtration. The residue was then extracted with THF (200 mL) and the solvent removed *in vacuo*. The crude product was heated in acetonitrile before being allowed to cool and filtered. The retentate was washed with acetonitrile and isopropanol and dried to give an off-white solid. Yield = 26 mg (61 %).

^{1}H NMR (601 MHz, Chloroform-*d*) δ 8.96 (d, *J* = 2.4 Hz, 2H, H_F), 8.51 (d, *J* = 8.2 Hz, 2H, H_D), 8.39 (d, *J* = 5.6 Hz, 2H, H_A), 8.07 (dd, *J* = 8.2, 2.4 Hz, 2H, H_E), 7.75 (d, *J* = 2.5 Hz, 2H, H_C), 6.60 (dd, *J* = 5.6, 2.5 Hz,

2H, H_B), 4.50 (s, 2H, H_G), 4.10 (dd, *J* = 5.8, 2.5 Hz, 4H, H_H), 2.30 (t, *J* = 2.5 Hz, 2H, H_I). HR-ESI-MS: *m/z* 209.0948 (predicted [M+2H]+ = 209.0947), 417.1831 (predicted [M+H]+ = 317.1822).

^{1}H NMR (601 MHz, DMSO-d_6) δ 9.12 (dd, *J* = 2.4, 0.9 Hz, 2H, H_F), 8.46 (dd, *J* = 8.3, 0.9 Hz, 2H, H_D), 8.34 (dd, *J* = 8.3, 2.4 Hz, 2H, H_E), 8.25 (d, *J* = 5.6 Hz, 2H, H_A), 7.75 (d, *J* = 2.4 Hz, 2H, H_C), 7.10 (t, *J* = 5.9 Hz, 2H, H_G), 6.66 (dd, *J* = 5.6, 2.4 Hz, 2H, H_B), 4.03 (dd, *J* = 6.0, 2.4 Hz, 4H, H_H), 3.17 (t, *J* = 2.4 Hz, 2H, H_I).

Synthesis of L36

CuAAC reaction

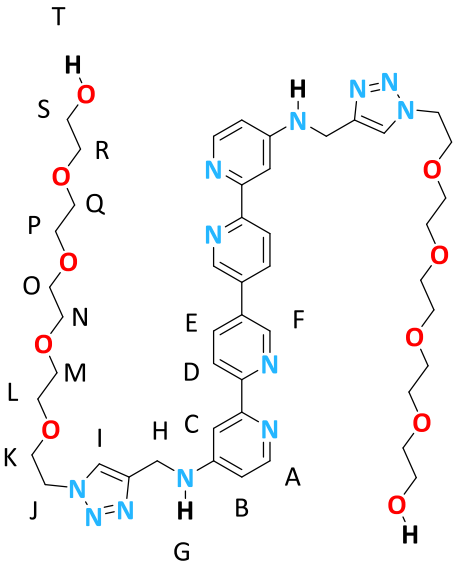

L33 was suspended in DCE (10 mL). Cu/C (81.4 mg) and trimethylamine (20 µL, dried over NaOH) were added. The mixture was sparged with N_2 and heated at 60 °C for 72 h. The mixture was allowed to cool and filtered onto celite. The retentate was extracted with DMF and the solvent removed *in vacuo*. The residue was washed with methanol and collected as an off-white powder. Detected by not isolated.

^{1}H NMR (601 MHz, DMSO-d_6) δ 9.09 (d, *J* = 2.4 Hz, 2H, H_F), 8.44 (d, *J* = 8.3, 2H, H_D), 8.31 (dd, *J* = 8.3, 2.4 Hz, 1H, H_E), 8.20 (d, *J* = 5.6 Hz, 1H, H_A), 7.75 (d, *J* = 2.4 Hz, 1H, H_C), 7.22 (t, *J* = 5.8 Hz, 1H, $H_{I?}$), 6.67 (dd, *J* = 5.7, 2.4 Hz, 1H. H_B). HR-ESI-MS: *m/z* 472.2419 (predicted [M+2H]+ = 427.2429). Not isolated in sufficient yield for ^{13}C.

Synthesis of L38

*Synthesis of **N19** by S_NAr*

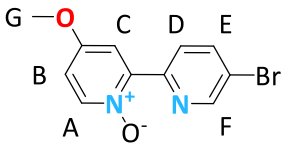

N5 (1.01 g, 3.40 mmol) and NaOH (1.16 g, 29.06 mmol) were dissolved in methanol (200 mL). The reaction mixture was heated at 75 °C for 3 h. The reaction was allowed to cool to room temperature and diluted with a DCM/water mixture (550 mL:300 mL). The aqueous layer extracted with DCM (3 x 250 mL) and the solvent removed from combined organic fractions *in vacuo*. Water (150 mL) was added to the residue and the mixture extracted with DCM (5 x 150 mL), the combined organic fractions were dried over $MgSO_4$ and the solvent *in vacuo* to give an off-white solid. Yield = 0.86 g (91%).

^{1}H NMR (400 MHz, DMSO-*d*6) δ 8.92 (d, *J* = 8.6 Hz, 1H, H_D), 8.87 (d, *J* = 2.5 Hz, 1H, H_F), 8.31 – 8.26 (m, 1H, H_A), 8.21 (dd, *J* = 8.6, 2.5 Hz, 1H, H_E), 7.66 (d, *J* = 3.6 Hz, 1H, H_C), 7.14 (dd, *J* = 7.3, 3.7 Hz, 1H, H_B), 3.89 (s, 3H, H_G). ^{13}C NMR (126 MHz, Chloroform-*d*) δ 157.7, 150.5, 148.1, 146.9, 141.9, 139.2, 126.9, 121.9, 113.5, 111.1, 56.4. HR-ESI-MS: *m/z* 280.9920 (predicted [M+H]+ = 280.9920)

*Synthesis of **N20** by S_NAr*

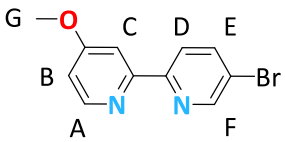

N7 (0.103 g, 0.37 mmol) and NaOH (0.166 g, 4.14 mmol) dissolved in methanol (50 mL). and was heated at 75 °C for 1 h. The reaction was allowed to cool to room temperature. The mixture was diluted with DCM/water mixture (25 mL: 25 mL) and the aqueous layer extracted with DCM (3 x 100 mL). The combined organic fractions were washed with water (50 mL) and dried over $MgSO_4$ and the solvent removed *in vacuo* to give an off-white solid. Yield = 88 mg (90%).

^{1}H NMR (500 MHz, Chloroform-*d*) δ 8.71 (d, *J* = 2.4 Hz, 1H, H_F), 8.47 (d, *J* = 5.6 Hz, 1H, H_A), 8.32 (d, *J* = 8.5 Hz, 1H, H_D), 7.94 (d, *J* = 2.7 Hz, 1H, H_C), 7.93 (dd, *J* = 8.5, 2.4 Hz, 1H, H_E), 6.86 (dd, *J* = 5.6, 2.7 Hz, 1H, H_B), 3.95 (s, 3H, H_G). ^{13}C NMR (126 MHz, Chloroform-*d*) δ 166.9, 157.2, 154.6, 150.5, 150.2, 139.6, 122.7, 121.4, 111.2, 106.2, 55.5. HR-ESI-MS: *m/z* 264.99798 (predicted $[M+H]_+$ = 264.99710)

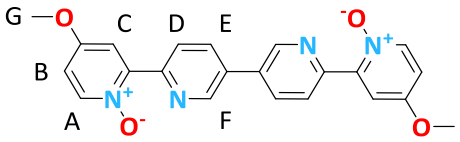

N19 (0.502 g, 1.79 mmol), $Pd(PPh_3)_4$ (0.102 g, 0.089 mmol) and $(Bu_3Sn)_2$ (0.50 mL, 1.09 mmol) were suspended in toluene (40 mL) and then sparged with N_2. The reaction mixture was heated at 100 °C for 48 h. The reaction mixture was concentrated *in vacuo* and the crude product was purified via column chromatography (Eluent: 1% trimethylamine/ DCM) to give the off-white solid product. Yield = 0.238 g (66%).

^{1}H NMR (400 MHz, DMSO-d_6) δ 9.24 (d, J = 2.4 Hz, 2H, H_F), 9.11 (d, J = 8.4 Hz, 2H, H_D), 8.42 (dd, J = 8.4, 2.4 Hz, 2H, H_E), 8.30 (d, J = 7.3 Hz, 2H, H_A), 7.77 (d, J = 3.6 Hz, 2H, H_C), 7.15 (dd, J = 7.3, 3.6 Hz, 2H, H_B), 3.92 (s, 6H, H_G). ^{13}C NMR (126 MHz, DMSO-d_6) δ 156.3, 149.1, 147.4, 145.9, 141.6, 113.5, 111.2, 56.3, 52.0, 27.7, 7.2. HR-ESI-MS: *m/z* 403.1363 (predicted [M+H]+ = 403.1401).

N-oxide reductions

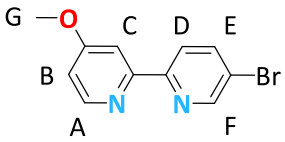

N19 Reduction with Fe (0)

N19 (0.25 g, 0.90 mmol) and Fe (fillings, 0.27 g, 4.84 mmol) were suspended in acetic acid (40 mL) and heated at 80 °C for 2 h under N_2. The mixture was allowed to cool to room temperature and a solution of NaOH (1.35 g, 38.52 mmol), EDTA (2.80 g, 9.59 mmol) in water (40 mL) and ammonia (80 mL) was added slowly. The mixture was extracted with chloroform (3 x 150 mL) and the combined organic phases were dried over $MgSO_4$. The solvent was removed *in vacuo* and the crude product was crystallised from hot toluene to give an off-white solid. Yield =0.193 g, (81%). Characterisation matched previous synthesis. (See above)

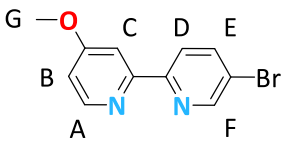

N20 Reduction with BPin

N19 (13.7 mg, 0.00487 mmol) and bis(pin)diboron (12.6 mg, 0.0049 mmol) were dissolved in CD_3CN (0.5 mL) in a sealed NMR tube and heated at 70 °C for 1 h. Ethylenediamine (65 µL, 0.9747 mmol) was added and the reaction stirred for two hours. Water (0.5 mL) was added and the aqueous layer

extracted with dichloromethane (3 x 0.5 mL). The organic phases were combined, dried over $MgSO_4$ and concentrated *in vacuo.* Characterisation matched previous synthesis. (See above)

L38

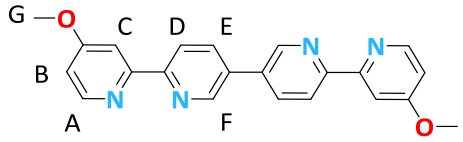

N21 (0.24 g, 0.59 mmol) and bis(pinacolato)diboron (0.30 g, 1.19 mmol) were dissolved in acetonitrile (60 mL) and sparged with N_2. The reaction mixture was heated at 70 °C for 4.5 h. The reaction was allowed to cool, ethylenediamine (1.6 mL, 23.93 mmol) was added and stirred for 1 h. Water (25 mL) was added to the reaction mixture and it was extracted using dichloromethane (3 x 25 mL). The organic fractions were combined, dried over $MgSO_4$ and concentrated *in vacuo.* The crude product was purified using column chromatography (Gradient eluent: dichloromethane/trimethylamine/ methanol: 100:0:0 to 99:1:0 to 94:1:5) to give product as off-white solid. Yield = 0.12 g (54%).

^{1}H NMR (601 MHz, DMSO-d_6) δ 9.16 (d, J = 2.1 Hz, 2H, H_F), 8.55 (d, J = 5.6 Hz, 2H, H_A), 8.52 (d, J = 8.2 Hz, 2H, H_D), 8.40 (dd, J = 8.2, 2.1 Hz, 2H, H_E), 8.00 (d, J = 2.2 Hz, 2H, H_C), 7.08 (dd, J = 5.6, 2.2 Hz, 2H, H_B), 3.95 (s, 6H, H_G). ^{13}C NMR (126 MHz, DMSO-*d*6) δ 166.3, 156.6, 154.6, 150.8, 147.4, 135.3, 132.6, 110.8, 106.0, 73.5, 24.9. HR-ESI-MS: *m/z* 371.1496 (predicted [M+H]+ = 371.1503)

Cage formations

*Co_4(**L38**)$_6$(NO_3)$_{12}$ (C38) by direct formation*

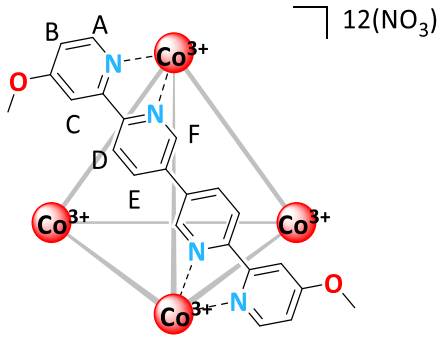

$Co(NO_3)_2.6(H_2O)$ (27.5 mg, 0.094 mmol) and **L38** (50.5 mg, 0.14 mmol) were suspended in a mixture of degassed water/acetonitrile (9:1, 6 mL) and sparged with N_2 and heated at 60 °C for 16 h. $(NH_4)_2Ce(NO_3)_6$ (79.6 mg, 0.145 mmol) dissolved in acetonitrile (6 mL) and added using a syringe pump at a rate of 6.0 µL/min. Acetonitrile (20 mL) was added to precipitate the product. The yellow product was isolated by filtration onto celite, washed with acetonitrile and then eluted with water (15 mL). The combined filtrates were concentrated *in vacuo* and loaded onto a size-exclusion column (Sephadex LH-20). The progress of the column was tracked from the appearance of a yellow band and

the product fractions identified by ^{1}H NMR. The fractions containing product were combined and freeze-dried to give a pale solid. Yield = 4.6 mg (6%).

^{1}H NMR (500 MHz, D_2O) δ 8.76 (d, *J* = 8.2 Hz, 1H, H_D), 8.47 (d, *J* = 2.7 Hz, 1H, H_C), 7.87 (d, *J* = 8.2 Hz, 1H, $_E$), 7.45 (s, 1H, H_F), 7.39 (d, *J* = 7.0 Hz, 1H, H_A), 7.35 (dd, *J* = 7.0, 2.5 Hz, 1H, H_B), 4.16 (s, 3H, H_G). ^{13}C NMR (126 MHz, D_2O) δ 171.4, 155.8, 155.3, 151.6, 149.0, 144.1, 138.0, 125.9, 117.1, 115.1, 57.7. ^{1}H DOSY NMR (500 MHz, D_2O): D = 1.91 x 10^{-6} cm^2 s^{-1}; calculated hydrodynamic radius = 12.5 Å.

Ligand exchange reactions

C38

C19 (5.1 mg, 1.8 µmol) was dissolved in a mixture of D_2O (842 µL) and CD_3CN (98 µL) in an NMR tube. A ^{1}H NMR was collected and **L38** (8.2 mg, 22 µmol) was added and another ^{1}H NMR was taken. The reaction was then sealed and heated at 75 °C. It was periodically allowed to cool for 30 minutes, monitored by ^{1}H NMR and returned to heating.

Co_4(L20)$_5$(L35)$(NO_3)_{12}$

C20 (3.0 mg, 1 µmol) was dissolved in a mixture of D_2O (450 µL) and CD_3CN (50 µL) in an NMR tube and a ^{1}H NMR was collected. **L35** (0.4 mg, 1 µmol) was added and another ^{1}H NMR was taken. The reaction was then sealed and heated at 75 °C. It was periodically allowed to cool for 30 minutes, monitored by ^{1}H NMR and returned to heating.

3.5 References

1 G. Yu, M. Zhang, M. L. Saha, Z. Mao, J. Chen, Y. Yao, Z. Zhou, Y. Liu, C. Gao, F. Huang, X. Chen and P. J. Stang, *J. Am. Chem. Soc.*, 2017, **139**, 15940–15949.

2 F. Kiessling, M. E. Mertens, J. Grimm and T. Lammers, *Radiology*, 2014, **273**, 10–28.

3 G. M. Mortimer, N. J. Butcher, A. W. Musumeci, Z. J. Deng, D. J. Martin and R. F. Minchin, *ACS Nano*, 2014, **8**, 3357–3366.

4 P. R. Symmers, M. J. Burke, D. P. August, P. I. T. Thomson, G. S. Nichol, M. R. Warren, C. J. Campbell and P. J. Lusby, *Chem. Sci.*, 2015, **6**, 756–760.

5 J. E. M. Lewis, A. B. S. Elliott, C. J. McAdam, K. C. Gordon and J. D. Crowley, *Chem. Sci.*, 2014, **5**, 1833–1843.

6 J. Han, A. Schmidt, T. Zhang, H. Permentier, G. M. M. Groothuis, R. Bischoff, F. E. Kühn, P. Horvatovich and A. Casini, *Chem. Commun.*, 2017, **53**, 1405–1408.

7 D. Fujita, K. Suzuki, S. Sato, M. Yagi-Utsumi, Y. Yamaguchi, N. Mizuno, T. Kumasaka, M. Takata, M. Noda, S. Uchiyama, K. Kato and M. Fujita, *Nat. Commun.*, 2012, **3**, 1093–1102.

8 D. A. Roberts, B. S. Pilgrim and J. R. Nitschke, *Chem. Soc. Rev.*, 2018, **47**, 626–644.

9 D. Zhao, S. Tan, D. Yuan, W. Lu, Y. H. Rezenom, H. Jiang, L.-Q. Wang and H.-C. Zhou, *Adv. Mater.*, 2011, **23**, 90–93.

10 Z. Li, T. S. Seo and J. Ju, *Tetrahedron Lett.*, 2004, **45**, 3143–3146.

11 S. Han, Z. Ma, R. Hopson, Y. Wei, D. Budil, S. Gulla and B. Moulton, *Inorg. Chem. Commun.*, 2012, **15**, 78–83.

12 Z. Ma, S. Han, R. Hopson, Y. Wei and B. Moulton, *Inorganica Chim. Acta*, 2012, **388**, 135–139.

13 J. Dommerholt, F. P. J. T. Rutjes and F. L. van Delft, *Top. Curr. Chem.*, 2016, **374**, 1–20.

14 R. Chakrabarty and P. J. Stang, *J. Am. Chem. Soc.*, 2012, **134**, 14738–14741.

15 M. Wang, W.-J. Lan, Y.-R. Zheng, T. R. Cook, H. S. White and P. J. Stang, *J. Am. Chem. Soc.*, 2011, **133**, 10752–10755.

16 D. A. Roberts, A. M. Castilla, T. K. Ronson and J. R. Nitschke, *J. Am. Chem. Soc.*, 2014, **136**, 8201–8204.

17 T. Kan and T. Fukuyama, *Chem. Commun.*, 2004, **4**, 353–359.

18 G. Yan and M. Yang, *Org. Biomol. Chem.*, 2013, **11**, 2554–2566.

19 S. Abou-Shehada, M. C. Teasdale, S. D. Bull, C. E. Wade and J. M. J. Williams, *ChemSusChem*, 2015, **8**, 1083–1087.

20 S. Wagaw and S. L. Buchwald, *J. Org. Chem.*, 1996, **61**, 7240–7241.

21 R. Shetty, D. Nguyen, D. Flubacher, F. Ruggle, A. Schumacher, M. Kelly and E. Michelotti, *Tetrahedron Lett.*, 2007, **48**, 113–117.

22 M. J. Burke, The University of Edinburgh, 2016.

23 D. P. Nair, M. Podgórski, S. Chatani, T. Gong, W. Xi, C. R. Fenoli and C. N. Bowman, *Chem. Mater.*, 2014, **26**, 724–744.

24 E. K. Riga, D. Boschert, M. Vöhringer, V. T. Widyaya, M. Kurowska, W. Hartleb and K. Lienkamp, *Macromol. Chem. Phys.*, 2017, **218**, 1700273–1700282.

25 N. Salewska and M. J. Milewska, *J. Heterocycl. Chem.*, 2014, **51**, 999–1003.

26 B. P. Hubbard, A. P. Gomes, H. Dai, J. Li, A. W. Case, T. Considine, T. V Riera, J. E. Lee, S. Y. E, D. W. Lamming, B. L. Pentelute, E. R. Schuman, L. A. Stevens, A. J. Y. Ling, S. M. Armour, S. Michan, H. Zhao, Y. Jiang, S. M. Sweitzer, C. A. Blum, J. S. Disch, P. Y. Ng, K. T. Howitz, A. P. Rolo, Y. Hamuro, J. Moss, R. B. Perni, J. L. Ellis, G. P. Vlasuk and D. A. Sinclair, *Science*, 2013, **339**, 1216–1219.

27 D. Wenkert and R. B. Woodward, *J. Org. Chem.*, 1983, **48**, 283–289.

28 G.-J. ten Brink, I. W. C. E. Arends, M. Hoogenraad, G. Verspui and R. A. Sheldon, *Adv. Synth. Catal.*, 2003, **345**, 497–505.

29 E. Howard and W. F. Olszewski, *J. Am. Chem. Soc.*, 1959, **81**, 1483–1484.

30 H. P. Kokatla, P. F. Thomson, S. Bae, V. R. Doddi and M. K. Lakshman, *J. Org. Chem.*, 2011, **76**, 7842–7848.

31 V. Vaněk, J. Pícha, B. Fabre, M. Buděšínský, M. Lepšík and J. Jiráček, *European J. Org. Chem.*, 2015, **2015**, 3689–3701.

Chapter 4: *In Vitro* Raman Spectroscopy of Alkyne Labelled $Co^{III}_4L_6$ Tetrahedra

4.1 Introduction

4.1.1 *In vivo* Imaging of Capsules

With the suitability of our cage systems for biological applications a greater understanding the behaviour of the cages in a biological setting was of great interest. Cellular imaging of the cages could give more insight into their behaviour within organisms.

A number of groups have used fluorescence microscopy to the study biological behaviour of cages in a cellular environment. Though many ligands are fluorescent themselves, this is often quenched by coordination to the metal centres.[1] This means that the cages can only be indirectly imaged through the fluorescence of guests or ligands after disassembly.

The Yoshizawa group used the fluorescence of an anthracene-containing ligand to study the uptake and degradation of M_2L_4 cages $\mathbf{C4_{a,b}}$ in cells (Fig. 4.1.1). This study implied the uptake of both the cages and free ligands, though this may have been partially aided by the inclusion of ethanol in the cell solution which would be expected to increase cell permeability.[2] They observed that the less stable palladium cage $\mathbf{C4_a}$ showed similar uptake to the free ligand, leading to fluorescence in the cytoplasm of the cell, while the platinum cage $\mathbf{C4_b}$ caused fluorescence to be observed in the nucleus of the cell (Fig, 4.1.1, (c), ii-iv). These results suggest that the more stable $\mathbf{C4_b}$ is able to penetrate the nucleus of the cell while the palladium variants were degraded in the cytoplasm. The fact that the more stable assembly has weaker fluorescence signal, demonstrates the limitation of fluorescence for imaging stable coordination species.[3]

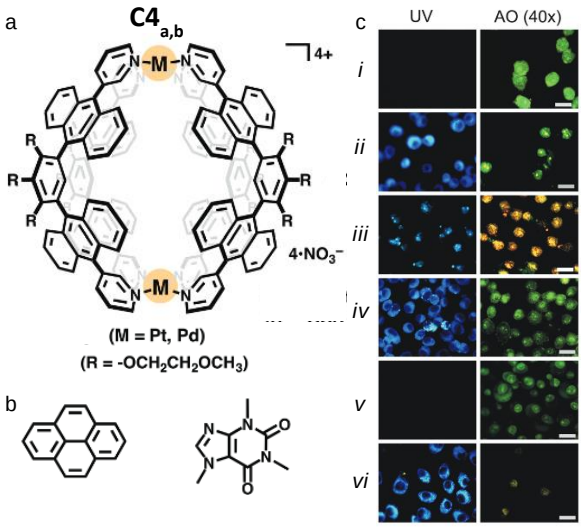

Figure 4.1.1: (a) M_2L_4 system (M = Pd, $\mathbf{C4_a}$ or Pt, $\mathbf{C4_b}$, R = -$OCH_2CH_2OCH_3$) used by Yoshizawa and co-workers, containing fluorescent anthracene panels. (b) Selection of guest tested in fluorescence studies. (c) Microscopy images (bright-field and fluorescence light under UV-light excitation) of (i)

untreated vital HT-29 cells, and cells treated for 4 h with 10μM solutions of (ii) ligand, (iii)Pt_2L_4 , (iv)Pd_2L_4, (v)Pt_2L_4·(pyrene)$_2$, and (vi) Pd_2L_4·(pyrene)$_2$. The fluorescence images under green-light excitation of (ii–vi) the treated and (i) the untreated HT-29 cells stained with acridine orange (AO), and visualized with 40× objectives (in AO (40×) respectively). The unstained cells are visualized with the 40× objective; all the scale bars mark 30μm. Adapted from 3.

Isaacs and co-workers were also able to indirectly image cellular behaviour by appending a fluorescent pro-drug onto the outside of a $Pd_{12}L_{24}$ cage using cucurbit[8]uril inclusion chemistry (**C9$_b$**, Fig.1.4.4).[4] Similarly Zheng and co-workers bound a tethered fluorescein inside Fujita's M_6L_4 truncated octahedron, which was then loaded into an anionic polymeric matrix to permit cellular imaging (**C8**, Fig. 1.4.3). They also showed the release of cis-platin from a bound fluorescein-platinum (IV) prodrug.[5]

In a similar manner, Therrien and co-workers were able to investigate their ruthenium trigonal prism (**C7**) through the release of a fluorescent pyrene guest in greater detail (Fig. 4.1.2).[6] They were able to show that the fluorescence was far higher within the cells when the host-guest complex was administered, rather than just the guest. They were also able to quantify the uptake of the guest through use of flow cytometry to investigate the effect of relative concentrations of guest and cage. Their results showed that the uptake of the cage was not linear with either concentration of host-guest complex or exposure time. Again, as fluorescence could only be observed by guest release, these results give limited information about the state of the cage and the nature of drug release.

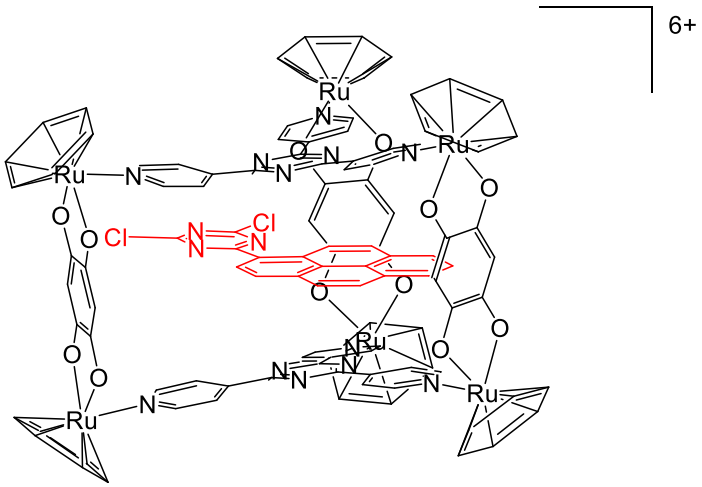

*Figure 4.1.2: Therrien and co-workers' triangular prism (**C7**) and fluorescent pyrene guest.*

In contrast, Stang and co-workers used assemblies based on ligands which show aggregation-induced emission and fluorescence, which is stronger when molecular rotation is restricted, either through aggregation or coordination. This permitted the active imaging of the assemblies within cells and even *in vivo.*[7]

The Lusby group have previously explored a range of options that would permit the fluorescent imaging of our robust $Co_4(\mathbf{L})_4(NO_3)_{12}$ tetrahedra. The cages **C15** and **C14** (Fig. 4.1.3 (a)) were found to bind a number of organic fluorophores (Fig. 4.1.3 (b)) but none were found to have sufficiently high association constants to allow cellular imaging. Therefore, attempts were made to tether a fluorophore to a tightly bound triisopropylsilanol guest (Fig. 4.1.3 (c)) but this was ultimately ineffective due design and solubility limits. Additionally, the inclusion of a fluorescent iridium metal complex into the ligand **L40** (Fig. 4.1.3, (d)) was trialled but the bulky groups were found to prevent cage formation due to their steric bulk.

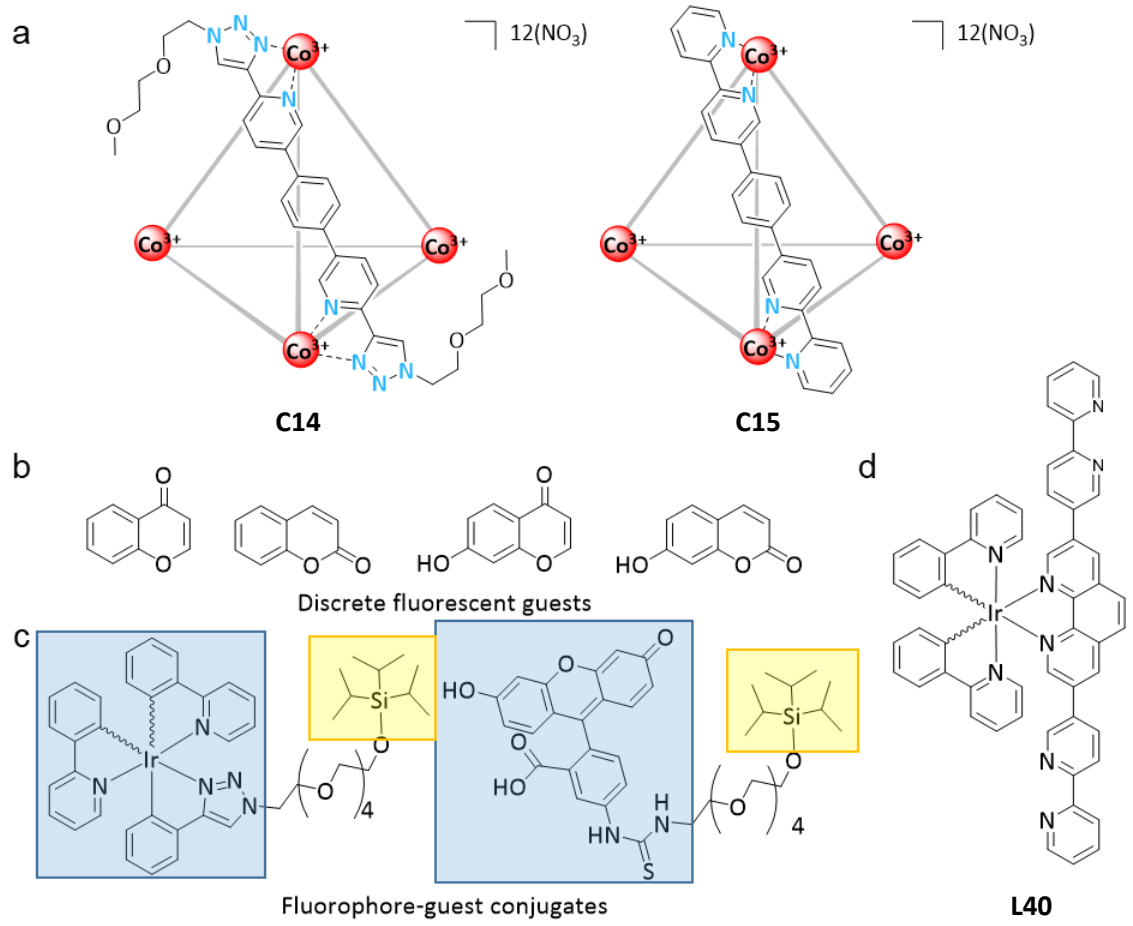

Figure 4.1.3: (a) ***C14*** *and* ***C15****, (b) Small fluorescent weakly binding guests of* ***C14*** *and* ***C15****, (c) Fluorophores (blue) tethered to a strongly binding triisopropyl silyl group (yellow), (d)* ***L40*** *containing fluorescent iridium complex.*

It is a commonly encountered problem in fluorescence microscopy that fluorophores are difficult to introduce into a molecule. Many common fluorophores, such as fluorescein and iridium complexes, have high molecular weights meaning that their incorporation is likely to significantly change the biological and physiochemical properties of the molecule of interest.

4.1.2 Raman Spectroscopy for Bioimaging

Raman spectroscopy represents a very attractive alternative approach to other cellular imaging methods as it uses very small spectroscopic "handles" that can be incorporated with little perturbation of molecular properties. Raman spectroscopy is similar to IR spectroscopy and uses the interaction of photons molecular vibrations to analyse compounds. The technique detects inelastically scattered photons, which have had an interaction with vibrational modes of the substrate to change the wavelength of the scattered photons. Most photons are scattered in an elastic manner and will therefore have the same energy as the incident photons. However, a small number of photons will be scattered inelastically, when they induce a change in polarizability of the molecule which couple to a molecular vibration. These photons are scattered at a different energy to the incident photons and can be detected to give a Raman spectrum.

Raman spectroscopy has other properties that make it an attractive imaging technique. It is largely non-destructive, using relatively low energy excitation and therefore allowing imaging of living cells. Cellular components can be visualised through detection of characteristic bands (Fig. 4.1.4); proteins can be detected by the peaks of amide carbonyl groups (1657 cm^{-1}), CH of phenylaniline (1033 cm^{-1}) and lipids can be detected by measuring the intensity of the CH_3 groups (2880 cm^{-1}). Importantly water has no signal and cells have a "silent region" in their Raman spectra between 1800-2800 cm^{-1}, in which few cellular components have any Raman signal. This means that signals in this range are easily detected due to minimal "noise".

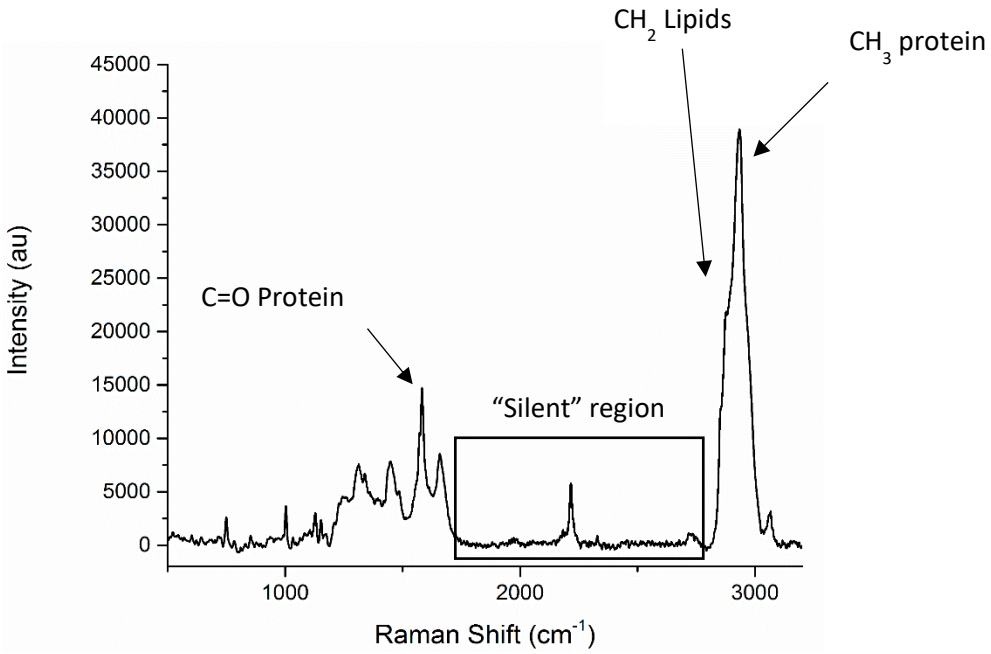

Figure 4.1.4: Spontaneous Raman spectra of HeLa cell pellet with characteristic vibrations and silent region highlighted.

A number of chemical groups have active Raman vibrations in the "silent region", including nitriles, azides, deuterium-carbon bonds and alkynes. Studies have shown that alkynes in general give the strongest signal out of these groups.[8] These groups are also small a and apolar making them easier to incorporate into a species of interest than large fluorophores

An alkyne tagged analogue of thymidine, originally developed for "click" labelling of cells with fluorescent groups,[9] was found to be to be suitable for direct imaging with Raman spectroscopy. Analysis of the 5-ethynyl-2-deoxyuridine (**EdU**, Fig. 4.1.5) signal in combination with that of the lipids and cytochrome in the cell was able to provide evidence for the accumulation of the alkyne-labelled species within the nucleus of HeLa cells.[10]

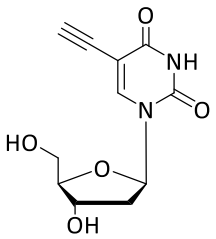

*Figure 4.1.5: Structure of **EdU**, a common Raman spectroscopic alkyne standard.*

This Raman imaging approach has been developed for simultaneous imaging of two different compounds within cells. Live-cell imaging has led to the technique providing insight into the cellular distribution of alkyne labelled lead drug compounds.[11]

Spontaneous Raman is the most common imaging variant, using a fixed wavelength laser which simultaneously stimulates all the Raman bands of the sample and giving a full spectrum. While this is effective for obtaining single spectra and has been used imaging cells,[12] the technique is insensitive as only a fraction of photons are scattered inelastically. This means the techniques requires relatively high concentrations of analyte and extended acquisition times to capture images, approximately 30 minutes for a single image, which can severely limit the suitability of the technique for imaging.[13]

A newer technique, known as stimulated Raman scattering (SRS), was developed to overcome this low signal problem. This technique uses two aligned lasers, wherein the difference in wavelength between the two beams matches a molecular vibration. When this vibration is stimulated it causes an intensity loss in one beam and an intensity gain in the other. Conversely, when no vibration is excited, then no change in the beam intensity occurs. Therefore, changes in beam intensity can be measured to detect the corresponding vibration. These measurements can be performed across a sample to give contrast images.[14] This technique is more sensitive, able to detect species at far lower concentrations, and far quicker, greatly decreasing acquisition time. This has greatly increased the feasibility of time-lapse cell

imaging, with SRS images being able to be collected in a matter of minutes or even seconds.[15] This allows real time imaging of living cells and tissue, allowing direct visualisation of drug uptake and metabolism.[11]

It was theorised that this technique could be informative for imaging the uptake of the metallosupramolecular cages in cells. The rigid, linear nature of alkynes permits their incorporation into ligands used in supramolecular cage assembly. Specifically, it was envisaged that an alkyne spacer could be placed between the two bipyridine groups of **L19** and/or **L20** without interfering with tetrahedron formation (Fig. 4.1.6). Assuming this is successful, stimulated Raman microscopy promises the possibility of being able to directly image intact cages within cells. This could provide a far greater understanding of uptake, distribution, guest release and metabolism of the cages within cells. This could significantly inform ongoing research into the biomedical applications of cage compounds.

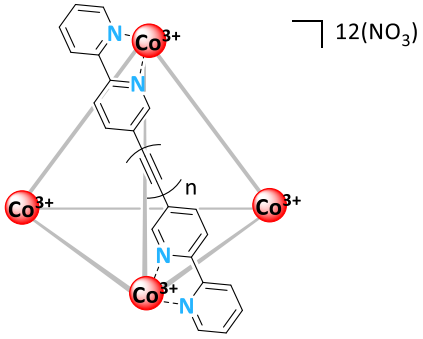

Figure 4.1.6: Proposed structure of tetrahedra formed from Raman active alkyne containing ligands (n = 1 or 2).

4.2 Results and Discussion

4.2.1 Synthesis of Alkyne Containing Cobalt (III) Tetrahedra

In order to closely match our existing cages, it was proposed that the alkynes could be used as central linkers in a M_4L_6 *bis*-bidentate ligand (Fig. 4.2.1). The *bis*-alkyne was proposed in order to attempt to have a more intense Raman signal. These would be close analogues of the previous M_4L_6 systems such as **L15**, hopefully meaning they would behave in a similar manner for formation, solubility and, more importantly, biological behaviour.

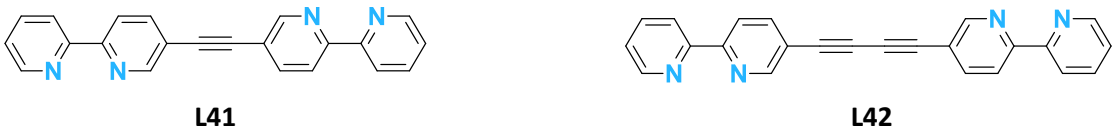

L41 **L42**

Figure 4.2.1: Proposed alkyne containing ligands.

Both ligands were synthesised by modified literature procedures, heavily relying on Sonagashira cross-coupling methodology, as outlined in Scheme 4.2.1.[16] However, the *bis*-alkyne ligand **L42** was found to be far less stable than the *mono*-alkyne ligand, **L41**, decomposing at room temperature over several days. Multiple alkyne containing groups are prone to instability.[17,18] While **L42** might be stable at lower temperatures, this instability was less than desirable and pointed to further problems with the subsequent cage compound, **C42** (Scheme 4.2.2, n = 2) and it was not further pursued.

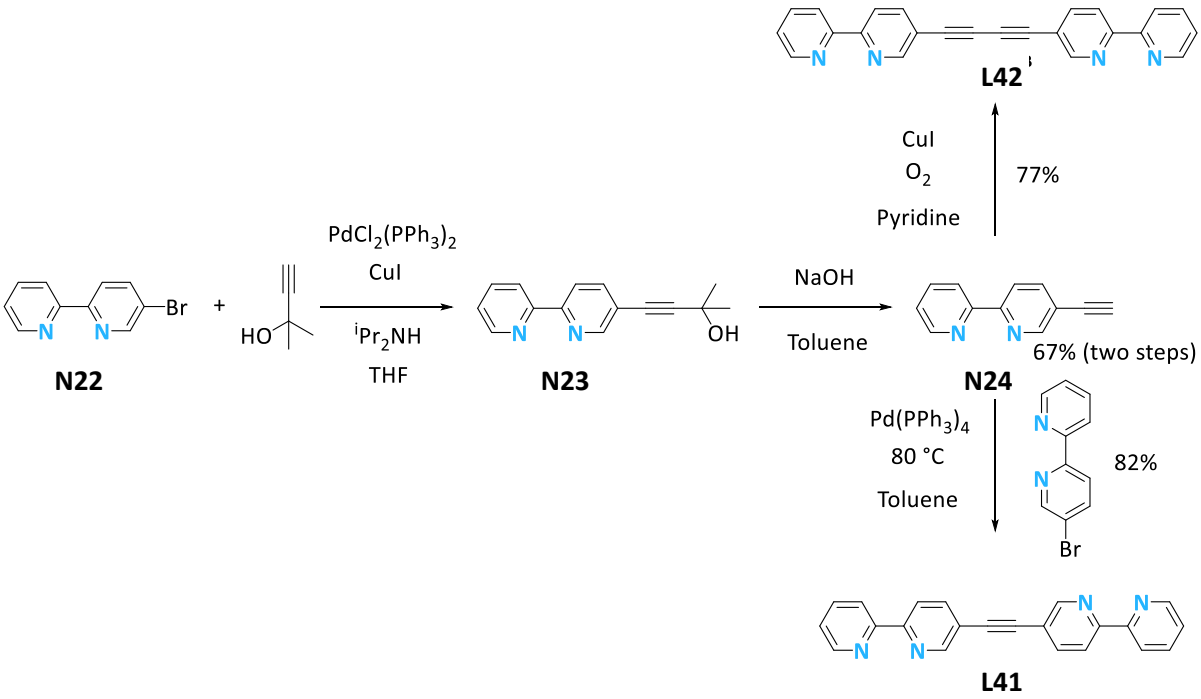

*Scheme 4.2.1: Synthesis of alkyne containing ligands **L41** and **L42**.*

Both **L41** and **L42** underwent cage formation using the "assembly-followed-by-fixing" method, giving single high symmetry species in excellent yields. Both compounds showed characterisation that was consistent with previous tetrahedra and is very similar to the parent, **C19** cage (Fig. 4.2.2).

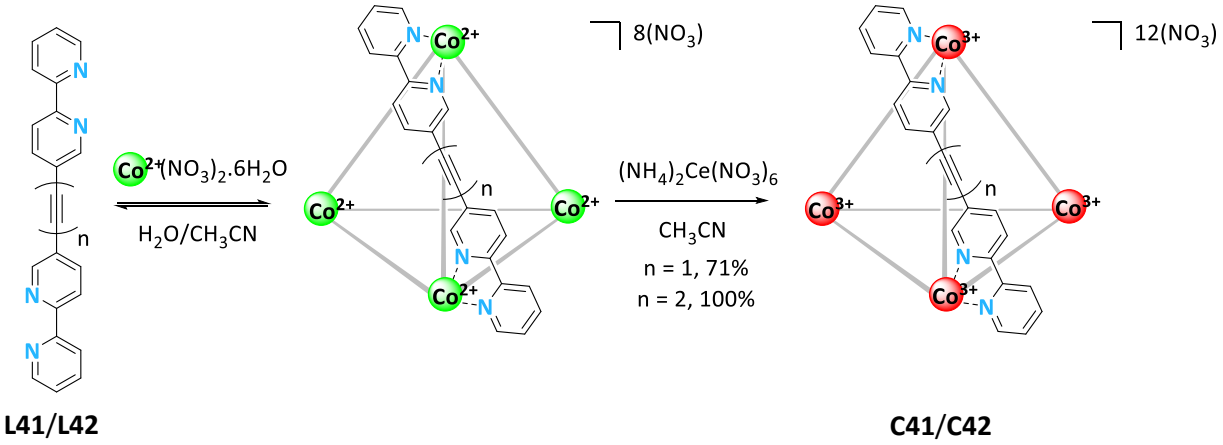

*Scheme 4.2.2: Synthesis of **C41** (n = 1) and **C42** (n = 2).*

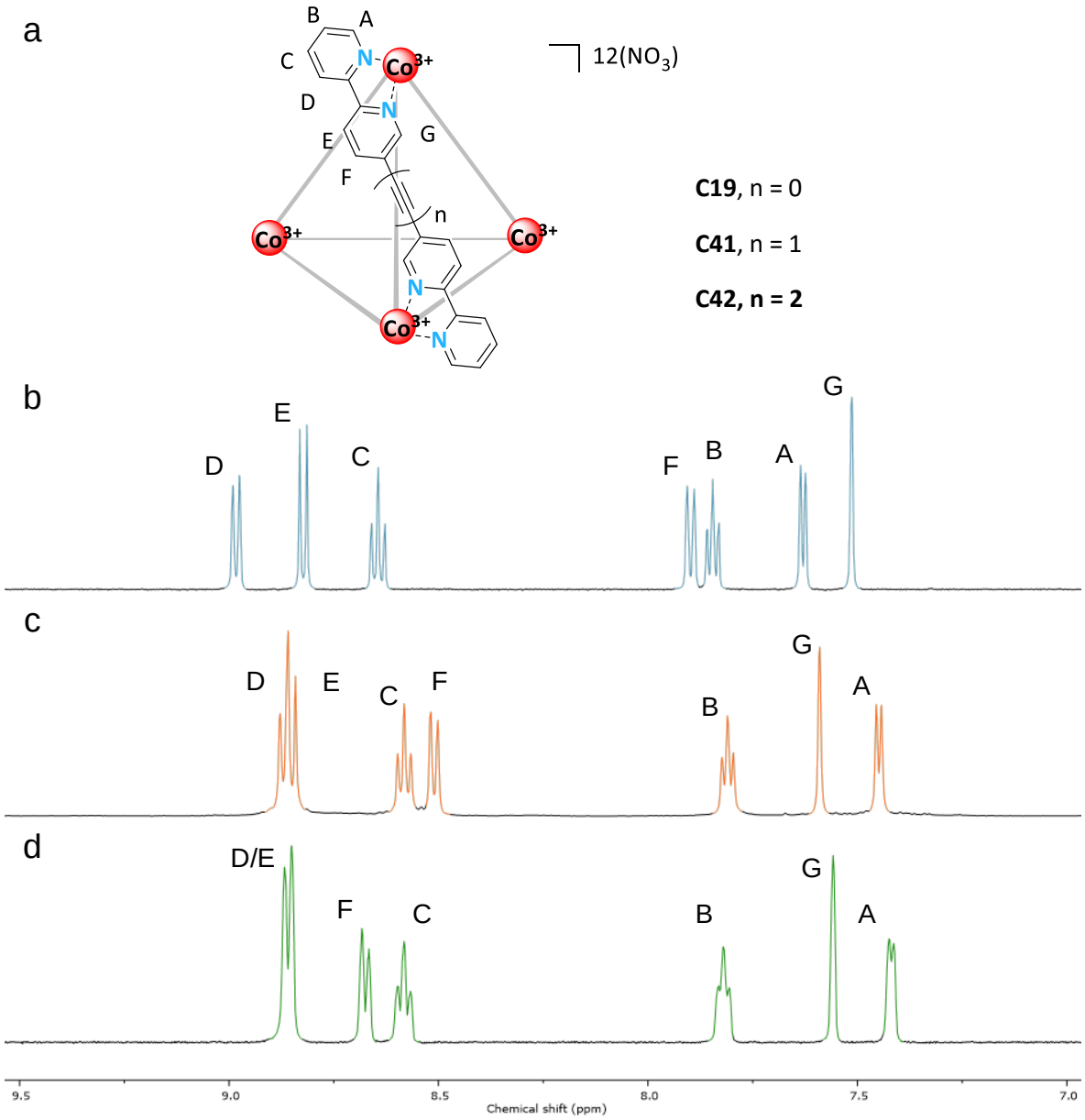

*Figure 4.2.2: (a) Depiction of Cage and partial ^{1}H NMR (500 MHz, D_2O) of (b) **C19** (n = 0), (c) **C41** (n = 1), (d) **C42** (n = 2).*

4.2.2 Guest binding Studies

While the cages were not designed for guest binding, their host-guest properties were still considered worth investigating. They would be expected to have significantly different guest binding properties to **C19** and **C15**. The alkyne central linkers will alter the size of the assemblies with the estimated average metal-metal distances are shown in Table 4.2.1. The tetrahedron of **L41** is therefore of an intermediate size to **C19** and **C15**, while that of **L42** would be slightly larger. This size difference will lead to different cavity volumes making them suitable for different size guests.

Table 4.2.1: Estimated cobalt-cobalt distances of various tetrahedra. Estimated using Spartan 10' models of assemblies.

Assembly	Average M-M distance / Å
C19	9.30
C41	11.58
C15	13.24
C42	13.93

The small surface area of the alkyne would be expected to lead to the cage less effectively demarcating the cavity and therefore reducing the hydrophobic driving force for guest binding. Preliminary guest screening of the **C41** cage was assessed to see if the cage is still suitable for the binding of anions. The screening appeared to show binding of several anions in common with **C19**, including SiF_6^{2-}, ReO_4^-, BF_4^- and ClO_4^- (Fig. 4.2.3). This common binding across different size assemblies implies that electrostatics are a large driving force for the binding of these anions. Though the lack of PF_6^- binding, which bound very strongly in **C19**, implying that other factors also have an influence.

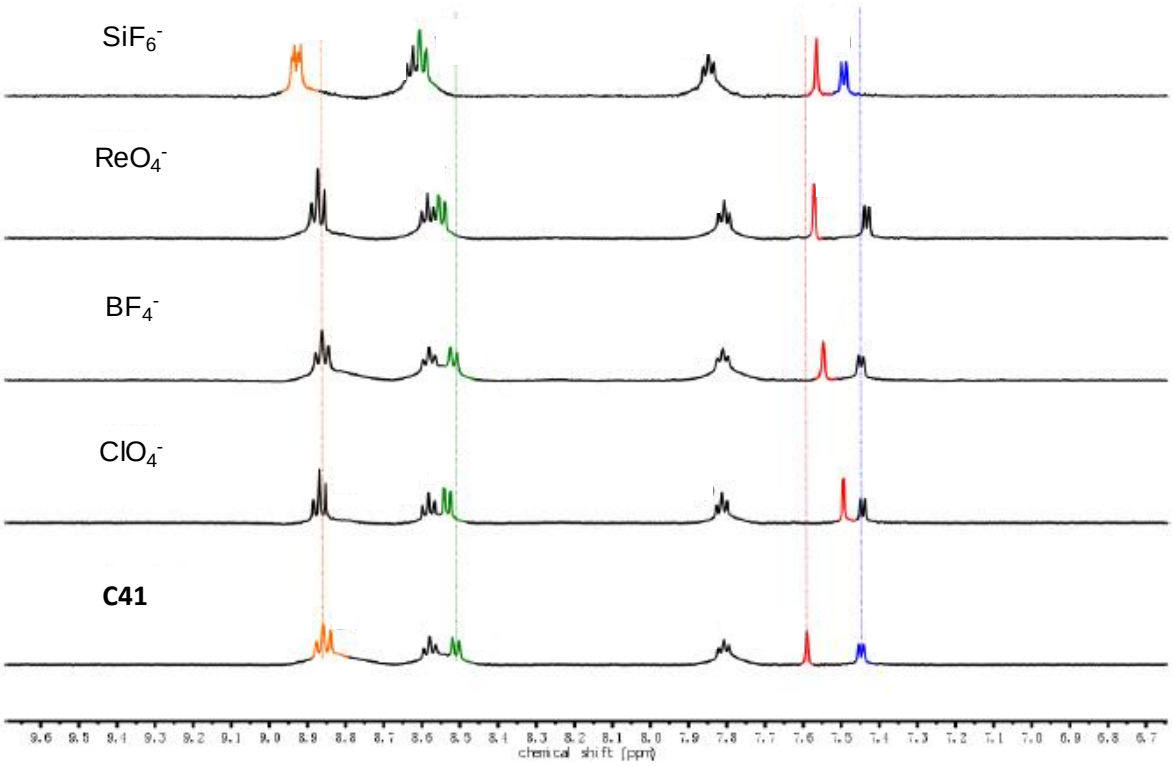

*Figure 4.2.3: Partial ^{1}H NMR (500 MHz, D_2O): Binding studies of different anions with **C41**.*

Further exploration of these differences may be of interest and determination of the binding constants of these anions would allow more direct comparison of binding between the different cages. Screening

of organic guests, which would be more dependent on the hydrophobic effect, would allow exploration of the effect of porosity on the cage.

4.2.3 Spontaneous Raman Spectroscopy Studies

Solution phase Raman spectra of the cage were taken but comparison with the ligand proved difficult as there was no single solvent in which both species were soluble. The cage also was ill suited to Raman spectroscopy in the solid phase as it appeared to decompose under exposure to the laser and give a broad spectroscopic peak. **L41** had limited solubility in water miscible solvents such as methanol, ethanol, water and DMSO. **L41** was found to be soluble to 10 mM in 1M HCl but not HNO_3, while **C41** was readily soluble in both 1 M DNO_3 and DCl. Solutions of the ligand and cage were mixed. The peaks of the cage remained stationary while the ligand shifts changed dramatically. Addition of more **L41** did not cause its ^{1}H NMR peaks to shift further, so the change does not appear to be concentration dependant and the solution appeared to be stable over multiple days.

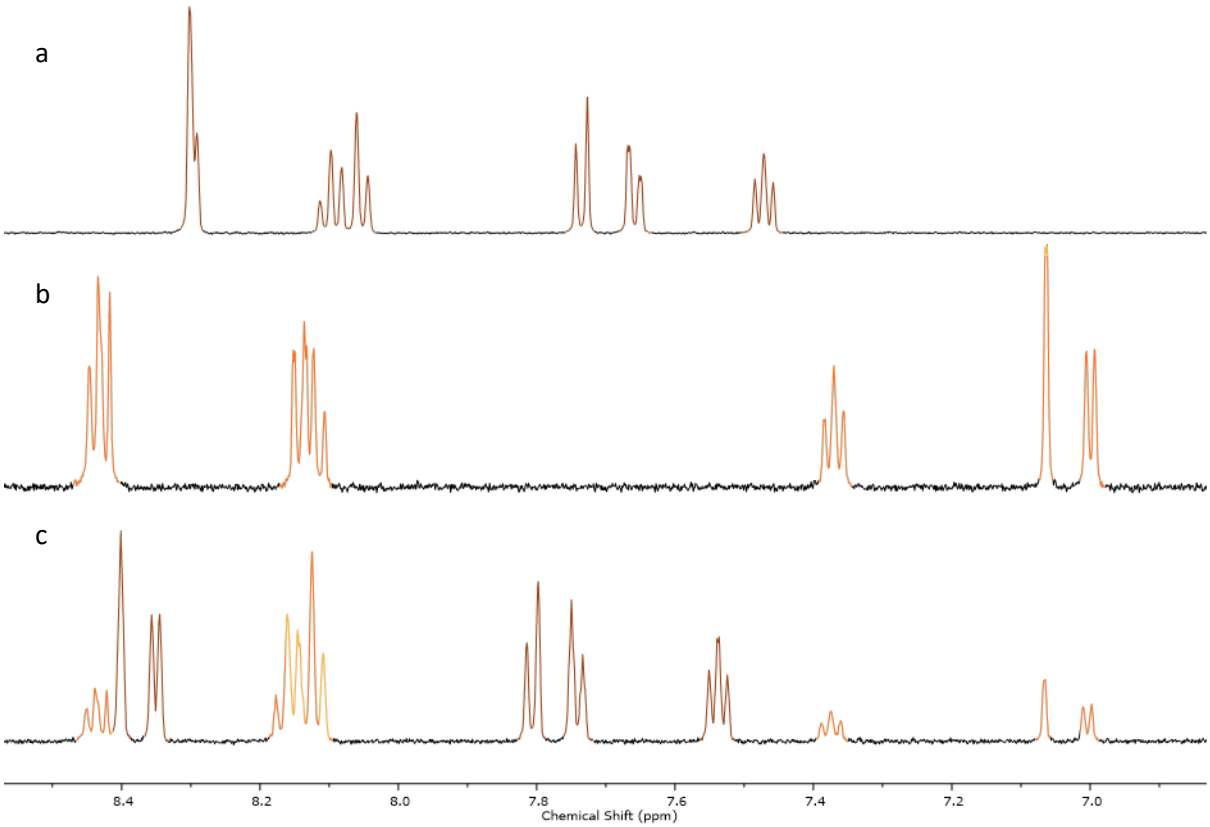

*Figure 4.2.4: Partial ^{1}H NMR (500 MHz, 1 M DCl, D_2O) of (a) **L41**, (b) **C41**, (c) **L41** and **C41**. **L41** (Brown), **C41** (Orange).*

With a common solvent identified, **C41** and **L41** were analysed using spontaneous Raman spectroscopy in a number of different solutions. These results appear to show that the vibration of the alkyne in **L41** is relatively insensitive to the chemical environment, differing only a few

wavenumbers between organic solvents and aqueous acid. The acidic solutions of **L41** gave a signal at a marginally higher wavenumber than in organic solvent, which was found to not differ at concentrations of 1 mM and 5 mM or in pH 0 or 0.7 solutions. Estimation of the pK_a of **L41** predicts that it would largely exist as the doubly protonated form in this pH range and protonation might be expected to have an effect on the electron density of the alkyne group. Combining the acidic and organic solutions gave intermediate peak positions, implying some intermediate state.

C41 was investigated in a smaller number of solutions due to limited material. The alkyne vibration in the cage was at a higher wavenumber than uncoordinated **L41** and appeared to appear at a slightly wider variation of values. This increase in wavenumber from ligand to cage was also observed by Crowley and co-workers with a Pd_2L_4 paddlewheel system.[19] The wavenumber of the vibration of **C41** also increases in wavenumber when in acidic solution (Fig. 4.2.5). It might be expected that the coordination of the ligand makes it less sensitive to changes in the polarity and pH of the solvent, so it would appear that other factors to consider. One such explanation is the change in counteranion, as in water, the counter anions are NO_3^-. While in the acidic solutions, there will be a large excess of Cl^- anions. Interactions of these anions with the alkynes may affect their Raman signal especially with the proximity of the alkyne moieties to the central cavity.

*Table 4.2.2: Alkyne Raman signal maximum of **L41** and **C41** in various solvents.*

Solvent		Alkyne peak maxima / cm^{-1}	
Concentration		**L41**	**C41**
5 mM	1 mM		
1 mM HCl		2228	2253
DMF		2220	-
	H_2O	(Insoluble)	2239
	DMSO	2221	2245
	DMSO/EtOH	2221	-
	1 mM HCL	2228	2253
	0.2 mM HCl	2228	-
	1:1 0.2 mM HCl/DMSO	2226	-
	9:1 0.2 mM HCl/ DMSO	2223	-

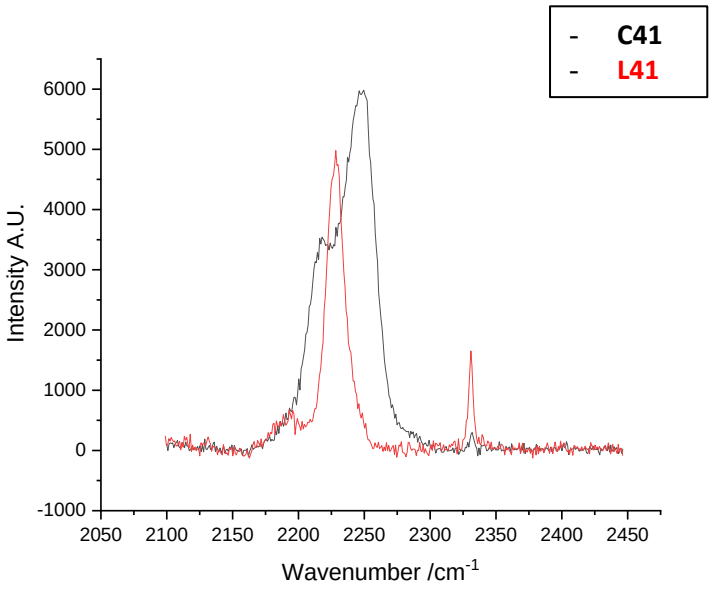

*Figure 4.2.5: Spontaneous Raman spectra (2100-2450 cm^{-1}) of 1 mM **L41** and **C41** in 1 M HCl.*

This difference between vibrational wavenumber of **C41** and **L41** mean that Raman spectroscopy could potentially distinguish between the cage and free ligand. This could make it a powerful tool when imaging, as it may provide information on the state of cage, as well its localisation.

Both **C41** and **L41** have complex peaks in the Raman spectra, both appearing to possess two signals in the expected region, with this second peak being far more pronounced in **C41** (Fig. 4.2.5). The reason for these secondary peaks is uncertain as both species appeared pure and of high symmetry by ^{1}H NMR studies (Fig. 4.2.2).

*Table 4.2.3: Alkyne Raman signals of of 1 mM **L41** and **C41** in 1 M HCl.*

Sample	Main peak (cm^{-1})	Secondary Peak (cm^{-1})
L41	2228	2193
C41	2249	2217

One explanation is the far greater time resolution of Raman spectroscopy over NMR. NMR spectra are time averaged over a far longer time frame and it is possible that a dynamic process not apparent by NMR is being detected by Raman.[20] It is also possible that these secondary peaks represent some form of conformation change in the species. Severe conformational changes have been proposed to occur in cages to allow ingress and egress of guests into cage cavities and could be expected to be occurring constantly in solution.[21] It is possible that these dynamic conformational changes are differentiated by Raman while not being detected by NMR.

The cause of the two peaks cannot be discerned without further study. Model mono-nuclear complexes, such as those depicted in Figure 4.2.6, with appended alkynes could provide insight into effect of coordination to metals on the alkyne vibration. It would also allow exploration of whether these additional peaks are due to the symmetry or dynamics of the tetrahedron.

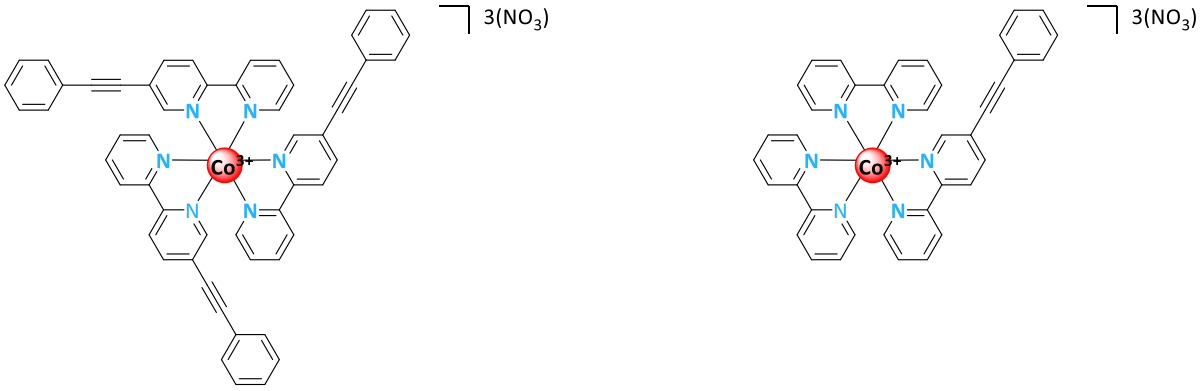

Figure 4.2.6: Potential mono-nuclear complexes for investigation of coordination on alkyne Raman signals.

Comparison of the cross-section of the vibration would also be of interest. The compound **EdU** (Fig. 4.1.5) has been used as a standard alkyne Raman compound to which intensity of scattering can be compared.[11] Assessment of the strength of the scattering would also aid in the optimisation of cell imaging as it would indicate limits of detection and could allow analysis of concentration. Quantification of the intensity of the Raman bands of the ligand and cage could also provide insight into the effect of coordination has on the polarizability of an alkyne in a ligand.

4.2.4 Cellular uptake

Initial cellular uptake studies were undertaken, and HeLa cells were dosed with **C41**, pelleted and assessed with spontaneous Raman spectroscopy. This cell pellet did show a Raman band in the cell silent region consistent with an alkyne. However, this Raman band had a wavenumber of 2219 cm^{-1} (Fig. 4.2.7), which is more consistent with solid **L41** rather than **C41** in an aqueous solution (Table 4.2.2). This, in combination with the observation of solid material appearing to precipitate onto the surface of the cells, could mean that Raman signal might correspond to solid ligand rather than cage.

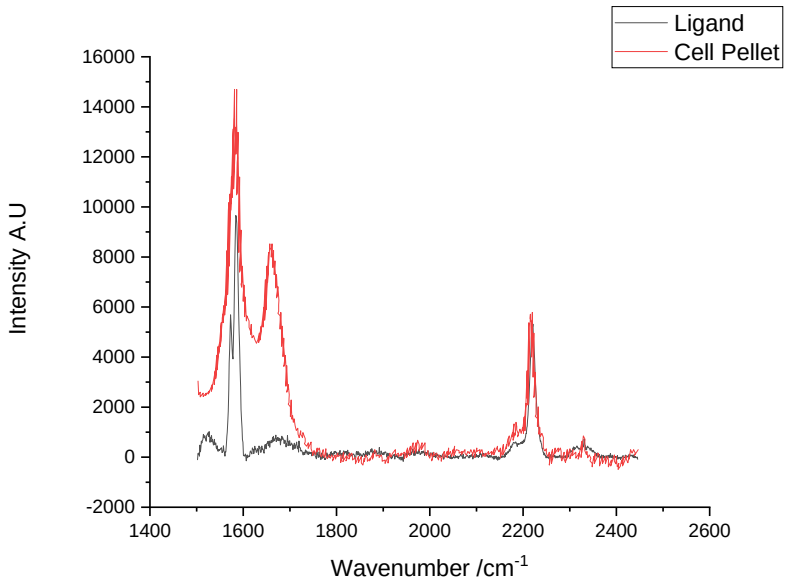

*Figure 4.2.7: Spontaneous Raman spectra of solid **L41** (black line) and cell pellet treated with **C41** (100 mM, cell media) for three hours (red line).*

Precipitated ligand could be caused by decomposition of the cage in media, as was observed with **C19** (see Chapter 2). **C41** could suffer similar instability and the insoluble ligand could be precipitating onto surface of the cells, meaning the alkyne signal detected might not indicate cellular cage uptake.

4.2.5 Stimulated Raman Spectroscopy Studies

Stimulated Raman spectroscopy was identified as means to investigate the behaviour of the **C41** in media and cells. The technique is able to image a sample quickly and would allow spatial analysis of sample to detect the difference between precipitated solid and the bulk solution.

Solutions of **C41** were assessed by spontaneous and stimulated Raman in order to check whether there was good agreement between the two techniques (Fig. 4.2.8). The two results gave marginally different results, with the highest peak in the stimulated Raman spectrum being 2449 cm^{-1} compared to 2245 cm^{-1} for the spontaneous equivalent. It is possible this small difference may be caused by the lower number data of points that can be collected when using stimulated Raman compared to spontaneous. It also possible that differences between the two techniques may lead to slight differences in temperature or light source when the data is collected.

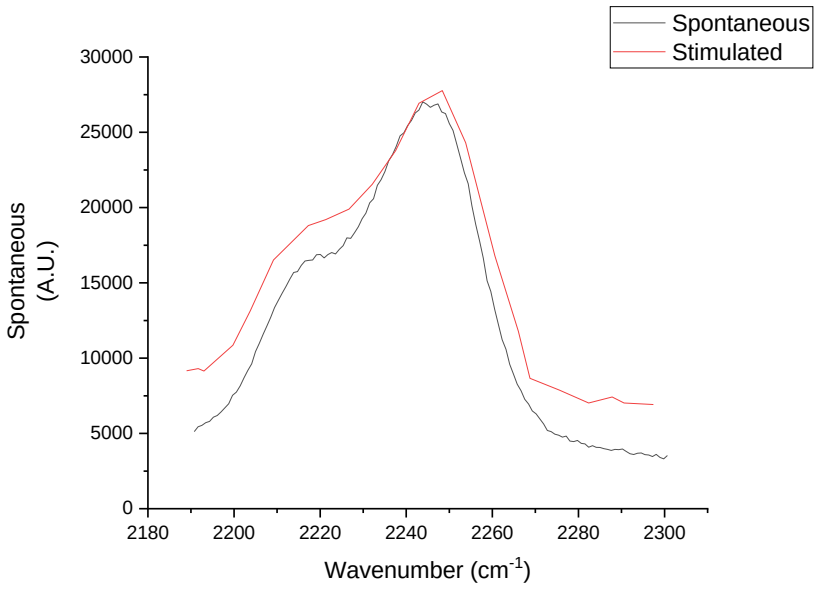

*Figure 4.2.8: Stimulated (red line) and spontaneous (black line) Raman spectra of **C41** (1 mM) in water.*

As it had been indicated that cage and ligand could be differentiated by the wavenumber of their alkyne peak, media solutions of **C41** were analysed by stimulated Raman spectroscopy. Comparison of solutions of **C41** in water and media found that they have similar alkyne vibrations with the highest signal at 2248 cm^{-1} (Fig. 4.2.9). However, continued observations of the solutions led to no change in pure aqueous solution, while solid precipitated from the media solution within an hour.

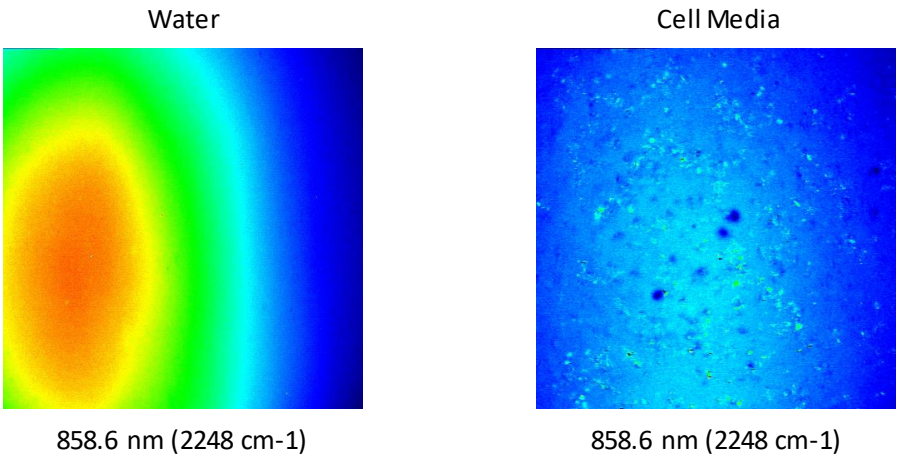

*Figure 4.2.9: Stimulated Raman scattering image of **C41** (1 mM) in water (left) and cell media (right). Image shows Intensity of Raman signal at 2248 cm^{-1}, Blue (low) to high (red).*

Stimulated Raman spectroscopy allows the separate analysis of the solution and precipitate. This showed that the alkyne vibration of the bulk solution was consistent with **C41**. In contrast, the solid precipitate had a different Raman vibration, with maximum signal at 2223 cm^{-1}, a wavenumber very

similar to that of free **L41** (Fig. 4.2.10). Furthermore, the precipitation of the poorly soluble material is likely to suggest free ligand, which is not water soluble. When the mixture was extracted with deuterated chloroform, ^{1}H NMR showed the presence of free **L41**, confirming cage decomposition.

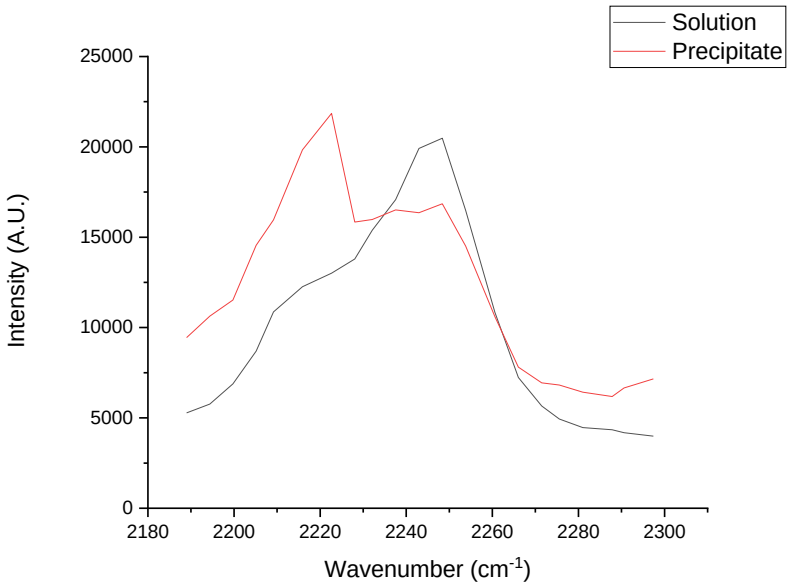

*Figure 4.2.10: Stimulated Raman Spectra of solution and precipitate of **C41** in DMEM eagle media (0.1 mM). 2190-2300 cm^{-1}.*

4.2.6 Investigation of the Stability of C41

As previously discussed, the most likely pathway for cage degradation in biological media is by reduction of the metal centres followed disassembly of the cage (see Chapter 2). Therefore, the glutathione assay previously described in Chapter 2 was repeated with **C41** to assess if it is degraded in a similar manner.

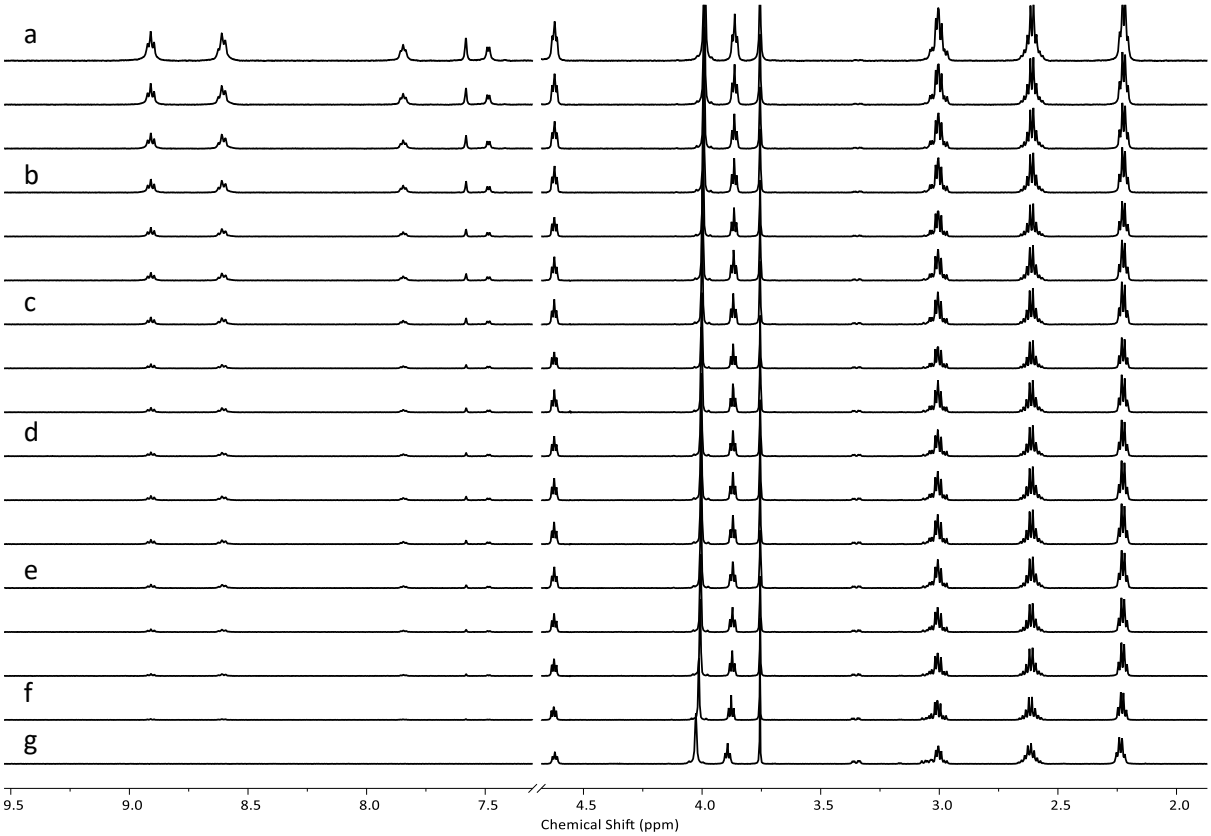

*Figure 4.2.11: Partial ^{1}H NMR (600 MHz, D_2O, 1 M PBS) of **C41** in presence of 10 equivalents of glutathione over time (descending). a) 0 h, b) 3 h, c) 7 h, d) 10 h, e) 12 h, f) 16 h, g) 38 h.*

C41 was found to be stable in phosphate buffered saline (PBS) and upon the addition of the glutathione was observed to degrade. Interestingly, **C41** appears to decompose slower than **C19**, remaining detectable in solution after 15 hours, though it had entirely decomposed after 20 hours. Limited precipitation was observed in the sample, implying that the reduced species remained soluble, in contrast to the cell media experiments in which precipitate was apparent.

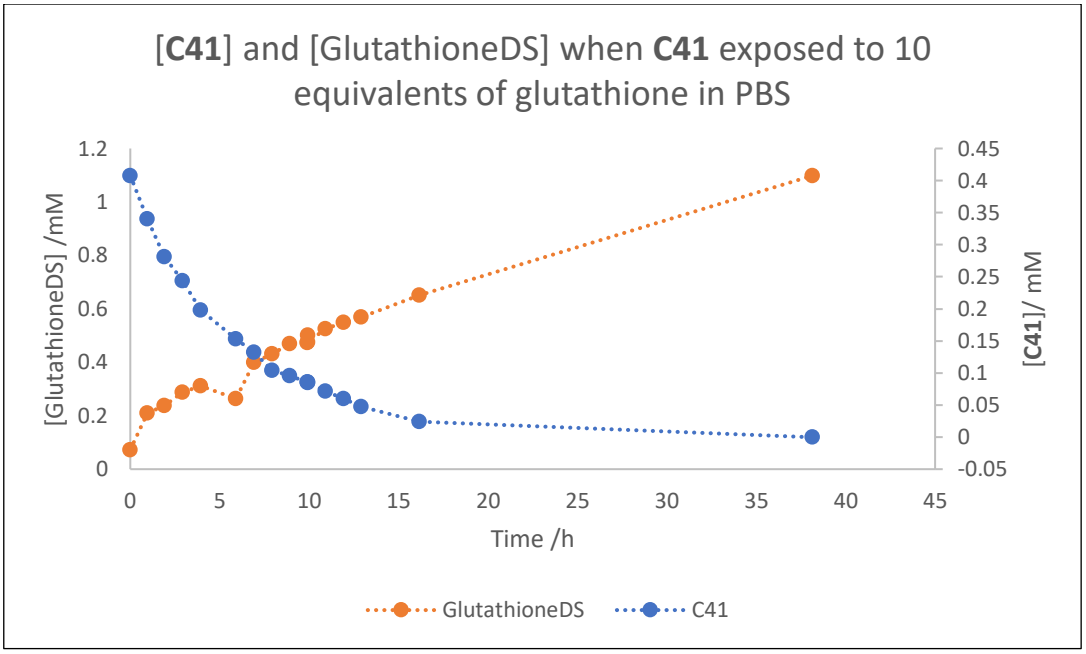

*Figure 4.2.12: Concentration of **C41** and Glutathione disulfide (glutathioneDS), when **C41** exposed to 10 equivalents of glutathione in pH 7.4 phosphate buffered saline.*

These results imply **C41** has an intermediate stability between **C19** and **C20**. The alkyne containing ligand would also be expected to more flexible than the ligands without central linkers, which might be expected to decrease the overall stability of the assembly by reduction of preorganization and cooperativity. However, this could also reduce steric strain on the assembly which may explain the apparent greater stability.

4.2.7 Stimulated Raman Cell Imaging

Despite the stability concerns of, it was proposed that **C41** be investigated for its cellular uptake through stimulated Raman microscopy. This would allow determination of whether the cage is truly taken up by cells or if the positive cell pellet result was in fact due to ligand precipitation.

Therefore, HeLa cells were dosed with a 100 µM solution of **C41** (the higher end of the expected concentrations of analyte)[22] for two hours before they were washed, fixed and investigated by SRS. The precipitation of the solid proved problematic as it formed crystals on the surface of the cells, leading to image saturation and sample damage. The crystals appeared most concentrated around the cells, most likely as the cells present the best nucleation sites. Imaging the sample at a variety of different wavenumber values showed that the precipitated solid (Fig. 4.2.13, (d)) had a Raman signal very similar to **L41** (Fig. 4.2.7). The crystallised ligand is also fluorescent, making for difficulties in acquiring Raman images. The fluorescence limited the number of wavelengths that could be investigated, such as those of the cellular components that are typically used to identify cell topology.

Despite these issues, images of the cells could still be obtained at alkyne wavenumbers and appeared to show some uptake of **C41**.

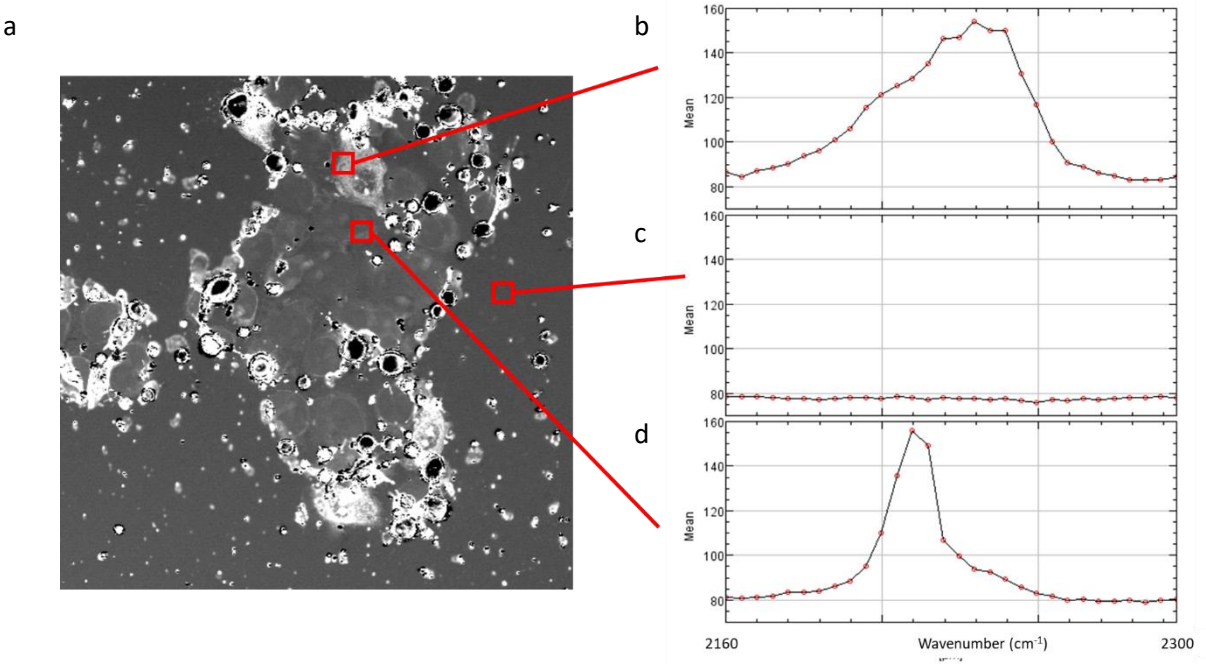

*Figure 4.2.13: (a) Stimulated Rama image of HeLa cell treated with **C41** (Intensity of Raman signal at 2230 cm^{-1}). Local Raman sweep (2160-2300 cm^{-1}) of (b) cell cytoplasm, (c) bulk solution, (d) solid precipitate. Data collected by Martin Lee.*

A number of cells show an alkyne Raman signal concentrated throughout the cytoplasm that had a maximum signal at 2230 cm^{-1}. This broad peak overlaps with both the wavenumber expected for intact **C41** (2239 cm^{-1}) and precipitated **L41** (2220 cm^{-1}), implying that it might represent a mixture of different states of cage and may show degradation of the cage within cells.

Other cells exhibited signals which were concentrated throughout the cells including the nucleus and nucleolus (Fig. 4.2.14). Unfortunately, the precipitated solid restricted transmission images, meaning the structure of the cells could not be confirmed.

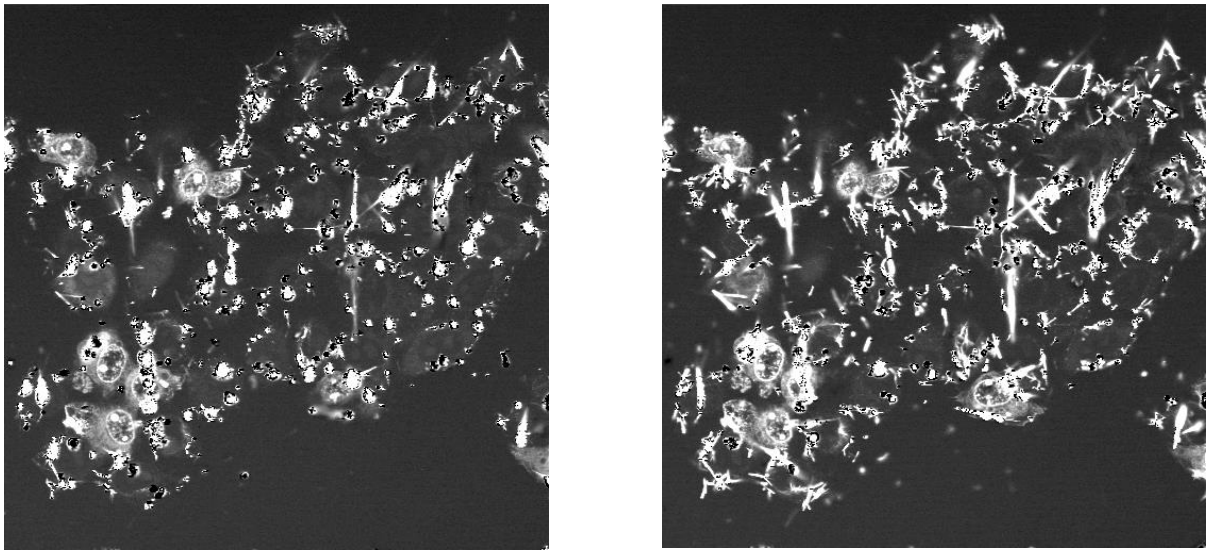

2260 cm^{-1} 2225 cm^{-1}

*Figure 4.2.14: Stimulated Raman spectroscopic images of HeLa cells dosed with **C41** (0.1 mM). Intensity of Raman signal at respective wavenumber. Data collected by Martin Lee.*

Despite the limitations of the data, it does appear to show that **C41** is taken up into HeLa cells and appears to be particularly concentrated within the nucleus and nucleolus of these cells. In order to distinguish between the precipitated material and that in solution within cells, fluorescence images were collected. As the free ligand is fluorescent and this is switched-off upon coordination to the metal ions and the assembly of the cage, this was identified as a means to distinguish between cage and precipitated ligand.

Collection of a fluorescence image and overlaying it with the Raman spectra appears to show separation of the fluorescence and Raman signal (Fig. 4.2.15), implying that the crystalline material is solid ligand and the material taken up by cells is intact **C41**. This presents the possibility of using Raman and fluorescence microscopy in tandem to provide additional information about the state of the alkyne containing cages within the cell sample.

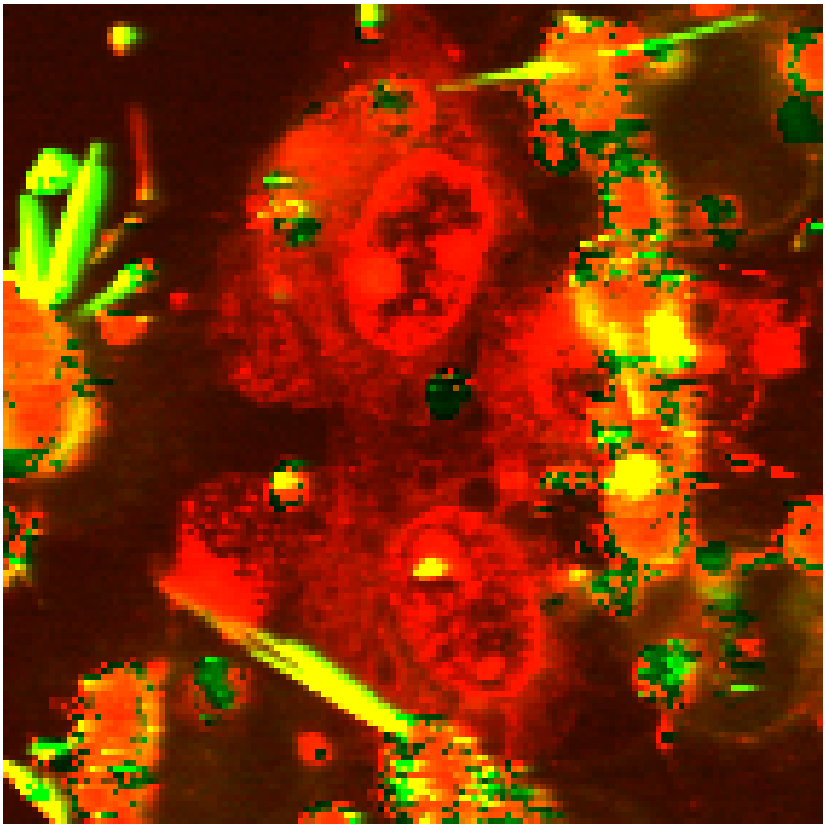

*Figure 4.2.15: Overlayed fluorescence image and stimulated Raman image (2225 cm^{-1}) of cells dosed with **C41** (0.1 mM). Intensity of Raman signal at 2225 cm^{-1} depicted in red and fluorescence depicted in green. Data collected by Martin Lee.*

More data is required to confirm the findings of these experiments and this will would be greatly aided by preventing the precipitation from occurring. Development of an effectively stabilised alkyne containing cage might be one means of reducing this precipitate. Alternatively, lower concentrations of **C41** could be administered in order to reduce the amount of precipitate that is formed. Additionally, **C41** could be administered to the cells in less chemically complex solutions, such as phosphate buffered saline or incomplete media. These solutions are compatible with cells for short periods, giving a window in which cage compounds could be administered with reduced degradation.[23]

4.2.8 Attempted Functionalisation of L41 to Increase Stability

As **C41** showed similar instability to the previous **C19** systems, it was proposed that it could be modified in a similar manner to increase its stability, prevent degradation and facilitate imaging. Therefore, an amine functionalised alkyne containing ligand, **L43**, was proposed (Fig. 4.2.16).

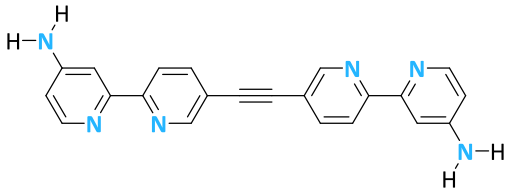

*Figure 4.2.16: Proposed amine functionalised alkyne containing ligand **L43**.*

L43 was only synthesised with partial success during the course of this investigation (Scheme 4.2.3). The synthesis progressed with the Sonogashira coupling of trimethylsilylacetylene and **N7** to give **N24**, followed by deprotection to produce **N25** and a further coupling with another equivalent of **N7** to give intermediate **N26**. Finally, this was subjected to conditions that could selectively reduce nitro groups. Unfortunately, **L43** appeared to be unstable; it could be precipitated from solution as an off-white solid but quickly turned to a black sticky oil upon attempts to isolate. This happened almost immediately upon isolation and occurred after further extractions with a number of solvents.

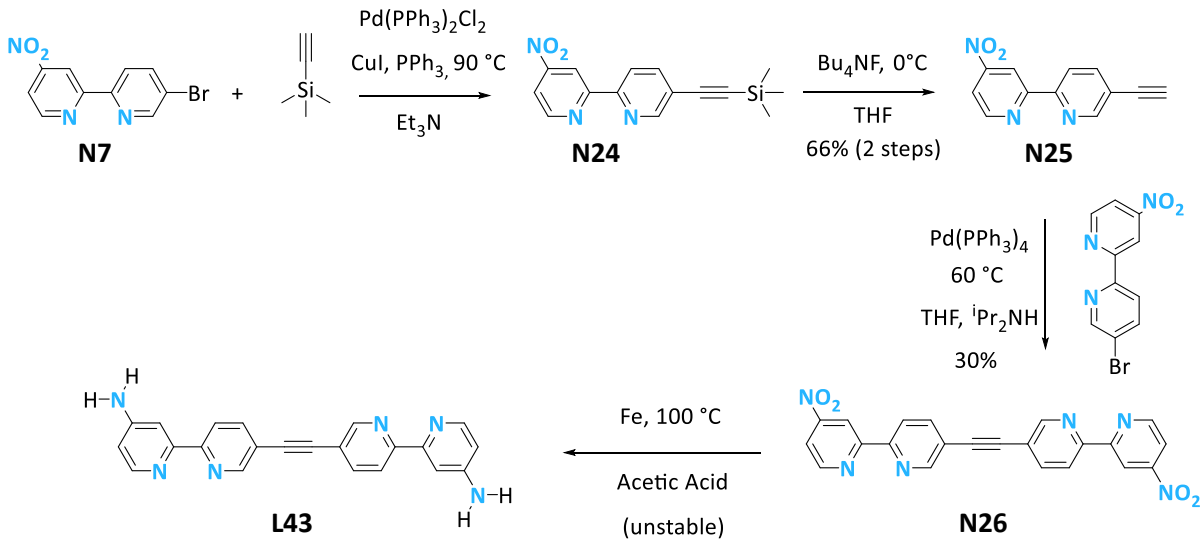

*Scheme 4.2.3: Attempted synthesis of **L43**.*

Repetition of the reaction gave a similar result and it was suggested that the ligand was decomposing on contact with air. However, cage formation was attempted in the hope that some of the ligand persisted and the decomposition products would not interfere with cage formation. **L43** initially appeared to behave well in the reaction, forming an orange solution upon heating and resonding similarly to previous systems to oxidation and isolation. However, the product was found to have a very broad ^{1}H NMR spectrum (Fig. 4.2.17, (b)).

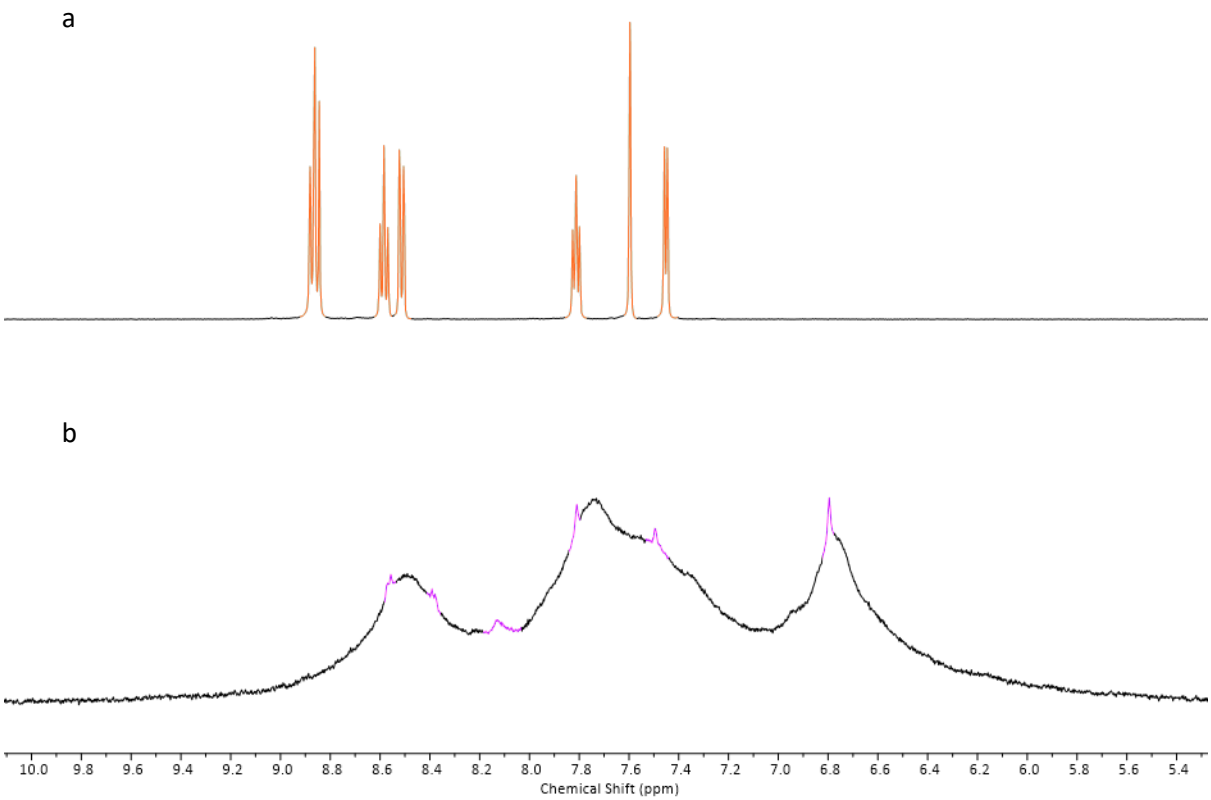

Figure 4.2.17: Partial ^{1}H NMR (600 MHz, D_2O) of (a) ***C41,*** *(b) The product of the direct cage formation with* ***L43****.*

This broad spectrum could be a result of the degradation of the ligand or similar speciation issues as those encountered with cage formation of **L20** and **L38** (see Chapters 2 and 3). It was therefore proposed that the cage formation could be attempted by ligand exchange in the same manner as **C20**, using the preorganisation of **C41** to avoid speciation issues.

This cage formation by ligand exchange was found to give a similar broad spectrum to the direct formation though with slightly better-defined peaks (Fig. 4.2.18). This implies that the broadness of the spectra is a result of instability of the ligand rather than kinetically trapped byproducts. It is possible that the peaks represent the **L43** tetrahedron and that it could be purified, however the issues with the stability of the **L43** imply this may not be the case.

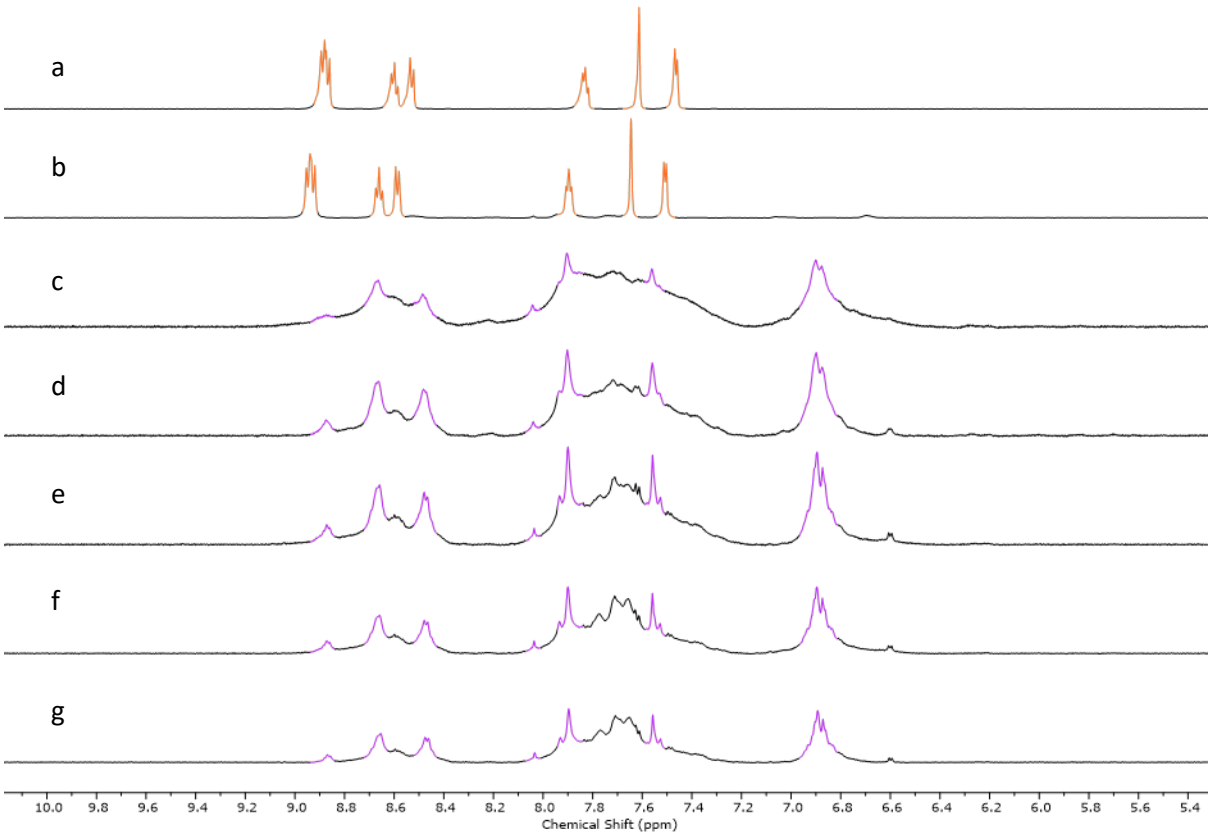

*Figure 4.2.18: Partial ^{1}H NMR (600 MHZ, 9:1 D_2O/CD_3CN) of reaction of **C41** and **L43**. (a) Before addition of **L43**, (b) After addition of **L43**, (c) After 24 h heating at 75 °C, (d) After 2 days heating at 75 °C, (e) After 5 days heating at 75 °C, (f) After 7 days heating at 75 °C, (g) After 24 days heating at 75 °C. **C41** highlighted in orange, proposed **L43** highlighted in purple.*

An alternative functionalisation to stabilise **C41** would be to use a methyl ether functionalised bipyridine rather than an amine (Fig. 4.2.19). These groups could be introduced in the same manner as in **L38** (Chapter 3) and would preclude the need for harsh reduction reactions. Hopefully, the methyl ether groups would provide a stable ligand with a robust tetrahedron.

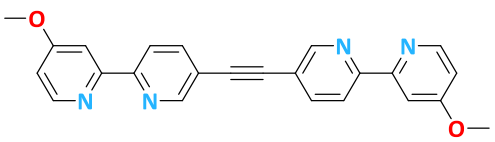

Figure 4.2.19: Alternative functionalised alkyne containing ligand.

4.3 Summary

Raman spectroscopy was identified as a potentially powerful means of investigating the *in vitro* behaviour of appropriately labelled robust metallosupramolecular cages. The technique offers several advantages over fluorescent imaging, including smaller labels and lack of metal coordination quenching. Therefore, the alkyne containing ligand, **L41**, was synthesised and successfully assembled into a tetrahedron **C41**. Spontaneous Raman spectroscopy of both the ligand and cage found different alkyne Raman bands which were dependent on solvent.

Initial cell uptake studies of **C41** were hampered by degradation of the cage in cell media and a subsequent glutathione assay indicated that **C41** was reductively in a similar manner to **C19**. Despite its instability, cell uptake experiments were undertaken with **C41**. This experiment was also hampered by the degradation of the cage but appeared to show the cellular uptake of **C41**, proving the potential Raman spectroscopy has as a method to investigate the cellular uptake of supramolecular cages. The ability to differentiate the state of the cage through the wavenumber of the Raman signal and the fluorescence of the free ligands indicates the technique may be used to give significant insight into the biological fate of our cage systems that will inform future biomedical applications.

The synthesis of an amine functionalised variant of the ligand, aiming to increase the stability of the resultant cage, was unsuccessful due to problems with decomposition of the ligand.

4.4 Experimental

General Information

As described in Chapter 2.

Abbreviations used in this text:

DMSO	Dimethylsulfoxide
DMF	*N,N*-dimethylformamide
THF	Tetrahydrofuran
DCM	Dichloromethane
NMR	Nuclear Magnetic Resonance
DOSY	Diffusion ordered spectroscopy
RT	Room temperature
EDTA	Ethylenediaminetetraacetic acid
Na_4EDTA	Ethylenediaminetetraacetic acid tetrasodium salt
MS	Mass Spectrometry
PBS	Phosphate buffered saline
DMEM	Dulbecco's modified eagle medium

Ligand Synthesis

4.1

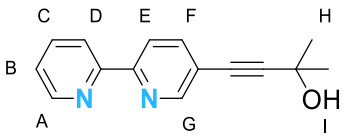

N22 (507 mg, 2.16 mmol), CuI (85 mg, 0.445 mmol) and $Pd(PPh_3)_4$ (147 mg, 0.13 mmol) were placed in a Schlenk flask under N_2. 2-Methyl-3-butyn-2-ol (0.4 mL, 4.127 mmol) and diisopropylamine (20 mL) were added and the reaction was sparged with N_2 for five minutes and stirred for 24 h at RT. The black reaction was diluted with Na_4EDTA (100 mL, 0.25 M, NaOH) and stirred for 0.5 h. The solvent was concentrated *in vacuo* and water (100 mL) was added to the residue and the mixture was extracted with dichloromethane (4 × 100 mL). The combined organic fractions were washed with brine (3 × 100 mL) and dried over $MgSO_4$. The solvent was removed *in vacuo* and the crude product purified by silica

flash chromatography (eluent, gradient: dichloromethane/ triethylamine/diethyl ether 99:1:0 to 98:1:2) to give a brown oil. This was diluted with saturated $NaHCO_3$ solution (100 mL) and extracted with dichloromethane (3 × 100 mL). The organic phases were dried over $MgSO_4$ and the solvent removed *in vacuo* to give a brown oil, which was used without further purification. Crude yield = 571 mg.

^{1}H NMR (601 MHz, Chloroform-*d*) δ 8.70 (dd, *J* = 2.1, 1.0 Hz, 1H$_G$), 8.68 (ddd, *J* = 4.8, 1.8, 0.9 Hz, 1H, H$_A$), 8.40 (dd, *J* = 8.1, 1.0 Hz, 1H, H$_D$), 8.37 (dd, *J* = 8.1, 1.0 Hz, 1H, H$_E$), 7.85 – 7.80 (m, 2H, H$_{C\&F}$), 7.32 (ddd, *J* = 7.5, 4.8, 1.2 Hz, 1H, H$_B$), 2.17 (s, 1H, H$_I$), 1.66 (s, 6H, H$_H$). Not isolated.

4.2

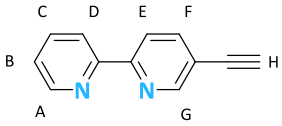

N23 (571 mg, 2.39 mmol) and NaOH (982 mg, 24.55 mmol) were suspended in toluene (100 mL) and refluxed for 5 h. The reaction was allowed to cool and diluted with dichloromethane (50 mL) and water (50 mL), separated and the aqueous phase was extracted with dichloromethane (3 × 30 mL). The combined organic phases were collected and dried over $MgSO_4$. The solvent was removed *in vacuo*. The crude product was purified by silica gel chromatography (eluent: ethyl acetate/ hexane (1:9)) to give the product as a colourless solid. Yield (two steps) = 260 mg (67%).

^{1}H NMR (500 MHz, Chloroform-*d*) δ 8.77 (d, J = 2.0 Hz, 1H, H$_G$), 8.69 (ddd, J = 4.7, 1.8, 0.9 Hz, 1H, H$_A$), 8.44 –8.38 (m, 1H, H$_D$), 8.40 –8.38 (m, 1H, H$_E$), 7.90 (dd, J = 8.2, 2.0 Hz, 1H, H$_F$), 7.83 (td, J = 7.6, 1.8 Hz, 1H, H$_C$), 7.32 (ddd, J = 7.6, 4.7, 1.1 Hz, 1H, H$_B$), 3.29 (s, 1H, H$_H$). ^{13}C NMR (126 MHz, Chloroform-*d*) δ 155.6, 155.5, 152.4, 149.5, 140.2, 137.1, 124.2, 121.6, 120.4, 119.3, 81.4, 80.9. HR-ESI MS: *m/z* 181.0768 (predicted [M+H]+= 181.0760), 203.0588 (predicted [M+Na]+= 203.0580).

L41

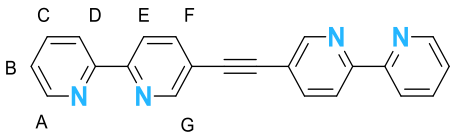

N24 (235 mg, 1.30 mmol), **N22** (313 mg, 1.33 mmol) and $Pd(PPh_3)_4$ (152 mg, 0.13 mmol) were suspended in toluene (100 mL) and NEt_3 (20 mL). The mixture was sparged with N_2 and heated at 80 °C for 12 h. The mixture was allowed to cool and the off-white precipitate was collected by filtration

and washed with toluene and acetonitrile. The crude product was crystallised from hot acetonitrile to give pale yellow needle crystals. Yield = 339 mg (77%).

^{1}H NMR (500 MHz, Chloroform-*d*) δ 8.85 (dd, J = 2.2, 0.9 Hz, 2H, H_G), 8.70 (dd, J = 4.8, 1.9 Hz, 2H, H_A), 8.46 –8.44 (m, 2H, H_E), 8.44 –8.42 (m, 2H, H_D), 7.98 (dd, J = 8.2, 2.1 Hz, 2H, H_F), 7.84 (td, J = 7.7, 1.8 Hz, 2H, Hc), 7.33 (ddd, J = 7.5, 4.8, 1.2 Hz, 2H, H_B). ^{13}C NMR (126 MHz, Chloroform-*d*) δ 155.5, 155.5, 151.8, 149.5, 139.6, 137.1, 124.2, 121.6, 120.6, 119.8, 90.6. HR-ESI MS: *m/z* 335.1302 (predicted [M+H]+= 335.1291), 357.1108 (predicted [M+Na]+ = 357.1111).

L42

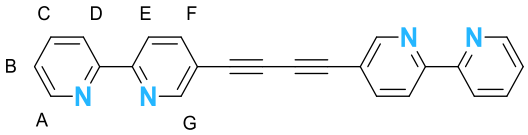

N24 (50 mg, 0.28 mmol) and CuCl (27 mg, 0.28 mmol) were suspended in pyridine (11 mL). The reaction was sparged with O_2 for 1 h and stirred at RT for 12 h. The reaction was diluted with Na_4EDTA (0.25 M, 6 mL) and water (18 mL) and the mixture was stirred for 1 h. The white crystalline product was collected by filtration, washed with diethyl ether and water and then dried *in vacuo*. Yield = 41 mg (82 %).

^{1}H NMR (601 MHz, Chloroform-*d*) δ 8.83 (s, 1H, H_G), 8.70 (d, *J* = 4.8 Hz, 1H, H_A), 8.45 –8.44 (m, 1H, H_E), 8.44 –8.42 (m, 2H, H_D), 7.95 (dd, *J* = 8.3, 2.1 Hz, 1H, H_F), 7.84 (td, *J* = 7.7, 1.7 Hz, 1H, H_C), 7.34 (t, *J* = 6.2 Hz, 1H, H_B). Compound decomposed before ^{13}C could be acquired. HR-ESI MS: *m/z* 358.1307 (predicted [M+H]+= 359.1291), 381.1122 (predicted [M+Na]+= 381.1111).

N24

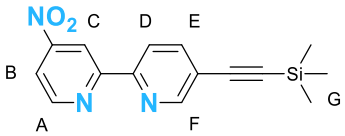

N7 (741 mg, 2.65 mmol), PPh_3 (20 mg, 0.077 mmol), CuI (14 mg, 0.075 mmol) and $Pd(PPh_3)_2Cl_2$ (84 mg, 0.12 mmol) were dissolved in trimethylamine (20 mL) under N_2. Trimethylsilylacetylene (0.39 mL, 260 mg, 2.65 mmol) was added and the mixture was sparged with N_2 for ten minutes, then heated at 90 °C for 16 h. The mixture was allowed to cool and Na_4EDTA solution (0.25 M, 100 mL) was added and the mixture was stirred for 1 h before being diluted with dichloromethane (70 mL) and water (50 mL), the layers were separated and the aqueous phase was extracted with dichloromethane (100 mL × 2). The solvent was removed *in vacuo* from the combined organic phases. The crude product was

dissolved in dichloromethane and passed through a silica plug, the solvent removed *in vacuo* and used without further purification. Crude yield = 776 mg.

^{1}H NMR (500 MHz, Chloroform-*d*) δ 9.15 (dd, *J* = 2.2, 0.7 Hz, 1H, H_C), 8.94 (dd, *J* = 5.3, 0.7 Hz, 1H, H_A), 8.78 (dd, *J* = 2.1, 0.9 Hz, 1H, H_F), 8.42 (dd, *J* = 8.2, 0.9 Hz, 1H, H_D), 8.01 (dd, *J* = 5.3, 2.2 Hz, 1H, H_B), 7.91 (dd, *J* = 8.2, 2.1 Hz, 1H, H_E), 0.29 (s, 9H, H_G). Product not isolated or further characterised.

N25

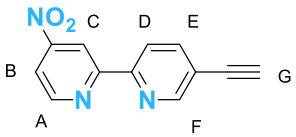

N24 (712 mg, 2.39 mmol) placed in a flask under N_2. Anhydrous THF (20 mL) was added and the resulting black solution was cooled to 0 °C. Bu_4NF (1 M in THF, 2.61 mL, 2.61 mmol) was added and the mixture was stirred at 0 °C for 1 h. The mixture was diluted with water (250 mL) and allowed to warm to room temperature. The reaction was extracted with dichloromethane (3 × 50 mL) and the combined organic phases were dried over $MgSO_4$ before the solvent was removed *in vacuo* to give the crude product as a brown powder. Crude product purified by dry loading onto a silica gel purification column (eluent, gradient: dichloromethane/diethyl ether 100:0 to 70:30) to give product as a brown solid. Yield = 392 mg (66%, over two steps).

^{1}H NMR (601 MHz, Chloroform-*d*) δ 9.16 (d, *J* = 2.2 Hz, 1H, H_C), 8.95 (d, *J* = 5.3 Hz, 1H, H_A), 8.82 (dd, *J* = 2.2, 0.9 Hz, 1H, H_F), 8.45 (dd, *J* = 8.2, 0.9 Hz, 1H, H_D), 8.03 (dd, *J* = 5.3, 2.2 Hz, 1H, H_B), 7.95 (dd, *J* = 8.2, 2.2 Hz, 1H, H_E), 3.35 (s, 1H, H_G). HR-ESI: *m/z* 226.0613 (predicted $[M+H]^+$ = 226.0857).

N26

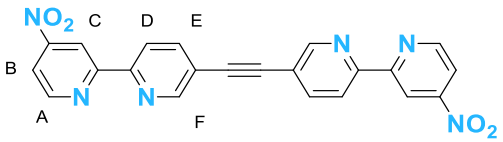

N24 (176 mg, 0.78 mmol), **N7** (354 mg, 1.28 mmol), CuI (17 mg, 0.087 mmol), $Pd(PPh_3)_4$ (98 mg, 0.85 mmol) were dissolved in THF (10 mL) and Et_2NH (5 mL) and heated at 60 °C for 5 days. Na_4EDTA solution (50 mL, 0.25 mM) was added and the mixture stirred for 30 minutes before being extracted with chloroform (3 × 50 mL). The combined organic phases were dried over $MgSO_4$, the solvent was removed *in vacuo.* The residue was then extracted with toluene and the solvent removed *in vacuo*. The crude product was crystallized from hot isopropanol. Yield = 107 mg (30 %).

^{1}H NMR (500 MHz, Chloroform-*d*) δ 9.20 (dd, *J* = 2.2, 0.7 Hz, 2H, H_F), 8.98 (dd, *J* = 5.3, 0.7 Hz, 2H, H_E), 8.92 (dd, *J* = 2.1, 0.9 Hz, 2H, H_C), 8.53 (dd, *J* = 8.2, 0.9 Hz, 2H, H_A), 8.06 – 8.03 (m, 4H, $H_{B\&E}$). HR-ESI: *m/z* 425.0972 (predicted $[M+H]^+$ = 425.0993).

C43

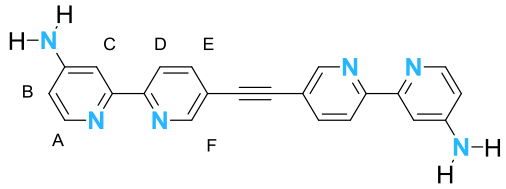

N26 (107 mg, 0.29 mmol) and Fe (powdered, 138 mg, 2.48 mmol) were suspended in acetic acid (20 mL) and sparged with N_2 and heated at 100 °C for 2 h. The mixture was allowed to cool and a solution of EDTA (1.4461 g) and NaOH (994.3 mg) dissolved in ammonium hydroxide (60 mL, 30%) and water (20 mL) were added. The mixture was stirred for 2 days. The crude product was collected by filtration and extracted with chloroform/methanol (1:1, 3 × 50 mL) and the solvent was removed *in vacuo*. The residue was extracted with acetonitrile (3× 50 mL) and precipitated with diethyl ether to give a grey/black waxy solid. Crude yield = 40 mg.

^{1}H NMR (500 MHz, DMSO-d_6) δ 8.85 (dd, *J* = 2.2, 0.9 Hz, 1H, H_F), 8.38 (dd, *J* = 8.2, 0.9 Hz, 1H, H_D), 8.12 (d, *J* = 5.5 Hz, 1H, H_A), 8.09 (dd, *J* = 8.2, 2.2 Hz, 1H, H_E), 7.66 (d, *J* = 2.4 Hz, 1H, H_C), 6.54 (dd, *J* = 5.5, 2.4 Hz, 1H, H_B), 6.21 (s, 4H, H_{NH}). Compounds instability prevented further characterisation.

Cage Synthesis

C41

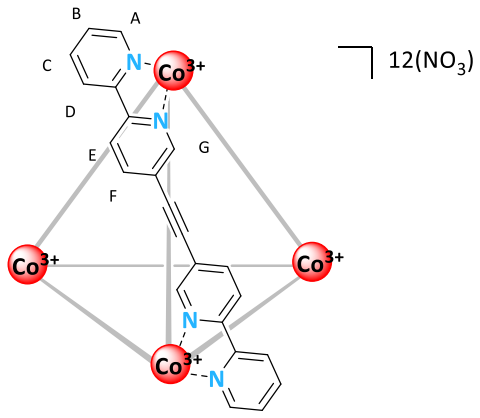

L41 (27.5 mg, 82.3 µmol) and cobalt (II) nitrate hexahydrate (16.0 mg, 54.9 µmol) were suspended in a degassed mixture of water and acetonitrile (1:2, 3.8 mL). The mixture was sparged with N_2, then heated at 50 °C for 0.5 h. The reaction was allowed to cool before $(NH_4)_2Ce(NO_3)_6$ (45.1 mg, 82.3 µmol) in acetonitrile (1.5 mL) was added via syringe pump (25 µLmin^{-1}). Some turbidity was observed,

addition of acetonitrile (20 mL) fully precipitated the product, which was collected onto celite and washed with acetonitrile. The product was eluted with water and the solution freeze-dried to give a yellow solid. Yield = 29 mg (71%).

^{1}H NMR (500 MHz, D_2O) δ 8.87 (d, *J* = 7.7 Hz, 12H, H_D), 8.85 (d, *J* = 8.6 Hz, 12H, H_E), 8.58 (apt, *J* = 7.7 Hz, 12H, H_C), 8.51 (d, *J* = 8.6 Hz, 12H, H_F), 7.81 (apt, *J* = 6.9 Hz, 12H, H_B), 7.59 (s, 12H, H_G), 7.45 (d, *J* = 6.0 Hz, 12H, H_A).^{13}C NMR (126 MHz, D_2O) δ 155.3, 155.0, 152.7, 151.1, 146.5, 144.2, 131.68, 128.1, 126.8, 124.9, 90.2. Calculated hydrodynamic radius = 11.6 Å.

C42

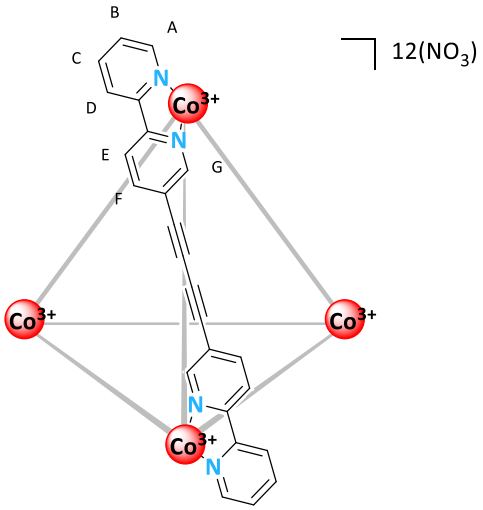

L42 (20.2 mg, 56.4 µmol) and cobalt (II) nitrate hexahydrate (10.8 mg, 37.2 µmol) were suspended in a degassed mixture of water and acetonitrile (1:2, 2.6 mL). The mixture was sparged with N_2, then heated at 50 °C for 0.5 h. The reaction was allowed to cool before $(NH_4)_2Ce(NO_3)_6$ (30.6 mg, 55.8 µmol) in acetonitrile (0.96 mL) was added via syringe pump (25 µLmin^{-1}). Some turbidity was observed, addition of acetonitrile (20 mL) fully precipitated the product, which was collected onto celite and washed with acetonitrile. The product was eluted with water and the solution freeze-dried to give the yellow title compound. Yield = 29 mg (100%).

^{1}H NMR (601 MHz, D_2O) δ 8.86 (d, *J* = 8.2 Hz, 12H, H_D), 8.85 (d, *J* = 8.5 Hz, 12H, H_E), 8.67 (d, *J* = 8.5, 1.8 Hz, 12H, H_F), 8.58 (t, *J* = 7.9 Hz, 12H, H_C), 7.82 (t, *J* = 6.7 Hz, 12H, H_B), 7.55 (d, *J* = 1.6 Hz, 12H, H_G), 7.42 (d, *J* = 6.0 Hz, 12H, H_A). ^{13}C NMR (126MHz, D_2O) δ 155.3, 155.0, 153.6, 151.2, 147.2, 144.3, 131.8, 128.1, 126.7, 124.9, 80.4, 77.8. Calculated hydronamic radius = 13.9 Å

L43

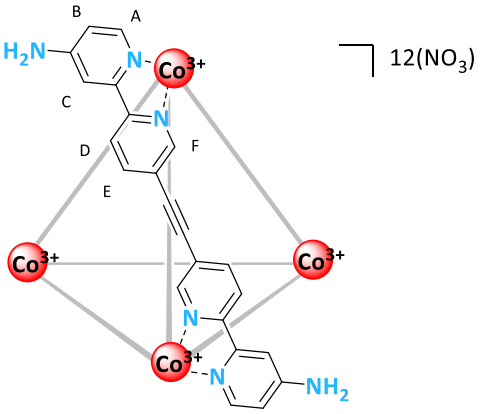

Direct formation

L43 (27.5 mg, 0.78 mmol) and cobalt (II) nitrate hexahydrate (14.6 mg, 0.05 mmol) were suspended in degassed mixture of water and acetonitrile (3.45 mL, 5:1) under N_2. The mixture was sparged with N_2 and heated at 60 °C for 24 h. The reaction was allowed to cool before $(NH_4)_2Ce(NO_3)_6$ (42.2 mg, 0.077 mmol) in acetonitrile (1.5 mL) was added via syringe pump (25 $\mu L min^{-1}$). Acetonitrile (20 mL) was added causing an orange precipitate, which was collected onto celite, washed with acetonitrile and eluted with water and the mixture freeze dried to give an orange solid.

By ligand exchange

L43 (impure, 7.9 mg, 0.021 mmol) was added to a solution of **C41** (5.8 mg, 842 µL D_2O, 98 µL CD_3CN) in an NMR tube. The tube was sealed and a ^1H NMR was taken before the tube was heated at 75 °C, while periodically being allowed to cool for 30 minutes to be analysed by ^1H NMR, before being returned to heating.

Glutathione Assay

A 1 mM solution of cage was prepared in deuterated PBS (1 M, pH 7.4, 1mM ^{t}BuOH). NMR samples were prepared (0.5 mL) and to one PBS (0.1 mL) was added and to another glutathione (100 mM, 0.1 mL) was added. The samples are then monitored by ^1H NMR to find the lifetime of the assemblies.

C41 in PBS

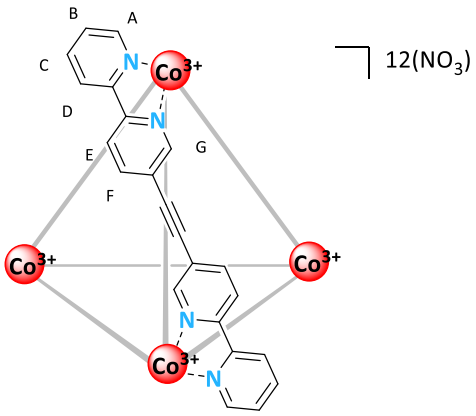

^{1}H NMR (500 MHz, D_2O) δ 8.94 – 8.84 (m, 24H, $H_{D/E}$), 8.67 – 8.52 (m, 24H, $H_{C/F}$), 7.84 (t, *J* = 7.0 Hz, 12H, H_B), 7.58 (s, 12H, H_G), 7.48 (d, *J* = 6.0 Hz, 12H, H_A).

Spontaneous Raman Spectroscopy

William Grantham, Alisia Sim

The spontaneous Raman spectra were obtained using a confocal Raman spectrometer (inVia Raman microscope, Renishaw) at room temperature. A 297 mW (206 mW after objective) 785 nm diode laser was used to excite the sample through a 20× N.A.075 objective (Leica Biosystems). The recorded spectral range for a grating was 1200 g mm^{-1}. The total data acquisition was performed during 60 s using Wire software. All spectra acquired at λ_{ex} = 785 nm were background subtracted using a background correction algorithm.

Two-photon fluorescence and Stimulated Raman Scattering (SRS) Microscopy

Kristal Sepp, Martin Lee

Images were obtained using a custom-built multi-modal microscope setup. A picoEmerald (APE, Berlin, Germany) laser provided tuneable pump laser (720-990 nm, 7ps, 80 MHz repetition rate) and a spatially and temporally overlapped Stokes laser (1064 nm, 5-6- ps, 80 MHz repetition rate). The output beam was inserted into the scanning unit of an Olympus FV1000MPE microscope using a series of dielectric mirrors and 2× lens based beam-expanding module. The resulting 2.4 mm beam were expanded by a further 3.6× lens within the microscope and directed into an Olympus XLP25XWMP N.A. 1.05 objective lens using a short-pass 690 nm dichroic mirror (Olympus). The objective was under filled to achieve higher power transmissions through the microscope which were shown to be essential to detect the SRS signal. Backscattered emission signals from two-photon fluorescence was separated from any backscattered excitation light using a short pass 690 nm dichroic mirror and IR cut filter (Olympus). A series of filters and dichroic mirrors were then used to deconvolve the different

emission signals onto one of 4 available photo-multiplier tubes (PMT). ER-Tracker Green two-photon fluorescence signals were filtered using FF552-Di02,FF483/639-Di01 and FF510/84 (Semrock).

Cellular Uptake Studies

HeLa cells were treated with either **C41** (1 mM, in DMEM complete eagle media, 30 min), or DMEM complete eagle media (2 h) and then washed with PBS prior to fixing with formaldehyde (3.7% in PBS, 10 min, 37 °C) before washing with PBS prior to trypsinisation and dilution with DMEM. The resulting cell suspension was centrifuged at 175 g and the cell pellet was washed with DMEM/PBS (1/1 v/v; 10 mL) and re-centrifuged (2×). The cell pellet was transferred to CaF_2 coverslips for analysis by spontaneous Raman spectroscopy using λ_{ex} = 785 nm.

4.5 References

1 C. M. Drain and J.-M. Lehn, *J. Chem. Soc. Chem. Commun.*, 1994, **53**, 2313–2315.

2 N. Strickland, A. J. Mulholland and J. N. Harvey, *Biophys. J.*, 2006, **90**, L27–L29.

3 A. Ahmedova, R. Mihaylova, D. Momekova, P. Shestakova, S. Stoykova, J. Zaharieva, M. Yamashina, G. Momekov, M. Akita and M. Yoshizawa, *Dalton Trans.*, 2016, **45**, 13214–13221.

4 S. K. Samanta, D. Moncelet, V. Briken and L. Isaacs, *J. Am. Chem. Soc.*, 2016, **138**, 14488–14496.

5 Z. Yue, H. Wang, D. J. Bowers, M. Gao, M. Stilgenbauer, F. Nielsen, J. T. Shelley and Y.-R. Zheng, *Dalton Trans.*, 2018, **47**, 670–674.

6 O. Zava, J. Mattsson, B. Therrien and P. J. Dyson, *Chem. Eur. J.*, 2010, **16**, 1428–1431.

7 M. Zhang, S. Li, X. Yan, Z. Zhou, M. L. Saha, Y.-C. Wang and P. J. Stang, *Proc. Natl. Acad. Sci.*, 2016, **113**, 11100–11105.

8 H. Yamakoshi, K. Dodo, A. Palonpon, J. Ando, K. Fujita, S. Kawata and M. Sodeoka, *J. Am. Chem. Soc.*, 2012, **134**, 20681–20689.

9 A. Salic and T. J. Mitchison, *Proc. Natl. Acad. Sci.*, 2008, **105**, 2415–2420.

10 H. Yamakoshi, K. Dodo, M. Okada, J. Ando, A. Palonpon, K. Fujita, S. Kawata and M. Sodeoka, *J. Am. Chem. Soc.*, 2011, **133**, 6102–6105.

11 W. J. Tipping, M. Lee, A. Serrels, V. G. Brunton and A. N. Hulme, *Chem. Sci.*, 2017, **8**, 5606–5615.

12 W. Wang, J. Zhao, M. Short and H. Zeng, *J. Biophotonics*, 2015, **8**, 527–545.

13 L. Opilik, T. Schmid and R. Zenobi, *Annu. Rev. Anal. Chem.*, 2013, **6**, 379–398.

14 C. W. Freudiger, W. Min, B. G. Saar, S. Lu, G. R. Holtom, C. He, J. C. Tsai, J. X. Kang and X. S. Xie, *Science*, 2008, **322**, 1857–1861.

15 B. G. Saar, C. W. Freudiger, J. Reichman, C. M. Stanley, G. R. Holtom and X. S. Xie, *Science*, 2010, **330**, 1368–1370.

16 V. Grosshenny, F. M. Romero and R. Ziessel, *J. Org. Chem.*, 1997, **62**, 1491–1500.

17 T. Luu, E. Elliott, A. D. Slepkov, S. Eisler, R. McDonald, F. A. Hegmann and R. R. Tykwinski, *Org. Lett.*, 2005, **7**, 51–54.

18 S. M. E. Simpkins, M. D. Weller and L. R. Cox, *Chem. Commun.*, 2007, 4035–4037.

19 A. B. S. Elliott, J. E. M. Lewis, H. van der Salm, C. J. McAdam, J. D. Crowley and K. C. Gordon, *Inorg. Chem.*, 2016, **55**, 3440–3447.

20 S. C. Epstein, A. R. Huff, E. S. Winesett, C. H. Londergan and L. K. Charkoudian, *Nat. Commun.*, 2019, **10**, 2227–2233.

21 A. V. Davis and K. N. Raymond, *J. Am. Chem. Soc.*, 2005, **127**, 7912–7919.

22 T. Zhu, S. Cao, P.-C. Su, R. Patel, D. Shah, H. B. Chokshi, R. Szukala, M. E. Johnson and K. E. Hevener, *J. Med. Chem.*, 2013, **56**, 6560–6572.

23 T. Yao and Y. Asayama, *Reprod. Med. Biol.*, 2017, **16**, 99–117.

Conclusions

This project explored the biomedical applications of robust metallosupramolecular cages. This included identification and solution of an instability issue, the development of a cage capable of altering the biological uptake of radiotracer, progress towards bioconjugation of the cages, and a means of investigating their cellular behaviour.

The previously developed **C19** cobalt (III) tetrahedra were found to be reductively degraded by biological reductants and therefore unsuitable for biological applications. Therefore, a more stable variant of the cage, **C20**, was developed. Synthesis of this tetrahedron was complicated by the strengthened interactions leading to kinetically trapped biproducts during the self-assembly process. This problem was overcome by utilising **C19** as a tetrahedral template for the formation of **C20** to prevent formation of these biproducts.

C20 proved to possess similar properties to **C19** but with the desired resistance to degradation, as shown by persistent binding of $[^{99m}Tc]TcO_4^-$ in serum, and significantly reduced degradation by glutathione in PBS. Therefore, **C20** was trialled *in vivo* by administering $[^{99m}Tc]TcO_4^-$ bound within **C20** to mice. The bound guest proved to significantly increase the uptake in the liver over the free anion, in a novel example of a guest molecule being retained by a "naked" metallosupramolecular capsule *in vivo*.

Methods of altering the biological properties of **C20** were explored to allow control of the cage's uptake. A pendant primary alkyne was introduced into the ligand, suitable for functionalisation via copper catalysed alkyne azide cycloaddition reactions with a wide variety of groups. Additionally, a methylether group was explored as an alternative to the amine group of **L20**, successfully resulting in the **C38** tetrahedron.

Stimulated Raman spectroscopy was identified as a promising means of investigating the cellular behaviour of cages. This required the incorporation of a Raman active alkyne group into the ligand **L41**, which was successfully assembled into the tetrahedron **C41**. Degradation of the cage led to precipitation of fluorescent ligand, interfering with the Raman technique. However, the Raman signal of the intact cage appeared to be present within the cells, indicating the potential of the technique with further refinement.

A cage capable of a biomedical application was developed and progress made towards biological targeting and in-depth investigation of the cellular interactions of the cages. These results clearly demonstrate the potential for these cage systems as viable biomedical tools, capable of altering the biological behaviour of a guest molecule with clear avenues for expansion to further develop and improve the technology.

Tetrahedron and Ligand Glossary

Previous Projects

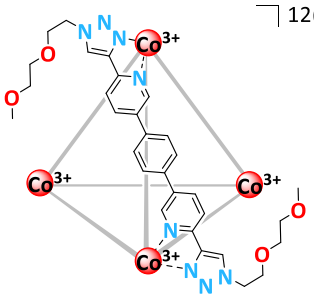

C14

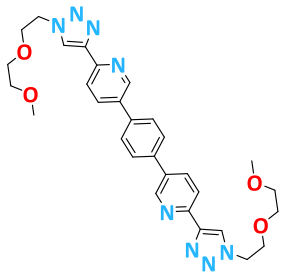

L14

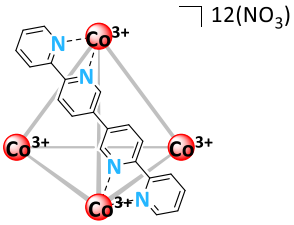

C19

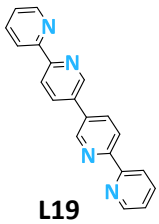

L19

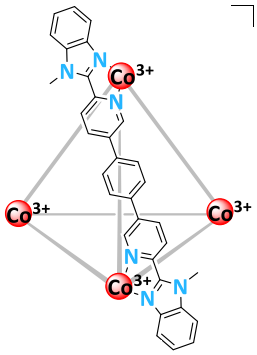

C16

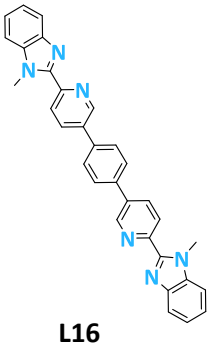

L16

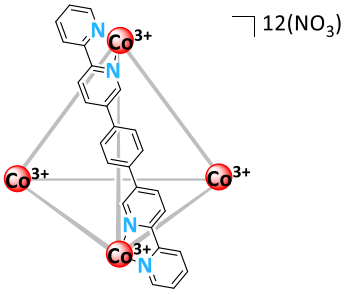

C15

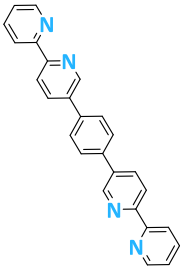

L15

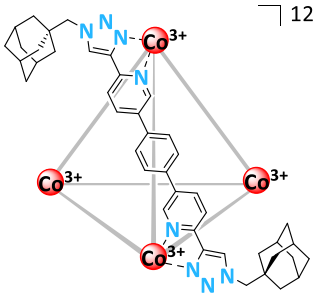

C24

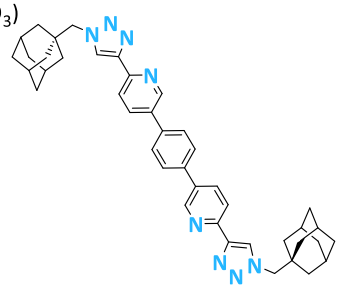

L24

Chapter 2

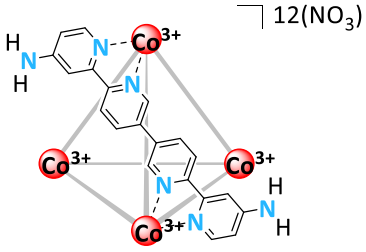

C20

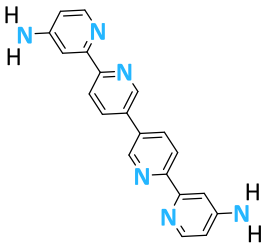

L20

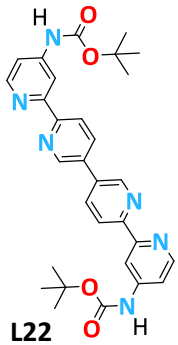

L22

Chapter 3

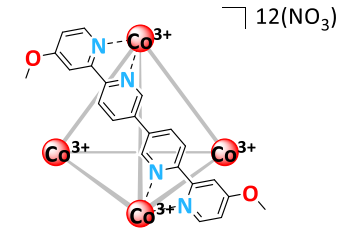

C38

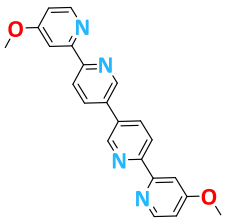

L38

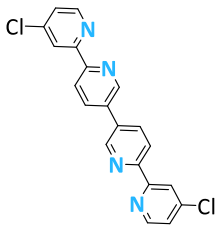

L33

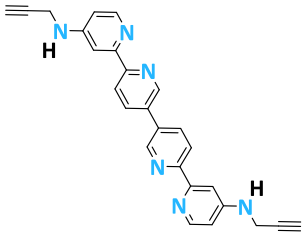

L35

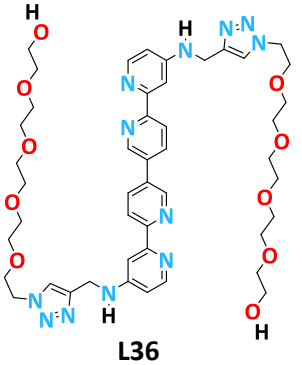

L36

Chapter 4

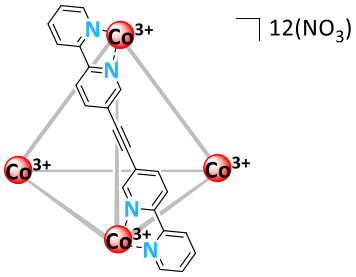

C41

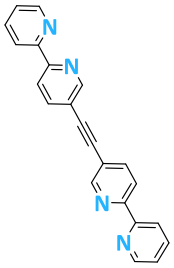

L41

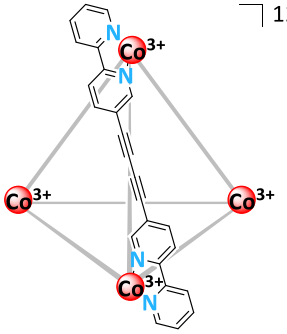

C42

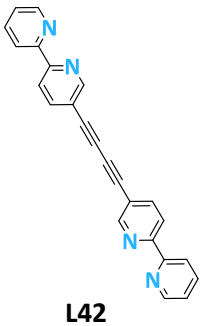

L42

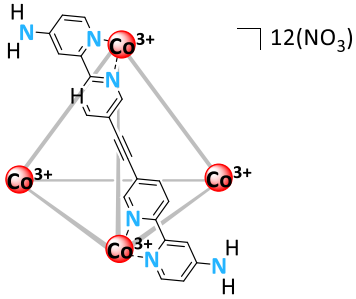

C43

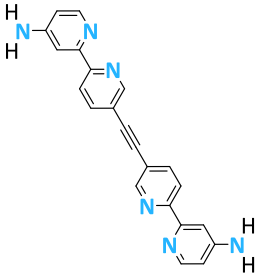

L43